Antibacterial Drug Mining from Endophytic Fungi and Characterization of Lead Compounds

Inaugural dissertation

for the attainment of the title of doctor
in the Faculty of Mathematics and Natural Sciences
at the Heinrich Heine University Düsseldorf

presented by

Lin Wang

from Hubei, P. R. China

Düsseldorf, 08, 2022

From the Institute of Pharmaceutical Biology and Biotechnology
at the Heinrich Heine University Düsseldorf

Published by permission of the Faculty of Mathematics and Natural Sciences
at Heinrich Heine University Düsseldorf

Supervisor: Prof. Dr. rer. Nat. Rainer Kalscheuer
Co-supervisor: Prof. Dr. Dr. hc. Peter Proksch

Date of oral examination: 30/08/2022

Devoted to my parents

Jiaxue Wang and Chuanju Zhang

And

Mrs. Shaohong Ha

CONTENTS

Abstract

To face the challenge of bacterial resistance spreading and the demand for novel therapeutic agents active against multidrug-resistant microbial pathogens, bioactive compounds from nature have historically made a major contribution to development of new antibiotics and have inspired the design of optimized structural analogues. While fungi are generally a well-studied, biotechnologically valuable group of organisms, endophytic fungi that colonize plant hosts are less well investigated. Since endophytic fungi occupy very diverse environments from tropical to arctic habitats and have adapted to complex ecological niches, they promise to provide a rich source of novel and structurally divers secondary metabolites. This dissertation describes the investigation of bioactive secondary metabolites from two endophytic fungi, *Clonostachys rosea* and *pestalotiopsis chamaeropis*. An "OSMAC" (One Strain Many Compounds) approach was applied to induce silent gene clusters to exploit biochemical diversity of these fungi by changing the composition of solid rice medium, e.g., by adding different salts. The structure of isolated secondary metabolites was elucidated by NMR spectra and HRESIMS data, whereas the absolute configuration of new compounds was determined by optical rotation, ECD analysis and X-ray diffraction.

Isolated compounds were screened for their antibacterial activity against nosocomial bacterial pathogens such as *Staphylococcus aureu*s, *Enterococcus faecalis*, *Enterococcus faecium*, *Escherichia coli*, *Acinetobacter baumannii* and *Streptococcus pneumoniae*, against *Mycobacterium tuberculosis*, against the pathogenic fungus *Candida albicans*, as well as against human immunodeficiency virus HIV-1 and SARS-CoV-2.

First manuscript:

Asperphenalenones isolated from the biocontrol agent Clonostachys rosea and their

antimicrobial activities

Ten asperphenalenones were isolated from the endophytic fungus *Clonostachys rosea* isolated from the plant *Conyza canadensis.* Eight new asperphenalenones F-M were first reported and their structures were elucidated by NMR, HREIMS and ECD calculation. Asperphenalenones F and H exhibited pronounced antibacterial activity against methicillin-resistant *Staphylococcus aureus* (MRSA) with minimal inhibitory concentrations (MIC) of 12.5 μM and 25 μM, respectively. AdditionallyAdditionally, asperphenalenone B exhibited low antiviral activity against human immunodeficiency virus HIV-1 replication with no cytotoxicity against the human T lymphocyte Jurkat cell line.

Second manuscript:

Roseazine A with a 1,3-benzodioxol-2,5-diazabicyclo[2.2.1]heptan skeleton from endophytic fungus Clonostachys rosea

One unprecedented roseazine A (**1**), containing 1, 3-benzodioxole-2, 5-diazabicyclo [2.2.1] heptane skeleton, together with a new crystal compound chrysine E and five known cytochalasins were isolated from endophytic fungus *Clonostachys rosea*. Their structures were elucidated by a combination of different NMR spectroscopic and mass spectrometric analyses, as well as single-crystal X-ray diffraction. Aspochalasin B showed moderate activity against both wild type and methicillin-resistant *Staphylococcus aureus* with MICs of 25 μM. Furthermore, aspochalasins I exhibited weak antibacterial activity against *Mycobacterium tuberculosis* H37Rv.

Third manuscript:

Studies on antibacterial activity of Pestalotic acid A against methicillin-resistant Staphylococcus aureus

Pestalotic acid derivatives were isolated from solid rice cultures of *Pestalotiopsis chamaeropis.* An "OSMAC" approach was applied by adding different sodium or ammonium salts to the rice medium. Addition of 3.5% NaI induced a significant enrichment of the metabolite pattern of pestalotic acid derivatives indicated by HPLC analysis. Bioactivity screening displayed that pestalotic acid A has significant antimicrobial activity against MRSA with a MIC_{90} of 6.25 μM. The strong bactericidal killing effects with low cytotoxicity make pestalotic acid A a promising candidate for further research. Mode of action studies indicated that pestalotic acid A might compromise the integrity of the bacterial cell membrane in MRSA.

Zusammenfassung

Angesichts der Ausbreitung bakterieller Resistenzen und der Nachfrage nach neuen therapeutischen Wirkstoffen gegen multiresistente mikrobielle Krankheitserreger haben bioaktive Verbindungen aus der Natur in der Vergangenheit einen wichtigen Beitrag zur Entwicklung neuer Antibiotika geleistet und die Entwicklung optimierter struktureller Analoga inspiriert. Während Pilze im Allgemeinen eine gut erforschte, biotechnologisch wertvolle Gruppe von Organismen darstellen, so sind endophytische Pilze, die innere Gewebe von Pflanzenwirten besiedeln, weniger gut untersucht. Da endophytische Pilze sehr unterschiedliche Lebensräume von den Tropen bis zur Arktis besiedeln und sich an komplexe ökologische Nischen angepasst haben, versprechen sie eine ergiebige Quelle neuartiger und strukturell vielfältiger Sekundärmetaboliten zu sein. Diese Dissertation beschreibt die Untersuchung bioaktiver Sekundärmetabolite aus zwei endophytischen Pilzen, *Clonostachys rosea* und

pestalotiopsis chamaeropis. Es wurde ein "OSMAC"-Ansatz (One Strain Many Compounds) angewandt, um stille Gencluster zu induzieren und die biochemische Vielfalt dieser Pilze zu nutzen. Dazu wurde die Zusammensetzung des verwendeten Reismediums z. B. durch die Zugabe verschiedener Salze verändert. Die Struktur der isolierten Sekundärmetaboliten wurde durch NMR-Spektren und HRESIMS-Daten aufgeklärt, während die absolute Konfiguration der neuen Verbindungen durch optische Rotation, ECD-Analyse und Röntgenbeugung bestimmt wurde.

Die isolierten Verbindungen wurden auf ihre antibakterielle Aktivität gegen nosokomiale bakterielle Krankheitserreger wie *Staphylococcus aureus*, Enterococcus faecalis, *Enterococcus faecium*, *Escherichia coli*, *Acinetobacter baumannii* und *Streptococcus pneumoniae*, gegen *Mycobacterium tuberculosis*, gegen den pathogenen Pilz *Candida albicans* sowie gegen das menschliche Immunschwächevirus HIV-1 und SARS-CoV-2 untersucht.

Erstes Manuskript:

Aus dem Biokontrollagens Clonostachys rosea isolierte Asperphenalenone und ihre antimikrobiellen Aktivitäten

Zehn Asperphenalenone wurden aus dem endophytischen Pilz *Clonostachys rosea* isoliert, der endophytisch in der Pflanze *Conyza canadensis* lebt. Acht neue Asperphenalenone F-M wurden erstmals beschrieben und ihre Strukturen durch NMR, HREIMS und ECD-Analyse aufgeklärt. Die Asperphenalenone F und H zeigten eine deutliche antibakterielle Aktivität gegen Methicillin-resistenten *Staphylococcus aureus* (MRSA) mit minimalen Hemmkonzentrationen (MHK) von 12,5 μM bzw. 25 μM. Außerdem zeigte Asperphenalenon B eine geringe antivirale Aktivität gegen die Replikation des humanen Immundefizienzvirus HIV-1 ohne Zytotoxizität gegen die humane T-Lymphozyten-Jurkat-Zelllinie.

Zweites Manuskript:

Roseazin A mit einem 1,3-benzodioxol-2,5-diazabicyclo[2.2.1]heptan-Skelett aus dem endophytischen Pilz Clonostachys rosea

Roseazin A, das ein neuartiges 1,3-benzodioxol-2,5-diazabicyclo[2.2.1]heptan-Skelett aufweist, wurde zusammen mit dem neuen Kristallverbindung Chrysin E und fünf bekannten Cytochalasinen aus dem endophytischen Pilz *Clonostachys rosea* isoliert. Ihre Strukturen wurden durch eine Kombination verschiedener NMR-spektroskopischer und massenspek−trometrischer Analysen sowie Einkristall-Röntgenbeugung aufgeklärt. Aspochalasin B zeigte mäßige Aktivität sowohl gegen sensitiven als auch gegen Methicillin-resistenten *Staphylococcus aureus* mit MHKs von 25 μM. Darüber hinaus zeigte Aspochalasine I eine schwache Aktivität gegen *Mycobacterium tuberculosis* H37Rv.

Drittes Manuskript:

Studien zur antibakteriellen Aktivität des Naturstoffs Pestalotinsäure A gegenüber Methicillin-resistentem *Staphylococcus aureus*

Pestalotinsäurederivate wurden aus festen Reiskulturen von *Pestalotiopsis chamaeropis* isoliert. Ein “OSMAC“-Ansatz wurde angewendet, indem dem Reismedium verschiedene Natrium- oder Ammoniumsalze zugesetzt wurden. Durch Zugabe von 3,5 % NaI wurde eine signifikante Diversifizierung des Sekundärmetabolitenprofils von Pestalotinsäurederivaten induzierten, was durch HPLC-Analyse nachgewiesen wurde. Das Bioaktivitäts-Screening zeigte, dass Pestalotinsäure A eine signifikante antimikrobielle Aktivität gegen MRSA mit einem MIC_{90} von 6,25 μM aufweist. Die starke bakterizide Abtötungswirkung bei geringer

Zytotoxizität macht Pestalotinsäure A zu einem vielversprechenden Kandidaten für eine weitere funktionale Charakterisierung. Studien zur Wirkungsweise zeigten, dass Pestalotin-säure A die Integrität der bakteriellen Zellmembran bei MRSA beeinträchtigen könnte.

Chapter 1 General Introduction

Deaths caused by infections continue to claim millions of lives each year, particularly in lower-resource settings where many people cannot access quality health services. Especially, respiratory infections remain the world's most deadly communicable disease, ranked as the 4th leading cause of death, including amongst others tuberculosis (TB). Even though the number of deaths decreased substantially, respiratory infections still claimed 2.6 million lives in 2019.[1] Based on the world health organization (WHO) statistics, globally a total of about 10 million people fell ill with *Mycobacterium tuberculosis* (Mtb), the causative agent of TB, in 2020[2], which led to about 1.5 million fatalities. Moreover, studies have found 20% of postoperative surgical site infections (SSIs) are caused by *Staphylococcus aureus* (*S. aureus*), identified as the most common SSI pathogen.[3] Additionally, before the COVID-19 pandemic, *Streptococcus pneumoniae* was the leading cause of community-acquired pneumonia worldwide . In 2017, the WHO published a list of pathogenic microorganisms, which have an urgent need for new therapeutics. Amongst others, *Acinetobacter baumannii* is listed due to its high antimicrobial resistance rates, which set an alert for infections caused by this gram-negative microorganism.[4]

1.1 Nosocomial bacterial pathogens

Nosocomial pathogens include bacteria, viruses, and fungal cells. According to the WHO, around 15% of all hospitalized patients suffer from these infections, demonstrating the large impact bacterial infections have on public health.[5] The majority of life-threatening infection are caused by the group of ESKAPE pathogens including *Enterococcus faecium*, *Staphylococcus aureus*, *Klebsiella pneumoniae*, *Acinetobacter baumannii*, *Pseudomonas aeruginosa*, and *Enterobacter spp*.. While bacterial infections have large impact on human health and pose enormous economic burden to the society in general, especially patients in hospitals and health-care facilities are critically in risk.[6] The following will give a short overview about some

pathogenic bacteria, which were studied in the projects reported in this thesis.

1.1.1 *Staphylococcus aureus*

S. aureus is a gram-positive bacterium that is cocci-shaped and tends to be arranged in clusters with a diameter of approximately 1 μm. Colonies on solid medium are golden or yellow, characterized by a thick layer (approximately 15-80 nm) of peptidoglycan above the smooth cell membrane.

S. aureus is commonly found on the skin and mucous membranes in humans and exhibits a wide variety of clinical characters. It is estimated that 15% of the population carry *S. aureus* asymptomatically as part of the normal flora, some of them might have high rates up to 80% colonization.[7] The ability of *S. aureus* to cause infection is mostly attributed to particular cell wall constituents. So far, more than 30 antigens have been discovered including cell surface proteins such as *staphylococcal* protein A (SPA). SPA can bind to immunoglobulins of many species with high affinity, which makes it a useful reagent for immunoassays and immunoglobulin purification. However, poor reactivity with some immunoglobulins subclasses including human IgG3 and murine IgG1 cause some limitations in application.[8]

S. aureus infections cause a wide range of diseases and syndromes, including pneumonia, infection on soft tissue and most community-associated invasive infections. Further, the pathophysiology is highly depending on the type of *S. aureus* infection. The typical virulence factors of *S. aureus* are the α-toxin and the Panton-Valentine leukocidin (PVL), which particularly contribute to disease development.[9] Toxic Shock Syndrome Toxin 1 (TSST-1) and staphylococcal toxins are important virulence factors in infectious sepsis and toxic shock syndrome.[10] Bacterial cell wall proteins, such as fibrinogen-binding proteins, clumping factors, and teichoic acids mediated the binding of the bacterial cells to extracellular matrix proteins and fibronectin in infectious endocarditis.[11] An increasing problem is the Methicillin-resistant *S. aureus* (MRSA), which resists treatment with a wide range of different antibiotics classes,

amongst other penicillins, carbapenems, and glycopeptides like vancomycin that was used as an effective treatment for a long time.[12]

1.1.2 *Mycobacterium tuberculosis*

Mtb is a class of elongated and slightly curved bacilli with a size of approx. 1-4 μm × 0.4 μm, named for its tendency to branch. Mtb is an obligate aerobe bacterium, requires high nutrient, and grows best at pH 6.5-6.8. Mtb is a slow growing bacterium and colonies on solid media can be observed after 3-4 weeks of incubation at 37 °C. They are characterized as dry, solid, yellow, and shaped as a cauliflower.

10 million people fall ill with TB every year, and 1.5 million people die from TB annually, despite being a preventable and curable disease, making it one of the world's top infectious killer only second to SARS-CoV-2 in recent years[13] TB is a poverty related disease mostly endemic to Subsaharan Africa and South East Asia, as can be estimated from reported TB incidence rates shown in Figure 1.

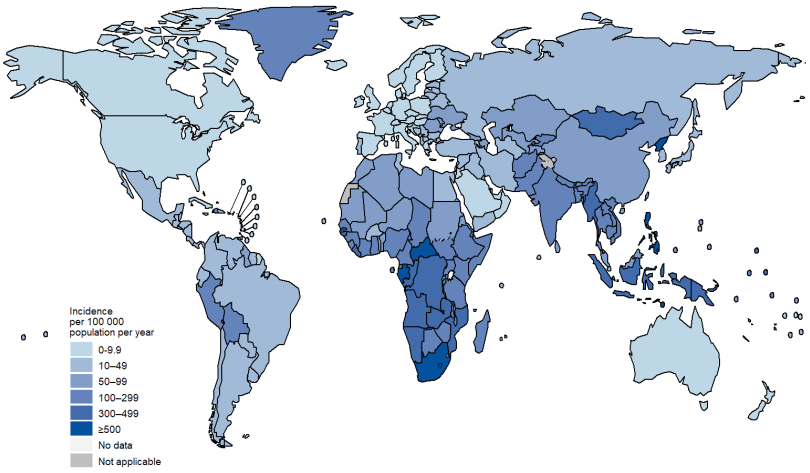

Figure 1: The estimated TB incidence rates in 2020 from WHO. Produced from: Global Tuberculosis Report 2021, WHO, 2021.

The TB bacteria can attack any part of the body, but not everyone infected with TB bacteria becomes sick (called latent TB infection). In most cases when infection with TB bacteria occur,

the body is able to fight against the invading bacteria and can limit their growth and dissemination.[14] TB is endotoxin free and also doesn't produce exotoxins or invasive enzymes. The pathogenesis mainly depends on the large amount of various peculiar lipids in the cell wall. The tubercle bacilli are effectively phagocytosed by alveolar macrophages but are able to stall the normal innate antimicrobial effector functions and multiply in the arrested and only partially acidified phagolysosomes of these immune cells. Other immune cells are recruited to the site if infection and form granulomatous structures, that limit dissemination but at the same time protect the bacteria from effective adaptive immune responses by B- and T-cells. After lysis of infected macrophages in the core of the granulomas, the bacteria become extracellular and are able to spread via the bloodstream or lymphatic channels to other tissues and organs after an infection has occurred in the lung.[15]

Drug-resistant Mtb strains have emerged as a threat to public health worldwide. The unusually thick and lipid-rich cell envelope of mycobacteria builds a natural permeability barrier against antibiotics. Furthermore, after penetrating the cell envelope, antibiotics might be affected by one or more anti-Tb resistance mechanisms including: 1, modification of drugs by Tb enzymes;[16] 2, the presence of Tb efflux pumps; 3, the modulation of TB gene expression,[17] and 4, intrinsic factors like acquisition of genetic mutations.[18] Most mutations related to drug resistance occur in genes coding for drug targets or drug activating enzymes through single nucleotide polymorphisms (SNPs) and insertion-deletions (indels). In contrast, horizontal transfer of resistance genes is not commonly reported in TB[19] Until now, single-step chromosomal mutations are the main causes of drug resistance in TB. Development of clinically relevant levels of resistance and of resistances against multiple drugs likely is a consequence of a step-wise acquisition and fixation.[20]

1.1.3 *Streptococcus pneumoniae*

S. pneumoniae is a gram-positive bacterium with alpha-hemolytic properties. As a significant human pathogenic bacterium, *S. pneumoniae* was discovered for causing pneumonia in the 1880s. [21] Cells of *S. pneumoniae* are spearhead-shaped, arranged in pairs, and form small colonies with round and smooth surfaces on blood agar plates. Similar to S. aureus, *S. pneumoniae* is an opportunistic pathogen and often found as commensal bacterium in the nasopharynx of humans without generally causing disease.[22]

S. pneumoniae infection is the most frequent cause of leading community pneumonia among the elder or young children.[23] The bacterium produces a polysaccharide capsule that is an important virulence factor. High fever, chills, cough, bloody sputum and chest pain are characteristics of *S. pneumoniae* infections in clinical manifestations.

1.2 Antibiotic resistance crisis

Antibiotics are medicines widely used to prevent and treat bacterial infections. Antibiotic resistance occurs after the use of medicines in response to bacteria once they have infected humans or animals, which make them harder to treat.[24] Nowadays, antibiotic resistance is becoming one of the biggest threat to human health, food security and social development that can affect anyone in any age at any country. A growing number of resistances are rising to dangerous levels worldwide.

1.2.1 Cause of antibiotic resistance

Causes of the antibiotic resistance crisis can be summarized in the following aspects: (1) Overuse. Several antibiotics can be bought for use in humans or animals without doctor's prescription in some regions or countries. This lack of regulation allows easy access, which promotes overuse, misuse, and therefore the spread of resistances.[25] (2) Inappropriate prescription. For patients with unspecific symptoms of a respiratory infection, broad-spectrum antibiotics are often prescribed without proper diagnosis. However, respiratory infections are mostly caused by viral and not by bacterial pathogens. This contributes to the promotion of

resistant bacteria, questions therapeutic benefit and exposes patients to potential side effects.[26] (3) Non-adherence to drug regimens. Patients frequently do not strictly adhere to treatment regiments and will have non-regular intake of drugs or terminate therapy prematurely after symptoms have improved. This leads to extended episodes of sub-inhibitory antibiotic concentrations in this cohort of patients, which promotes mutations in the target or the activating enzymes.[27] (4) Another driving factor is the extensive use of antibiotics in agriculture. The agricultural use of antibiotics also affects the environmental microbiome especially in livestock. Ingested by humans when they consume food, this results in the spread and transfer of resistant bacteria to humans through farm animals.[28] Additionally, residual amounts of antibiotics can occasionally be found in food products generated from livestock, and this inadvertent intake of antibiotics promotes the emergence of resistant bacteria in the same way an incomplete therapy would do. (5) Another factor are also economic interest. Compared to other pharmaceuticals, the development of antibiotics is considered economically less attractive. Changes in standards for clinical trial design made the research and development particularly challenging, especially during the past two decades due to increased regulations by the FDA in the USA and the EMA in the EU. Studies comparing antibiotics with placebo are considered unethical and require a large sample population at consequently high costs for the industry.[29] Thus, major pharma companies have abandoned antibiotic development programs, which has led to a strong curtailing of new antibiotics in the last decades. More research and development (R&D) is vital and thus the WHO has published a list of priority pathogens for R&D of new antibiotics (Table 1).

Table 1: Priority pathogens list for R&D of new antibiotics. Reproduced from WHO publication-antibacterial agents in clinical development 2019.[30]

Critical Priority	*Acinetobacter baumannii*, carbapenem-resistant
	Pseudomonas aeruginosa, carbapenem-resistant
	Enterobacteriaceae, carbapenem-resistant, ESBL-producing
High Priority	*Enterococcus faecium*, vancomycin-resistant
	Staphylococcus aureus, methicillin-resistant, vancomycin-intermediate and resistant
	Helicobacter pylori, clarithromycin-resistant
	Campylobacter spp., fluoroquinolone-resistant
	Salmonellae, fluoroquinolone-resistant
	Neisseria gonorrhoeae, cephalosporin-resistant, fluoroquinolone-resistant
Medium Priority	*Streptococcus pneumoniae*, penicillin-non-susceptible
	Haemophilus influenzae, ampicillin-resistant
	Shigella spp., fluoroquinolone-resistant

1.2.2 Mechanisms of resistance

The mechanisms of resistance mainly can be concluded as: limiting uptake of drugs, activation of efflux, target modification, and drug inactivation. These mechanisms may be native to the microorganisms, or acquired from other microorganisms by vertical or horizontal gene transfer (Figure 2).[31]

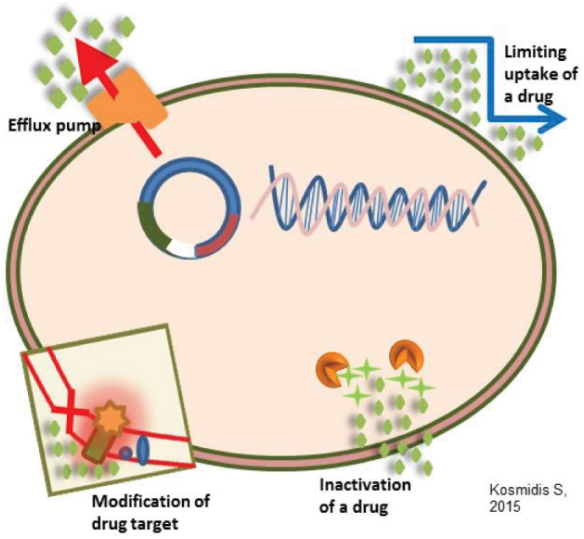

Figure 2: General antimicrobial resistance mechanisms against antibiotics. Produced from: An overview of the antimicrobial resistance mechanisms of bacteria. *AIMS Microbiol*. 2018.[31]

1.2.2.1 Limiting drug uptake

The presence of the lipopolysaccharide (LPS-) containing outer membrane layer in gram-negative bacteria provides a natural barrier to certain types of molecules like large antimicrobial agents. Thus, it prevents certain antibiotics to enter the cell and confers high intrinsic resistance. Substances can, however, enter the cell through porin channels especially for hydrophilic molecules. Resistance can occur due to mutations in the porin channels or by the alternation of porin expression resulting in decreased uptake of the drug. For example, the *Enterobacteriaceae* resistance to carbapenems typically relies on reduce porin expression.[32] The outer membrane of mycobacteria consist of a high content of specific lipids allowing easier access of hydrophobic drugs to the cell such as rifampicin and the fluoroquinolones.[33] On the other hand, the high content of mycolic acids and arabinogalactan increase the resistance for the bacteria towards acidic pH and some antibiotics. Additionally, the wax film-like lipoarabinomannan layer masks the immunogenic potential of mycobacteria and increases its pathogenic potential. Some bacteria, such as mycoplasma, lack a cell wall, and thus they are resistant to all drugs which target the cell wall including β-lactams and glycopeptides.[34] Gram-positive bacteria doesn't have an outer membrane like gram-negative bacteria, and drugs have easier access. But when *S. aureus* is treated with vancomycin, it responds to the treatment by producing a thickened cell wall, which makes it difficult for the drug to enter the cell and provides different level resistance to vancomycin.[35] Persisters and biofilms are a form of bacterial growth that can withstand antibiotic treatment without being resistant mutants but tolerant subpopulations. Persisters are characterized by a slowed metabolism where e.g. DNA and protein synthesis are donwregulated. This renders the persistent cells phenotypically resistant to antibiotics like fluoroquinolones and tetracyclines, which would interfere in the DNA and protein synthesis, respectively. Biofilms are a form of bacterial growth that form micro-communities of cells on biotic and abiotic surfaces. Induced by quorum sensing, the bacteria produce and secrete polymers, i.e., DNA, polysaccherides, and proteins that form an extracellular matrix, which is

a physical barrier surrounding the cells and thereby protecting the imbedded bacteria from antibiotics or influences of the immune system. The biofilm-incorporated bacteria can tolerate antibiotic concentration up to 1000-fold of the MIC of their planktonic counterparts.[36]

1.2.2.2 Activation of efflux

All bacteria can encode genes for efflux pumps that are either constitutively expressed or induced under a certain environmental stimulation. Functional efflux pumps play an important role for other cellular processes, in particular biofilm formation and virulence.[37] Efflux pumps are critical for the bacterial susceptibility and are major determinants of antibiotic resistance. In general, according to the structure and energy source, efflux pumps can be divided into five families (Figure 3):

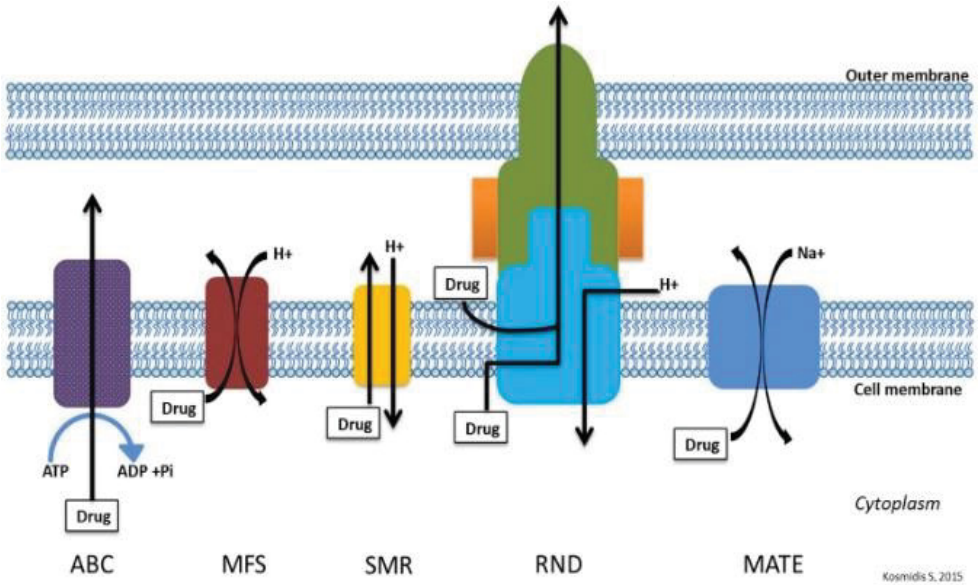

Figure 3: Five Possible multi drug efflux systems for antimicrobial resistance in activation of efflux. Produced from: An overview of the antimicrobial resistance mechanisms of bacteria. *AIMS Microbiol*. 2018.[32]

Efflux pumps of the resistance-nodulation-division (RND) family consist of an inner membrane pump, a periplasmic adaptor protein and an outer membrane channel and are found in Gram-negative bacteria.[38] Major facilitator superfamily (MFS) pumps are responsible for

efflux-mediated resistance in most bacteria.[39] Small multidrug resistance (SMR) transporters comprise approximately 100–140 amino acids for four transmembrane α-helices and are majorly responsible for transport of lipophilic compounds.[40] For example, QacC in *S. aureus* and EmrA in *E. coli* transport toxic organic cations.[41, 42] Multidrug and toxin extrusion (MATE) efflux pumps form a large family of secondary active transporters comprising a single polypeptide chain and mediate drug export driven by the electrochemical gradient force.[43] ATP-binding cassette (ABC) transporters are a widespread family of transporters in bacteria, archaea and eukaryotes. ABC pumps couple the hydrolysis of ATP to the translocation of solutes, for example PatAB from *Streptococcus pneumoniae* that confers resistance to fluoroquinolones.[44-46]

1.2.2.3 Target modification

There are multiple components in the bacterial cell that may be targets of antimicrobial agents, in reverse these targets might become one of factors involved in resistance. Post-transcriptional modification by addition of chemical groups to the target protein or mutation of the corresponding gene sequence are main ways to obtain resistance at target modification.

Most resistance-mediating mutations commonly occur directly in the gene encoding the target protein. For example, the main mechanism for the fluoroquinolone resistance are mutations in the *gyrA* subunit of DNA gyrase and/or the *parC* subunit of topoisomerase II, which determine the quinolone-resistance.[47] Another example is sulfonamides and trimethoprim, which competitively inhibit the active site of enzyme of metabolic pathways. Mutations in these enzymes lead to structural changes and interfere with drug binding.[48] Methylation is one mechanism of target modifications, e.g., resistance to macrolides are obtained from methylation of an adenine residue in the 23S ribosomal RNA.[49] One typical mechanism of resistance to the *β*-lactam drugs is through change in the structure or number of PBPs (penicillin-binding proteins), which form peptidoglycan in the cell wall.[50]

1.2.2.4 Drug inactivation

Degradation of the drug and transfer of a chemical group to the drug are two main ways in which bacteria inactivate drugs before they reach their targets. The typical example of antibiotic degradation are *β*-lactam antibiotics degraded by hydrolyzing enzymes. The *β*-lactamase enzymes bind the *β*-lactam ring by active site serine residue to perform hydrolysis.[51] However, the coordinated zinc ion can catalyze hydrolysis for metallo-*β*-lactamases.[52] The degradation by hydrolysis can be further verified by macrolide esterase enzymes, which target ester bonds within the cyclic macrolide molecules resulted in high-level resistance.[53] In addition, transfer of acetyl, phosphoryl, and adenyl groups were also identified to inactivate the drugs.

1.3 Antibacterial chemotherapy and development

1.3.1 Mechanisms of antibiotics

The discovery of antibiotics has saved innumerable lives and lead infections can be effectively controlled and prevented. Antibiotics address various targets and engage different mechanisms such as disruption of the cell membrane, cell integrity, inhibition of ATP Synthesis, protein synthesis, cell wall synthesis, mycolic acid synthesis, DNA replication, inhibition of metabolism and others. In the following, the most common targets and antibiotics are introduced.

1.3.1.1 Inhibition of cell wall

Bacterial cells are surrounded by a cell wall made of peptidoglycan consisting of long sugar polymers crosslinked by peptide bridges that is crucial to a bacterium's ability to survive environmental conditions. Maintenance of the peptidoglycan layer is accomplished by the activity of transglycosylases and penicillin-binding proteins (PBPs). The primary targets of the *β*-lactam agents are PBPs. The cyclic amide ring in *β*-lactam agents has a structure similar to the terminal d-alanyl-d-alanine dipeptide of peptidoglycan and is used as a substrate for the

PBPs during the acylation phase of cross link formation. The inhibition of cell wall synthesis leads to changes not only of cell shape and size but also induces cell stress responses and eventually cell lysis.[54, 55] In comparison, most glycopeptide antibiotics (for example, vancomycin) also inhibit peptidoglycan synthesis but they do so by binding the D-alanyl D-alanine portion in the peptide side chain of the precursor peptidoglycan subunit, blocking cell wall synthesis by a different mechanism than β-lactams.[56]

1.3.1.2 Inhibition of DNA replication

Quinolones inhibit the enzyme of bacterial DNA gyrase, which is a type II topoisomerases that introduces negative supercoiling into DNA in a ATP dependent manner by causing double strand breaks in the DNA double helix. This activity is essentially required for DNA synthesis.[57, 58] After the binding of quinolones to DNA gyrase, the DNA replication is blocked resulting in bacteriostasis or cell death.[59] However, this effect depends on the concentration of quinolones and is at least partially reversible after withdrawal of the drug. Notably, several studies have shown that the effects of quinolones on DNA gyrase induces the DNA stress response. RecA can be activated when DNA is damaged and promotes self-cleavage of the LexA repressor protein, inducing the expression of stress response genes such as DNA repair enzymes.[60] In reverse, preventing the activation of the stress response reduces the formation of drug-resistance.[61]

1.3.1.3 Inhibition of RNA synthesis

The semi-synthetic antibiotic family of rifamycin inhibits the synthesis of mRNA by binding to DNA-dependent RNA-polymerase.[62,63] Rifamycin interacts with the DNA-RNA polymerase complex.[64] While initial reactions and function of RNA polymerase are not significantly impaired (i.e., binding of the DNA template and formation of the open complex), the bound rifamycins directly block of the elongating RNA once transcripts reach 2–3 nucleotides in lenght.[63] Rifamycins are very potent and broad spectrum antibiotics. However,

rifamycins lead to strong induction of cytochrome P450 enzymes, and thus rifamycins can adversely interfere with other drugs.

1.3.1.4 Inhibition of protein synthesis

The pathway of bacterial protein synthesis is directed by ribosomes located in the cytoplasm that occurs in three sequential phases (initiation, elongation and termination).[65] Bacterial 70S ribosomes are composed of two subunits of 50S and 30S, which form the 70S holo complex at the initiation step of protein synthesis and separate at the termination step.[66] Drugs inhibiting proteins biosynthesis can interact with both ribosomal subunits: the 50S inhibitors and 30S inhibitors. 50S ribosome inhibitors include streptogramins, oxazolidinones, amphenicols, macrolides, and lincosamin.[67] 50S ribosome inhibitors block the initiation of protein translation or translocation of peptidyl tRNAs to reach the inhibition of peptidyl transferase reaction.[68] The 30S ribosome inhibitors block the access of aminoacyl tRNAs to the ribosome like tetracyclines and aminocyclitols.[69] The conformation of the complex loaded with aminoacyl tRNA at the ribosome changes and tRNA mismatching and protein mistranslation occurs when aminoglycosides bind to 16S rRNA, a component of the 30S ribosomal subunit.[70, 71]

1.3.2 Development of antibiotics

The introduction of antibiotics into clinical use created a milestone of chemotherapy in the 20th century. Antibiotics are not only used to treat infectious diseases but are also prophylactically applied in cancer treatment, organ transplantation and open-heart surgery area.[72] The history of the clinical use of antibiotics looks back to the groundbreaking discoveries of pioneers such as Paul Ehrlich and Alexander Fleming. Paul Ehrlich developed salvarsan and neo-salvarsan in the 19th century, which represented the first systematic screening approach in drug discovery.[73] Sulfonamides were developed by Gerhard Domagk in 1932 and represent the first broad spectrum antibiotic used in the clinic, and congeners are still in clinical used today. Alexander Fleming discovered penicillin in 1928. However, only years later Howard Florey

and Ernest Chain described the purification of penicillin in large quantities that led to mass production and distribution in 1945. Back at this time, the mode of action of penicillin was still unknown.[74] The first aminoglycoside, streptomycin, was discovered by American biochemist Selman Waksman in 1943. However, streptomycin causes potential side effects and is significantly toxic to kidneys and ear.[75] Chloramphenicol was discovered from the soil bacterium *Streptomyces venezuelae* in 1947.[76] The first tetracycline was found as new class of antibiotic in natural products and exhibited effects against a wide range of infections in 1948.[77] The macrolides were first discovered from the soil bacterium *Streptomyces erythraeus* in the 1950s and were used as an alternative treatment of *Streptococcus* infections in people who are allergic to penicillin.[78] Quinolones were discovered in 1962 with a wide antibacterial spectrum against both gram-positive and gram-negative bacteria.[79] Notably, most antibiotics were discovered during this "golden age of antibiotics", but from the 1970s less and less new antibiotics were discovered and brought to the clinic (Figure 4). This hiatus in antibiotic discovery was metaphored as "all low-hanging fruit had been harvested".[80]

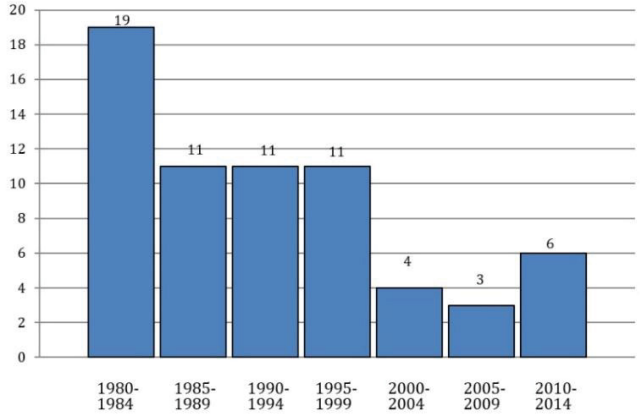

Figure 4: Decreasing number of new antibiotics developed and approved in the past three decades. Produced from The antibiotic resistance crisis: part 1: causes and threats. Pharmacy and Therapeutics. 2015; 40 (4):277-283.

1.4 The source of antibiotics

The discovery of the majority of antimicrobial compounds were from soil-dwelling microorganisms. The production of antibacterial agents by bacteria was reported by the turn of

the 20th century and the first clinical use of antibiotic was described from an extract of *Bacillus pycyaneus* verified as a mixture of the quorum sensing inhibitors phenazine and 2-alkyl-4-hydroxy-quinolones later.[81] This was a pioneer work and marked the starting point to discover antimicrobial compounds from microorganism. In the next decades, most reported antibiotics (tetracyclines, glycopeptides, aminoglycosides) used in clinic today were originally isolated from actinomycetes, especially from the genus *Streptomyces*, which highlights the capability of microorganism to produce antibiotics.

It is well known that fungi, ranked as the second biggest kingdom of organisms in nature, are one of the most important resources for the discovery of bioactive compounds.[82] From the history of drug discovery, fungal secondary metabolites provided a number of important drugs. For example, the *β*-lactam penicillin is the most successful example of natural product application in modern science and technology.[83] Semi-synthetic derivatives of cephalosporin C was described from fungus *Acremonium chrysogenum* in 1948. Then, another class of antibiotics tetracyclic fusidic acid was reported from fungus *Fusidium coccineum* in 1960.[84] Thus, fungi are regarded as a potential goldmine for the production of pharmaceuticals.

1.5 Activation of silent gene clusters

Natural products (NPs) are critical sources of drug molecules for hundred years. Most antibiotics in clinical use originate from microorganism and a large number of secondary metabolites supply broad options for pharmaceutical scientist. From available genome sequences it is obvious that in almost all microorganism the number of identified potential biosynthetic gene clusters (BGC), that code for the biosynthetic pathways of natural products, is exceeding the number of compounds that can actually be isolated from a given organism and indicates a great biogenetic potential to produce many secondary metabolites. Unfortunately, however, most BGCs are not expressed under laboratory conditions, and thus only a very restricted number of secondary metabolites are produced. Therefore, development of methods

to activate these silent BGCs is essential for current antibiotic discovery.[85] From reported publications commonly used strategies for silent BGC activation can be described in the following three aspects:

1.5.1 "OSMAC" approach

One strategy focuses on the fermentation itself by changing the culture conditions by altering the nutrient composition of the medium or adjust the physical conditions such as pH, light, temperature, aeration, or even the shape of culture vessels which was introduced by Zeeck and named as One Strain MAny Compounds (OSMAC).[86] Nowadays, more and more studies verified this is effective for microorganisms to express diverse secondary metabolisms. Factors for nutritional condition include the type of carbon and nitrogen sources. Wang and coworkers changed solid rice medium to Czapek medium which resulted in three new mixed terpenoids.[87] The addition of 2% tryptophan to solid rice medium resulted in the isolation of a new bismacrolactone from the endophytic fungus *Trichocladium sp.* by Tran-Cong *et al*.[88] Furthermore, the addition of salts (MgSO4, NaNO3, and NaCl) to solid Czapek medium led to nine new secondary metabolites from the endophytic fungus *Bulgaria inquinans.*[89] These examples highlight that variation of the medium composition is an effective method for expansion and diversification of the fungal secondary metabolite profile.

In addition, physical factors also affect the metabolite patterns. Fanelli and his colleagues set a success example using different light wavelength to culture of the fungus *Bipolaris maydis* demonstrating that a shift to white light allowed the highest production of secondary metabolites, while blue and green light showed an inhibitory effect, reducing the production of secondary metabolites to 50%, as well as red and yellow but at a lower level.[90] In summary, the OSMAC approach is a strong tool to stimulate the biosynthesis of secondary metabolites, but it is inherently empirical as the impact of an perturbation is unpredictable.[91]

1.5.2 Co-cultivation

The co-cultivation strategy requires the use of at least two different microorganisms in a reaction environment, which is inspired by microbial competition in the real natural environment.[92] In this environment, microorganisms compete for space and nutrients, which might spontaneously induce microbes to produce signal molecules that inhibit the growth of other organisms or change the metabolism of themselves to improve the survival in complex conditions. Eventually, this competition results in the activation of silent BGCs and accumulation of cryptic metabolites.[93] When the fungal endophyte *Fusarium tricinctum* is co-cultured with the bacterium *Bacillus subtilis* on solid rice medium, it resulted in an up to 78-fold increase in the accumulation of secondary metabolites spanning a broad range of structurl diversity including cyclic depsipeptides, fusaristatin A and three new natural compounds that were only present in the co-cultures.[94] Up to date, several publications have reported the induction of new or bioactive metabolites by the co-cultivation approach and proved that it is an effective strategy to trigger new secondary metabolites or enhance the production of low-amount compounds from fungi. Even though co-cultivation of fungi and bacteria were frequently reported, the mechanisms underlying BCG activation during co-cultivation of fungi-fungi, fungi-bacteria or bacteria-bacteria were rarely studied and are largely still unclear.

1.5.3 Epigenetic modification

Epigenetic modulation can be used to increase the expression of secondary metabolic genes without alteration of the encoding sequence.[95] The epigenetic modifiers which are used for gene silencing in fungal cells mainly include two groups of chemicals. DNA methyltransferase (DNMT) inhibitors such as trichostatin A (TSA), suberoylanilide hydroxamic acid (SAHA) and histone deacetylase (HDAC) inhibitors such as 5-azacytidine (5-AC) and 5-aza-2'-deoxcytidine (decitabine).[96] One example is the endophytic fungus *Eupenicillium sp*. LG41 that was subjected to epigenetic modulation. Nicotinamide was used based on NAD^+ dependent histone

deacetylase (HDAC) inhibitor and led to enhanced production of two new decalin-containing compounds, eupenicinicols C and D.[97] Furthermore, another successful application is the marine-derived fungus *Microascus sp*. that was induced to produce a new cyclodepsipeptide by histone deacetylase inhibitor SAHA, which enabled the biosynthesis of EGM-556.[98]

1.6 Aims and significance of the study

Antibiotics saved millions of lives since they were introduced, and at one point in history it was believed that we had won the war against microorganisms. However, with the development of resistant bacteria evolved in the last decades, more and more antibiotics are no longer as effective as before. Further challenges we are facing now are that the golden age of antibiotics has passed and less new antibiotics are available. Together with the abuse of antibiotics in agriculture or human health care, this is becoming a great threat for humans.

To overcome this future critical problem, we put our efforts in the discovery of new antibiotics. Historically, the development of antibacterial drugs has taught us that natural sources represent a promising possibility to find new lead structures due to the diversity which organic synthesis or drug design by artificial intelligence are unmatched.

The primary aim of this study is to identify potential new antimicrobial lead structure especially for critical resistant bacteria such as MRSA, *A. baumannii*, *M. tuberculosis* and currently challenging viruses, such as HIV and SARS-CoV-2. To achieve this aim, several fungi were isolated from soil and plants in Germany and China. Among them, two interesting endophytic fungal strains were fermented, active compounds were isolated and purified based on the bioactivity tracking. To expand the diversity of secondary metabolites or enhance the antimicrobial activity under standard laboratory condition, "OSMAC" and co-cultivation experiments were performed to activate silent gene clusters. The structure of pure compounds was elucidated by high-resolution electrospray ionization mass spectrometry, 1D and 2D NMR spectroscopy, specific optical rotation, ECD calculations and X-ray diffraction. Searching for

new antimicrobial compounds, the isolated molecules were screened following the Clinical and Laboratory Standards Institute (CLSI) guidelines. Hit compounds were further tested for their cytotoxicity against human cell lines, such as THP-1, MRC-5, HEK-293, HUH-7 and CLS-54 cell lines. Promising compounds, offering a therapeutic index greater than 10, were subsequently characterized by their inhibitory effect *in vitro* and determination of the mode of action.

We stand on the shoulders of giants to enjoy the achievements of science. Today, we wish we can contribute to the efforts of lead structure mining from nature for further quest of new antibacterial drug.

References to chapter 1

[1] WHO. The top 10 causes of death. 9th, December, 2020.

[2] WHO. Global tuberculosis reported, 2021.

[3] Hardtstock, F., Heinrich, K, Wilke, T. et.al. Burden of Staphylococcus aureus infections after orthopedic surgery in Germany. *BMC Infect Dis*. 2020; 20, 233.

[4] WHO, news, publishes list of bacteria for which new antibiotics are urgently needed 27 February 2017.

[5] Haque M, Sartelli M, McKimm J, et.al. Health care-associated infections–an overview. *Infect Drug Resist*. 2018; 11, 2321-2333.

[6] Mulani MS, Kamble EE, Kumkar SN, et.al. Emerging strategies to combat ESKAPE pathogens in the era of antimicrobial resistance: a review. *Front. Microbiol*. 2019; 10, 539.

[7] Tong SY, Davis JS, Eichenberger E, et.al. *Staphylococcus aureus* infections: epidemiology, pathophysiology, clinical manifestations, and management. *Clin Microbiol Rev*. 2015; 28, 603-61.

[8] Scott MA, Davis JM, Schwartz KA. *Staphylococcal* protein A binding to canine IgG and IgM. *Vet. Immunol. Immunopathol*. 1997; 59, 205-212.

[9] Le KY, Otto M. Quorum-sensing regulation in staphylococci-an overview. *Front Microbiol*. 2015; 6.1174.

[10] Salgado-Pabón W, Breshears L, Spaulding AR, et.al. Superantigens are critical for *Staphylococcus aureus* Infective endocarditis, sepsis, and acute kidney injury. mBio. 2013; 20, 4(4), 494-513.

[11] DeLeo FR, Diep BA, Otto M. Host defense and pathogenesis in *Staphylococcus aureus* infections. *Infect Dis Clin North Am*. 2009; 23, 17-34.

[12] Smith TL, Pearson ML, Wilcox KR, et.al. Emergence of vancomycin resistance in *Staphylococcus aureus*. *N Engl J Med*. 1999; 340:493-501.

[13] WHO, *Mycobacteria tuberculosis*. Key facts. 2021.

[14] CDC, *Mycobacteria tuberculosis*, Basic TB Facts. 2016.

[15] CDC, Chapter 2: Transmission and Pathogenesis of *Tuberculosis*.

[16] Gygli SM, Borrell S, Trauner A, et.al. Antimicrobial resistance in *Mycobacterium tuberculosis*: mechanistic and evolutionary perspectives, *FEMS Microbiol. Rev*. 2017; 41, 354-373.

[17] Kester JC, Fortune SM. Persisters and beyond: Mechanisms of phenotypic drug resistance and drug tolerance in bacteria. *Crit. Rev. Biochem. Mol. Biol*. 2014; 49, 91-101.

[18] Allué-Guardia A, García JI, Torrelles JB. Evolution of drug-resistant *Mycobacterium tuberculosis* strains and their adaptation to the human lung environment. *Front. Microbiol*. 2021; 04. 612675.

[19] Dookie N, Rambaran S, Padayatchi N, et.al. Evolution of drug resistance in *Mycobacterium tuberculosis*: a review on the molecular determinants of resistance and implications for personalized care. *J. Antimicrob. Chemother*. 2018; 73, 1138-1151.

[20] Cohen KA, Abeel T, McGuire AM, et.al. Evolution of extensively drug-resistant tuberculosis over four decades: Whole genome sequencing and dating analysis of *Mycobacterium tuberculosis* isolates from *KwaZulu-Natal*. *Int. J. Microbiol*. 2015; 29, 24-25.

[21] Ryan KJ, Ray CG. Sherris medical microbiology: An Introduction to Infectious Diseases 4th edition. *McGraw-Hill Medical.* 2003. ISBN: 978-0838585290.

[22] CDC. Laboratory methods for the diagnosis of meningitis, Chapter 8: Identification and characterization of *Streptococcus pneumoniae*; 2016

[23] European Centre for Disease Prevention and Control. Factsheet about pneumococcal disease.

[24] WHO. Antibiotics resistance, July 2020

[25] Michael CA, Dominey-Howes D, Labbate M. The antibiotic resistance crisis: causes, consequences, and management. *Front. Public Health*. 2014; 2, 145.

[26] Lushniak BD. Antibiotic resistance: a public health crisis. *Public. Health. Rep*. 2014; 129, 314-316.

[27] Viswanathan VK. Off-label abuse of antibiotics by bacteria. *Gut Microbes*. 2014; 5, 3-4.

[28] Golkar Z, Bagazra O, Pace DG. Bacteriophage therapy: a potential solution for the antibiotic resistance crisis. *J Infect Dev Ctries*. 2014; 8, 129-136.

[29] Wright GD. Something old, something new: revisiting natural products in antibiotic drug discovery. *Can J Microbiol*. 2014; 60,147-154.

[30] WHO, 2019 antibacterial agents in clinical development: an analysis of the antibacterial clinical development pipeline. 2019.

[31] Reygaert WC. An overview of the antimicrobial resistance mechanisms of bacteria. *AIMS Microbiol*. 2018; 4, 482-501.

[32] Kumar A, Schweizer HP. Bacterial resistance to antibiotics: active efflux and reduced uptake. *Adv Drug Deliver Rev*. 2005; 57, 1486-1513.

[33] Lambert PA. Cellular impermeability and uptake of biocides and antibiotics in gram-positive bacteria and mycobacteria. *J Appl Microbiol*. 2002; 92, 46-54.

[34] Bébéar CM, Pereyre S. Mechanisms of drug resistance in mycoplasma pneumoniae. *Curr Drug Targets*. 2005; 5, 263-271.

[35] Miller WR, Munita JM, Arias CA. Mechanisms of antibiotic resistance in enterococci. *Expert Rev Anti-Infe*. 2014; 12, 1221-1236.

[36] Mah TF. Biofilm-specific antibiotic resistance. *Future Microbiol*. 2012; 7, 1061-1072.

[37] Baugh S. Ekanayaka AS, Piddock LJV, et.al. Loss of or inhibition of all multidrug resistance efflux pumps of Salmonella enterica serovar Typhimurium results in impaired ability to form a biofilm. *J. Antimicrob. Chemother*. 2012; 67, 2409-2417.

[38] Tikhonova EB, Zgurskaya HI. AcrA, AcrB, and TolC of *Escherichia coli* form a stable intermembrane multidrug efflux complex. *J. Biol. Chem.* 2004; 279, 32116-32124.

[39] Poole, K. Efflux-mediated antimicrobial resistance. *J. Antimicrob. Chemother*. 2005; 56,

20-51.

[40] Yerushalmi H, Lebendiker M, Schuldiner, S. Negative dominance studies demonstrate the oligomeric structure of EmrE, a multidrug antiporter from *Escherichia coli*. *J. Biol. Chem*. 1996; 271, 31044-31048.

[41] Paulsen IT, Brown MH, Dunstan SJ, et.al. Molecular characterization of the *staphylococcal* multidrug resistance export protein QacC. *J. Bacteriol*. 1995; 177, 2827-2833.

[42] Yerushalmi H, Lebendiker M, Schuldiner SE. An *Escherichia coli* 12-kDa multidrug transporter, exchanges toxic cations and H^+ and is soluble in organic solvents. *J. Biol. Chem*. 1995; 270, 6856-6863.

[43] He, GX, Kuroda T, Mima T. et al. An H($^+$)-coupled multidrug efflux pump, PmpM, a member of the MATE family of transporters, from *Pseudomonas aeruginosa*. *J. Bacteriol*. 2004; 186, 262-265.

[44] Garvey MI, Piddock LJV. The efflux pump inhibitor reserpine selects multidrug-resistant *Streptococcus pneumoniae* strains that overexpress the ABC transporters PatA and PatB. *Antimicrob. Agents Chemother.* 2008; 52, 1677-1685.

[45] Lin HT, Bavro VN, Barrera NP. et al. MacB ABC transporter is a dimer whose ATPase activity and macrolide-binding capacity are regulated by the membrane fusion protein MacA. *J. Biol. Chem*. 2009; 284, 1145-1154.

[46] Marrer E, Schad K, Satoh A. et al. Involvement of the putative ATP dependent efflux proteins PatA and PatB in fluoroquinolone resistance of a multidrug resistant mutant of *Streptococcus pneumoniae*. *Antimicrob. Agents Chemother*. 2006; 50, 685-693.

[47] Ruiz J. Mechanisms of resistance to quinolones: target alterations, decreased accumulation and DNA gyrase protection. The *J. Antimicrob. Chemother*. 2003; 51, 1109-1117.

[48] Vedantam G, Guay GG, Austria NE, et al. Characterization of mutations contributing to sulfathiazole resistance in *Escherichia coli*. *Antimicrob Agents. Chemother*. 1998; 42:88-93.

[49] Weisblum B. *Erythromycin* resistance by ribosome modification. *Antimicrob Agents.*

Chemother. 1995; 39, 577-585.

[50] Reygaert W. Methicillin-resistant *Staphylococcus aureus* (MRSA): molecular aspects of antimicrobial resistance and virulence. *Clin Lab Sci*. 2009; 22, 115-119.

[51] Bush LM, Calmon J, Johnson CC. Newer penicillins and beta-lactamase inhibitors. *Infect. Dis. Clin. North Am*. 1995; 9, 653-686.

[52] Nordmann P, Poirel L. Emerging carbapenemases in gram-negative aerobes. *Clin. Microbiol. Infect*. 2002; 8, 321-331.

[53] Biskri L, Mazel D. *Erythromycin Esterase* Gene ere (A) is located in a functional gene cassette in an unusual Class 2 Integron. *Antimicrob Agents. Chemother*. 2003, 47, 3326-3331.

[54] Waxman DJ, Yocum RR, Strominger JL. Penicillins and cephalosporins are active site-directed acylating agents: evidence in support of the substrate analogue hypothesis. *Philos. Trans. R. Soc. Lond. B Biol. Sci*. 1980; 289, 257-271.

[55] Josephine HR, Kumar I, Pratt RF. The perfect penicillin? Inhibition of a bacterial DD-peptidase by peptidoglycan-mimetic *β*-lactams. *J. Am. Chem. Soc*. 2004; 126, 8122-8123.

[56] Džidić S, Šušković J, Kos B. Antibiotic resistance mechanisms in bacteria: Biochemical and genetic aspects. *Food Technol Biotechnol*. 2008; 46, 11-21.

[57] Cabral JH, Jackson AP, Smith CV, et al. Crystal structure of the breakage-reunion domain of DNA gyrase. *Nature*. 1997; 388, 903-906.

[58] Heddle J, Maxwell A. Quinolone-binding pocket of DNA gyrase: role of GyrB. *Antimicrob. Agents Chemother*. 2002; 46, 1805-1815.

[59] Drlica K, Malik M, Kern RJ, et.al. Quinolone-mediated bacterial death. *Antimicrob. Agents Chemother.* 2008; 52, 385-392.

[60] Courcelle J, Hanawalt PC. RecA-dependent recovery of arrested DNA replication forks. *Annu. Rev. Genet*. 2003; 37, 611-646.

[61] Cirz RT, Chin JK, Andes DR, et al. Inhibition of mutation and combating the evolution of antibiotic resistance. *PLoS Biol*. 2005; 3, 176.

[62] Mariani R, Maffioli S, Bacterial RNA polymerase Inhibitors: An Organized Overview of their Structure, Derivatives, Biological Activity and Current Clinical Development Status, *Curr Med Chem*. 2009; 16, 430-454.

[63] Campbell EA, Nataliya K, Arkady M, et.al. Structural mechanism for rifampicin inhibition of bacterial RNA polymerase. *Cell*. 2001; 104, 901-912.

[64] Kono Y. Oxygen enhancement of bactericidal activity of rifamycin SV on *Escherichia coli* and aerobic oxidation of rifamycin SV to rifamycin S catalyzed by manganous ions: the role of superoxide. *J. Biochem*. 1982; 91, 381-395.

[65] Garrett RA, Douthwaite SR, Liljas A, et.al. The Ribosome: Structure, Function, Antibiotics, and Cellular Interactions ASM Press. 2000. ISBN: 978-1-683-67252-4.

[66] Nissen P, Hansen J, Ban N, Moore PB et.al. The structural basis of ribosome activity in peptide bond synthesis. *Science*. 2000; 289, 920-930.

[67] Katz L, Ashley GW. Translation and protein synthesis: macrolides. *Chem. Rev*. 2005; 105, 499-528.

[68] Patel U, Yan YP, Frank WHJ, et.al. Oxazolidinones mechanism of action: inhibition of the first peptide bond formation. *J. Biol. Chem*. 2001; 276, 37199-37205.

[69] Chopra I, Roberts M. Tetracycline antibiotics: mode of action, applications, molecular biology, and epidemiology of bacterial resistance. *Microbiol Mol. Biol. Rev*. 2001; 65, 232-260.

[70] Davis BD. Mechanism of bactericidal action of aminoglycosides. *Microbiol. Rev*. 1987; 51, 341-350.

[71] Davies J, Gorini L, Davis BD. Misreading of RNA codewords induced by aminoglycoside antibiotics. *Mol. Pharmacol*. 1965; 1, 93-106.

[72] Hutchings MI, Truman AW, Wilkinson B. Antibiotics: past, present and future. *Curr Opin Microbiol*. 2019; 15, 72-80.

[73] Otten H, Domagk and the development of the sulphonamides. *J. Antimicrob. Chemother*. 1986; 17, 689-690.

[74] Abraham EP, Chain E, Fletcher CM, et.al. Further observations on penicillin. The Lancet. 1941; 16, 177-189.

[75] Forge, A. Schacht, J. Aminoglycoside Antibiotics. *Audiol Neurootol* 2000; 5, 3-22.

[76] Wiest DB, Cochran JB, Tecklenburg FW, et.al. Chloramphenicol toxicity revisited: A 12-year-old patient with a brain abscess. *J Pediatr Pharmacol Ther.* 2012; 17, 182-188.

[77] Nelson ML, Levy SB. The history of the tetracyclines. *Ann. N.Y. Acad. Sci*. 2011; 1241, 17-32.

[78] Parsons V. Ten important moments in the history of antibiotic discovery. July 2017.

[79] Andriole VT. The Quinolones: Past, Present, and Future. *Clin. Infect. Dis*. 2005; 41, 113-119.

[80] Katz L, Baltz RH. Natural product discovery: past, present, and future. *J Ind Microbiol Biotechnol*, 2016; 43,155-176.

[81] Hays EE, Wells IC, Katzman PA, et.al. Antibiotic Substances produced by *Pseu-domonas aeruginosa*. *Biol. Chem*. 1945; 159.725-750.

[82] Hawksworth DL. The magnitude of fungal diversity: the 1.5 million species estimate revisited. *Mycol. Res*. 2001; 105, 1422-1432.

[83] Demain AL, Elander RP. The β-lactam antibiotics: past, present, and future. *Antonie van Leeuwenhoek*. 1999; 75, 5-19.

[84] Godtfredsen WO, Jahnsen S, Lorck H, et.al. Fusidic Acid: a New Antibiotic. *Nature*, 1962; 193, 987.

[85] Liu Z, Zhao Y, Huang C, et.al. Recent Advances in Silent Gene Cluster Activation in Streptomyces. *Front. Bioeng. Biotechnol*. 2021; 9,632230.

[86] Bode HB, Bethe B, Höfs R, et.al. Big effects from small changes: possible ways to explore nature's chemical diversity. *Chem.Bio.Chem*. 2002; 3, 619-627.

[87] Wang QX, Bao L, Yang XL, et.al. Tricycloalternarenes F-H: three new mixed terpenoids produced by an endolichenic fungus *Ulocladium sp*. using OSMAC method. *Fitoterapia*. 2013;

85, 8-13.

[88] Tran-Cong NM, Mándi A, Kurtán T, et.al. Induction of cryptic metabolites of the endophytic fungus *Trichocladium sp*. through OSMAC and co-cultivation. *RSC Adv*. 2019; 9, 27279-27288.

[89] Ariantari NP, Georgios D, Attila M, et.al. Expanding the chemical diversity of an endophytic fungus *Bulgaria inquinans*, an ascomycete associated with mistletoe, through an OSMAC approach. *RSC Adv*., 2019; 9, 25119-25132.

[90] Fanelli F, Reveglia P, Masi M, et.al. Influence of light on the biosynthesis of ophiobolin A by *Bipolaris maydis*. *Nat. Prod. Res*. 2017; 31, 909-917.

[91] Zhang, MM, Qiao Y, Ang EL, ey.al. Using natural products for drug discovery: the impact of the genomics era. *Expert Opin Drug Discov*. 2017; 12, 475-487.

[92] Bertrand S, Bohni N, Schnee S, et.al. Metabolite induction via microorganism co-culture: a potential way to enhance chemical diversity for drug discovery. *Biotechnol. Adv*. 2014; 32, 1180-1204.

[93] Daletos G, Ebrahim W, Ancheeva E, et.al. "Microbial coculture and OSMAC approach as strategies to induce cryptic fungal biogenetic gene clusters." Chemical biology of natural products. CRC press, 2017; 233-284.

[94] Ola AR, Thomy D, Lai DW, et.al. Inducing Secondary Metabolite Production by the Endophytic Fungus *Fusarium tricinctum* through Coculture with Bacillus subtilis. *J. Nat. Prod*. 2013; 76, 11, 2094-2099.

[95] Zheng YG, Wu J, Chen Z, et.al. Chemical regulation of epigenetic modifications: opportunities for new cancer therapy. *Med. Res. Rev*. 2008; 28, 645-687.

[96] Cole PA. Chemical probes for histone-modifying enzymes. *Nat. Chem. Biol*. 2008; 4, 590-597.

[97] Li G, Souvik K, Christopher G, et.al. Epigenetic modulation of endophytic *eupenicillium sp*. LG41 by a histone deacetylase inhibitor for production of decalin-containing compounds. *J.*

Nat. Prod. 2017; 80, 4, 983-988.

[98] Vervoort HC, Drašković M, Crews P. Histone deacetylase inhibitors as a tool to up-regulate new fungal biosynthetic products: isolation of eGM-556, a Cyclodepsipeptide, from *microascus sp*. *Org. Lett*. 2011; 13, 3, 410-413.

Chapter 2 – Manuscript 1

Asperphenalenones isolated from the biocontrol agent *Clonostachys rosea* and their antimicrobial activities

Journal submission: Journal of Agricultural and Food Chemistry

Overall contribution to the manuscript:

- Cultures fermentation
- Compounds isolation
- Structure elucidation
- Determination of minimal inhibitory concentrations (Gram-positive bacteria and *Candida albicans*)
- Cytotoxicity assay against human T lymphocyte Jurkat cells
- Manuscript writing

Asperphenalenones isolated from the biocontrol agent *Clonostachys rosea* and their antimicrobial activities

Lin Wang, [1] Anna-Lene Kiffe-Delf, [1] Philipp Niklas Ostermann, [2] Ying Gao, [1] Lasse van Geelen, [1] Hao-Fu Dai, [3] You-Xing Zhao, [3] Heiner Schaal, [2] Attila Mándi, [4] Tibor Kurtán, [4] Zhen Liu, [5,*] Rainer Kalscheuer[1,*]

[1] Institute of Pharmaceutical Biology and Biotechnology, Heinrich Heine University Düsseldorf, Universitätsstrasse 1, 40225 Düsseldorf, Germany.

[2] Institute of Virology, University Hospital Düsseldorf, Heinrich Heine University Düsseldorf, Universitätsstrasse 1, 40225 Düsseldorf, Germany.

[3] Institute of Tropical Bioscience and Biotechnology, Chinese Academy of Tropical Agricultural Sciences, Haikou 571101, China.

[4] Department of Organic Chemistry, University of Debrecen, Egyetem tér 1, 4002 Debrecen P.O.B. 400, Hungary.

[5] Key Laboratory of Study and Discovery of Small Targeted Molecules of Hunan Province, School of Medicine, Hunan Normal University, Changsha 410013, China.

[*]Corresponding authors. E-mail address:

Zhen Liu: zhenfeizi0@sina.com

Rainer Kalscheuer: rainer.kalscheuer@hhu.de; ORCID ID orcid.org/0000-0002-3378-2067

ABSTRACT: *Clonostachys rosea* is a fungus widely distributed on earth and has a high capacity to adapt to complex environments in soil, plants or sea. It is an endophyte that can be used as a potential biocontrol agent to protect plants from pathogenic fungi, nematodes and insects. However, the spectrum of secondary metabolites produced by *C. rosea* has only been scarcely studied. In the present study, eight new phenalenones, asperphenalenones F-M (**1**-**8**), together with the two known derivatives asperphenalenones E and B (**9** and **10**) were isolated from the axenic rice culture of this fungus. The structures of the new compounds were elucidated by NMR, HREIMS and ECD analyses. Asperphenalenones J-M (**5**-**8**) are unusual phenalenone adducts, which are conjugated to diterpenoid glycosides. Asperphenalenones **F** and **H** showed moderate antibacterial activity against methicillin-resistant *Staphylococcus aureus* with minimal inhibitory concentrations of 12.5 and 25 μM, respectively. Asperphenalenone **B** exhibited low antiviral activity against human immunodeficiency virus HIV-1 replication. Furthermore, asperphenalenones **F** and **H** exhibited low cytotoxicity against Jurkat cells, while all other compounds were devoid of cytotoxicity.

KEYWORDS: *Clonostachys rosea*, *Asperphenalenones*, *Antibacterial activity*, *Methicillin-resistant Staphylococcus aureus* (MRSA), *Anti-HIV activity*.

INTRODUCTION

The ascomycete *Clonostachys rosea* (family Bionectriaceae) shows wide distribution all over the world. The fungus inhabits subarctic, temperate, subtropical and tropical regions of the world[1] owing to its pronounced ability to adapt the complex environments that enables it to withstand a wide range of physical (temperature, ultraviolet light), chemical (pesticides, disinfectant) or biological (bacteria, virus) stressors. *C. rosea* can colonize living plants as an endophyte and, due to its mycoparasitic properties, might be usable as a biologic control agent as it showed antagonistic effects against a wide variety of plant pathogenic fungi such as *Fusarium* seed borne diseases of cereals,[2] *Botrytis cinerea* sporulation on rose debris,[3] strawberry gray mold,[4] and *Fusarium* head blight of wheat.[5] Furthermore, it can detoxify the mycotoxin zearalenone, which is produced by several *Fusarium* species and can affect health and performance of livestock, through the enzyme zearalenone lactonohydrolase.[6] The emergence time and emergence of carrot seed were consistently improved when *C. rosea* was applied during a commercial drum priming process,[7] and co-inoculation of *C. rosea* together with the fungus *Beauveria bassiana* controlled insect pests and suppressed grey mould in greenhouse tomatoes and sweet peppers when vectored by bumble bees.[8] Strong inhibition to gastrointestinal nematodes in sheep was shown when combining *Bacillus thuringienasis* and *C. rosea* isolates.[9-10] Despite its potential beneficial applications in agriculture and livestock, however, the profile of secondary metabolites produced by *C. rosea* is largely unknown, and only few compounds have been reported. For example, bisorbicillinoids have open-ended cage structures and displayed antibacterial activity.[11] Clonostach acids exhibited phytotoxicity against lettuce and enhanced the production of secondary metabolites.[12] Unique cyclic heptapeptides exhibited significant cytotoxicity against the L5178Y mouse lymphoma cell.[13] TMC 151 series of compounds, which are reduced polyketide derivatives isolated from *C. rosea*, exhibited antibacterial properties,[14] while eburicol displayed significant antiproliferative activity against MCF-7 cells.[15] Two novel indole alkaloids featuring clonorosins A and B were

isolated, and clonorosins A was active against *Fusarium oxysporum* with an MIC value of 50 μg/mL.[16] These reports on diverse bioactivities with potential applicability in agriculture or human health motivated us to further study the secondary metabolite profile of *C. rosea* with a special focus on compounds potentially exhibiting antimicrobial properties.

While methicillin-resistant *Staphylococcus aureus* (MRSA), a Gram-positive pathogen of nosocomial infections not only resistant against beta-lactam antibiotics but also multi-resistant against several classes of antibiotics. Seriously, this situation becomes increasingly worse. Roughly one-third of healthy human individuals carry *S. aureus*, and around 2% of people carry MRSA.[17] Furthermore, MRSA is responsible for several difficult-to-treat infections in human being including skin and soft tissue infections, septicemia, endocarditis, pneumonia, enteritis, meningitis, osteomyelitis as well as toxic shock syndrome, and represents a significant global health threat, resulting in extensive mortality and burden on global healthcare systems.[18] Thus, to overcome this increasing threaten, new and bioactive compounds are urgently needed.

MATERIALS AND METHODS

General experimental procedure

Optical rotations were recorded by a PerkinElmer-241 MC polarimeter. Electrospray ionization mass spectra (ESI-MS) were obtained utilizing a HP1100 Agilent Finnigan LCQ Deca XP Thermoquest mass spectrometer and high-resolution electrospray ionization mass spectra (HRESIMS) were obtained with a UHR-QTOF Maxis 4G mass spectrometer. 1D and 2D NMR spectra were measured by Bruker Avance III 300 or 600 NMR spectrometers, using TMS as an internal standard. HPLC for analysis was performed by a Dionex P580 system with a photodiode array detector (UVD340S) and an Eurospher II C_{18} column (125×4 mm, L×ID, Knauer), while semi-preparative HPLC was done with a Lachrom-Merck Hitachi system (L7100 Pump, L7400 UV detector and a 300×8 mm i.d., 10 mm, Eurospher II C_{18} column) employing a mixture of MeOH-H_2O or MeCN-H_2O. Merck MN silica gel 60M (0.04–0.063

mm) and Sephadex LH-20 were used as stationary phases for column chromatography. Thin-layer chromatography (TLC) was carried out using pre-coated silica gel 60 F254 plates (Merck) with detection under UV light at 254 and 365 nm wavelengths.

Fungus material

The fungal strain *C. rosea* was isolated from the plant *Conyza canadensis* collected in April 2018 in Beijing, P.R. China, on solid medium containing 7.5 g of Bacto agar, 7.5 g of malt extract, and 0.125 g of chloramphenicol in 500 mL of demineralized water by subpassaging until an axenic culture was obtained. PCR amplification of the internal transcribed spacer region from chromosomal DNA followed by Sanger sequencing was done according to a previously reported protocol to identify the fungal strain (the DNA sequence was deposited in GenBank under accession number: OL597994).[19] The strain was deposited and cryopreserved in a −80 °C freezer in our laboratory.

Fermentation, extraction and isolation

Mycelium of *C. rosea* was grown aerobically on solid rice medium in twenty 1 L Erlenmeyer flasks each containing autoclaved 100 g rice and 110 mL water at 22 °C and incubated for 24 days. Fermented rice cultures were fragmented to small pieces before being extracted with 500 mL EtOAc for each flask, which was soaked overnight. Harvested extracts were combined and concentrated by rotary evaporator to yield a final crude EtOAc extract (39.2 g). The crude extract was fractionated via vacuum liquid chromatography (VLC) on silica gel with a gradient of *n*-hexane/EtOAc (100:0, 80:20, 60:40, 40:60, 20:80, 0:100) and dichloromethane/methanol (100:0, 60:40, 20:80, 0:100) as elution solvent to obtain seven fractions (Fr.1-Fr.7). Fraction Fr.6 (2.6 g) was further separated by Sephadex LH-20 column with MeOH to get five sub-fractions Fr.6.1-Fr.6.5. Sub-fraction Fr.6.1 (1.1 g) was chromatographed by VLC on silica gel using dichloromethane/methanol (80:20, 70:30, 60:40,

50:50, 40:60) as mobile phase, followed by separation using semi-preparative HPLC with a mixture of acetonitrile and H_2O to yield **1** (1.5 mg), **2** (2.7 mg), **3** (2.1 mg), **4** (7.0 mg), **9** (37.5 mg) and **10** (4.3 mg). Sub-fraction Fr.6.4 (0.9 g) was eluted on silica gel using dichloromethane/methanol (60:40, 50:50, 40:60, 30:70), followed by purification using semi-preparative HPLC with MeOH-H_2O as mobile phase to obtain **5** (4.2 mg), **6** (10.7 mg), **7** (3.6 mg), and **8** (4.5 mg).

Asperphenalenone **F** (**1**) Brown gum; $[\alpha]_D^{25}$ -48.9 (MeOH); UV (MeOH) λ_{max} (nm): 340, 258, 215; ECD (c 3.20x10^{-4} M, MeOH) λ_{max} ($\Delta\varepsilon$) 393 (−1.23), 349 (−0.32), 329 (+1.49), 303sh (+1.18), 278 (+1.73), 255 (+4.37), 236sh (+3.99), 209 (−5.44) nm; HRESIMS *m/z* 625.3371 $[M + H]^+$ (calcd for $C_{36}H_{48}O_9$, 624.3298); ^1H and ^{13}C NMR data see table 1.

Asperphenalenone **G** (**2**) Brown gum; $[\alpha]_D^{25}$ +6.4 (MeOH); UV (MeOH) λ_{max} (nm) : 342, 257, 213; ECD (c 3.20x10^{-4} M, MeOH) λ_{max} ($\Delta\varepsilon$) 380 (−0.39), 331 (+0.63), 251 (+1.25), 234sh (+1.07), 225 (+1.23), 207 (−3.39), 196sh (−1.63) nm; HRESIMS *m/z* 625.3377 $[M + H]^+$ (calcd for $C_{36}H_{48}O_9$, 624.3298); ^1H and ^{13}C NMR data see table 1.

Asperphenalenone **H** (**3**) Brown gum; $[\alpha]_D^{25}$ +98.2 (MeOH); UV (MeOH) λ_{max} (nm): 335, 257, 212; ECD (c 3.35x10^{-4} M, MeOH) λ_{max} ($\Delta\varepsilon$) 419sh (−0.25), 386 (−0.95), 360 (+0.64), 325 (+2.77), 293sh (−0.63), 266 (−0.95), 254sh (+4.28), 248 (+4.84), 228 (+0.71), 219 (+3.28), 206 (−12.28) nm; HRESIMS *m/z* 597.3052 $[M + Na]^+$ (calcd for $C_{34}H_{44}O_9$, 596.2985); ^1H and ^{13}C NMR data see table 1.

Asperphenalenone **I** (**4**) Brown gum; $[\alpha]_D^{25}$ +46.9 (MeOH); UV (MeOH) λ_{max} (nm): 344, 258, 214; ECD (c 3.13x10^{-4} M, MeOH) λ_{max} ($\Delta\varepsilon$) 389 (−1.09), 328 (+0.65), 302sh (+0.66), 280 (+0.69), 255 (+2.74), 235sh (+2.19), 209 (−4.06) nm; HRESIMS *m/z* 639.3165 $[M + H]^+$ (calcd for $C_{36}H_{46}O_{10}$, 638.3091); ^1H and ^{13}C NMR data see table 1.

Asperphenalenone **J** (**5**) Brown gum; $[\alpha]_D^{25}$ +47.5 (MeOH); UV (MeOH) λ_{max} (nm): 344, 258, 212; ECD (c 2.54x10^{-4} M, MeOH) λ_{max} ($\Delta\varepsilon$) 422sh (−0.77), 389 (−1.16), 346 (−0.41), 328 (+1.12), 302sh (+1.28), 282 (+1.53), 254 (+4.16), 236sh (+3.67), 209 (−4.47) nm; HRESIMS

m/z 804.4159 $[M + NH_4]^+$ (calcd for $C_{42}H_{58}O_{14}$, 786.3827); ^1H and ^{13}C NMR data see table 2.

Asperphenalenone **K** (**6**) Brown gum; $[\alpha]_D^{25}$ -6.9 (MeOH); UV (MeOH) λ_{max} (nm): 343, 258, 214; ECD (c 2.59x10^{-4} M, MeOH) λ_{max} ($\Delta\varepsilon$) 377 (−1.04), 350 (−1.00), 328 (+3.21), 283 (+0.51), 267 (−0.26), 254 (+4.17), 237sh (+3.67), 219 (+2.67). 208 (−7.30) nm; HRESIMS *m/z* 790.4006 $[M + NH_4]^+$ (calcd for $C_{41}H_{56}O_{14}$, 772.3670); ^1H and ^{13}C NMR data see table 2.

Asperphenalenone **L** (**7**) Brown gum; $[\alpha]_D^{25}$ +89.6 (MeOH); UV (MeOH) λ_{max} (nm): 344, 258, 216; ECD (c 8.47x10^{-5} M, MeOH) λ_{max} ($\Delta\varepsilon$) 427 (−0.28), 386 (+0.13), 351 (−0.65), 301 (+0.75), 280sh (+0.71), 257 (+1.20), 241sh (+0.93), 223 (+1.30), 208 (−1.84), 202sh (−1.48) nm; HRESIMS *m/z* 804.4159 $[M + NH_4]^+$ (calcd for $C_{42}H_{58}O_{14}$, 786.3827); ^1H and ^{13}C NMR data see table 2.

Asperphenalenone **M** (**8**) Brown gum; $[\alpha]_D^{25}$ +47.5 (MeOH); UV (MeOH) λ_{max} (nm): 344, 258, 211; ECD (c 2.41x10^{-4} M, MeOH) λ_{max} ($\Delta\varepsilon$) 417sh (−0.90), 399 (−1.03), 328 (+1.25), 307sh (+1.00), 277 (+0.97), 255 (+2.92), 241sh (+2.57), 221 (+0.81), 208 (−3.38) nm; HRESIMS *m/z* 846.4278 $[M + NH_4]^+$ (calcd for $C_{44}H_{60}O_{15}$, 828.3932); ^1H and ^{13}C NMR data see table 2.

Compound **9** and **10** were identified as asperphenalenones **E** and **B**, respectively, by comparison of their NMR and MS data with the literature.[20]

Hydrolysis of Asperphenalenone K (6)

2.2 mg of compound **6** was added to 2 mL of 15% HCl and maintained for 5 h at 90 °C. Afterwards, the resulting solution was dried under reduced pressure followed by partition between H_2O and CH_2Cl_2. The aqueous phase contained α-D-mannose identified by R_f value on TLC plate spayed with anhydrous 5% H_2SO_4 reagent.[21]

Culture of microorganism and virus strains

Mueller Hinton broth was used for cultivation of nosocomial bacterial strains including *Staphylococcus aureus* ATCC 25923, *Staphylococcus aureus* ATCC 70669 (MRSA/VISA),

Enterococcus faecalis ATCC 51299, and *Enterococcus faecium* ATCC 35667. All bacteria were grown aerobically at 37 °C. *Candida albicans* strain ATCC 24433 was incubated in YPD medium (yeast extract 10 g/L, peptone 20 g/L, D-glucose 20 g/L) at 37 °C aerobically. *Mycobacterium tuberculosis* strain H37Rv was cultured aerobically at 37 °C in Middlebrook 7H9 broth supplemented with 0.5% glycerol, 0.05% tyloxapol and 10% (v/v) ADS enrichment yielding final concentrations of 5% bovine serum albumin fraction V, 2% glucose, and 0.85% sodium chloride, respectively. SARS-CoV-2 was propagated in infected Vero cells maintained in DMEM medium supplemented with 2% heat-inactivated fetal calf serum, 4.5 g/L glucose, 0.11 g/L sodium pyruvate, stable glutamine, and 1% penicillin/streptomycin solution. HIV was propagated in Jurkat cells maintained in RPMI 1640 medium supplemented with 5% heat-inactivated fetal calf serum.

Determination of Minimal Inhibitory Concentration (MIC)

All compounds were tested for their antimicrobial bioactivities against the gram-positive nosocomial bacterial pathogens *S. aureus, E. faecalis* and *E. faecium*, against *M. tuberculosis* as well as against the pathogenic fungus *C. albicans*. The broth microdilution method was used in each case according to recommendations by the Clinical and Laboratory Standards Institute (CLSI) (CLSI, 2018).[22] All tests were repeated twice.

Briefly, nosocomial bacteria were grown aerobically in Mueller Hinton (MH) medium at 37 °C as shaking cultures at 180 rpm until reaching early log phase. Cell suspensions were then diluted to 1×10^6 CFU/mL ($OD_{600\,nm} \sim 0.1$) and seeded at a density of 5×10^5 CFU/well in a total volume of 100 μL in 96-well round bottom microtiter plates. The tested compounds were twofold serially diluted and added to the wells to yield final concentrations ranging from 0.78 – 100 μM. DMSO at a maximal concentration of 1% was used as solvent control, while moxifloxacin served as positive control. After aerobic incubation at 37 °C for 16-20 h, MICs were determined macroscopically.

Cells of *C. albicans* were incubated at 37 °C in YPD medium with shaking at 180 rpm overnight to promote growth of the cells in the yeast form. For inducing growth in the hyphae form, YP medium containing 5% proline was used, and cells were incubated at 30 °C with shaking at 80 rpm. Afterwards, cells were seeded in 96-well round bottom microtiter plates at a density of 1×10^6 CFU/mL containing twofold serial dilutions of compounds at final concentrations ranging from 0.78 – 100 μM in a total volume of 100 μL. 1% DMSO was used as solvent control while hygromycin B served as positive control.[23] The plates were incubated at 37 °C and 30 °C overnight for the yeast and the hyphae form, respectively, and growth inhibition was evaluated macroscopically.

Cells of *M. tuberculosis* were incubated at 37 °C in Middlebrook 7H9 medium with shaking at 180 rpm for four days. Afterwards, cells were seeded at density of 1×10^6 CFU/mL in 96-well round bottom microplate containing two-fold serial dilutions of compounds at final concentrations ranging from 0.78-100 μM in a total volume of 100 μL. Rifampicin served as positive control and DMSO at maximal concentration of 1% was used as solvent control. After plates were incubated at 37 °C for 5 days aerobically, resazurin solution (10 μl/well from 100 μg/ml stock, Sigma-Aldrich) was added to the cells and incubated for 16 h at room temperature for reduction of resazurin to resorufin by aerobic respiration of metabolically active cells. Next, *M. tuberculosis* cells were inactivated by incubation with formalin (10%, v/v, final concentration) for 30 min at room temperature. Subsequently, fluorescence was measured using a microplate reader (TECAN) (excitation 560 nm, emission 590 nm).

Determination of inhibition of *SARS-CoV-2* cytopathic effects

Vero cells were grown in 96-well white flat bottom cell culture plate overnight in DMEM supplemented with 2% FCS and 1% penicillin/streptomycin solution at 37 °C, 5% CO_2 to a final density of $2x10^4$ cells/well. Afterwards, the medium was removed and 50 μL fresh medium containing the tested compounds at a concentration of 100 μM were added to each well and

incubated for 1 hour. Next, further 50 μL growth medium containing SARS-CoV-2 was added to yield a tissue culture infectious dose of 50% (TCID50) and incubated for another 2 hours at 37 °C with 5% CO_2. Subsequently, the inoculum was removed and replaced by 100 μL fresh medium containing the tested compounds at a concentration of 100 μM . After 72 h incubation, host cell viability was measured using ViroTiter Glo (Promega) following the manufacturer's manual. All tests were done in triplicates.

Cytotoxicity assay

Compounds **1-10** were tested for cytotoxicity against Jurkat cell line (Human T Lymphocyte cells). Cells were grown in RPMI 1640 medium supplemented with 10% FCS at 37 °C with 5% CO_2 before diluted to a concentration of 1×10^6 cells/mL. Afterwards, cells were seeded into 96-well flat bottom microtiter plate containing twofold serial dilutions of the tested compounds to yield final concentrations ranging from 0.78-100 μM in a total volume of 100 μL and incubated at 37 °C with 5% CO_2 for 48 h. Next, 10 μL of resazurin solution (100 μg/mL) were added to each well and incubated for another 4 h before fluorescence was measured to quantify the survival of cells using a microplate reader (excitation, 540 nm; emission, 590 nm). DMSO was used as solvent control and growth was calculated relative to non-inoculated (0% growth) and untreated (100% growth) controls.[24]

HIV-1 infection and quantification of replication by HIV-1 exon 7 qPCR

In 1 mL of RPMI medium (Thermo Fisher Scientific, MA, USA) supplemented with 5% FCS (PAN Biotech, Germany), 1×10^6 Jurkat T-cells were infected with the HIV-1 molecular clone NL4-3[25] at an MOI of 0.005 for 6 hours in a 15 mL centrifugation tube at 37 °C in a humidified atmosphere. Afterwards, the cells were centrifuged at 400 × g for 5 min and washed once with 1 mL PBS. Cell pellets were resuspended in 1 mL of culture medium containing the compound1-10 at the indicated concentrations (50 μM, 12.5 μM, 25 μM, 100 μM, 100 μM, 100 μM, 100 μM, 100 μM, 25 μM, 50 μM) and transferred into T25 cell culture flasks. At 3 days

post-infection, the cells were transferred to 2 mL centrifugation tubes and centrifuged at 20,000 x g for 14 sec and washed once in 1 mL PBS and again centrifuged like before. Cell lysis was performed using 500 μL Solution D (4 M guanidinium thiocyanate, 25 mM sodium citrate, 0.5 % Sarcosyl, 100 mM beta-mercaptoethanol). RNA isolation was conducted via phenol-chloroform extraction. Therefore, a master mix containing 7.2 μl β-mercaptoethanol, 50 μl 2 M sodium acetate (pH 4) and 500 μl phenol per sample were added to the lysed cells. The samples were briefly vortexed and mixed with 103 μl of a chloroform/isoamyl alcohol mixture (ratio 24:1). Afterwards, the samples were vortexed for 15 sec, incubated on ice for 15 min and centrifuged for 20 min at approx. 10,000 x g at 4 °C. After centrifugation, 400 μl of the aqueous upper phase were mixed with the same amount of 100 % isopropanol and incubated at -20 °C for at least 1 h. Thereafter, the samples were centrifuged for 20 min at approx. 10,000 x g and 4 °C. The pellets were washed twice with 200 μL of ethanol (70 %) for 10 min at 10,000 x g at 4 °C and air-dried for 5 min at room temperature. The RNA was solubilized by adding 10 μL of H_2O.

For cDNA synthesis, 10 μL samples containing exactly 1 μg RNA were incubated at 70 °C for 5 min and afterwards cooled on ice for a few seconds. A total of 5 μL were mixed with 0.5 μl Oligo-d(T) primer (1:20 dilution) (Roche, Switzerland), 0.5 μL dNTPs (Qiagen, Germany) and 0.5 μL H_2O. After incubating this mixture for 5 min at 65 °C, 2 μL first strand buffer (Thermo Fisher Scientific, MA, USA), 0.5 μL DTT (Thermo Fisher Scientific, MA, USA), 0.5 μL RNAsin (Promega, WI, USA) and 0.5 μL Superscript III (Thermo Fisher Scientific, MA, USA) were added. The samples were then incubated at 50 °C for 60 min and subsequently at 72 °C for 15 min.

The amount of HIV-1 and cellular glyceraldehyde 3-phosphate dehydrogenase (GAPDH) transcripts was analyzed via quantitative PCR (qPCR). For this, the cDNA samples were diluted 1:10 and 2 μL of these dilutions were mixed with 6 μL H_2O, 1 μL forward primer (5' ACCCTGTTGCTGTAGCCA3' (GAPDH), 5' TTGCTCAATG CCACAGCCAT 3' (HIV-1 exon 7)), 1 μL reverse primer (5' CCACTCCTCCACCT TTGAC 3' (GAPDH), 5'

TTTGACCACTTGCCACCCAT 3' (HIV-1 exon 7)) and 10 μL qPCR master mix (Primer Design, UK). The qPCR samples were filled into glass capillaries (Roche, Switzerland) via centrifugation at 68 × g for 5 sec and analyzed using the Light Cyler 1.5 capillary-based qPCR system. The samples were run in triplicates and were subject to the following PCR program: Segment 1 (Amplification) 1. 95 °C for 10 sec; 2. 60 °C for 60 sec (42 cycles); Segment 2 (Melting Curve) 1. 95 °C for 0 sec; 2. 63 °C for 30 sec; 3. 95 °C for 0 sec with a slope of 0.1 °C/sec (1 cycle). The data were analyzed using the comparative C_T method.[26]

Computational Section

Mixed torsional/low-mode conformational searches were carried out by means of the Macromodel 10.8.011 software using the MMFF with an implicit solvent model for $CHCl_3$ applying a 21 kJ/mol energy window.[27] Geometry reoptimizations of the resultant conformers [ωB97X/TZVP level[28] with PCM solvent model for MeOH], TDDFT-ECD and OR calculations [B3LYP/TZVP, BH&HLYP/TZVP, CAM-B3LYP/TZVP and PBE0/TZVP levels with PCM solvent model for MeOH] were performed with Gaussian 09 package.[29] ECD spectra were generated as sums of Gaussians with 2100 cm^{-1} width at half-height, using dipole-velocity-computed rotational strength values.[30] Boltzmann distributions were estimated from the ωB97X energies. Visualization of the results was performed by the MOLEKEL software package.[31]

RESULTS AND DISCUSSION

Compound **1** was obtained as brown gum. Its molecular formula of $C_{36}H_{48}O_9$ was determined by HRESIMS, indicating 13 degrees of unsaturation. The ^{1}H NMR spectrum of **1** displayed an aromatic proton at δ_H 7.03 (s, H-8), three olefinic protons at δ_H 5.32 (t, H-25), 5.06 (t, H-21) and 5.05 (t, H-17), an oxygenated methylene at δ_H 4.12 (d, H-33a) and 4.06 (d, H-33b), an oxygenated methine at δ_H 3.26 (dd, H-29), and six methyl groups at δ_H 2.96 (s, H-15), 2.18 (s, H-14), 1.56 (s, H-34), 1.29 (s, H-35), 1.16 (s, H-31) and 1.13 (s, H-32). The above NMR

data of **1** was closely related to those of the co-isolated known phenalenone derivative, asperphenalenone E (**9**), except for the presence of an additional methoxy group in **1** at δ_C 56.3 and δ_H 3.99 (s). The location of this methoxy group at C-7 in **1** was confirmed by the HMBC correlations from protons of the methoxy group to C-7 (δ_C 161.3). Detailed analysis of the 2D NMR spectra of **1** revealed that its remaining structure was identical to that of **9** (Figure 1 + 2). The ROESY correlations between H-17/H_2-19, H-21/H_2-23, and H-25/H_2-27 demonstrated the double bonds at C-17/C-18, C-21/C-22 and C-25/C-26 were *E*, *E*, *Z* configurations, respectively. The ECD spectrum (Fig. S2) of **1** showed a good agreement with the ECD spectrum of the known compound asperphenalenone A[20] (Fig. S3) in the region 200-400 nm. Furthermore, it was also similar to the experimental ECD of **3**, for which we performed TDDFT-ECD calculations on a truncated model compound to confirm the previous configurational assignments of related derivatives (*vide infra*). In fact, the ECD spectra of all the new derivatives **1**-**8** showed similar ECD patterns, high wavelength negative transition around 380-420 nm with weak or average intensity, a positive transition around 325 nm, two or more positive transitions in the range of 220-250 nm and a negative one around 205-210 nm, suggesting the same absolute configuration of the C-1 chirality center of the isolated compounds. Thus, the absolute configuration of C-1 was established as (*S*) in **1**, while its side chain with a C-29 chirality center was similar to those of known compounds asperphenalenone E[20], aspergillussanones A[32] and aspergillussanones K and L,[33] for which (29*R*) absolute configuration was suggested tentatively. Thus, the structure of **1** was elucidated as drawn in Figure 1, representing a new phenalenone derivative, for which the trivial name asperphenalenone F is given.

The HRESIMS data of compound **2** indicated the same molecular formula of $C_{36}H_{48}O_9$ as that of **1**. Comparison of the ^{1}H and ^{13}C NMR data of **1** and **2** (Table 1) revealed that both compounds differ in the position of the methoxy group. In compound **2** the methoxy group was attached to C-1 based on the HMBC correlations from protons of the methoxy group (δ_H 3.11)

and H_2-16 (δ_H 2.58) to C-1 (δ_C 87.4) (Figure 2). The positive Cotton effect at around 250 nm in the ECD spectrum (Fig. S4) of **2** suggested the absolute configuration of C-1 was identical to **1** and **3** as (*S*). In addition, the absolute configuration of C-29 was assigned to be (*R*) configuration on basis of **1**. The structure of **2**, named as asperphenalenone **G**, was elucidated as drawn in Figure 1.

The molecular formula of asperphenalenone H (**3**) was determined as $C_{34}H_{44}O_9$ by HRSIMS. When comparing the NMR data of **3** and **1**, the obvious differences were the disappearance of the methoxy group and the replacement of the aromatic methyl by an aromatic proton (δ_H 6.17, s, H-12) in **3**. The HMBC correlations from H-12 to C-3 (δ_C 101.2) and C-10 (δ_C 113.5), from Me-15 (δ_H 2.77) to C-8 (δ_C 117.1), C-9 (δ_C 149.9) and C-10, and from H-8 (δ_H 6.72) to C-5 (δ_C 106.6) and C-10 confirmed the location of the additional aromatic methine proton at C-12. Detailed analysis of the 2D NMR spectra of **3** (Figure 2) revealed that the remaining substructure and the relative configuration of the double bonds of **3** were identical to those of **1**. The ECD spectrum of **3** (Fig. S5) showed intense positive Cotton effects centered around 250 nm, which suggested homochiral (1*S*) absolute configuration with **1**. By checking the related literature on stereochemical analysis, it was found that ECD comparison of related derivatives with different chromophoric systems were performed (*e.g.* sculezonone A and herqueinone)[34] or the calculated TDDFT-ECD spectra showed only partial agreement with the experimental ones,[20] which raised some uncertainty in the previous configurational assignments. Therefore, we decided to perform TDDFT-ECD and OR (optical rotation) calculations for **3**.[35] Since the chiroptical properties were expected to be determined by the C-1 chirality center and the side-chain implies a large amount of flexibility enhancement, the calculations were performed for two truncated model systems containing either a methyl (**3modMe**) or ethyl group (**3modEt**) attached to the first double bonds of the side-chain (Figure 3).[36, 37] Previous studies showed that position of the truncation is important for the result and in the case of ECD spectroscopy, the first double bonds is worth to be kept in models of molecules containing more

than one isolated double bonds in the side-chain.[38]

MerckMolecular Force Field (MMFF) conformational search of (*S*)-**3modMe** and (*S*)-**3modEt** resulted in 36 and 94 initial conformers in a 21 kJ/mol energy window. These structures were re-optimized at the ωB97X/TZVP[28] PCM/MeOH level yielding 9 and 9 low-energy conformers over 1% Boltzmann population, respectively. ECD spectra computed at various levels of theory for these conformers gave acceptable to good agreement with the experimental ECD spectrum (Figure 4).

A level dependency was found for the applied combinations of methods underscoring to test several of them: the CAM-B3LYP and BH&HLYP functionals reproduced better the position and splitting of the transitions, while the PBE0 and B3LYP functionals reproduced better the relative intensities of the 219 and 248 nm transitions (Figure S5). Although the high-wavelength negative transition at 386 nm was not reproduced by the average ECD spectra, some low-energy conformers exhibited also this transition with a blue shift (Figure S6). Despite choosing a well performing DFT functional[39] for the optimization, the truncation may have altered the Boltzmann distribution. The same problem appeared in the OR calculations. We identified low-energy conformers with the OR value ranging from c.a. –450 to +430 (Tables S1and S2) and the real population of these could be somewhat different from the computed Boltzmann distribution. The computed average OR values for **3modEt** were around 0, while for **3modMe** between +13 and +25. Although the sign of these latter ones matches the experimental $[\alpha]_D$ value, the small average value comparing to the range of the conformers does not allow a solid assignment on the basis of the OR calculations. On the other hand, the ECD calculations of the truncated models could be applied to verify the (1*S*) absolute configuration in line with the literature examples. The absolute configuration of C-29 was assigned as (*R*) on the basis of **1**.

Based on the HRESIMS data, the molecular formula of **4** was determined as $C_{36}H_{46}O_{10}$. The ^1H and ^{13}C NMR data of **4** (Table 1) revealed closely structural similarity to **1** except for the replacement of the oxygenated methylene at C-33 (δ_H 4.12 and 4.06, δ_C 59.7) of **1** by a carbonyl

group (δ_C 169.2) in **4**, which was supported by the HMBC correlations from H-25 (δ_H 5.76) to C-33. The configurations of the three double bonds in **4** were elucidated as 17*E*, 21*E*, and 25*Z*, respectively, based on the NOE correlations between H-17/H_2-19, H-21/H_2-23, and H-25/H_2-27. The configuration at C-1 of **4** was identical (*S*) with **1** and **3** on the basis of the ECD spectrum (Fig. S6) showing positive Cotton effects at around 250 nm. The absolute configuration of C-29 was assigned to be (*R*) on the basis of **1**. The structure of **4**, named as asperphenalenone **I**, was elucidated as drawn in Figure 1.

Compound **5** was obtained as brown gum with molecular formula of $C_{42}H_{58}O_{14}$ as determined by HRSIMS. The ^{1}H and ^{13}C NMR (Table 1) of **5** were similar to those of **1**, suggesting that they shared the same structural fragment from C-1 to C-35. The remaining NMR signals in **5** included five oxygenated methines and an oxygenated methylene (CH-1′ to 5′ and CH_2-6′), constructing an additional pyranoside unit in **5**, which were evident from the COSY correlations between H-1′/H-2′/H-3′/H-4′/H-5′/H_2-6′ and the HMBC corelations from H-1′ to C-5′. Furthermore, the HMBC correlations from H-1′ (δ_H 4.47) to C-33 (δ_C 66.7) and from H_2-33 (δ_H 4.30) to C-1′ (δ_C 100.1) indicated that the pyranose residue was attached to C-33. Furthermore, hydrolysis was carried out and identified the pyranose residue as α-D-mannose by Rf values in TLC analysis. The coupling constant of H-1′ with 0.8 Hz also indicated α configuration for mannose. By comparing the experimental ECD spectra (Fig. S7), (*S*) absolute configuration was suggested for C-1 and C-29 was assigned to be (*R*) in **5** on basis of **1** and **3**. The structure of **5** was elucidated as drawn in Figure 1 and it named as asperphenalenone **J**.

The molecular formula of asperphenalenone K (**6**) was determined as $C_{41}H_{56}O_{14}$ by the HRSIMS data, missing a CH_2 unit when compared to **5**. The obvious difference between the NMR data of **6** and **5** was the disappearance of signals of the methoxy group in **6**. Detailed analysis of the 2D NMR spectra indicated that C-7 was attached to a hydroxy group in **6** rather than a methoxy group in **5** (Figure 2). The ECD spectrum (Fig. S8) of **6** suggested (*S*) absolute configuration for C-1 and C-29 was assigned as (*R*) on basis of **1**.

Asperphenalenone L (**7**) shared the same molecular formula as **5**. Comparison of their NMR data (Table 2) suggested that they are structurally similar. As expected, signals for the aromatic rings, the side chain and the pyranose unit were observed. However, the big differences of the chemical shifts of C-1 and C-7 between **5** and **7** (+2.5 and +3.4 ppm in **7**) suggested different location of the methoxy group. The HMBC correlation of the protons of the methoxy group (δ_H 3.27) to C-1 (δ_C 89.2) confirmed the attachment of the methoxy group at C-1 in **7** instead of C-7 in **5**. The ECD spectrum (Fig. S9) of **7** suggested that the absolute configuration of C-1 was identical to **1** and thus assigned as (*S*). The absolute configuration of C-29 was assigned as (*R*) on basis of **1**. The structure of **7** was elucidated as drawn in Figure 1 and it was named as asperphenalenone **L**.

Compound **8** gave a molecular formula of $C_{44}H_{60}O_{15}$ as determined by HRSIMS, thus differing from **5** by 42 additional mass units. This difference was accounted for an additional acetyl group, which was evident from the presence of an additional carbonyl carbon (δ_C 172.6) and an additional methyl group (δ_H 2.05 and δ_C 20.7) in the NMR spectra of **8** (Table 2). The location of this acetyl group at C-6′ was confirmed by the HMBC correlations from the methyl group (δ_H 2.05) and deshielded H_2-6′ (δ_H 4.41 and 4.22) to the carbonyl carbon (δ_C 172.6). The remaining structure of **8** was identical to that of **5**. The ECD spectrum (Fig. S10) of **8** suggested (*S*) absolute configuration for C-1 and C-29 was assigned as (*R*) on basis of **1**.

Compounds **1**−**8** exhibited significant activities against the tested gram-positive bacteria *S. aureus* ATCC 29213, *S. aureus* ATCC 70669, *E. faecium* ATCC 35667 and *E. faecalis* ATCC 51299 (Table 3). Notably, compound **1** and **2** showed pronounced activities against all tested strains, with compound **1** resulting in an MIC of 12.5 μM against MRSA. Compounds **1**-**8** did not display growth inhibitory activities against *M. tuberculosis* H37Rv and *C. albicans* as well as no antiviral effects on *SARS-CoV-2* up to the maximal tested concentration. When tested for their cytotoxic activity against human T lymphocyte Jurkat cell line, compound **1** and **3** showed low cytotoxic potential with IC_{50} of 30.8 μM and 40 μM, respectively, while the other

compounds were nearly not cytotoxic even at the highest tested concentration (Figure 5). Since the known compound asperphenalenone **A** has been reported to exhibit antiviral activity against HIV,[20] we studied the effect of the compounds on inhibiting replication of HIV in infected Jurkat cells. While most compounds were devoid of any substantial antiviral effects, compound **10** (asperphenalenone **B**) showed low anti-HIV activity resulting in ca. 70% decrease in viral transcript in treated HIV-infected Jurkat cells, whereas compound **9** (asperphenalenone **E**) even seemed to promote viral replication (Figure 6). Compared to asperphenalenone **A**, which displayed an IC_{50} values of 4.5 μM in an assay employing a VSV-G pseudotyped HIV-1,[20] the anti-HIV effect of compound **10** was relatively low (70% inhibition at 50 μM). Compared to the structure of asperphenalenone **A**, compound **10** has a carboxylate function at position C-33 instead of a hydroxyl group and an additional hydroxyl group substitution at C-30, suggesting that the increased polarity of compound **10** might impair anti-HIV activity.

In conclusion, eight new compounds **1**−**8** along with two known derivatives were obtained from the rice culture of the endophytic fungus *C. rosea*. The sugar constituent of the glycosylated compounds **5-8** was identified as D-mannose by TLC analysis of hydrolysis products. Remarkably, thus is the first report on glycosides being isolated from the rice culture of *C. rosea*, further expanding the diversity of natural compounds produced by this organism. In bioactivity screenings, compound **1** and **2** showed pronounced antibacterial activities against sensitive and drug-resistant isolates of the gram-positive pathogens *S. aureus*, *E. faecalis* and *E. faecium.* In a previous study, structurally related asperphenalenone derivatives isolated from an endophytic *Aspergillus* sp. exhibited not only antibacterial active against gram-positive bacteria but also against gram-negative bacteria such as *Pseudomonas aeruginosa* and *Escherichia coli*.[28] However, we could not detect any antibacterial properties of compounds **1**−**8** against these two gram-negative bacteria. Another asperphenalenone derivatives isolated from *Aspergillus* sp., aspergillussanone A, displayed cytotoxic activity against human oral carcinoma (KB) cell lines[27] as well as anti-HIV activity.[20] In our study, however, compounds

1−**8** were largely devoid of substantial cytotoxic or anti-HIV properties. Concerning antibacterial activities, compound **1**, **2** and **3** showed significant activities against MRSA and *E. faecium*, with **1** showing the strongest activities with MICs of 12.5 μM and 25 μM, respectively. In contrast, compound **9**, which only differs in position C-1 and C-7 compared to **1** and **2** was inactive. Thus, from the structure-activity relationship aspect, substitution by a methoxy group at position C-1 and C-7 obviously is crucial for antibacterial activity. However, also the side chain plays an indispensable role as well. If position C-33 was glycosylated, the activity against MRSA decreased from 12.5 to 100 μM when comparing **1** and **7**, and the same trend was seen when comparing activity of **2** and **8**. In summary, asperphenalenone derivatives from the biocontrol agent *C. rosea* might offer structural scaffolds to develop new antibiotics and anti-HIV drugs.

ASSOCIATED CONTENT

Supporting Information

AUTHOR'S INFORMATION

Lin Wang: E-mail: liwan103@hhu.de

Anna-Lene Kiffe-Delf: E-mail: ankif100@hhu.de

Philipp Niklas Ostermann: E-mail: Philipp.Ostermann@uni-duesseldorf.de

Ying Gao: E-mail: gaoying446@gmail.com

Lasse van Geelen: Lasse.Geelen@hhu.de

Hao-Fu Dai: daihaofu@itbb.org.cn

You-Xing Zhao: zhaoyouxing@itbb.org.cn

Heiner Schaal: E-mail: schaal@uni-duesseldorf.de

Attila Mándi: E-mail: mandi.attila@science.unideb.hu

Tibor Kurtán: E-mail: kurtan.tibor@science.unideb.hu

Zhen Liu: E-mail: zhenferizi0@sina.com

Rainer Kalscheuer: E-mail: rainer.kalscheuer@hhu.de

Funding

This work was financially supported by the China Scholarship Council, the Ministry of Education of China, for a doctoral scholarship awarded to L.W.. R.K. acknowledges financial support from the Stiftung zur Erforschung infektiös-immunologischer Erkrankungen. This work was further supported by the Jürgen Manchot Foundation (to P.N.O., H.S.) and by the Forschungskommission Düsseldorf (FoKo) (to H.S.). The research work of T.K. and A.M. was supported by the National Research, Development and Innovation Office (K138672, FK134653). The Governmental Information-Technology Development Agency (KIFÜ) is acknowledged for CPU time.

DECLARATION OF COMPETING INTEREST

The authors declare that there is no conflict of interests regarding the publication of this article.

REGERNCE

[1] Toledo, A. V.; Virla, E.; Humber, R. A.; Paradell, S. L.; López Lastra, C. C. First record of *Clonostachys rosea* (Ascomycota: Hypocreales) as an entomopathogenic fungus of *Oncometopia tucumana* and *Sonesimia grossa* (Hemiptera: Cicadellidae) in Argentina. *J. Invertebr. Pathol*. 2006, 92, 7−10.

[2] Roberti, R.; Veronesi, A.; Cesari, A.; Cascone, A.; Berardino, I.D.; Bertini, L.; Caruso, C. Induction of PR proteins and resistance by the biocontrol agent *Clonostachys rosea* in wheat plants infected with *Fusarium culmorum*. *Plant Sci*. 2008, 175, 339−347.

[3] Morandi, M. A. B.; Mattos, L. P. V.; Santos, E. R.; Bonugli, R. C. Influence of application time on the establishment, survival, and ability of *Clonostachys rosea* to suppress *Botrytis*

cinerea sporulation on rose debris. *Crop Prot*. 2008, 27, 77−83.

[4] Cota, L. V.; Maffia, L. A.; Mizubuti, E. S. G.; Macedo, P. E. F.; Antunes, R. F. Biological control of strawberry gray mold by *Clonostachys rosea* under field conditions. *Biol. Control*. 2008, 46, 515−522.

[5] Xue, A. G.; Chen, Y. H.; Voldeng, H. D.; Fedak, G.; Savard, M. E.; Längle, T.; Zhang, J. X.; Harman, G. E. Concentration and cultivar effects on efficacy of CLO-1 biofungicide in controlling *Fusarium* head blight of wheat. *Biol. Control*. 2014, 73, 2−7.

[6] Kosawang, C.; Karlsson, M.; Vélëz, H.; Rasmussen, P. H.; Collinge, D. B.; Jensen, B.; Jensen, D. F. Zearalenone detoxification by zearalenone hydrolase is important for the antagonistic ability of *Clonostachys rosea* against mycotoxigenic *Fusarium graminearum*. *Fungal Biol*. 2014, 118, 364−373.

[7] Bennett, A. J.; Mead, A.; Whipps, J. M. Performance of carrot and onion seed primed with beneficial microorganisms in glasshouse and field trials. *Biol. Control.* 2009, 51, 417−426.

[8] Kapongo, J. P.; Shipp, L.; Kevan, P.; Sutton, j. C. Co-vectoring of *Beauveria bassiana* and *Clonostachys rosea* by bumble bees (*Bombus impatiens*) for control of insect pests and suppression of grey mould in greenhouse tomato and sweet pepper. *Biol. Control*. 2008, 46, 508−514.

[9] Baloyi, M. A.; Laing, M. D.; Yobo, K. S. Use of mixed cultures of biocontrol agents to control sheep nematodes. Vet. *Parasitol*. 2012, 184, 367−370.

[10] Ahmed, M.; Laing, M. D.; Nsahlai, I. V. Use of *Clonostachys rosea* against sheep nematodes developing in pastures. *Biocontrol Sci Technol*. 2014, 24, 389–398.

[11] Zhai, M. M.; Qi, F. M.; Li, J.; Jiang, C. X.; Hou, Y.; Shi, Y. P.; Di, D. L.; Zhang, J. W.; Wu, Q. X. Isolation of secondary metabolites from the soil-derived fungus *Clonostachys rosea* yrs-06, a biological control agent, and evaluation of antibacterial activity. *J. Agric. Food Chem*. 2016, 64, 2298−2306.

[12] Supratman, U.; Suzuki, T.; Nakamura, T.; Yokoyama, Y.; Harneti, D.; Maharani, R.;

Salam, S.; Abdullah, F. F.; Koseki, T.; Shiono, Y. New metabolites produced by endophyte *Clonostachys rosea* b52. *Nat. Prod. Res*. 2019, 1-7.

[13] Abdel-Wahab, N. M.; Harwoko, H.; Müller, W. E. G.; Hamacher, A.; Kassack, M. U.; Fouad, M. A.; Kamel, M. S.; Lin, W. H.; Ebrahim, W.; Liu, Z.; Proksch, P. Cyclic heptapeptides from the soil-derived fungus *Clonostachys rosea*. *Bioorg Med Chem.* 2019, 27, 3954–3959.

[14] Okuda, T.; Kohno, J.; Kishi, N.; Asai, Y.; Nishio, M.; Komatsubara, S. Production of TMC-151, TMC-154 and TMC-171, a new class of antibiotics, is specific to 'gliocladium roseum' group. *Mycoscience*, 2000, 41, 239-253.

[15] Dias, A. C.D. S.; Couzinet-Mossion, A.; Ruiz, N.; Lakhdar, F.; Samira, E.; Samuel, B.; Lucie, O.; Christos, R.; Yves F. P.; Nazih, E. H.; Gaetane, W. C. Steroids from marine-derived fungi: evaluation of antiproliferative and antimicrobial activities of eburicol. *Mar. Drugs*, 2019, 17, 372.

[16] Jiang, C. X.; Yu, B.; Miao, Y. M,; Ren, H.; Xu, Q. H.; Zhao, C.; Tian, L. L.; Yu, Z.Q.; Zhou, P. P.; Wang, X. l.; Fang, J. G.; Zhang, J. W.; Zhang, J. Z.; Wu, Q.X. Indole Alkaloids from a soil-derived *Clonostachys rosea*. *J. Nat. Prod*. 2021, 84, 2468−2474.

[17] Gao, C.; Fan, Y. L.; Zhao, F., Ren, Q. C.; Wu, X.; Chang, L.; Gao, F. Quinolone derivatives and their activities against methicillin-resistant *Staphylococcus aureus* (MRSA). *Eur. J. Med. Chem*. 2018, 157, 1081-1095.

[18] Drougka, E.; Foka, A.; Liakpoulos, A.; Doudoulakakis, A.; Jelastopuli, E.; Chini, V.; Spiliopoulou, A.; Levidiotou, S.; Panagea, T.; Vogiatzi, A.; Lebessi, E.; Petinaki, E.; Spiliopoulou, I. A 12-year survey of methicillin-resistant *Staphylococcus aureus* infections in Greece: ST80-IV Epidemic? *Clin. Microbial. Infect*. 2014, 20, 796-803.

[19] Kjer, J.; Debbab, A,; Aly, A. H.; Proksch, P. Methods for isolation of marine-derived endophytic fungi and their bioactive secondary products. *Nat Protoc*. 2010, 5, 479-490.

[20] Pang, X..; Zhao, J. Y.; Fang, X. M.; Zhang, T.; Zhang, D. W.; Liu, H. Y.; Su, J.; Cen, S.; Yu, L. Y. Metabolites from the plant endophytic fungus *Aspergillus sp*. CPCC 400735 and their

anti-HIV activities. *J. Nat. Prod.* 2017, 80, 2595-2601.

[21] Elnaggar, M. S.; Ebrahim, W.; Mándi, A.; Kurtán, T.; Müller, W. E. G.; Kalscheuer, R.; Singab, A.; Lin, W. H.; Liu, Z.; Proksch, P. Hydroquinone derivatives from the marine-derived fungus Gliomastix sp. *RSC Adv*. 2017, 7, 30640-30649.

[22] CLSI. Methods for dilution antimicrobial susceptibility tests for bacteria that grow aerobically. CLSI standard M07 11th ed. Wayne, PA: Clinical and Laboratory Standards Institute; 2018.

[23] Gao, Y.; Wang, L.; Kalscheuer, R.; Liu, Z.; Proksch, P. Antifungal polyketide derivatives from the endophytic fungus *Aplosporella javeedii*. *Bioorg. Med. Chem*. 2020, 28, 115456.

[24] Rehberg, N.; Sommer, G. A.; Drießen, D.; Kruppa, M.; Adeniyi, E. T.; Chen, S.; Wang, L.; Wolf, K.; Tasch, B. O. A.; Ioerger, T. R.; Zhu, K.; Müller, J. J. T.; Kalscheuer, R. Nature-inspired (di)azine-bridged bisindole alkaloids with potent antibacterial in vitro and in vivo efficacy against methicillin-resistant *Staphylococcus aureus*. *J. Med. Chem*. 2020, 63, 12623−12641.

[25] Schmittgen, T. D.; Livak, K. J. Analyzing real-time PCR data by the comparative CT method. *Nat*. *Prot.* 2008, 3, 1101-1108.

[26] Adachi, A.; Gendelman, H. E.; Koenig, S.; Folks, T.; Willey, R.; Rabson, A.; Martin, M. A. Production of acquired immunodeficiency syndrome-associated retrovirus in human and nonhuman cells transfected with an infectious molecular clone. *J. Viro*. 1986, 59, 284-291.

[27] MacroModel. Schrödinger, L. L. C. 2015. http://www.schrodinger. com/ Macro-Model.

[28] Chai, J. D.; Head-Gordon, M. Systematic optimization of long-range corrected hybrid density functionals. *J. Chem. Phys.* 2008, 128, 084106

[29] Frisch, M. J.; Trucks, G. W.; Schlegel, H. B.; Scuseria, G. E.; Robb, M. A.; Cheeseman, J. R.; Scalmani, G.; Barone, V.; Mennucci, B.; Petersson, G. A.; et al. Gaussian 09, Revision E. 01; Gaussian: Wallingford, CT, USA, 2013.

[30] Stephens, P. J.; Harada, N. ECD cotton effect approximated by the Gaussian curve and

other methods. Chirality. 2010, 22, 229–233.

[31] Varetto, U. MOLEKEL 5.4; Swiss National Supercomputing Centre: Manno, Switzerland, 2009.

[32] Rukachaisirikul, V.; Rungsaiwattana, N.; Klaiklay, S.; Phongpaichit, S.; Borwornwiriyapan, K.; Sakayaroj, J. γ‑Butyrolactone, cytochalasin, cyclic carbonate, eutypinic acid, and phenalenone derivatives from the soil fungus *Aspergillus sp*. PSURSPG185. *J. Nat. Prod.* 2014, 77, 2375−2382.

[33] Gombodorj, S.; Yang, M.H.; Shang, Z. C.; Liu, R. H.; Li, T. X.; Yin, G. P.; Kong, L. Y. New phenalenone derivatives from *Pinellia ternata* tubers derived *Aspergillus* sp.. *Fitoterapia* 2017, 120, 72-78.

[34] Komatsu, K.; Shigemori, H.; Mikami, Y.; Kobayashi, J.: Sculezonones A and B, two metabolites possessing a phenalenone skeleton from a marine-derived fungus *Penicillium Species. J. Nat. Prod*. 2000, 63, 408-409.

[35] Mándi, A.; Kurtán, T. Applications of OR/ECD/VCD to the structure elucidation of natural products. *Nat. Prod. Rep*. 2019, 36, 889-918.

[36] Hou, X. F.; Yao, S., Mándi, A.; Kurtán, T.; Tang, C. P.; Ke, C. Q.; Li, X. Q.; Ye, Y. Bicunningines A and B, two new dimeric diterpenes from *Cunninghamia lanceolata*. *Org. Lett*. 2012, 14, 460-463.

[37] Gao, Y.; Stuhldreier, F.; Schmitt, L.; Wesselborg, S.; Guo, Z.; Zou, K.; Mándi, A.; Kurtán, T.; Liu, Z.; Proksch, P. Induction of new lactam derivatives from the endophytic fungus *Aplosporella javeedii* Through an OSMAC Approach. *Front. Microbiol.* 2020, 11, Article 600983.

[38] Mándi, A.; Swamy, M. M. M.; Taniguchi, T.; Anetai, M.; Monde, K. Reducing molecular flexibility by cyclization for elucidation of absolute configuration by CD calculations: daurichromenic acid. *Chirality.* 2016, 28, 453-459.

[39] Bremond, E.; Savarese, M.; Su, N. Q.; Perez-Jimenez, A. J.; Xu, X.; Sancho-Garcia, J. C.;

Adamo, C. Benchmarking density functionals on structural parameters of small-/medium-sized organic molecules. *J. Chem. Theory Comput.* 2016, 12, 459-465.

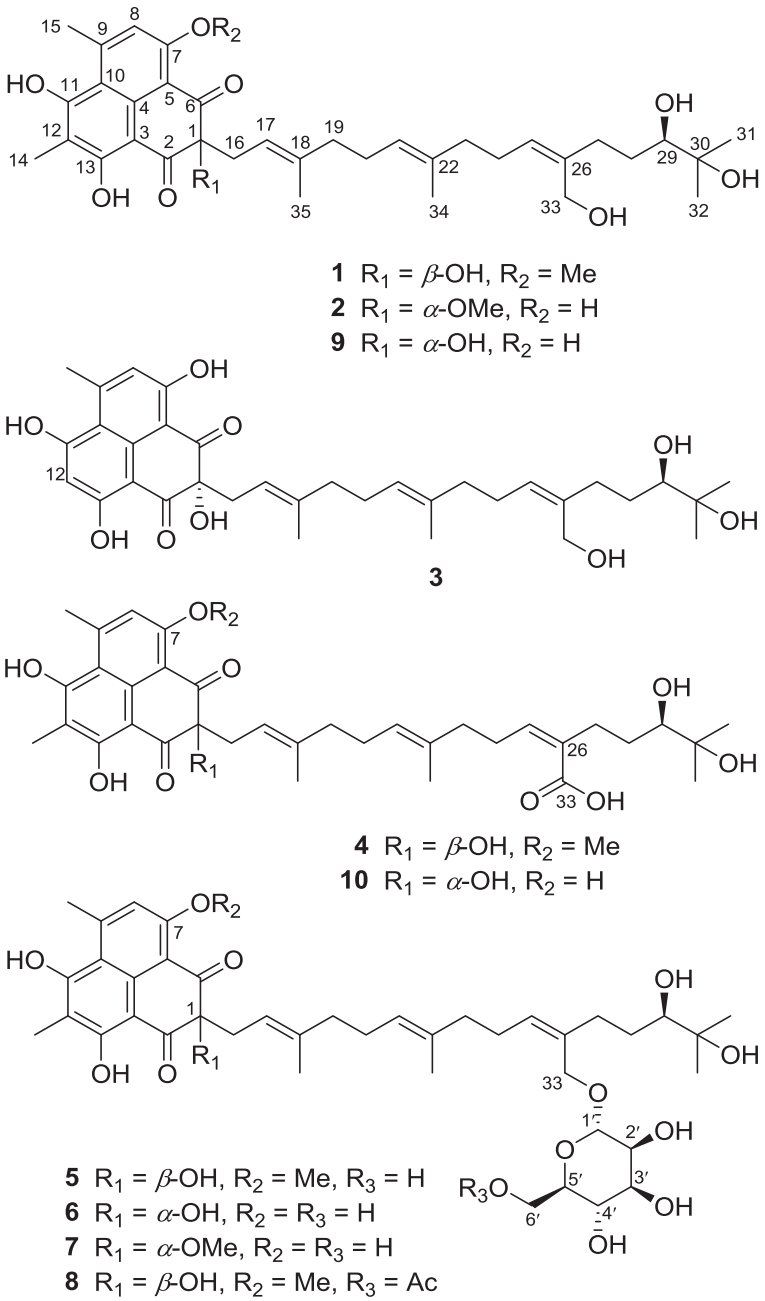

Figure 1. Structure of compounds **1-10**.

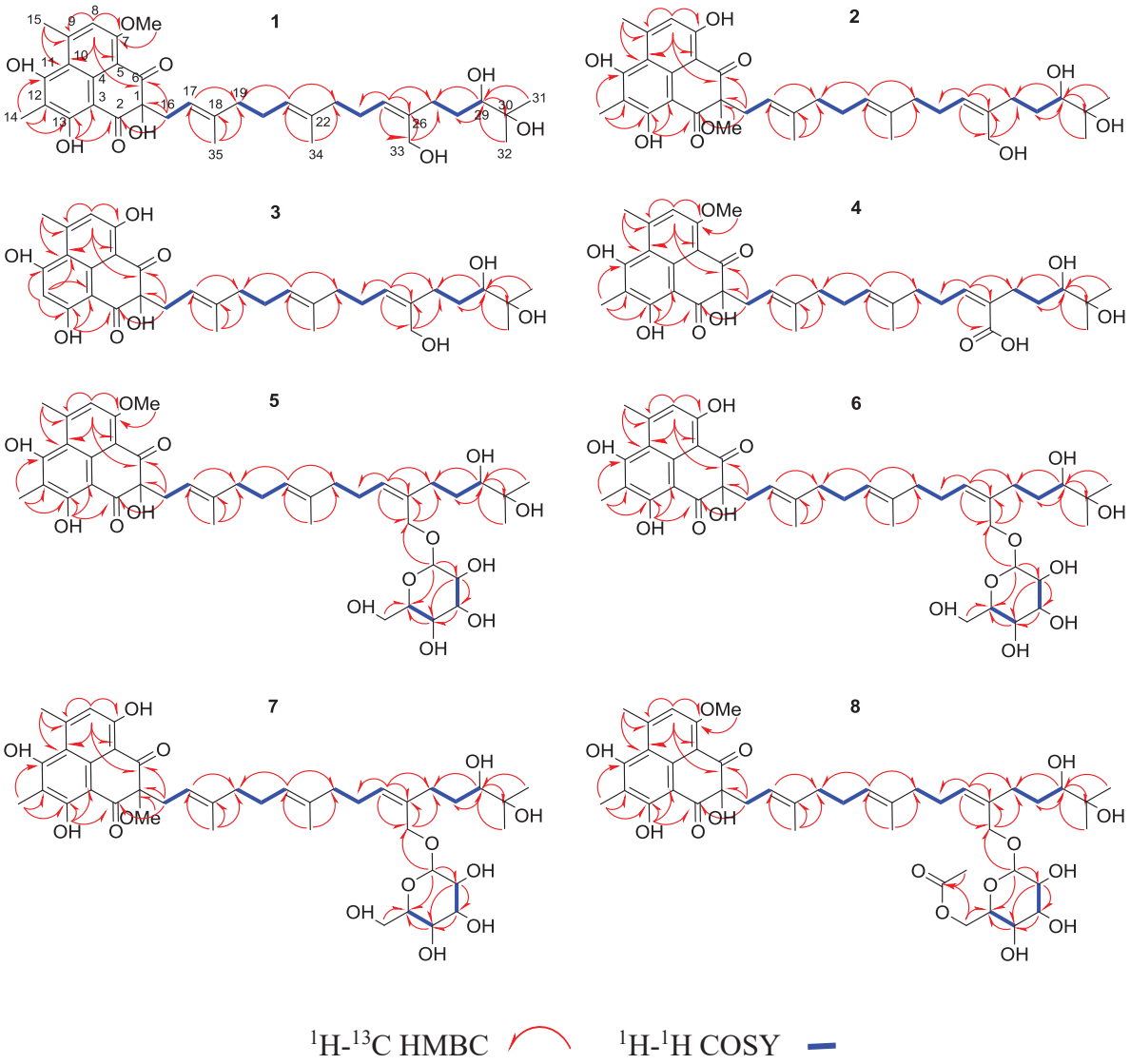

Figure 2. Key correlations of HMBC (H-C), COSY (H-H), and NOESY (H-H) compounds 1−8.

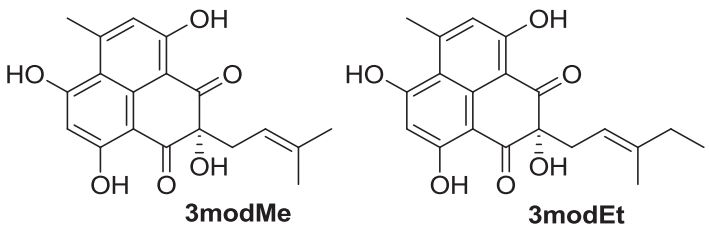

Figure 3. Structure of model compounds (*S*)-**3modMe** and (*S*)-**3modEt**.

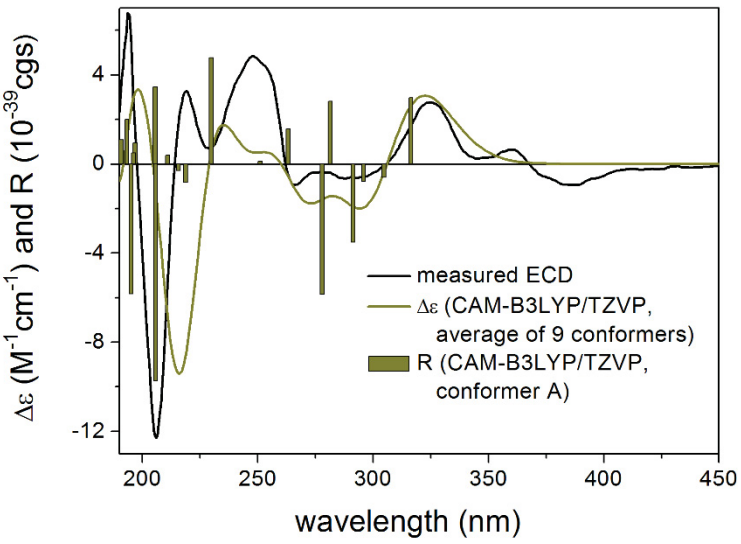

Figure 4. Experimental ECD spectrum of **3** in MeOH (black line) compared with the calculated CAM-B3LYP/TZVP PCM/MeOH spectrum of (*S*)-**3modEt** (dark yellow line). Level of DFT optimization: ωB97X/TZVP PCM/MeOH. Bars represent the rotational strengths of conformer A.

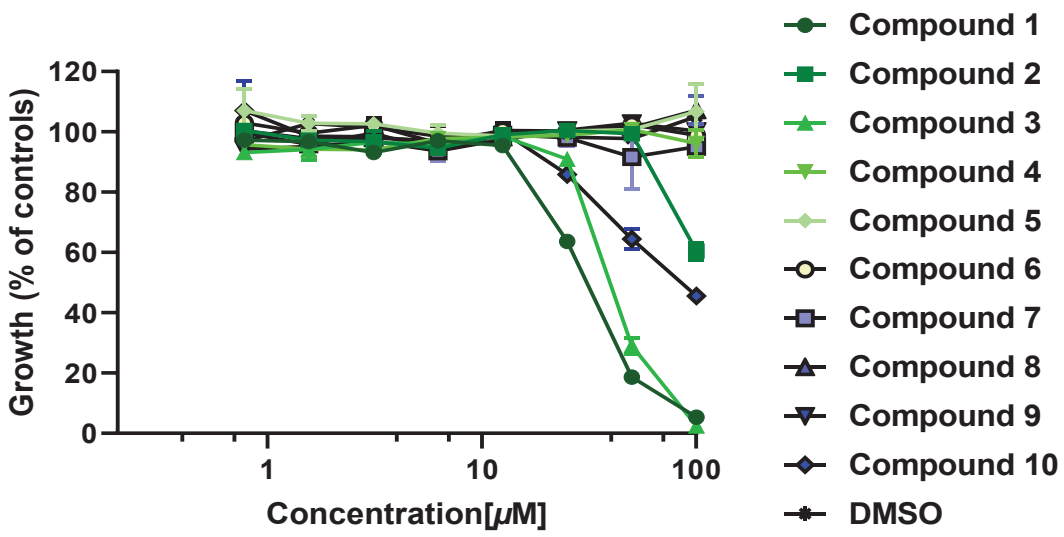

Figure 5. Cytotoxicity of compounds **1**-**10** against human T lymphocyte Jurkat cells. Compound **1** and **3** showed cytotoxic effects at a high contraction of 50 μM, but the rest of compounds was virtually devoid of cytotoxicity against Jurkat cells.

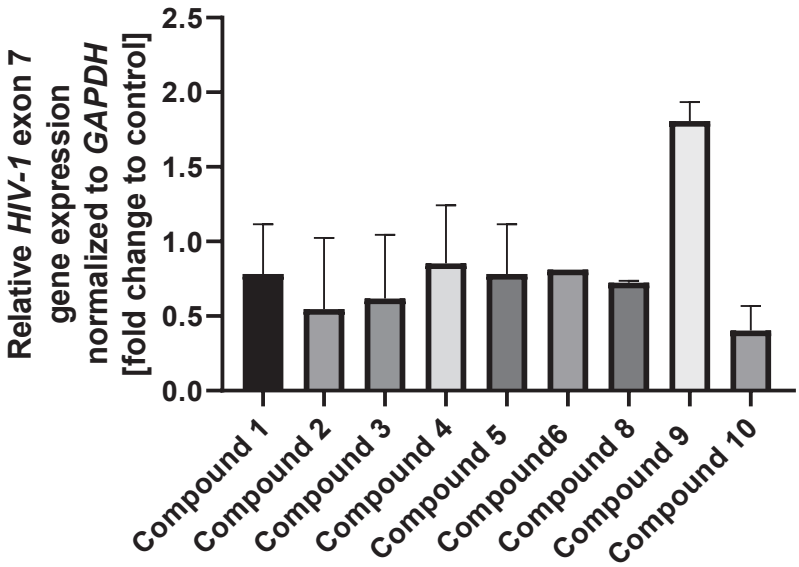

Figure 6. Inhibitory effects of isolated compounds on HIV-1 RNA replication in infected Jurkat cells. Compounds were tested at subcytotoxic concentrations as estimated from Figure 5. Compound **10** showed inhibitory activity leading to ca. 70% decrease in viral RNA at a concentration of 50 μM.

Table 1. NMR data for compounds **1**−**4**.

NO.	**1**[a]		**2**[b]		**3**[b]		**4**[b]	
	δ_C, type [c]	δ_H (J in Hz)	δ_C, type [c]	δ_H (J in Hz)	δ_C, type	δ_H (J in Hz)	δ_C, type	δ_H (J in Hz)
1	86.3, C		87.4, C		80.9, C		84.9, C	
2	198.2, C		196.6, C		198.8, C		196.0, C	
3	101.0, C		103.1, C		101.2, C		100.0, C	
4	136.9, C		136.3, C		138.0, C		136.1, C	
5	111.4, C		107.9, C		106.6, C		111.0, C	
6	200.2, C		201.9, C		203.4, C		197.8, C	
7	161.3, C		163.5, C		164.0, C		159.1, C	
8	114.0, CH	7.03, s	117.3, CH	6.70, s	117.1, CH	6.72, s	113.1, CH	6.97, s
9	148.7, C		150.4, C		149.9, C		145.7, C	
10	115.5, C		114.4, C		113.5, C		114.7, C	
11	165.3, C		165.0, C		164.0, C		165.1, C	
12	108.3, C		107.2, C		99.4, CH	6.17, s	106.6, C	
13	167.8, C		165.8, C		167.2, C		165.9, C	
14	7.6, CH_3	2.18, s	8.2, CH_3	2.04, s			8.1, CH_3	2.06, s
15	26.6, CH_3	2.96, s	26.2, CH_3	2.81, s	25.5, CH_3	2.77, s	26.1, CH_3	2.89, s
16	41.8, CH_2	2.60, dd (14.1, 8.0) 2.54, dd (14.1, 8.0)	40.8, CH_2	2.58, d (8.0)	41.4, CH_2	2.54, d (7.9)	40.1, CH_2	2.42, d (8.0)
17	117.2, CH	5.05, t (8.0)	114.8, CH	4.79, t (8.0)	115.4, CH	4.81, t (8.0)	116.9, CH	5.00, t (8.0)
18	141.1, C		140.4, C		139.8, C		138.2, C	
19	40.5, CH_2	1.83, m	39.3, CH_2	1.61, t (7.9)	39.4, CH_2	1.63, t (7.7)	39.4, CH_2	1.78, m
20	27.2, CH_2	1.84, m	25.9, CH_2	1.47, m	26.0, CH_2	1.51, m	26.0, CH_2	1.80, m
21	125.2, CH	5.06, t (7.0)	123.7, CH	4.87, t (7.0)	123.8, CH	4.89, t (6.9)	124.2, CH	5.03, t (6.9)
22	135.6, C		134.5, C		134.4, C		133.9, C	
23	40.6, CH_2	2.01, t (7.5)	39.5, CH_2	1.85, t (7.7)	39.6, CH_2	1.85, t (7.5)	38.7, CH_2	1.99, t (7.5)
24	26.9, CH_2	2.18, m	25.6, CH_2	2.03, m	25.6, CH_2	2.03, m	27.5, CH_2	2.42, m
25	128.6, CH	5.32, t (7.3)	125.1, CH	5.08, t (7.3)	125.1, CH	5.09, t (7.1)	138.7, CH	5.76, t (7.3)
26	139.3, C		139.8, C		139.7, C		138.1, C	
27	33.0, CH_2	2.40, m; 2.10, m	31.9, CH_2	2.27, m; 1.92, m	31.9, CH_2	2.27, m; 1.92, m	31.7, CH_2	2.40, m; 2.07, m

28	30.7, CH_2	1.75, m; 1.37, m	29.7, CH_2	1.61, m; 1.16, m	29.7, CH_2	1.61, m; 1.16, m	30.5, CH_2	1.60, m; 1.17, m
29	78.8, CH	3.26, dd (10.5, 1.7)	77.3, CH	3.04, dd (10.3, 1.5)	77.3, CH	3.04, dd (10.3, 1.6)	76.8, CH	3.04, dd (10.4, 1.8)
30	73.5, C		71.7, C		71.7, C		71.5, C	
31	25.3, CH_3	1.16, s	26.1, CH_3	1.01, s	26.2, CH_3	1.02, s	26.2, CH_3	1.02, s
32	24.7, CH_3	1.13, s	24.7, CH_3	0.96, s	24.7, CH_3	0.97, s	24.5, CH_3	0.96, s
33	59.7, CH_2	4.12, d (12.1) 4.06, d (12.1)	58.2, CH_2	3.90, d (12.0) 3.86, d (12.0)	58.2, CH_2	3.91, d (12.1) 3.86, d (12.1)	169.2, C	
34	15.8, CH_3	1.56, s	15.5, CH_3	1.37, s	15.5, CH_3	1.40, s	15.5, CH_3	1.51, s
35	15.9, CH_3	1.29, s	15.7, CH_3	1.29, s	15.7, CH_3	1.29, s	15.6, CH_3	1.21, s
1-OMe			54.1, CH_3	3.11, s				
7-OMe	56.3, CH_3	3.99, s					55.9, CH_3	3.89, s

[a] recorded at 600 MHz (^{1}H) and 150 MHz (^{13}C) in CD_3OD; [b] recorded at 600 MHz (^{1}H) and 150 MHz (^{13}C) in DMSO-d_6; [c] Data were extracted from HSQC and HMBC.

Table 2. NMR data for compounds **5**–**8**.

NO.	**5**[a]		**6**[a]		**7**[a]		**8**[a]	
	δ_C, type	δ_H (*J* in Hz)	δ_C, type	δ_H (*J* in Hz)	δ_C, type	δ_H (*J* in Hz)	δ_C, type	δ_H (*J* in Hz)
1	86.7, C		83.6, C		89.2, C		86.7, C	
2	198.4, C		201.2, C		200.2, C		198.4, C	
3	102.6, C		103.5, C		104.1, C		102.7, C	
4	138.0, C		137.2, C		137.5, C		138.1, C	
5	111.8, C		107.4, C		109.0, C		111.9, C	
6	200.4, C		203.5, C		203.2, C		200.1, C	
7	161.7, C		165.4, C		165.1, C		161.5, C	
8	114.5, CH	7.03, s	114.4, CH	6.72, s	119.0, CH	6.78, s	114.1, CH	7.04, s
9	148.9, C		151.2, C		151.8, C		148.9, C	
10	115.7, C		119.3, C		114.4, C		116.1, C	
11	165.2, C		164.7, C		165.7, C		166.6, C	
12	108.4, C		108.4, C		108.3, C		108.4, C	
13	168.1, C		167.4, C		167.3, C		168.6, C	
14	7.8, CH_3	2.18, s	7.8, CH_3	2.16, s	7.5, CH_3	2.19, s	7.7, CH_3	2.19, s
15	26.9, CH_3	2.96, s	26.8, CH_3	2.85, s	26.6, CH_3	2.88, s	26.7, CH_3	2.97, s
16	42.1, CH_2	2.60, dd (14.0, 8.1) 2.54, dd (14.0, 7.5)	43.8, CH_2	2.63, d (8.0)	42.5, CH_2	2.70, d (8.1)	42.1, CH_2	2.61, dd (14.0, 8.1) 2.55, dd (14.0, 7.5)
17	117.4, CH	5.05, dd (8.1, 7.5)	116.3, CH	4.87, t (8.0)	115.3, CH	4.82, t (8.1)	117.3, CH	5.05, dd (8.1, 7.5)
18	141.3, C		142.2, C		142.5, C		141.2, C	
19	40.9, CH_2	1.83, m	40.7, CH_2	1.68, t (7.9)	40.3, CH_2	1.64, t (7.9)	40.9, CH_2	1.84, m
20	27.5, CH_2	1.84, m	27.4, CH_2	1.58, m	27.1, CH_2	1.48, m	27.3, CH_2	1.84, m
21	125.7, CH	5.06, t (7.0)	125.5, CH	4.94, t (7.0)	125.1, CH	4.90, t (7.1)	125.7, CH	5.07, t (7.0)
22	135.7, C		135.6, C		135.4, C		135.3, C	
23	40.8, CH_2	2.00, t (7.5)	40.8, CH_2	1.95, t (7.6)	40.4, CH_2	1.93, t (7.4)	40.8, CH_2	2.02, t (7.3)
24	27.3, CH_2	2.20, m	27.2, CH_2	2.17, m	26.9, CH_2	2.15, m	27.1, CH_2	2.20, m
25	131.3, CH	5.44, t (7.2)	131.2, CH	5.41, t (7.3)	130.9, CH	5.41, t (7.2)	131.4, CH	5.46, t (7.3)
26	136.5, C		136.5, C		136.3, C		136.4, C	
27	33.6, CH_2	2.37, m; 2.10, m	33.6, CH_2	2.36, m; 2.09, m	33.3, CH_2	2.36, m; 2.08, m	33.3, CH_2	2.37, m; 2.09, m

28	31.2, CH_2	1.78, m; 1.36, m	31.2, CH_2	1.77, m; 1.36, m	30.9, CH_2	1.77, m; 1.34, m	31.0, CH_2	1.78, m; 1.36, m
29	79.2, CH	3.26, dd (10.5, 1.7)	79.2, CH	3.26, dd (10.5, 1.7)	78.9, CH	3.26, dd (10.8, 1.6)	79.2, CH	3.25, dd (10.5, 1.7)
30	73.8, C		73.8, C		73.6, C		73.7, C	
31	25.9, CH_3	1.16, s	25.8, CH_3	1.16, s	25.5, CH_3	1.16, s	25.4, CH_3	1.16, s
32	24.9, CH_3	1.12, s	24.9, CH_3	1.12, s	24.5, CH_3	1.12, s	24.6, CH_3	1.13, s
33	66.7, CH_2	4.30, s	66.7, CH_2	4.29, s	66.3, CH_2	4.29, s	66.3, CH_2	4.31, d (11.7) 4.24, d (11.7)
34	16.1, CH_3	1.56, s	16.0, CH_3	1.47, s	15.6, CH_3	1.43, s	16.0, CH_3	1.57, s
35	16.2, CH_3	1.29, s	16.1, CH_3	1.31, s	15.9, CH_3	1.36, s	16.0, CH_3	1.29, s
1′	100.1, CH	4.47, d (0.8)	100.1, CH	4.47, d (0.8)	99.8, CH	4.47, d (0.7)	99.7, CH	4.46, d (0.8)
2′	72.6, CH	3.83, dd (3.2, 0.8)	72.6, CH	3.83, dd (3.2, 0.8)	72.2, CH	3.83, dd (3.2, 0.8)	72.3, CH	3.84, dd (3.3, 0.8)
3′	75.4, CH	3.43, dd (9.5, 3.2)	75.4, CH	3.44, dd (9.5, 3.2)	75.1, CH	3.43, dd (9.6, 3.2)	75.1, CH	3.44, dd (9.5, 3.3)
4′	68.5, CH	3.59, t (9.5)	68.5, CH	3.59, t (9.5)	68.2, CH	3.59, t (9.6)	68.6, CH	3.57, t (9.5)
5′	78.2, CH	3.17, ddd (9.5, 5.5, 2.4)	78.2, CH	3.18, ddd (9.5, 5.4, 2.4)	77.9, CH	3.18, ddd (9.6, 5.4, 2.3)	75.5, CH	3.35, ddd (9.5, 6.5, 2.1)
6′	62.8, CH_2	3.86, dd (11.8, 2.4) 3.73, dd (11.8, 5.5)	62.8, CH_2	3.86, dd (11.9, 2.4) 3.73, dd (11.9, 5.4)	62.4, CH_2	3.86, dd (11.8, 2.3) 3.73, dd (11.8, 5.4)	65.0, CH_2	4.41, dd (11.8, 2.1) 4.22, dd (11.8, 6.5)
1-OMe					54.9, CH_3	3.27, s		
7-OMe	56.6, CH_3	3.99, s					56.5, CH_3	3.99, s
6′-OAc							20.7, CH_3 172.6, C	2.05, s

[a] recorded at 600 MHz (^1H) and 150 MHz (^{13}C) in CD_3OD; [b] Data were extracted from HSQC and HMBC.

Table 3. Anti-microbial activities of compounds **1-10**

	Minimal Inhibitory Concentration MIC (μM)									
Strain	**1**	**2**	**3**	**4**	**5**	**6**	**7**	**8**	**9**	**10**
Staphylococcus aureus ATCC 25923	100	100	>100	>100	>100	>100	>100	>100	>100	>100
Staphylococcus aureus ATCC 700669	12.5	100	25	100	100	>100	100	>100	>100	>100
Enterococcus faecium ATCC 35667	25	50	>100	>100	>100	>100	>100	>100	>100	>100
Enterococcus faecalis ATCC 51299	50	100	>100	>100	>100	>100	>100	>100	>100	>100
Mycobacterium tuberculosis H37Rv	>100	>100	>100	>100	>100	>100	>100	>100	>100	>100
Candia albicans yeast form	>100	>100	>100	>100	>100	>100	>100	>100	>100	>100
Candia albicans hyphae form	>100	>100	>100	>100	>100	>100	>100	>100	>100	>100
SARS-CoV-2	>100	>100	>100	>100	>100	>100	>100	>100	>100	>100

Staphylococcus aureus ATCC 700669: Methicillin, oxacillin and vancomycin resistance strain.

Staphylococcus aureus ATCC 25923: Standard strain.

Enterococcus faecium ATCC 35667: Standard strain.

Enterococcus faecalis ATCC 51299: Low-level vancomycin, amikacin, gentamycin, tobramycin, streptomycin resistance strain.

Candia albicans ATCC 24433: Standard strain.

Mycobacterium tuberculosis H37Rv: Standard strain.

SARS-CoV-2: Clinical isolate strain.

Graphic Abstract

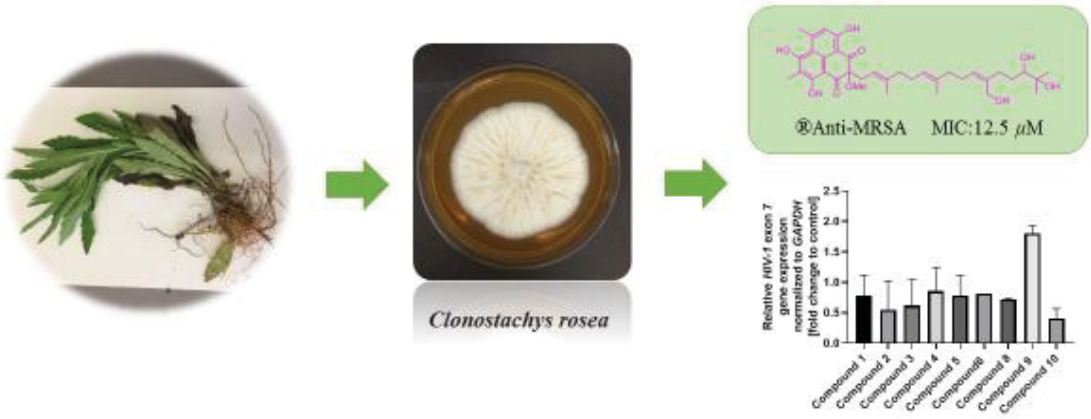

Supporting Information

Asperphenalenones isolated from the biocontrol agent *Clonostachys rosea* and their antimicrobial activities

Lin Wang, [1] Anna-Lene Kiffe-Delf, [1] Philipp Niklas Ostermann, [2] Ying Gao, [1] Lasse van Geelen, [1] Hao-Fu Dai, [3] You-Xing Zhao, [3] Heiner Schaal, [2] Attila Mándi, [4] Tibor Kurtán, [4] Zhen Liu, [5,*] Rainer Kalscheuer[1,*]

[1] Institute of Pharmaceutical Biology and Biotechnology, Heinrich Heine University Düsseldorf, Universitätsstrasse 1, 40225 Düsseldorf, Germany

[2] Institute of Virology, University Hospital Düsseldorf, Heinrich Heine University Düsseldorf, Universitätsstrasse 1, 40225 Düsseldorf, Germany

[3] Institute of Tropical Bioscience and Biotechnology, Chinese Academy of Tropical Agricultural Sciences, Haikou 571101, China

[4] Department of Organic Chemistry, University of Debrecen, Egyetem tér 1, 4002 Debrecen P.O.B. 400, Hungary

[5] Key Laboratory of Study and Discovery of Small Targeted Molecules of Hunan Province, School of Medicine, Hunan Normal University, Changsha 410013, China

[*]Corresponding authors. E-mail address:

Zhen Liu: zhenfeizi0@sina.com

Rainer Kalscheuer: rainer.kalscheuer@hhu.de;

CONTENT

Extraction and isolation

All compounds were guided on activity tracking approach to Isolated and purified. The strain *C. Rosea* was cultivated in solid rice medium containing 100 g rice and 110 ml water for 24 days at 22°C. Subsquently, culture was extracted by 500 mL EtOAc × 2 for each flask and shake with speed of 145 rpm overnight. The EtOAc crude extract (39.2 g) was subjected via vacuum liquid chromatography (VLC) on silica gel with gradient *n*-hexane / EtOAc (100:0, 80:20, 60:40, 40:60, 20:80, 0:100) and dichloroform / methanol (100:0, 60:40, 20:80, 0:100) as elution solvent to obtain seven fractions on the basis of TLC analysis. Afterwards, Seven fractions were tested their anti-MRSA activity under the guidance of CLSI and see fig.S1-A.

Fraction 6 was further separated by Sephadex LH-20 column with MeOH to get five sub-fractions Fr6.1- Fr. 6.5. Subsequently, the anti-MRSA activity were carried with same protocol and fraction 6.1 started show wake activity see fig.S1-B. Further, Fraction.6.1 was Chromatographed by VLC on silica gel respectively using dichloroform / methanol at 80:20, 70:30, 60:40, 50:50 and 40:60 as elution solvent yielded three sub-fractions (Fr.6.1.1- Fr.6.1.3) and their anti-MRSA activity were tested. Sub-fraction 6.1.2 exhibited strongest activity against MRSA at 100 mg/L see fig.S1-C, than followed by semi-preparative HPLC with a mixture of Acetonitrile and H_2O to yield compound **2** and **3**. Sub-fraction 6.1.1 and sub-fraction 6.1.3 were separated by semi-preparative HPLC with mixture of acetonitrile and water to yield compound **1**, **4**, and **9**, **10** respectively.

Fraction 6.4 was eluted on silica gel using dichloroform / methanol at 60:40, 50:50 40:60 and 30:70 to achieve four sub-fractions (Fr.6.4.1- Fr.6.4.4). Next was using MeOH-H_2O as mobile phase to obtain **5**. **6** and **7. 8** purification by Semi-preparative HPLC from

Fr. 6.4.2 and Fr.6.4.4 respectively. All isolated compounds were tested their activity against MRSA, see table 1.

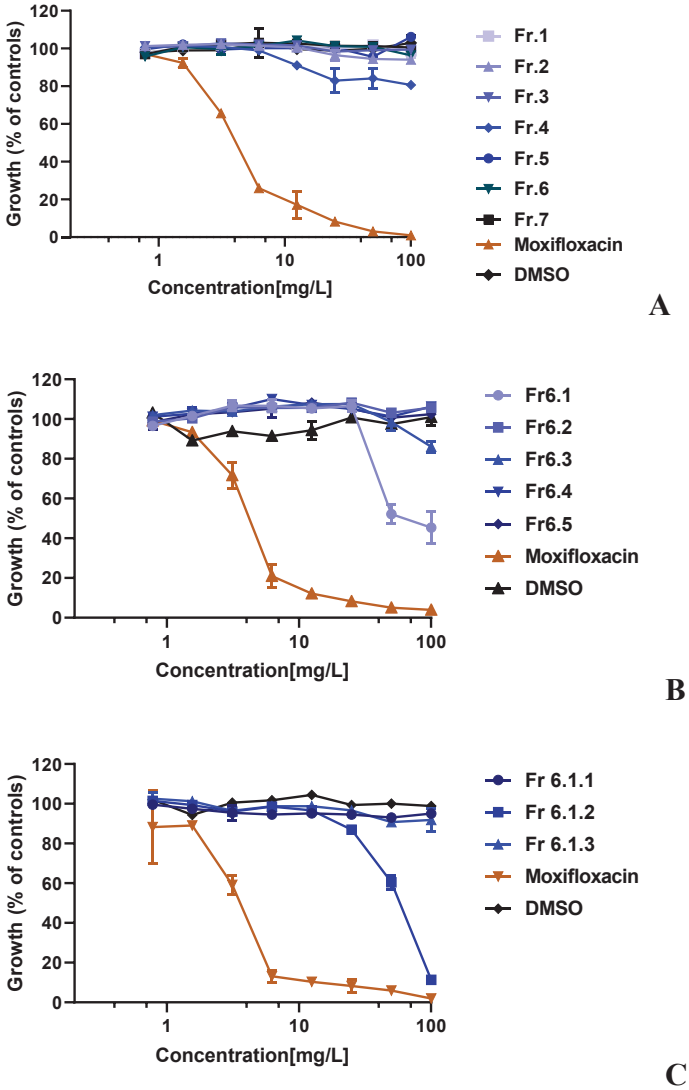

Fig. S1. Dose-response curves against MRSA with fractions and sub-tractions. Growth (% of control) was quantified by resazurin dye reduction assay for growth of MRSA. A: Fractions shown any activity against MRSA. B: Fr.6.1 started display wake activity with the dilution of crude extract. C: Fr.6.1 2 exhibited significant activity at concentration 100 mg/L after three times dilution.

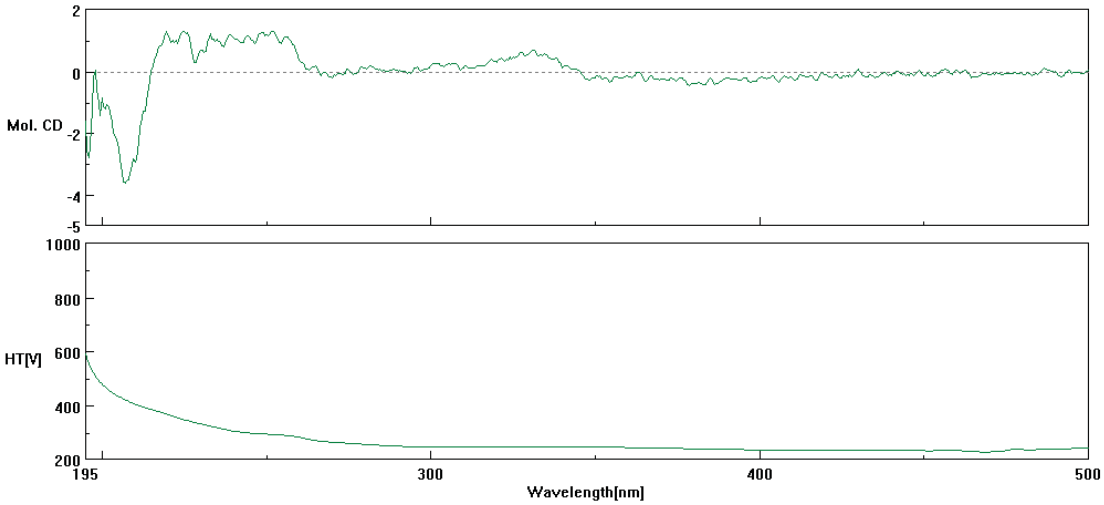

Fig.S2. Experimental CD spectrum of compound **1** in CAN

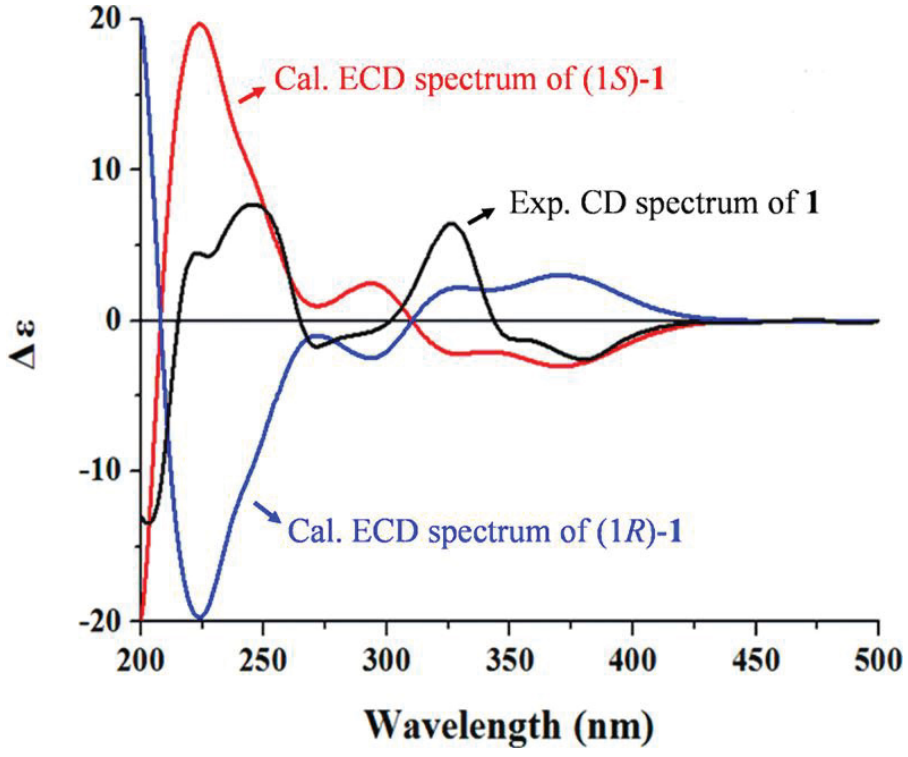

Fig.S3. Experimental ECD spectra of known compound asperphenalenone A in literature and the calculated ECD spectra of (1*S*)-1 and (1*R*)-1.

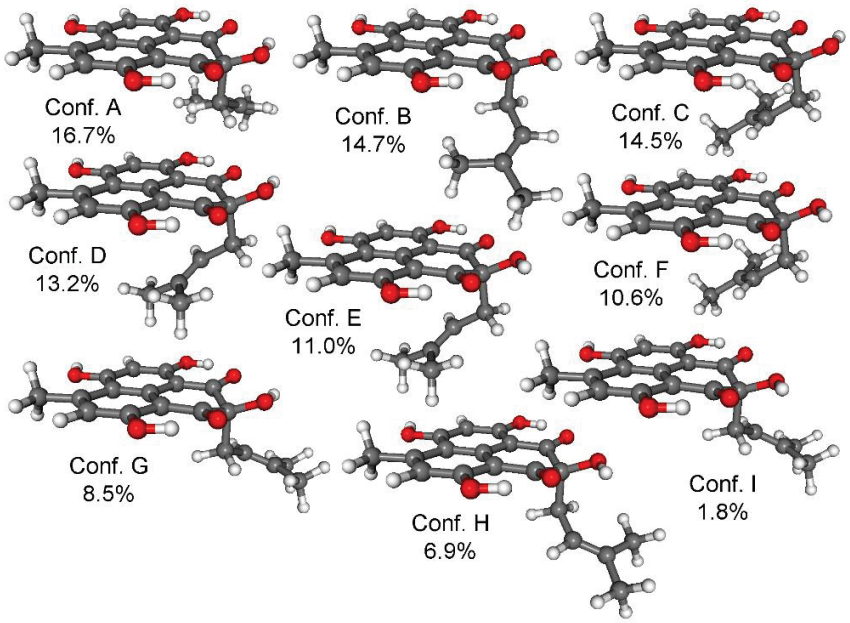

Fig. S4. Low-energy (≥ 1%) ωB97X/TZVP PCM/MeOH conformers of (S)-3modMe.

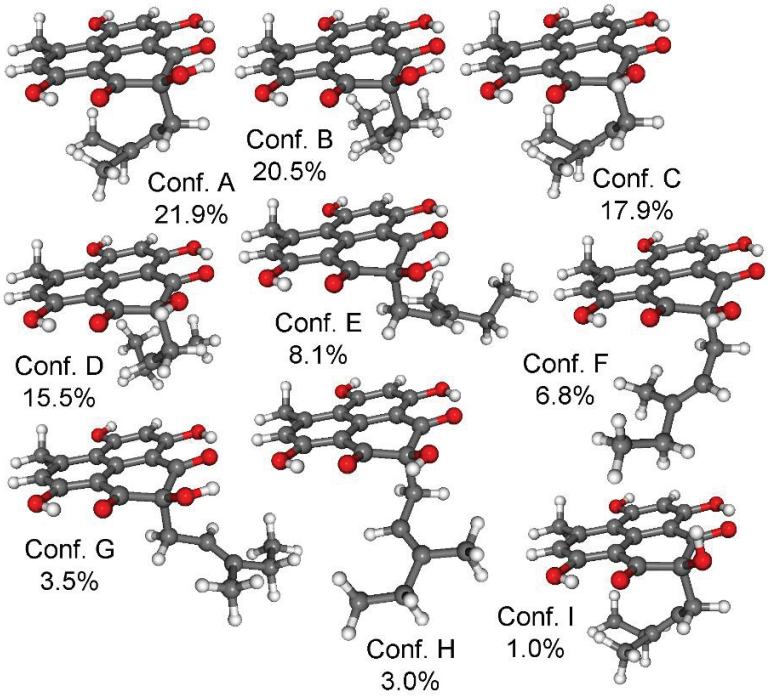

Fig. S5. Low-energy (≥ 1%) ωB97X/TZVP PCM/MeOH conformers of (S)-3modEt.

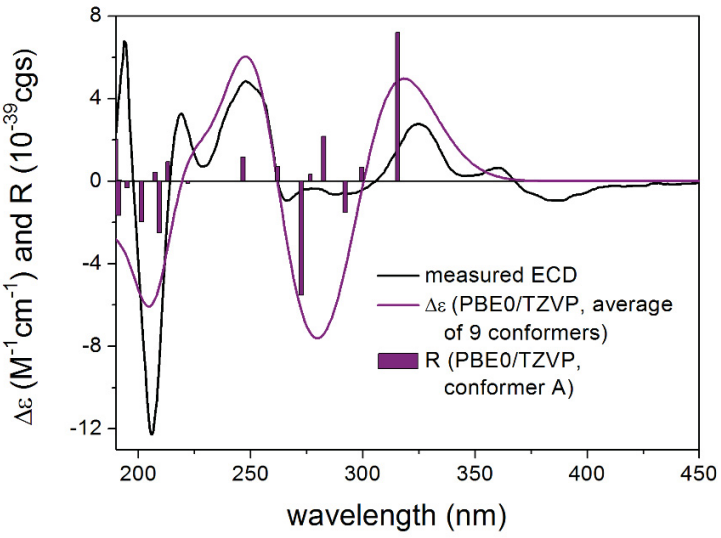

Fig. S6. Experimental ECD spectrum of 3 in MeOH (black line) compared with the calculated PBE0/TZVP PCM/MeOH spectrum of (*S*)-**3modMe** (purple line). Level of DFT optimization: ωB97X/TZVP PCM/MeOH. Bars represent the rotational strengths of conformer A.

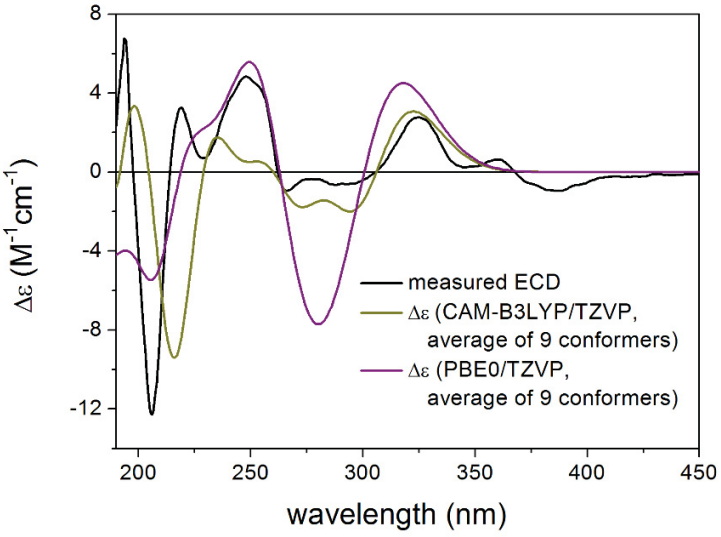

Fig. S7. Experimental ECD spectrum of 3 in MeOH (black line) compared with the calculated CAM-B3LYP/TZVP PCM/MeOH and PBE0/TZVP PCM/MeOH spectra of (*S*)-**3modEt** (olive and purple lines, respectively). Level of DFT optimization: ωB97X/TZVP PCM/MeOH.

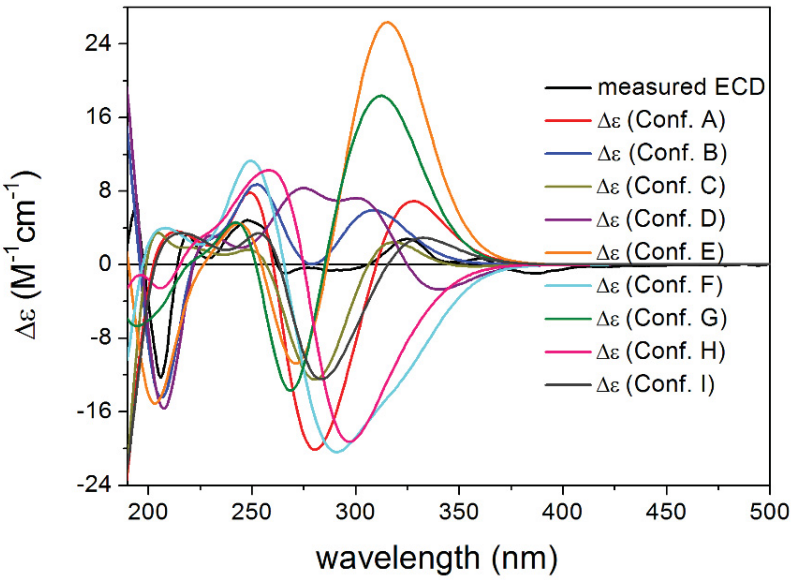

Fig. S8**.** Experimental ECD spectrum of 3 in MeOH (black line) compared with the calculated PBE0/TZVP PCM/MeOH spectra of the individual low-energy conformers of (*S*)-**3modEt** (color lines). Level of DFT optimization: ωB97X/TZVP PCM/MeOH.

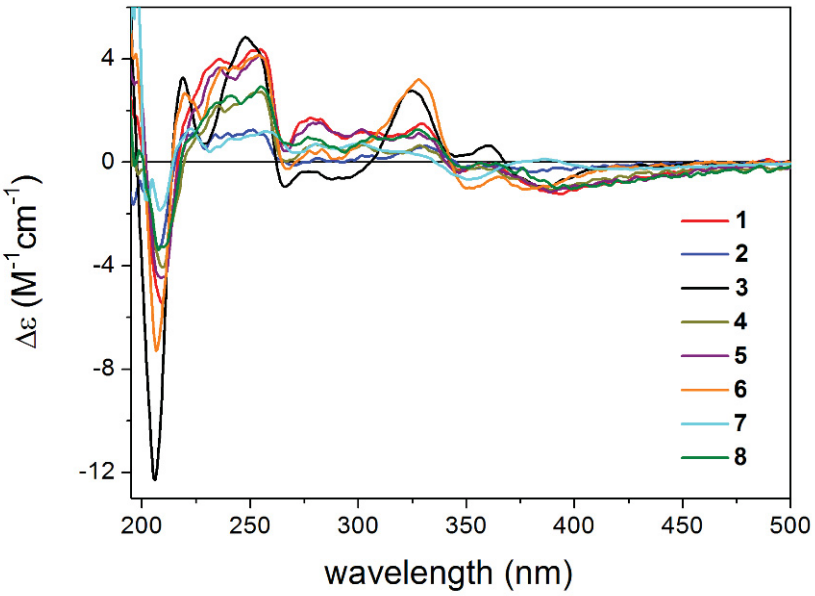

Fig. S9.Comparison of the experimental ECD spectra of 1-8 measured in MeOH.

Table S1. Boltzmann populations and specific optical rotations of the low-energy conformers of (S)-3modMe computed at various levels for the ωB97X/TZVP PCM/MeOH optimized MMFF conformers.

Conformer	Boltzmann population	B3LYP/TZVP	BH&HLYP/TZVP	CAM-B3LYP/TZVP	PBE0/TZVP
Conf. A	16.69%	447.72	320.78	341.74	421.16
Conf. B	14.69%	-429.98	-317.34	-332.75	-402.43
Conf. C	14.54%	180.86	144.88	153.34	176.41
Conf. D	13.17%	-130.51	-116.05	-119.68	-131.27
Conf. E	11.02%	-169.90	-147.47	-152.48	-165.69
Conf. F	10.65%	143.83	114.46	121.54	143.90
Conf. G	8.46%	272.48	169.96	182.52	257.30
Conf. H	6.92%	-283.39	-182.13	-192.93	-266.30
Conf. I	1.81%	217.13	127.75	139.99	207.46
Average	N/A	25.15	13.00	15.78	24.19

Table S2. Boltzmann populations and specific optical rotations of the low-energy conformers of (S)-3modEt computed at various levels for the ωB97X/TZVP PCM/MeOH optimized MMFF conformers.

Conformer	Boltzmann population	B3LYP/TZVP	BH&HLYP/TZVP	CAM-B3LYP/TZVP	PBE0/TZVP
Conf. A	21.88%	-166.74	-138.59	-144.19	-164.74
Conf. B	20.53%	204.65	160.92	170.06	199.29
Conf. C	17.87%	-186.20	-157.86	-162.86	-181.11
Conf. D	15.46%	179.74	137.26	146.61	177.80
Conf. E	8.07%	442.33	313.88	333.99	418.30
Conf. F	6.77%	-427.42	-312.65	-327.73	-401.92
Conf. G	3.47%	289.76	184.82	198.00	274.55
Conf. H	2.98%	-298.66	-196.20	-207.29	-281.54

Conf. I	0.98%	-180.09	-152.34	-157.65	-176.27
Average	N/A	6.30	-1.08	0.84	6.05

Table S3. Cartesian coordinates and energies of the low-energy conformers calculated at the ωB97X/TZVP PCM/MeOH level.

(*S*)-**3modMe**, Conf A

O	2.388905	2.179924	-1.303141
O	-2.272076	3.403179	0.387187
C	-4.655630	-0.695203	0.971764
O	-3.263694	-2.861269	0.219517
O	1.045668	-2.717468	-1.598672
O	0.151162	3.425611	-0.491323
O	2.207017	-0.403555	-1.813586
C	-2.182177	-2.149079	-0.133931
C	-1.092429	-2.784597	-0.676333
C	0.032145	-2.049656	-1.049003
C	-2.195817	2.077746	0.286103
C	-3.334063	1.342051	0.650069
C	-3.375001	-0.022221	0.556380
C	-2.221722	-0.727672	0.064964
C	0.150793	2.198873	-0.439931
C	-1.041270	1.422079	-0.140504
C	-1.057955	0.000464	-0.279235
C	0.085507	-0.670817	-0.815234
C	1.280058	0.059201	-1.143016
C	4.927063	-1.211476	1.436980
C	2.469369	-1.658263	1.805208
C	3.525526	-0.667991	1.400439
C	3.291694	0.586265	1.014807
C	1.960939	1.268932	0.923368
C	1.464674	1.445714	-0.552755
H	2.951287	1.527548	-1.744621
H	-1.418381	3.774223	0.067952
H	-5.106292	-1.235880	0.140009
H	-4.484222	-1.420238	1.766281
H	-5.362111	0.054646	1.325100
H	-3.123315	-3.795490	0.031971
H	1.732624	-2.063978	-1.855738
H	-1.096281	-3.856175	-0.838737
H	-4.196495	1.894294	1.002944
H	5.657431	-0.472644	1.105596
H	5.189166	-1.529322	2.450320
H	5.010984	-2.094530	0.796549
H	1.476757	-1.221844	1.909487
H	2.407884	-2.459373	1.060793
H	2.736397	-2.130427	2.754256
H	4.144082	1.195807	0.725291
H	1.194320	0.751214	1.501349
H	2.040070	2.284705	1.320499

ωB97X Energy = -1186.35542056 a.u.

(*S*)-**3modMe**, Conf B

O	-2.389604	2.168121	-1.303802
O	-1.005170	-2.729995	-1.583846
C	3.393391	-3.037189	0.261127
O	4.462042	-0.657923	0.889791
O	2.246159	3.430298	0.389080
O	-2.182764	-0.417096	-1.820906
O	-0.178870	3.428167	-0.453156
C	3.355830	0.021645	0.545419
C	3.335290	1.389223	0.644081
C	2.190432	2.104684	0.289031
C	-0.002870	-2.045766	-1.031963
C	1.134289	-2.769457	-0.648136
C	2.232423	-2.153887	-0.108903
C	2.226936	-0.726814	0.068171
C	-1.270342	0.053940	-1.141391
C	-0.067683	-0.672044	-0.804651
C	1.067145	0.010515	-0.270965
C	1.035408	1.434206	-0.132442
C	-0.159428	2.198192	-0.420274
C	-4.955691	-1.231495	1.382875
C	-2.502652	-1.688518	1.769402
C	-3.552492	-0.691477	1.365045
C	-3.311597	0.566237	0.995149
C	-1.978100	1.245890	0.922083
C	-1.468107	1.435453	-0.547855
H	-2.955501	1.517047	-1.741938
H	-1.697973	-2.089925	-1.853320
H	3.646598	-2.934279	1.315640
H	3.139367	-4.076913	0.059613
H	4.286364	-2.777100	-0.306186
H	5.146258	-0.047736	1.185593
H	1.378937	3.784152	0.080972
H	4.207158	1.934142	0.986362
H	1.126992	-3.841059	-0.805537
H	-5.036626	-2.105076	0.729198
H	-5.226750	-1.563160	2.389390
H	-5.681500	-0.486154	1.056103
H	-1.509207	-1.256440	1.883624
H	-2.777513	-2.166083	2.713492
H	-2.439240	-2.485005	1.020301
H	-4.159785	1.181438	0.705298
H	-2.057613	2.258250	1.327501
H	-1.217403	0.721282	1.501795

ωB97X Energy = -1186.35529972 a.u.

(*S*)-**3modMe**, Conf C

O	3.304102	1.189516	-1.401270
O	-0.798964	3.786068	0.076785
C	-4.384432	0.644471	0.337124
O	-3.658395	-1.864273	-0.259180
O	0.651314	-3.122603	-1.565056
O	1.583104	3.049433	-0.511720
O	2.496815	-1.327244	-1.604482
C	-2.379304	-1.531665	-0.490754
C	-1.489487	-2.491200	-0.905478
C	-0.158882	-2.153583	-1.146957
C	-1.128312	2.502433	-0.043289
C	-2.470382	2.164161	0.185485
C	-2.921626	0.877944	0.070999
C	-1.998270	-0.159640	-0.303041
C	1.198875	1.881197	-0.520841
C	-0.196306	1.513746	-0.365015
C	-0.636889	0.163671	-0.515187

C	0.292077	-0.844693	-0.925750
C	1.680529	-0.541908	-1.104102
C	0.308852	-1.102496	3.420440
C	1.941614	-2.268471	1.886255
C	1.375327	-0.963323	2.370292
C	1.736759	0.237136	1.919164
C	2.764234	0.534374	0.865501
C	2.236272	0.775190	-0.587461
H	3.722033	0.378958	-1.723490
H	0.161032	3.864598	-0.131566
H	-4.531339	-0.063673	1.151826
H	-4.860608	1.587987	0.600178
H	-4.884683	0.229830	-0.537325
H	-3.793789	-2.802528	-0.430400
H	1.538540	-2.724523	-1.719807
H	-1.807096	-3.516042	-1.057769
H	-3.150964	2.963359	0.452541
H	-0.535053	-1.678906	3.028059
H	0.688314	-1.647186	4.289697
H	-0.061988	-0.132224	3.753050
H	2.351478	-2.836176	2.726264
H	1.145494	-2.881708	1.451728
H	2.724338	-2.154838	1.137031
H	1.239971	1.106005	2.345570
H	3.296892	1.455007	1.114875
H	3.509735	-0.259171	0.784614

ωB97X Energy = -1186.35529005 a.u.

(*S*)-**3modMe**, Conf D

O	-3.326407	1.112483	-1.395540
O	-0.493947	-3.088512	-1.648196
C	3.907909	-1.858715	-0.265266
O	4.149272	0.732969	0.364832
O	0.650098	3.829130	0.184138
O	-2.414814	-1.393950	-1.646729
O	-1.698123	2.996114	-0.472303
C	2.855098	1.000171	0.131313
C	2.384841	2.281200	0.279216
C	1.041009	2.565529	0.042168
C	0.263691	-2.092068	-1.195202
C	1.612992	-2.380640	-0.942535
C	2.484861	-1.426155	-0.495140
C	2.009601	-0.085397	-0.281094
C	-1.658591	-0.567687	-1.138118
C	-0.242137	-0.814170	-0.950999
C	0.643105	0.211031	-0.498676
C	0.150172	1.541364	-0.309076
C	-1.241001	1.846056	-0.474794
C	-0.329585	-1.347695	3.331313
C	-1.967296	-2.441066	1.749657
C	-1.399848	-1.159926	2.292543
C	-1.759251	0.060467	1.896533
C	-2.783718	0.407238	0.855105
C	-2.251010	0.715028	-0.583311
H	-3.424469	2.064788	-1.258039
H	-1.398282	-2.726048	-1.797562
H	4.597506	-1.305528	-0.901876
H	4.214544	-1.680477	0.764742
H	4.004668	-2.921597	-0.482404
H	4.611515	1.534488	0.633041
H	-0.307403	3.873005	-0.039949
H	3.048196	3.087708	0.568541
H	1.951754	-3.393735	-1.121960

H	0.512998	-1.904365	2.908468
H	0.042361	-0.394111	3.708050
H	-0.705221	-1.933536	4.175072
H	-2.343577	-3.063328	2.566204
H	-2.773643	-2.292354	1.032605
H	-1.178784	-3.016842	1.253802
H	-1.258635	0.907975	2.359789
H	-3.320283	1.311801	1.153803
H	-3.526933	-0.381102	0.726231

ωB97X Energy = -1186.35519674 a.u.

(*S*)-**3modMe**, Conf E

O	-3.336562	1.100657	-1.395016
O	-0.520423	-3.119040	-1.595209
C	3.893398	-1.878246	-0.257579
O	4.150382	0.723055	0.325535
O	0.658490	3.824526	0.112413
O	-2.434127	-1.383132	-1.635843
O	-1.688121	3.006981	-0.474034
C	2.855029	0.989888	0.092466
C	2.387565	2.272862	0.217950
C	1.041619	2.557470	-0.015363
C	0.245927	-2.120386	-1.161725
C	1.594489	-2.408591	-0.911910
C	2.470375	-1.445965	-0.487167
C	2.002925	-0.098785	-0.296321
C	-1.655251	-0.577339	-1.116749
C	-0.251687	-0.836745	-0.931456
C	0.636048	0.200345	-0.510045
C	0.143926	1.533964	-0.350815
C	-1.256845	1.852632	-0.501236
C	-0.286739	-1.200942	3.383974
C	-1.903187	-2.370597	1.835849
C	-1.360379	-1.063388	2.340967
C	-1.745204	0.137729	1.911350
C	-2.779320	0.432959	0.863676
C	-2.256696	0.712100	-0.584228
H	-3.731994	0.282101	-1.724585
H	-1.420755	-2.759695	-1.757887
H	3.987960	-2.943823	-0.461847
H	4.581496	-1.333428	-0.902790
H	4.203587	-1.688030	0.769266
H	4.615070	1.528670	0.576413
H	-0.306155	3.859673	-0.095400
H	3.052471	3.083277	0.492769
H	1.931631	-3.424743	-1.075828
H	0.567032	-1.751854	2.976405
H	0.065591	-0.229902	3.734019
H	-0.650703	-1.770499	4.243850
H	-2.285203	-2.967567	2.668541
H	-2.700736	-2.259279	1.102083
H	-1.099792	-2.953914	1.374189
H	-1.262986	1.008400	2.350427
H	-3.507805	-0.374682	0.768113
H	-3.331775	1.337126	1.129670

ωB97X Energy = -1186.35502812 a.u.

(*S*)-**3modMe**, Conf F

O	3.295578	1.184642	-1.410919
O	-0.779840	3.791332	0.141738
C	-4.380176	0.664160	0.385402
O	-3.681046	-1.836388	-0.271072

O	0.616197	-3.101658	-1.609720
O	1.601224	3.031342	-0.519514
O	2.475316	-1.355278	-1.605478
C	-2.399633	-1.507971	-0.501850
C	-1.517122	-2.462988	-0.937244
C	-0.183382	-2.130496	-1.177417
C	-1.120381	2.511504	0.008899
C	-2.461200	2.177632	0.243838
C	-2.918766	0.894535	0.109954
C	-2.006623	-0.142902	-0.291619
C	1.188667	1.868051	-0.501674
C	-0.198791	1.519162	-0.330270
C	-0.643714	0.172979	-0.506738
C	0.279428	-0.827679	-0.945591
C	1.682829	-0.543211	-1.122682
C	0.353616	-1.225754	3.380062
C	1.995243	-2.332760	1.811763
C	1.414449	-1.047453	2.330015
C	1.756726	0.168389	1.905907
C	2.773581	0.505874	0.853876
C	2.233289	0.768573	-0.590567
H	3.376346	2.139268	-1.280689
H	0.172715	3.875494	-0.084392
H	-4.848897	1.604625	0.671583
H	-4.890553	0.268680	-0.492035
H	-4.522606	-0.059213	1.187433
H	-3.822582	-2.770268	-0.459878
H	1.509530	-2.703166	-1.748121
H	-1.839506	-3.484212	-1.103675
H	-3.136589	2.974798	0.529154
H	-0.032605	-0.268950	3.733559
H	-0.481567	-1.808476	2.978428
H	0.744966	-1.781607	4.236890
H	2.790298	-2.189353	1.081117
H	2.390915	-2.928706	2.638775
H	1.209680	-2.932267	1.340056
H	1.248232	1.019331	2.354201
H	3.294549	1.426792	1.129423
H	3.530014	-0.272589	0.743499

ωB97X Energy = -1186.35499594 a.u.

(*S*)-**3modMe**, Conf G

O	2.565987	0.894160	-1.533261
O	-1.492483	3.649936	-0.178350
C	-4.917530	0.564047	1.068837
O	-4.215636	-2.004928	0.746088
O	-0.084802	-3.410160	-0.942016
O	0.812535	2.833282	-0.982387
O	1.694399	-1.611077	-1.488984
C	-2.985372	-1.701696	0.302733
C	-2.134542	-2.704452	-0.090682
C	-0.852985	-2.397450	-0.546289
C	-1.794673	2.361071	-0.036064
C	-3.085181	2.053845	0.420403
C	-3.510761	0.762379	0.571763
C	-2.616147	-0.315197	0.244802
C	0.471261	1.685474	-0.709380
C	-0.881447	1.341090	-0.304707
C	-1.299989	-0.019272	-0.183946
C	-0.404324	-1.070711	-0.556505
C	0.942617	-0.781613	-0.967905
C	5.337779	-1.404326	1.379902
C	5.069182	1.060377	0.897127

C	4.394535	-0.265773	1.105158
C	3.076984	-0.466468	1.070191
C	2.017972	0.566238	0.827599
C	1.519367	0.589807	-0.658842
H	3.025547	0.060165	-1.700812
H	-0.576964	3.701367	-0.536087
H	-5.520565	0.013307	0.348004
H	-4.932315	-0.006621	1.996811
H	-5.380336	1.533960	1.245694
H	-4.348026	-2.958880	0.731595
H	0.760966	-3.032515	-1.272539
H	-2.446970	-3.741838	-0.063085
H	-3.748077	2.880456	0.645171
H	5.930968	-1.201191	2.276416
H	4.807596	-2.346648	1.522242
H	6.044708	-1.524775	0.553918
H	4.376105	1.866686	0.665999
H	5.641163	1.334503	1.788514
H	5.785101	0.987604	0.073576
H	2.716216	-1.479701	1.233765
H	1.163377	0.385817	1.485152
H	2.381015	1.574395	1.031772

ωB97X Energy = -1186.35477841 a.u.

(*S*)-**3modMe**, Conf H

O	2.569948	0.872451	1.524749
O	-0.138167	-3.408342	0.931704
C	-4.410703	-2.111434	-0.768644
O	-4.716220	0.542492	-0.996448
O	-1.440403	3.672451	0.163165
O	1.664773	-1.626768	1.491220
O	0.855093	2.830707	0.936627
C	-3.474090	0.806813	-0.559067
C	-3.061733	2.106815	-0.415108
C	-1.768876	2.390210	0.027649
C	-0.888513	-2.380196	0.539228
C	-2.183142	-2.666289	0.084526
C	-3.046198	-1.677446	-0.304745
C	-2.623611	-0.304374	-0.237607
C	0.931252	-0.788890	0.964399
C	-0.424933	-1.064723	0.550553
C	-1.304774	-0.002682	0.179699
C	-0.865099	1.353881	0.296302
C	0.489113	1.682756	0.684481
C	5.352982	-1.451865	-1.336181
C	5.080916	1.016866	-0.876702
C	4.407629	-0.310539	-1.081200
C	3.089403	-0.509678	-1.059338
C	2.029660	0.526837	-0.836270
C	1.524265	0.572223	0.647425
H	3.042725	0.042910	1.674918
H	0.712503	-3.050109	1.266864
H	-4.609123	-1.774232	-1.785233
H	-4.476909	-3.198152	-0.738632
H	-5.194588	-1.694694	-0.137191
H	-5.187780	1.363955	-1.171544
H	-0.517126	3.703132	0.508322
H	-3.729490	2.929907	-0.641042
H	-2.490025	-3.704704	0.059712
H	5.955596	-1.256465	-2.228087
H	6.051128	-1.565424	-0.501832
H	4.823807	-2.395114	-1.476036
H	4.385662	1.825962	-0.662498

H	5.785733	0.951207	-0.043037
H	5.665042	1.281822	-1.762952
H	2.729526	-1.523860	-1.218717
H	2.394126	1.531877	-1.052579
H	1.177708	0.338352	-1.494957

ωB97X Energy = -1186.35458962 a.u.

(*S*)-**3modMe**, Conf I

O	-2.567572	0.908656	1.561390
O	1.485232	3.651772	0.153971
C	4.890982	0.552730	-1.117273
O	4.192917	-2.014800	-0.773335
O	0.091713	-3.400772	1.000634
O	-0.824106	2.815952	1.005320
O	-1.672178	-1.619548	1.565271
C	2.969998	-1.706145	-0.311087
C	2.123523	-2.701954	0.104658
C	0.849414	-2.389702	0.581422
C	1.788631	2.362549	0.016044
C	3.072120	2.051352	-0.453881
C	3.491639	0.756573	-0.602433
C	2.601974	-0.319610	-0.256454
C	-0.460122	1.674392	0.714499
C	0.880416	1.342445	0.299503
C	1.291874	-0.021745	0.189296
C	0.398743	-1.063833	0.589550
C	-0.952605	-0.779262	1.028068
C	-5.308479	-1.454769	-1.422765
C	-5.063843	1.021227	-0.990900
C	-4.378356	-0.307123	-1.140526
C	-3.064445	-0.504118	-1.042126
C	-2.015161	0.536344	-0.795914
C	-1.521588	0.587134	0.691583
H	-2.576482	1.874077	1.623920
H	0.577925	3.712702	0.523331
H	5.501605	0.003171	-0.401989
H	4.891395	-0.022652	-2.042447
H	5.354182	1.520368	-1.304873
H	4.323215	-2.968874	-0.753995
H	-0.747005	-3.014329	1.345333
H	2.432563	-3.740547	0.081249
H	3.734645	2.874227	-0.692520
H	-6.047625	-1.555482	-0.622630
H	-5.865524	-1.278138	-2.347710
H	-4.771408	-2.399153	-1.518335
H	-5.614312	1.267164	-1.903785
H	-5.799420	0.969155	-0.183225
H	-4.381290	1.839081	-0.767579
H	-2.695457	-1.520816	-1.160405
H	-1.153716	0.351597	-1.443743
H	-2.379627	1.539457	-1.024197

ωB97X Energy = -1186.35332110 a.u.

(*S*)-**3modEt**, Conf A

O	-3.413904	1.193749	-1.360426
O	-0.363694	-2.771018	-2.146472
C	3.996364	-1.433805	-0.736754
O	4.079645	1.032334	0.302849
O	0.394215	3.893244	0.603441
O	-2.385102	-1.227090	-1.877530
O	-1.907089	3.018694	-0.143083

C	2.768165	1.248757	0.119912
C	2.223107	2.462872	0.455127
C	0.859147	2.690048	0.279711
C	0.342701	-1.794368	-1.581382
C	1.717109	-2.017280	-1.413702
C	2.539754	-1.075461	-0.859489
C	1.984371	0.183465	-0.440586
C	-1.669688	-0.421413	-1.283886
C	-0.236924	-0.599659	-1.149640
C	0.594559	0.412768	-0.581347
C	0.025238	1.670045	-0.201605
C	-1.383957	1.909854	-0.312628
C	-1.942922	-2.657573	1.352720
C	-0.368816	-1.683701	3.100652
C	-1.432349	-1.432417	2.059966
C	-1.837905	-0.189088	1.801802
C	-2.866132	0.239107	0.795161
C	-2.331057	0.750539	-0.580466
C	0.918401	-2.263681	2.512616
H	-3.582266	2.105800	-1.086958
H	-1.294273	-2.454480	-2.223040
H	4.626276	-0.731720	-1.281547
H	4.322227	-1.412989	0.302863
H	4.158555	-2.434279	-1.135483
H	4.496555	1.814594	0.679909
H	-0.568754	3.906415	0.397698
H	2.840703	3.259408	0.853218
H	2.115761	-2.967327	-1.747899
H	-2.863561	-2.479106	0.798332
H	-1.198389	-3.031573	0.642784
H	-2.125581	-3.460744	2.071359
H	-0.143857	-0.748554	3.619427
H	-0.763656	-2.378547	3.850484
H	-1.381405	0.616903	2.372801
H	-3.566949	-0.561172	0.552544
H	-3.449284	1.072221	1.197031
H	1.672643	-2.395936	3.290571
H	0.748055	-3.237178	2.047556
H	1.329633	-1.595080	1.751038

ωB97X Energy = -1225.67227205 a.u.

(*S*)-**3modEt**, Conf B

O	3.397040	1.312234	-1.318431
O	-0.581376	3.861281	0.516824
C	-4.330495	0.920625	0.229704
O	-3.724121	-1.498853	-0.742819
O	0.556781	-2.805816	-2.092366
O	1.770134	3.097281	-0.142991
O	2.491454	-1.130094	-1.835537
C	-2.421666	-1.211071	-0.887810
C	-1.570451	-2.150272	-1.414470
C	-0.215258	-1.860622	-1.562243
C	-0.973110	2.630312	0.199006
C	-2.336395	2.336181	0.348975
C	-2.851148	1.110370	0.027970
C	-1.974034	0.093582	-0.487843
C	1.329333	1.964809	-0.333050
C	-0.084842	1.651370	-0.252280
C	-0.590313	0.365010	-0.611972
C	0.297544	-0.625712	-1.139514
C	1.704333	-0.376027	-1.248349
C	1.947324	-2.516806	1.470610
C	0.356393	-1.516779	3.188374

C	1.417507	-1.279593	2.141663
C	1.807798	-0.038586	1.850752
C	2.839265	0.374642	0.841194
C	2.315972	0.833090	-0.557976
C	-0.932235	-2.107023	2.613931
H	3.793143	0.535071	-1.735846
H	0.386209	3.917770	0.336878
H	-4.831089	0.682039	-0.708018
H	-4.535206	0.100381	0.916876
H	-4.761505	1.834999	0.635142
H	-3.903602	-2.392471	-1.054607
H	1.468687	-2.440795	-2.164971
H	-1.937084	-3.121782	-1.724588
H	-2.980959	3.121124	0.725219
H	1.200311	-2.935525	0.789006
H	2.853276	-2.336740	0.892831
H	2.163761	-3.287936	2.214575
H	0.754513	-2.199351	3.947579
H	0.131334	-0.574304	3.693571
H	1.339620	0.777182	2.398091
H	3.401136	1.233811	1.214934
H	3.558321	-0.422524	0.641662
H	-1.352870	-1.443451	1.853173
H	-0.760773	-3.082082	2.152523
H	-1.679658	-2.238683	3.398503

ωB97X Energy = -1225.67221163 a.u.

(*S*)-**3modEt**, Conf C

O	-3.414253	1.234797	-1.337732
O	-0.420391	-2.786538	-2.121522
C	3.962285	-1.498265	-0.732659
O	4.095992	0.992156	0.239178
O	0.443146	3.891152	0.563981
O	-2.418990	-1.170623	-1.881904
O	-1.868652	3.048168	-0.103114
C	2.783032	1.219098	0.073328
C	2.253167	2.440701	0.400224
C	0.888052	2.680787	0.240498
C	0.304768	-1.817362	-1.566793
C	1.674783	-2.059037	-1.399210
C	2.511650	-1.118947	-0.861074
C	1.978940	0.156074	-0.461335
C	-1.672158	-0.401895	-1.268582
C	-0.253347	-0.611156	-1.139143
C	0.591104	0.403525	-0.592964
C	0.035429	1.670408	-0.228373
C	-1.381556	1.935266	-0.313158
C	-1.924569	-2.609316	1.402997
C	-0.353866	-1.611869	3.140390
C	-1.416524	-1.374621	2.095386
C	-1.825458	-0.135408	1.822929
C	-2.857798	0.277422	0.814188
C	-2.330000	0.776115	-0.568930
C	0.937535	-2.191631	2.561388
H	-3.792316	0.452713	-1.761944
H	-1.342811	-2.458939	-2.212289
H	4.601196	-0.823720	-1.301296
H	4.292591	-1.449451	0.304546
H	4.106609	-2.513206	-1.100416
H	4.525166	1.775100	0.600661
H	-0.527398	3.903162	0.380275
H	2.882200	3.235915	0.782897
H	2.060215	-3.018988	-1.720118

H	-2.121800	-3.398588	2.133135
H	-2.836998	-2.436660	0.833170
H	-1.172543	-3.000264	0.710419
H	-0.134295	-0.671033	3.651067
H	-0.747622	-2.301345	3.895713
H	-1.371964	0.678859	2.384476
H	-3.557563	-0.530646	0.591080
H	-3.441382	1.116367	1.200255
H	0.772629	-3.169401	2.103407
H	1.348947	-1.527329	1.796188
H	1.689494	-2.314787	3.343026

ωB97X Energy = -1225.67208092 a.u.

(*S*)-**3modEt**, Conf D

O	3.383869	1.282984	-1.359859
O	-0.545448	3.860043	0.561266
C	-4.323058	0.953009	0.290133
O	-3.757218	-1.454344	-0.734137
O	0.502264	-2.795368	-2.115535
O	1.797818	3.070370	-0.176931
O	2.456062	-1.184353	-1.835205
C	-2.451145	-1.179520	-0.881041
C	-1.612306	-2.119135	-1.422891
C	-0.253213	-1.843277	-1.574979
C	-0.954874	2.635511	0.239639
C	-2.317621	2.351946	0.403238
C	-2.844850	1.133000	0.072603
C	-1.984647	0.113762	-0.466919
C	1.324074	1.941081	-0.333199
C	-0.082812	1.649386	-0.226883
C	-0.598893	0.370823	-0.601690
C	0.278015	-0.616229	-1.151950
C	1.699095	-0.393113	-1.268282
C	1.980194	-2.556009	1.419605
C	0.396747	-1.575884	3.155934
C	1.452425	-1.326788	2.106635
C	1.837765	-0.082100	1.825318
C	2.857266	0.344882	0.809133
C	2.313272	0.813460	-0.578240
C	-0.891239	-2.166883	2.580819
H	3.530731	2.199711	-1.090781
H	0.415306	3.918729	0.361126
H	-4.740941	1.863386	0.717559
H	-4.837066	0.735818	-0.645524
H	-4.526247	0.121504	0.964059
H	-3.947092	-2.341806	-1.056983
H	1.421518	-2.437929	-2.176149
H	-1.989194	-3.084196	-1.740977
H	-2.952464	3.137104	0.794999
H	2.892927	-2.371603	0.854205
H	2.183305	-3.341338	2.152335
H	1.237171	-2.957051	0.723057
H	0.800123	-2.262800	3.908429
H	0.169685	-0.638139	3.669021
H	1.370812	0.726550	2.384194
H	3.421066	1.199521	1.193144
H	3.575992	-0.444974	0.585568
H	-1.636502	-2.306064	3.366152
H	-1.315813	-1.500192	1.824938
H	-0.717272	-3.138410	2.112940

ωB97X Energy = -1225.67194373 a.u.

(*S*)-**3modEt**, Conf E

O	1.798134	2.598834	-1.307073
O	-2.970080	3.109259	0.445246
C	-4.732704	-1.298800	0.975673
O	-3.036008	-3.231751	0.212110
O	1.185249	-2.439024	-1.646072
O	-0.582438	3.495835	-0.443185
O	1.984645	0.024523	-1.858381
C	-2.076082	-2.364587	-0.146484
C	-0.909882	-2.828237	-0.704185
C	0.089696	-1.932554	-1.080798
C	-2.704180	1.810502	0.322543
C	-3.721637	0.912474	0.680026
C	-3.564391	-0.441882	0.567987
C	-2.323423	-0.966108	0.063822
C	-0.406356	2.280971	-0.416305
C	-1.470585	1.335174	-0.122050
C	-1.281455	-0.071942	-0.279502
C	-0.058296	-0.563171	-0.833851
C	1.011587	0.337708	-1.166886
C	2.450490	-1.228860	1.754383
C	4.833122	-0.440585	1.342059
C	3.361578	-0.104681	1.342243
C	2.950930	1.109944	0.976074
C	1.538045	1.604484	0.910311
C	1.001051	1.727706	-0.557093
C	5.193185	-1.567588	0.373497
H	2.441774	2.041059	-1.766827
H	-2.180700	3.604431	0.128560
H	-4.459408	-1.988182	1.773645
H	-5.545818	-0.662757	1.322890
H	-5.090216	-1.903456	0.142863
H	-2.759397	-4.133638	0.017287
H	1.763578	-1.689263	-1.908043
H	-0.757451	-3.887340	-0.875092
H	-4.653054	1.329102	1.043475
H	2.839613	-1.721666	2.649369
H	1.430795	-0.904872	1.959437
H	2.403257	-1.991206	0.970348
H	5.406563	0.455131	1.091286
H	5.127903	-0.734330	2.356050
H	3.706765	1.834450	0.682923
H	0.858887	0.978335	1.490384
H	1.480813	2.616918	1.319475
H	4.885580	-1.316500	-0.644992
H	6.270921	-1.740483	0.367972
H	4.709420	-2.506922	0.649034

ωB97X Energy = -1225.67133038 a.u.

(*S*)-**3modEt**, Conf F

O	-1.798869	2.591617	-1.309184
O	-1.158652	-2.453739	-1.630333
C	3.132914	-3.432113	0.231131
O	4.529502	-1.246817	0.917546
O	2.955400	3.132635	0.440548
O	-1.968260	0.013067	-1.863412
O	0.566191	3.501141	-0.423437
C	3.543806	-0.404848	0.566402
C	3.726565	0.949408	0.680723
C	2.705105	1.831209	0.322427
C	-0.068999	-1.932189	-1.065627
C	0.944342	-2.820908	-0.682493
C	2.118056	-2.381030	-0.130014

C	2.323182	-0.971284	0.064541
C	-1.005373	0.334277	-1.166330
C	0.071167	-0.566481	-0.825813
C	1.289166	-0.066003	-0.274540
C	1.468773	1.344992	-0.120735
C	0.403358	2.281542	-0.407436
C	-2.469838	-1.241276	1.736248
C	-4.849261	-0.446507	1.317827
C	-3.376999	-0.113903	1.324254
C	-2.962107	1.101334	0.964661
C	-1.547853	1.592988	0.907889
C	-1.002523	1.722286	-0.555930
C	-5.208349	-1.571167	0.346219
H	-2.445402	2.035233	-1.765967
H	-1.743489	-1.714802	-1.902988
H	2.731198	-4.418491	0.003611
H	4.061636	-3.293987	-0.321179
H	3.384508	-3.390731	1.290291
H	5.292799	-0.750879	1.232726
H	2.153632	3.614770	0.128957
H	4.663848	1.356198	1.041856
H	0.779326	-3.877690	-0.852774
H	-1.449466	-0.920662	1.943283
H	-2.861627	-1.733935	2.630137
H	-2.423807	-2.003068	0.951634
H	-5.148371	-0.741205	2.330268
H	-5.419678	0.450969	1.066491
H	-3.715195	1.828784	0.671741
H	-1.490174	2.603598	1.321295
H	-0.872308	0.963516	1.488579
H	-6.286538	-1.740914	0.335759
H	-4.895620	-1.319641	-0.670598
H	-4.728562	-2.512266	0.622629

ωB97X Energy = -1225.67116454 a.u.

(*S*)-**3modEt**, Conf G

O	2.170828	-1.432357	1.599922
O	-2.129596	-3.572014	-0.091800
C	-5.109454	-0.010218	-1.208352
O	-4.119932	2.424491	-0.670650
O	0.077581	3.192003	1.247330
O	0.222506	-3.102811	0.841006
O	1.599323	1.152562	1.726746
C	-2.952975	1.942584	-0.214152
C	-2.004327	2.803963	0.278352
C	-0.789223	2.310902	0.752441
C	-2.270142	-2.249180	-0.145089
C	-3.494910	-1.754807	-0.618594
C	-3.756917	-0.413690	-0.685357
C	-2.754676	0.520802	-0.248748
C	0.030439	-1.904768	0.650579
C	-1.254414	-1.369860	0.231154
C	-1.502258	0.036480	0.199239
C	-0.504158	0.941772	0.679525
C	0.779123	0.461433	1.114931
C	4.756563	-1.598023	-0.706405
C	5.267811	0.842802	-1.057638
C	4.199893	-0.212126	-0.882918
C	2.900337	0.083827	-0.895139
C	1.757854	-0.875308	-0.745560
C	1.202115	-0.943212	0.719086
C	4.798857	2.274885	-1.262800
H	2.709065	-0.670549	1.854749

H	-1.241247	-3.759899	0.288415
H	-5.672832	-0.901283	-1.482123
H	-5.674196	0.546464	-0.461319
H	-5.020872	0.632309	-2.083507
H	-4.138036	3.384102	-0.588935
H	0.855805	2.691733	1.580403
H	-2.188307	3.871092	0.318239
H	-4.241604	-2.476459	-0.926532
H	3.990912	-2.353060	-0.541216
H	5.344381	-1.882934	-1.583970
H	5.436537	-1.619927	0.149883
H	5.925595	0.796240	-0.181856
H	5.898133	0.539691	-1.901950
H	2.611582	1.122702	-1.025807
H	0.945413	-0.588301	-1.418431
H	2.043502	-1.898010	-0.995401
H	5.657359	2.939843	-1.370922
H	4.187336	2.372094	-2.162746
H	4.208566	2.629621	-0.414743

ωB97X Energy = -1225.67053394 a.u.

(*S*)-**3modEt**, Conf H

O	-2.176566	-1.412271	1.593587
O	-0.028919	3.197915	1.232414
C	4.293214	2.560470	-0.700838
O	4.910024	-0.013949	-1.129400
O	2.087137	-3.597531	-0.097563
O	-1.572598	1.169042	1.729161
O	-0.260207	-3.102165	0.805947
C	3.727791	-0.459342	-0.673531
C	3.481726	-1.807030	-0.612862
C	2.252327	-2.278350	-0.149160
C	0.823177	2.299910	0.740420
C	2.052865	2.775163	0.263970
C	3.012382	1.929455	-0.224695
C	2.762644	0.513326	-0.244572
C	-0.768923	0.469036	1.111428
C	0.524060	0.939449	0.671434
C	1.509159	0.022512	0.193812
C	1.242340	-1.382729	0.225766
C	-0.045496	-1.902730	0.631356
C	-4.766555	-1.571315	-0.692417
C	-5.285925	0.870082	-1.026889
C	-4.214361	-0.183058	-0.864585
C	-2.915420	0.115827	-0.884326
C	-1.770445	-0.842949	-0.750607
C	-1.207405	-0.927772	0.710263
C	-4.822047	2.303815	-1.231822
H	-2.724025	-0.653022	1.835159
H	-0.813248	2.715412	1.572746
H	4.228359	3.641831	-0.588694
H	5.149210	2.198831	-0.132374
H	4.484989	2.326288	-1.747329
H	5.471697	-0.757058	-1.374319
H	1.188617	-3.765545	0.272957
H	4.233422	-2.524532	-0.920443
H	2.230813	3.842730	0.306209
H	-5.360274	-1.852105	-1.567312
H	-3.998052	-2.325624	-0.537505
H	-5.440072	-1.599941	0.168765
H	-5.922296	0.567892	-1.866957
H	-5.936479	0.819291	-0.145967
H	-2.629992	1.156090	-1.011242

H	-2.055927	-1.863151	-1.010485
H	-0.961279	-0.547950	-1.423904
H	-5.683050	2.966722	-1.332334
H	-4.226806	2.658245	-0.387130
H	-4.217232	2.404651	-2.135887

ωB97X Energy = -1225.67039109 a.u.

(*S*)-**3modEt**, Conf I

O	-3.469324	1.199850	-1.296566
O	-0.390209	-2.794051	-2.114207
C	3.982399	-1.489582	-0.715237
O	4.099545	0.992804	0.275314
O	0.441402	3.886629	0.576104
O	-2.387971	-1.218883	-1.876805
O	-1.858100	3.044978	-0.123004
C	2.787687	1.218829	0.097981
C	2.254232	2.438956	0.424449
C	0.890329	2.677106	0.254204
C	0.326824	-1.818670	-1.559958
C	1.697997	-2.055549	-1.388099
C	2.530529	-1.114883	-0.846783
C	1.990180	0.156761	-0.447631
C	-1.667985	-0.419031	-1.279030
C	-0.239278	-0.612408	-1.141667
C	0.601736	0.400307	-0.588207
C	0.042944	1.665533	-0.222305
C	-1.371915	1.928374	-0.320078
C	-1.964774	-2.610468	1.384969
C	-0.397228	-1.613907	3.125516
C	-1.454690	-1.375613	2.075625
C	-1.854600	-0.135303	1.795643
C	-2.878680	0.277894	0.779061
C	-2.333097	0.771425	-0.591036
C	0.892285	-2.203113	2.551741
H	-3.210301	1.514121	-2.168510
H	-1.316084	-2.465694	-2.198237
H	4.132034	-2.499953	-1.093507
H	4.621965	-0.806717	-1.273009
H	4.307519	-1.451858	0.324107
H	4.523995	1.775093	0.643620
H	-0.527015	3.897840	0.381114
H	2.879061	3.233699	0.814941
H	2.085999	-3.014954	-1.707841
H	-2.881480	-2.438516	0.822105
H	-1.216767	-2.997618	0.685864
H	-2.154304	-3.401491	2.115189
H	-0.173926	-0.672162	3.632910
H	-0.796895	-2.298229	3.882386
H	-1.399333	0.678671	2.356102
H	-3.576160	-0.527350	0.543579
H	-3.463882	1.118068	1.160230
H	1.308288	-1.544941	1.783701
H	1.642288	-2.326281	3.335251
H	0.722890	-3.182279	2.098368

ωB97X Energy = -1225.669

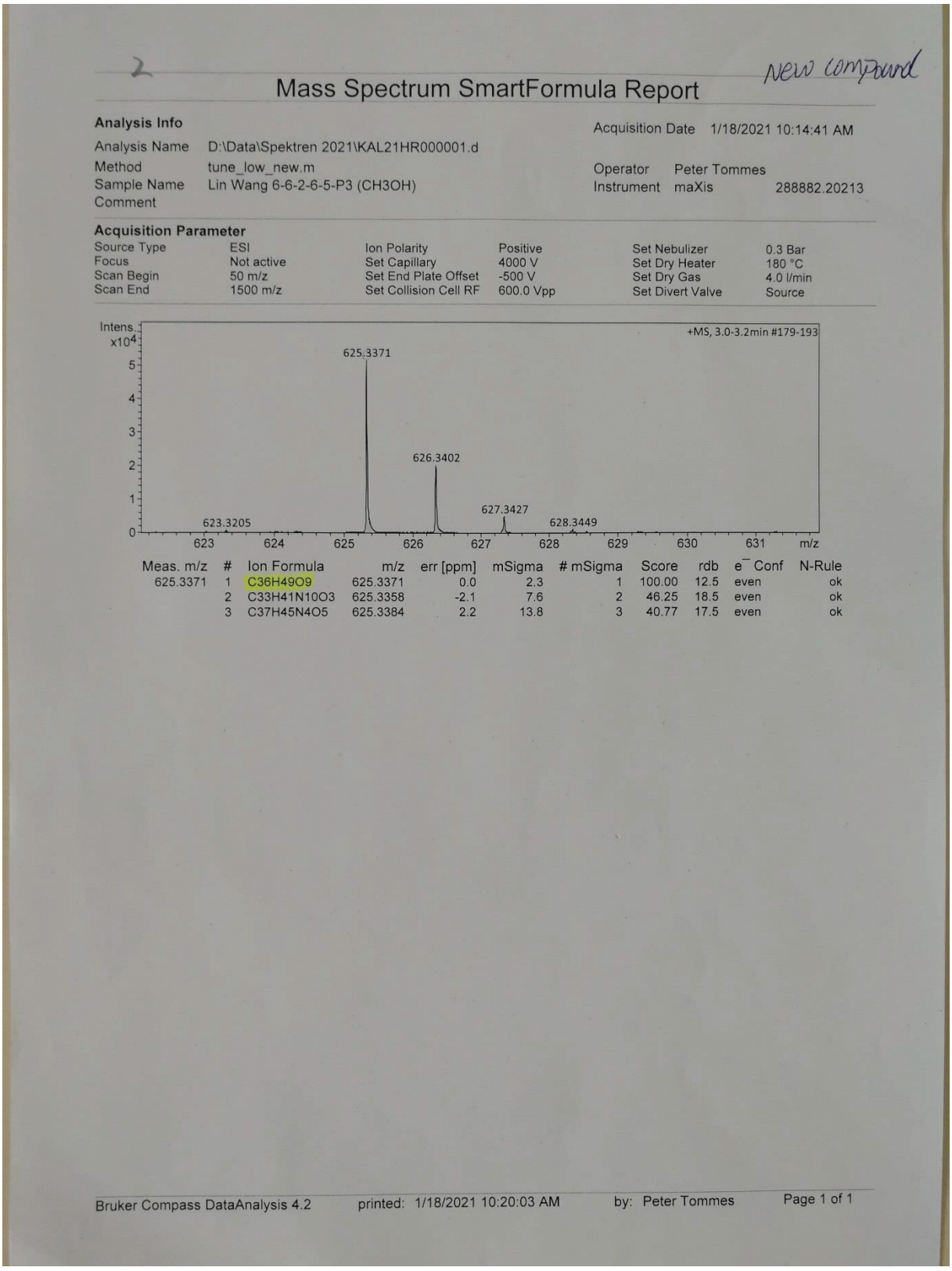

2 new compound

Mass Spectrum SmartFormula Report

Analysis Info

Analysis Name	D:\Data\Spektren 2021\KAL21HR000001.d	Acquisition Date	1/18/2021 10:14:41 AM
Method	tune_low_new.m	Operator	Peter Tommes
Sample Name	Lin Wang 6-6-2-6-5-P3 (CH3OH)	Instrument	maXis 288882.20213
Comment			

Acquisition Parameter

Source Type	ESI	Ion Polarity	Positive	Set Nebulizer	0.3 Bar
Focus	Not active	Set Capillary	4000 V	Set Dry Heater	180 °C
Scan Begin	50 m/z	Set End Plate Offset	-500 V	Set Dry Gas	4.0 l/min
Scan End	1500 m/z	Set Collision Cell RF	600.0 Vpp	Set Divert Valve	Source

Meas. m/z	#	Ion Formula	m/z	err [ppm]	mSigma	# mSigma	Score	rdb	e⁻ Conf	N-Rule
625.3371	1	C36H49O9	625.3371	0.0	2.3	1	100.00	12.5	even	ok
	2	C33H41N10O3	625.3358	-2.1	7.6	2	46.25	18.5	even	ok
	3	C37H45N4O5	625.3384	2.2	13.8	3	40.77	17.5	even	ok

Bruker Compass DataAnalysis 4.2 printed: 1/18/2021 10:20:03 AM by: Peter Tommes Page 1 of 1

Fig. S10. HRESIMS of Compound **1**

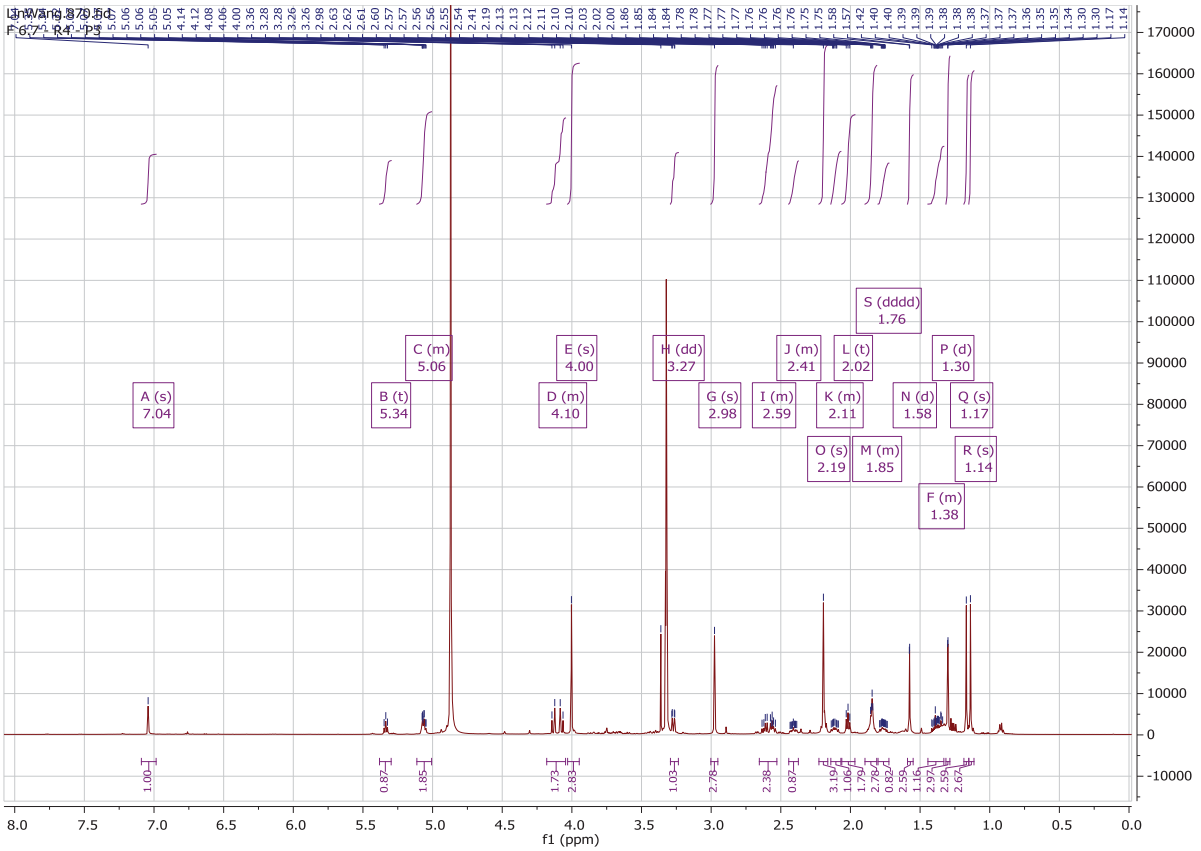

Fig. S11. ^{1}H NMR spectrum of Compound **1**

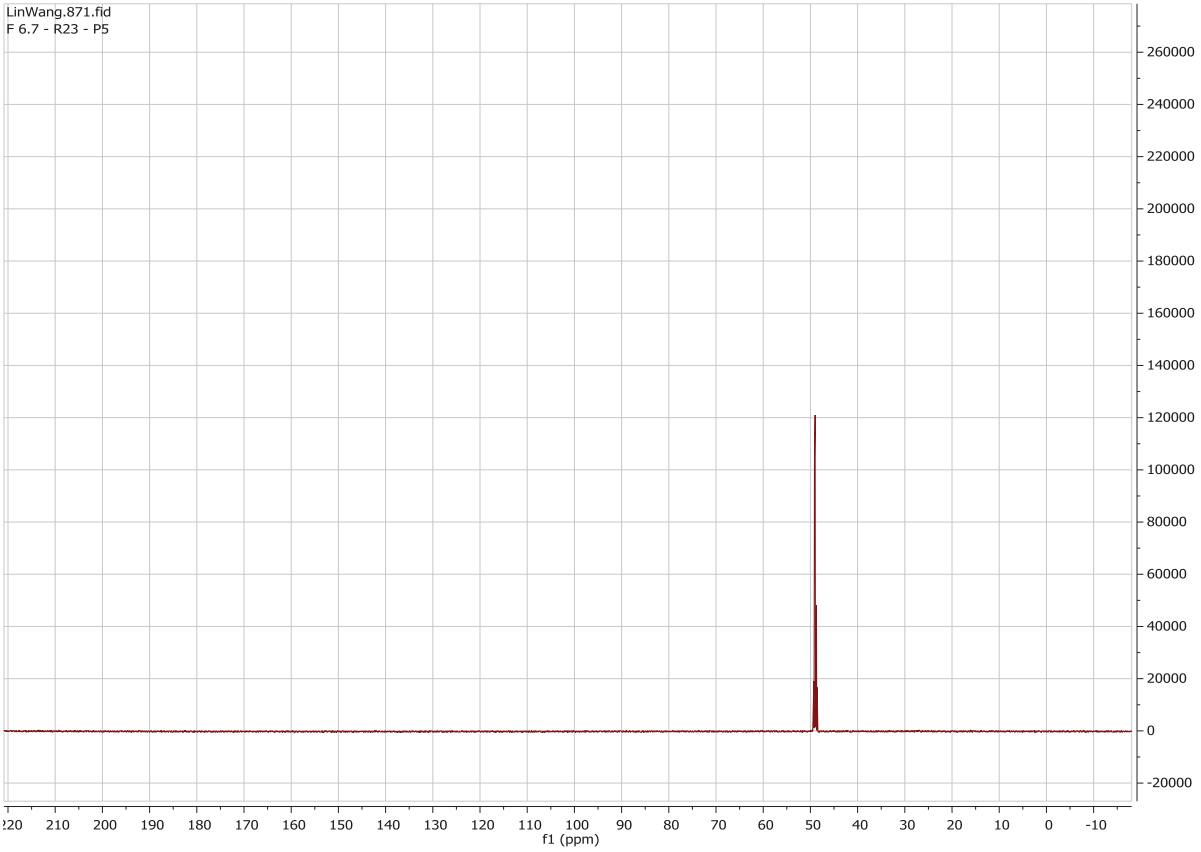

Fig. S12. ^{13}C NMR of Compound **1.**

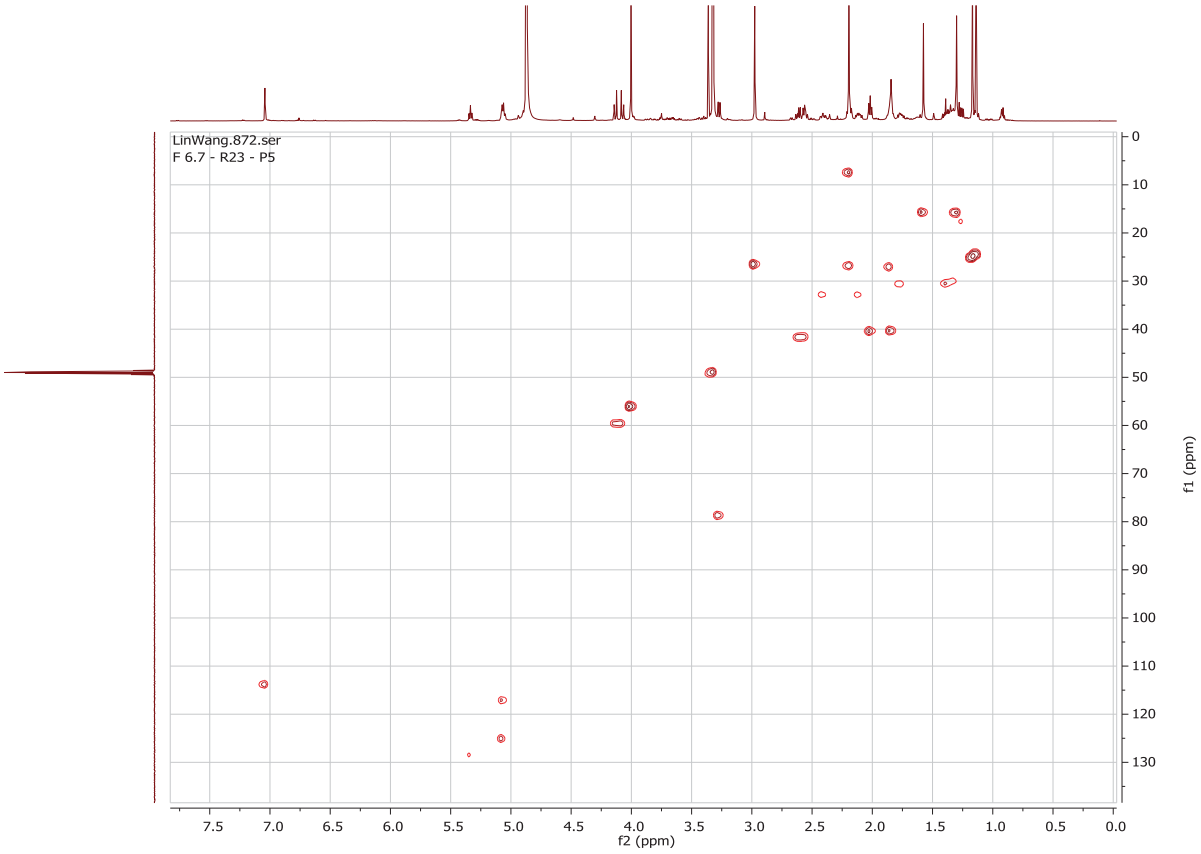

Fig. S13. ^{1}H-^{13}C HSQC of Compound **1**

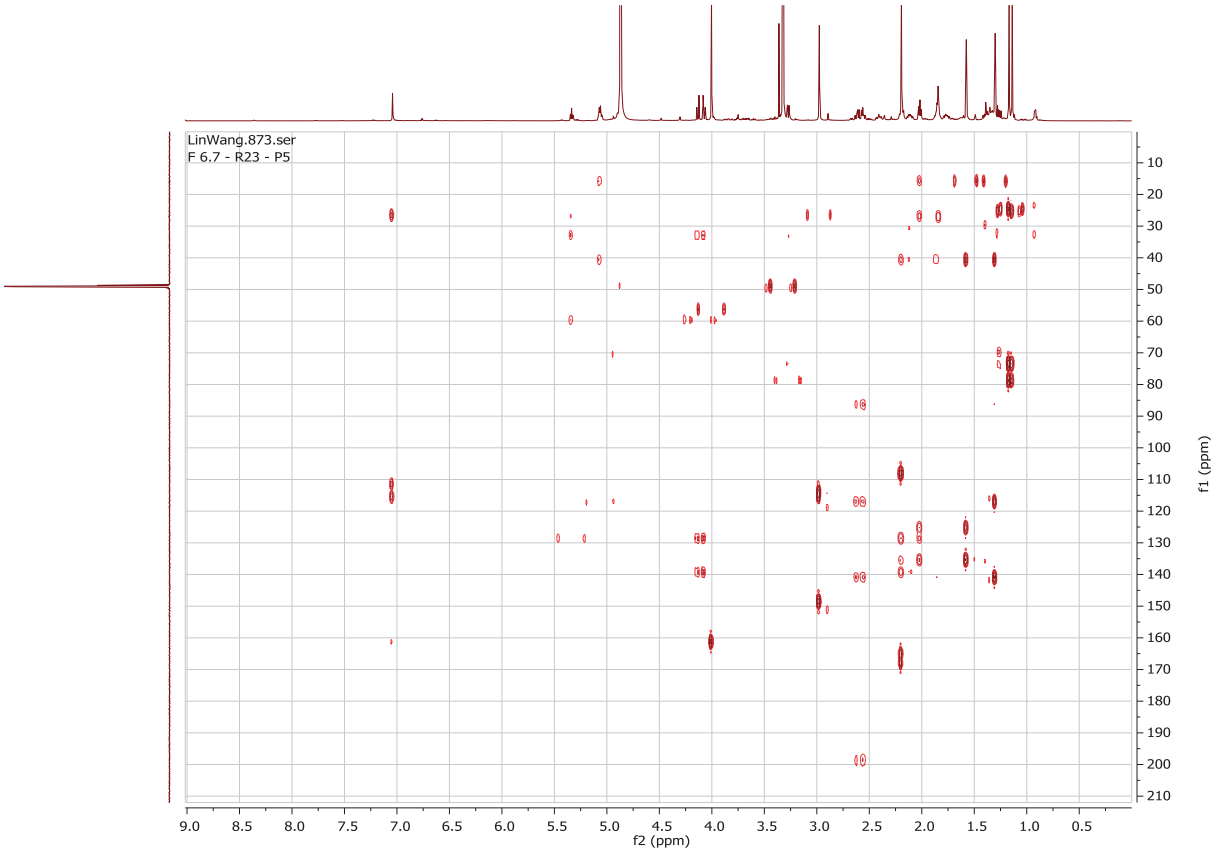

Fig. S14. ^{1}H-^{13}C HMBC of Compound **1**

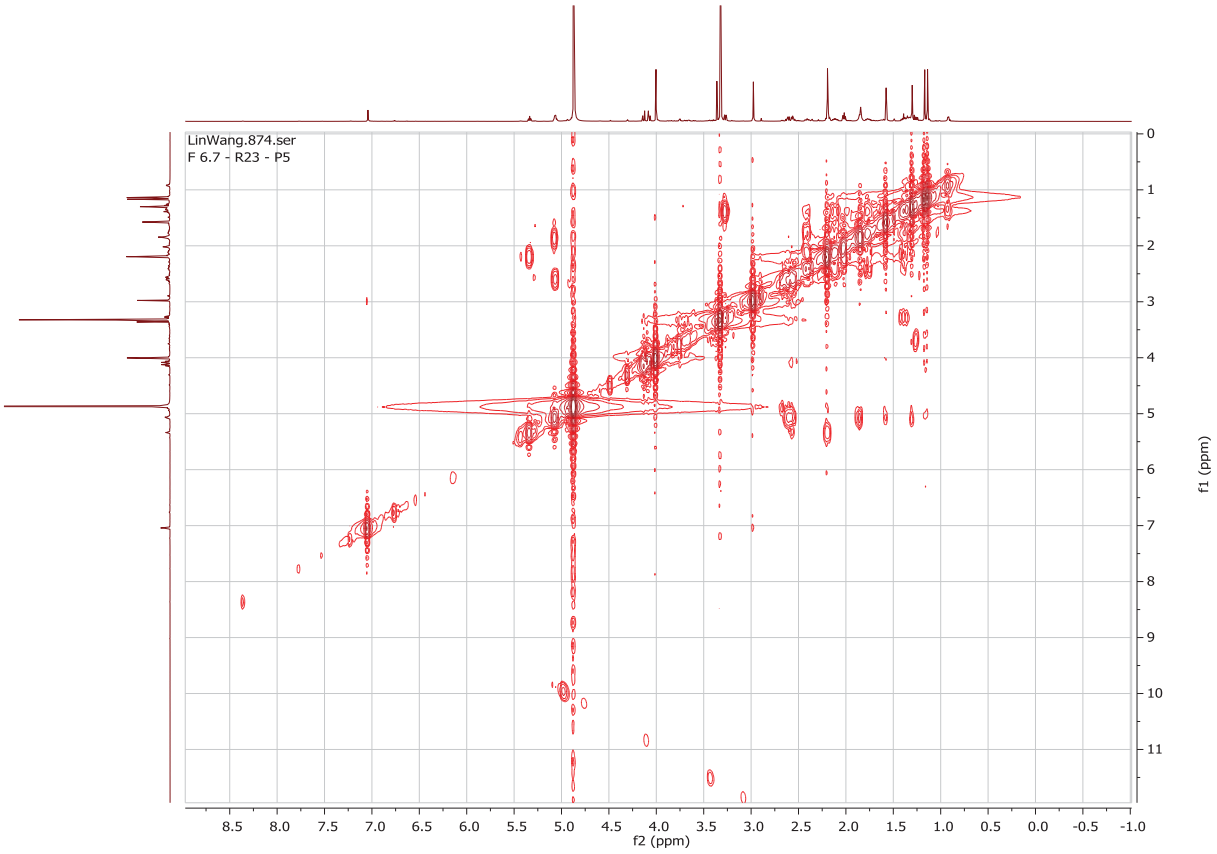

Fig. S15. ^{1}H-^{1}H COSY of Compound **1**

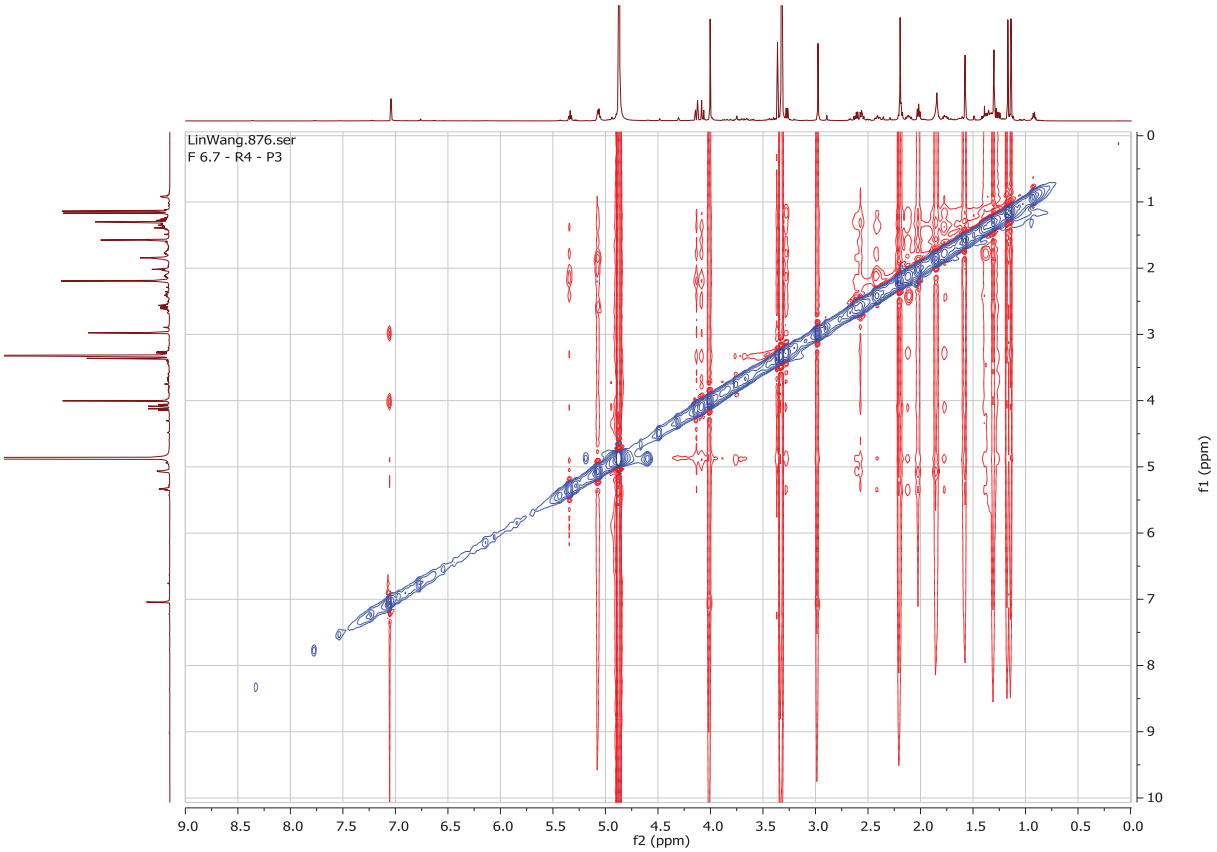

Fig. S16 ^{1}H-^{1}H ROESY of Compound **1**

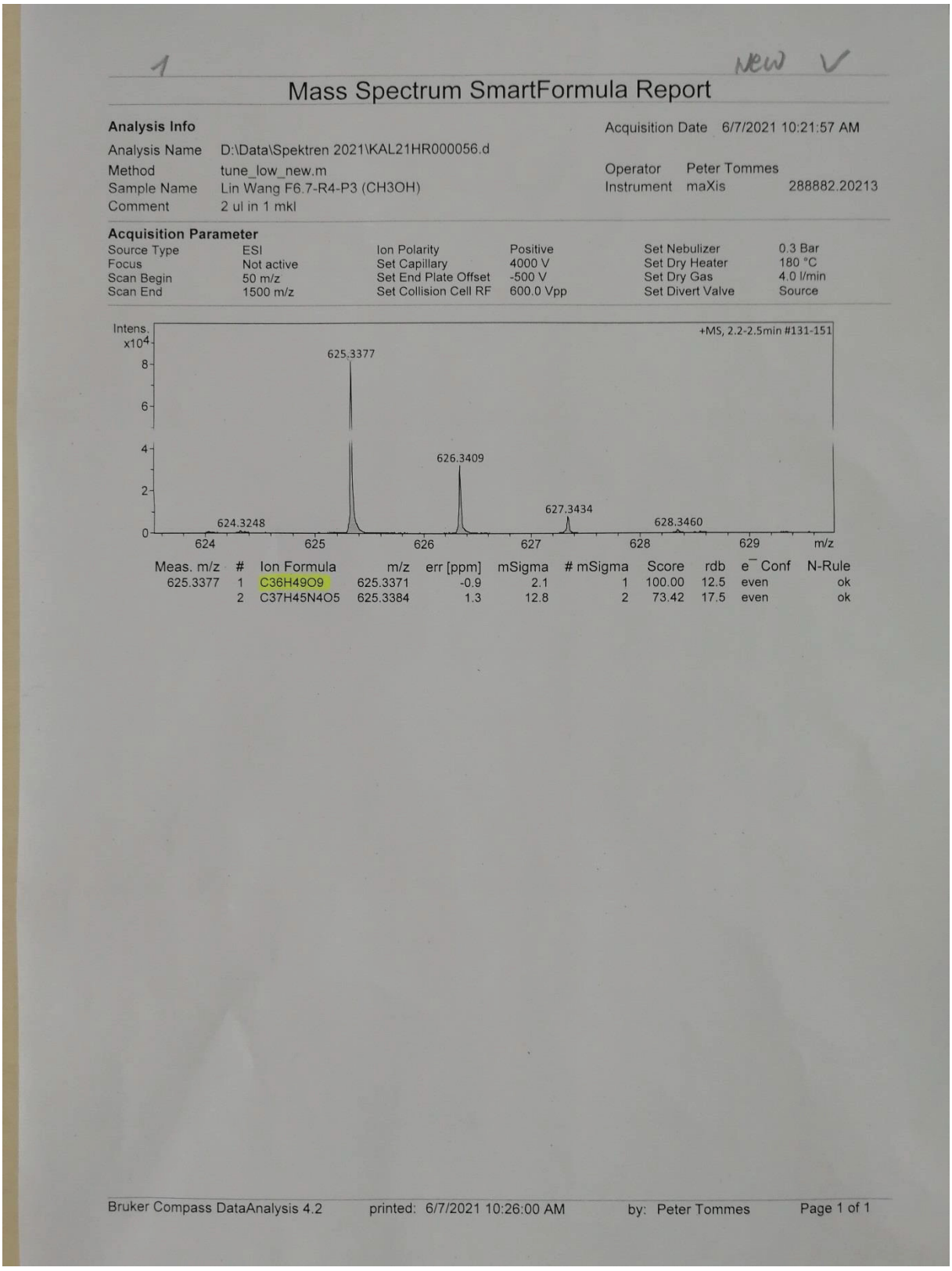

1 NEW ✓

Mass Spectrum SmartFormula Report

Analysis Info

Acquisition Date 6/7/2021 10:21:57 AM

Analysis Name	D:\Data\Spektren 2021\KAL21HR000056.d		
Method	tune_low_new.m	Operator	Peter Tommes
Sample Name	Lin Wang F6.7-R4-P3 (CH3OH)	Instrument	maXis 288882.20213
Comment	2 ul in 1 mkl		

Acquisition Parameter

Source Type	ESI	Ion Polarity	Positive	Set Nebulizer	0.3 Bar
Focus	Not active	Set Capillary	4000 V	Set Dry Heater	180 °C
Scan Begin	50 m/z	Set End Plate Offset	-500 V	Set Dry Gas	4.0 l/min
Scan End	1500 m/z	Set Collision Cell RF	600.0 Vpp	Set Divert Valve	Source

Meas. m/z	#	Ion Formula	m/z	err [ppm]	mSigma	# mSigma	Score	rdb	e⁻ Conf	N-Rule
625.3377	1	C36H49O9	625.3371	-0.9	2.1	1	100.00	12.5	even	ok
	2	C37H45N4O5	625.3384	1.3	12.8	2	73.42	17.5	even	ok

Bruker Compass DataAnalysis 4.2 printed: 6/7/2021 10:26:00 AM by: Peter Tommes Page 1 of 1

Fig. S17. HRESIMS of Compound **2**

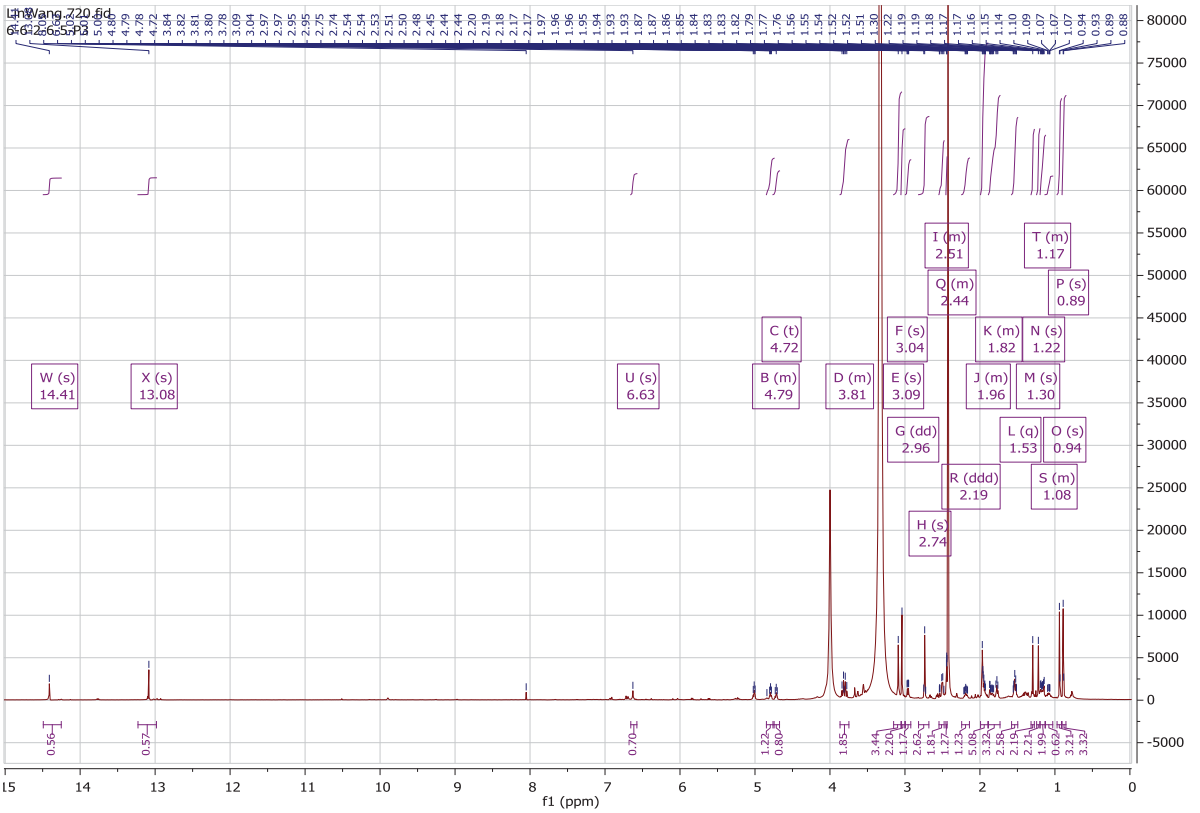

Fig. S18. ^{1}H NMR spectrum of Compound **2**

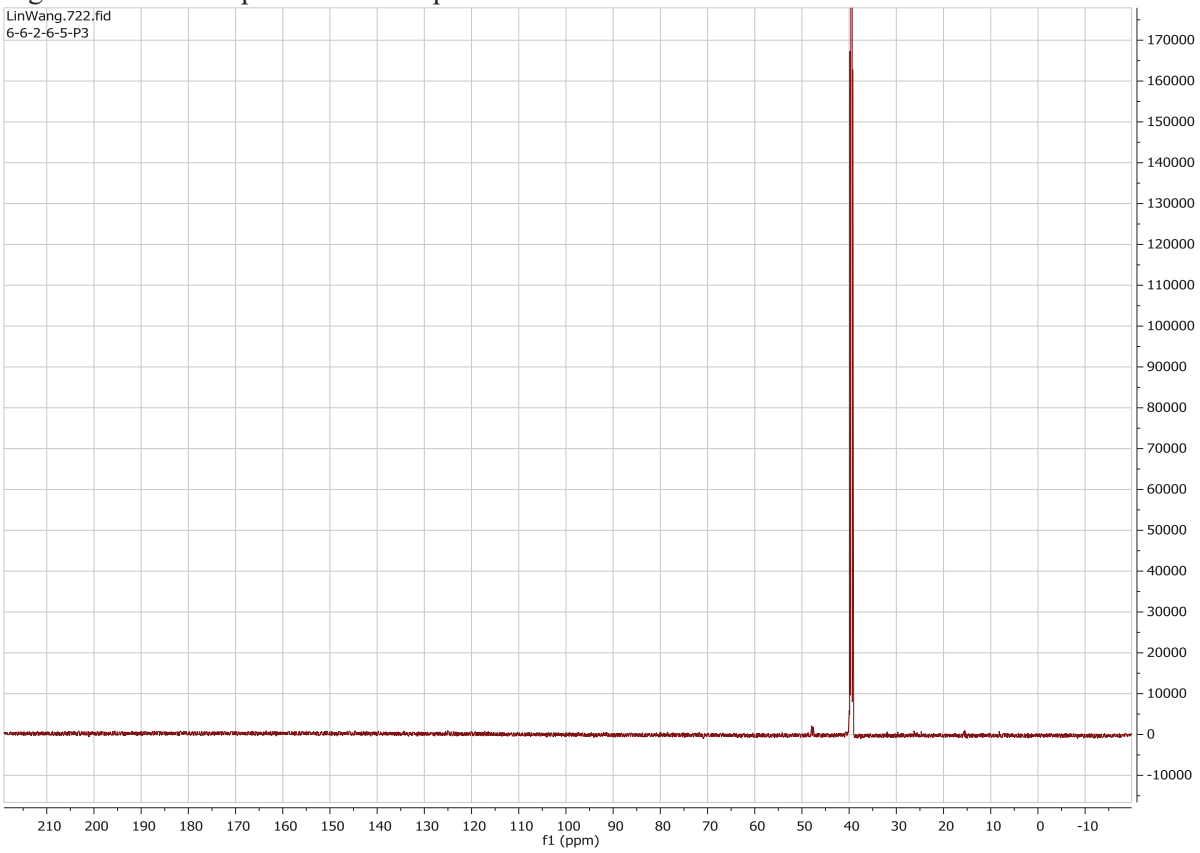

Fig. S19. ^{13}C NMR of Compound **2**

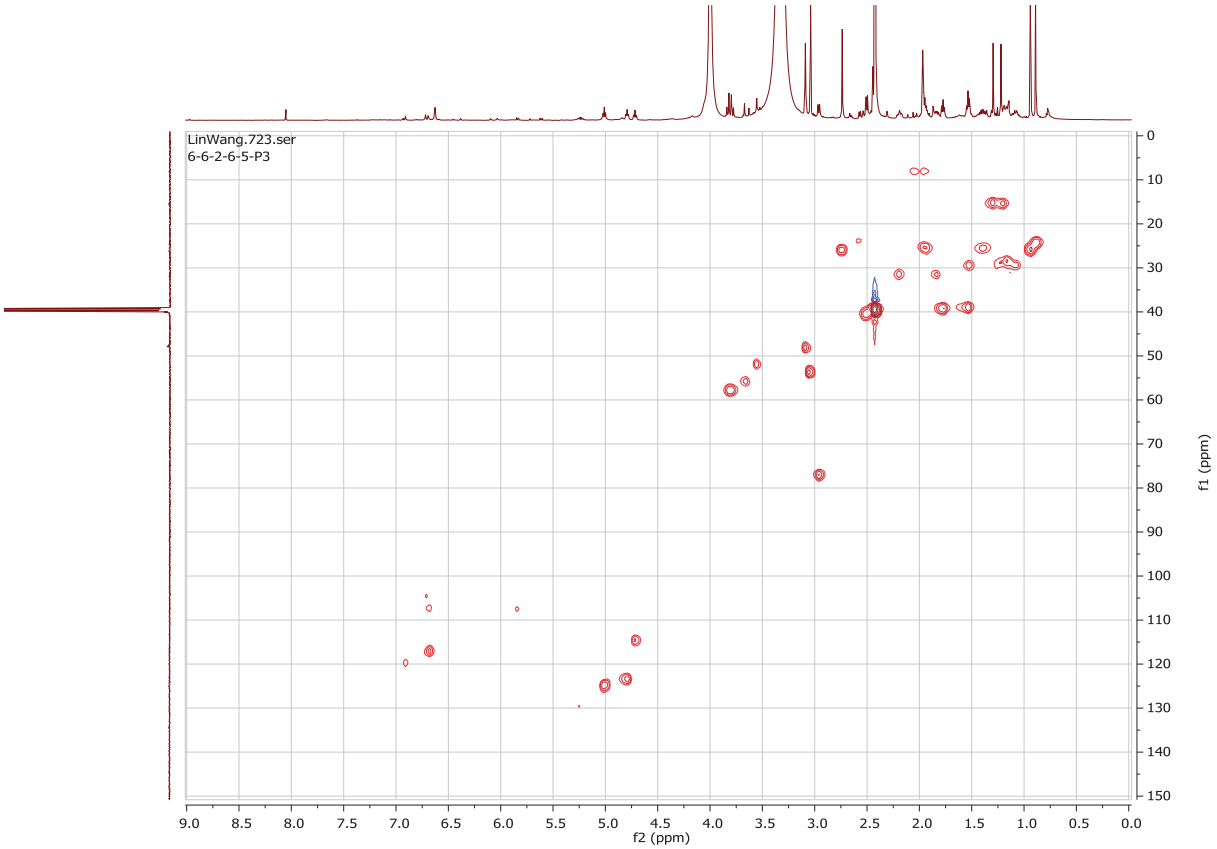

Fig. S20. ^{1}H-^{13}C HSQC of Compound **2**

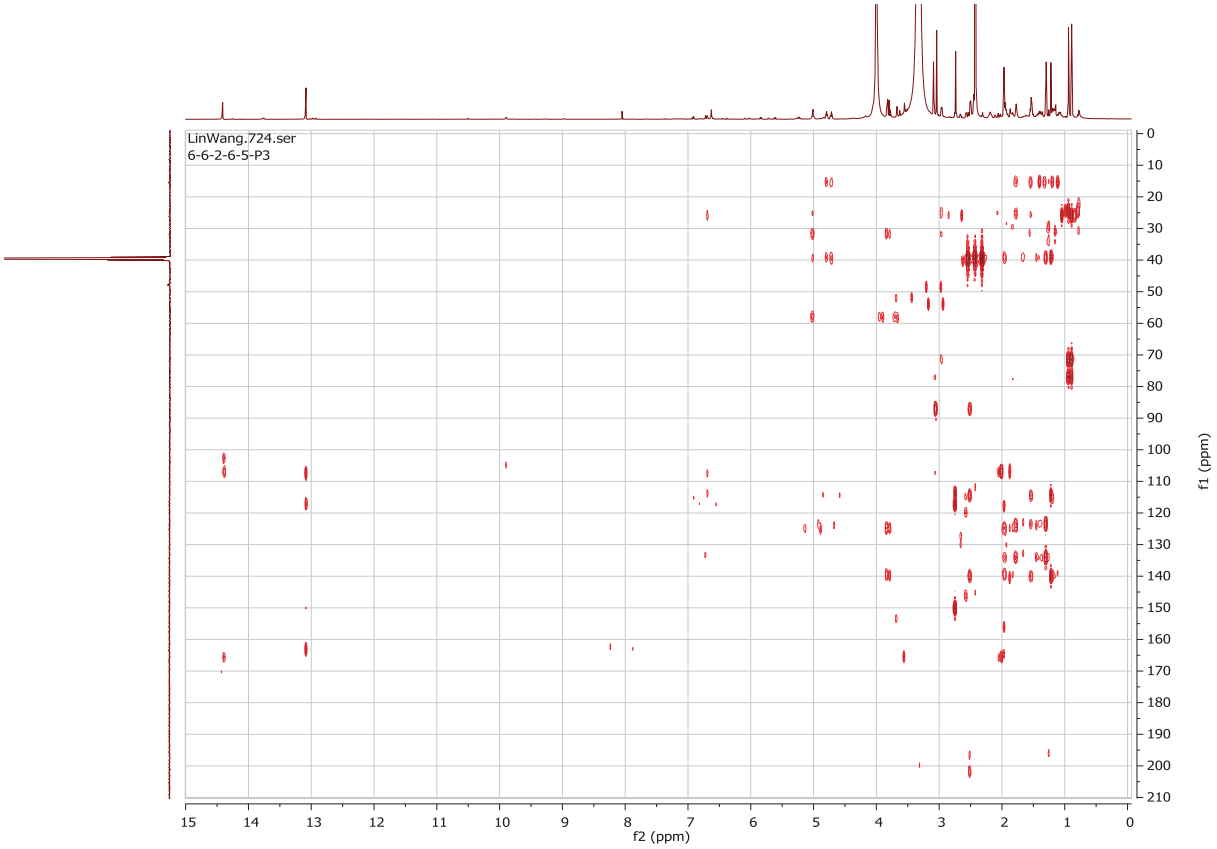

Fig. S21. ^{1}H-^{13}C HMBC of Compound **2**

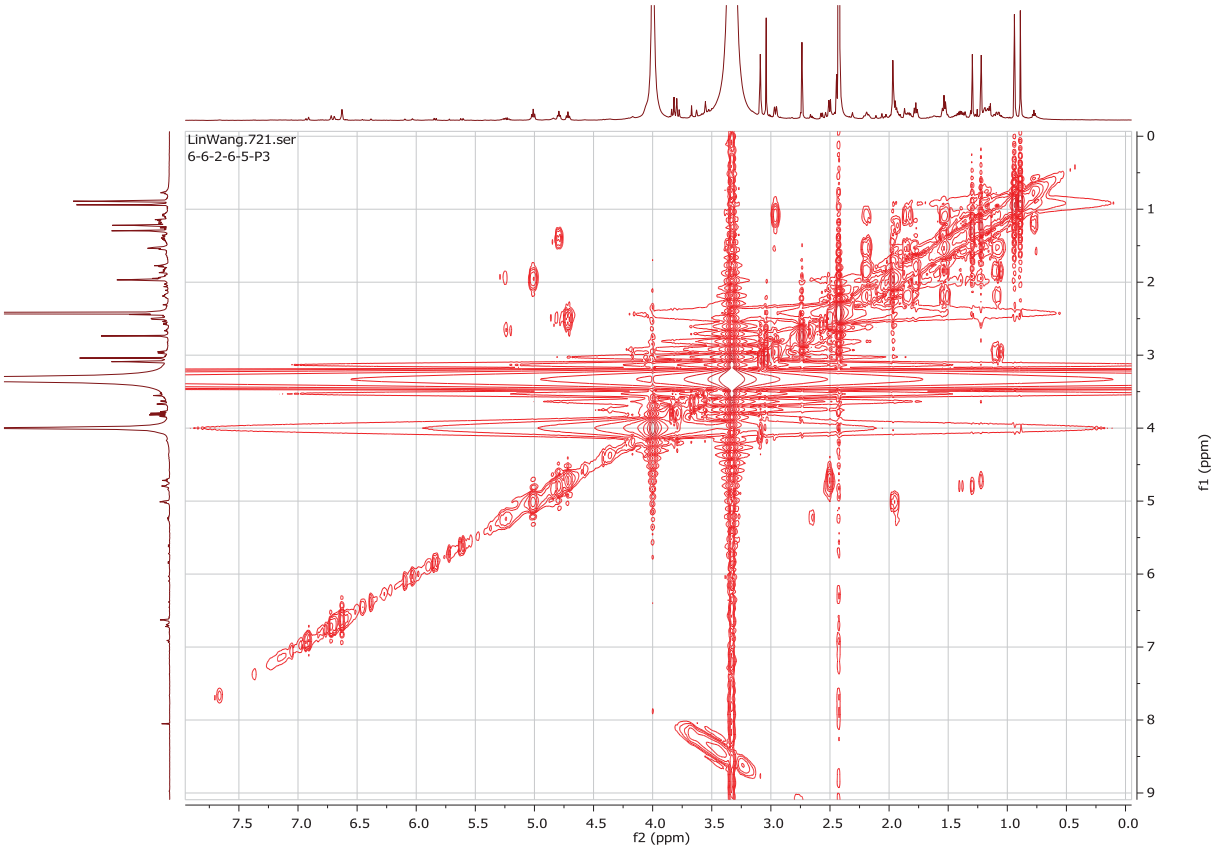

Fig. S22. ^{1}H-^{1}H COSY of Compound **2**

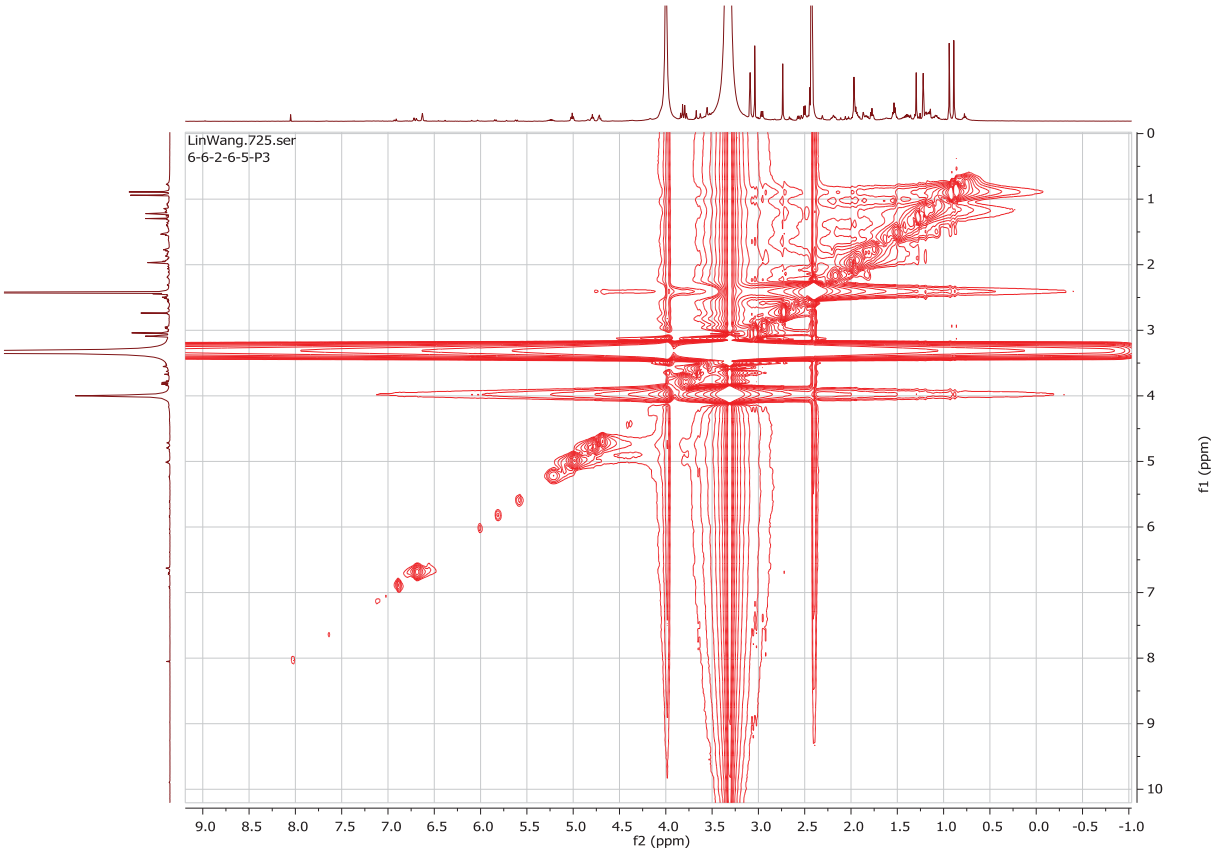

Fig. S23**.** ^{1}H-^{1}H ROESY of Compound **2**

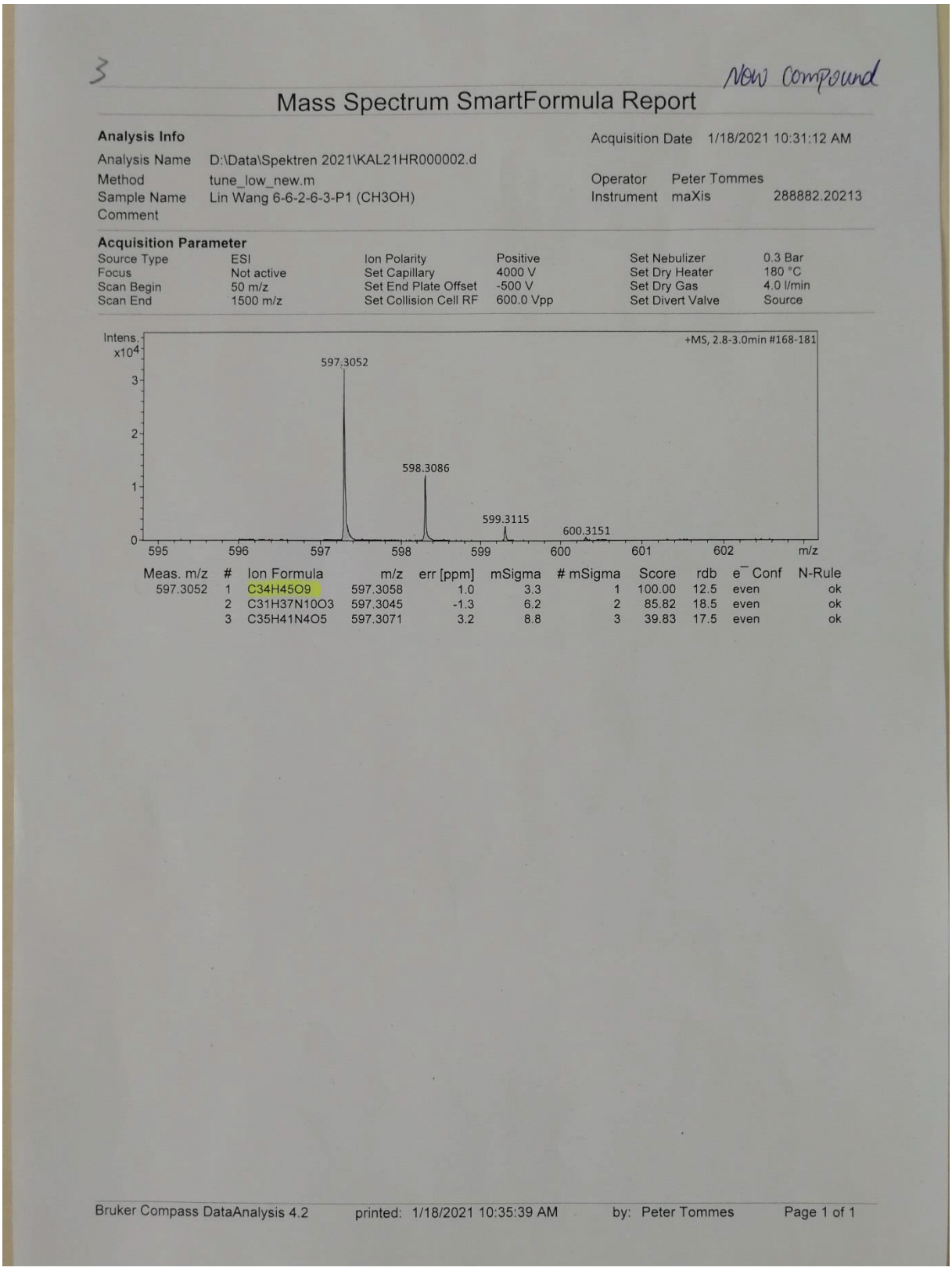

Fig. S24. HRESIMS of Compound **3**

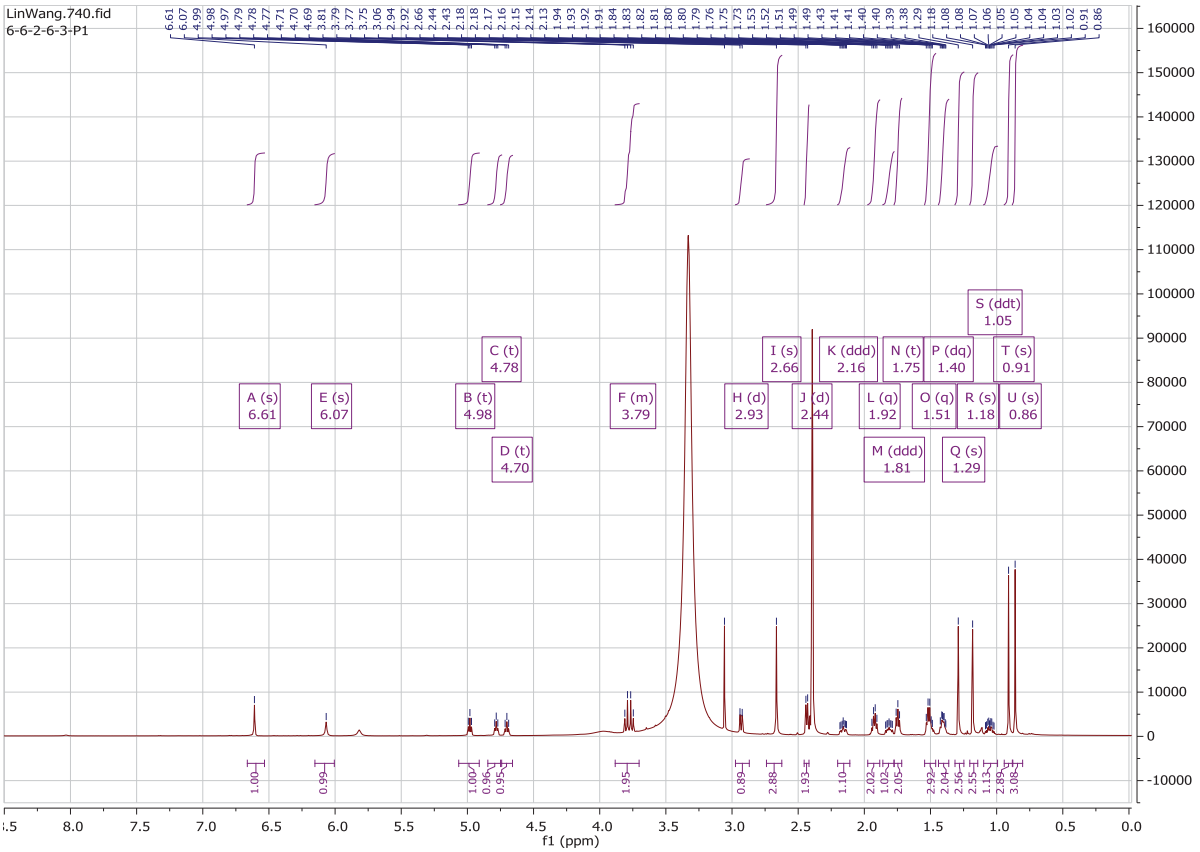

Fig. S25. ^{1}H NMR spectrum of Compound **3**

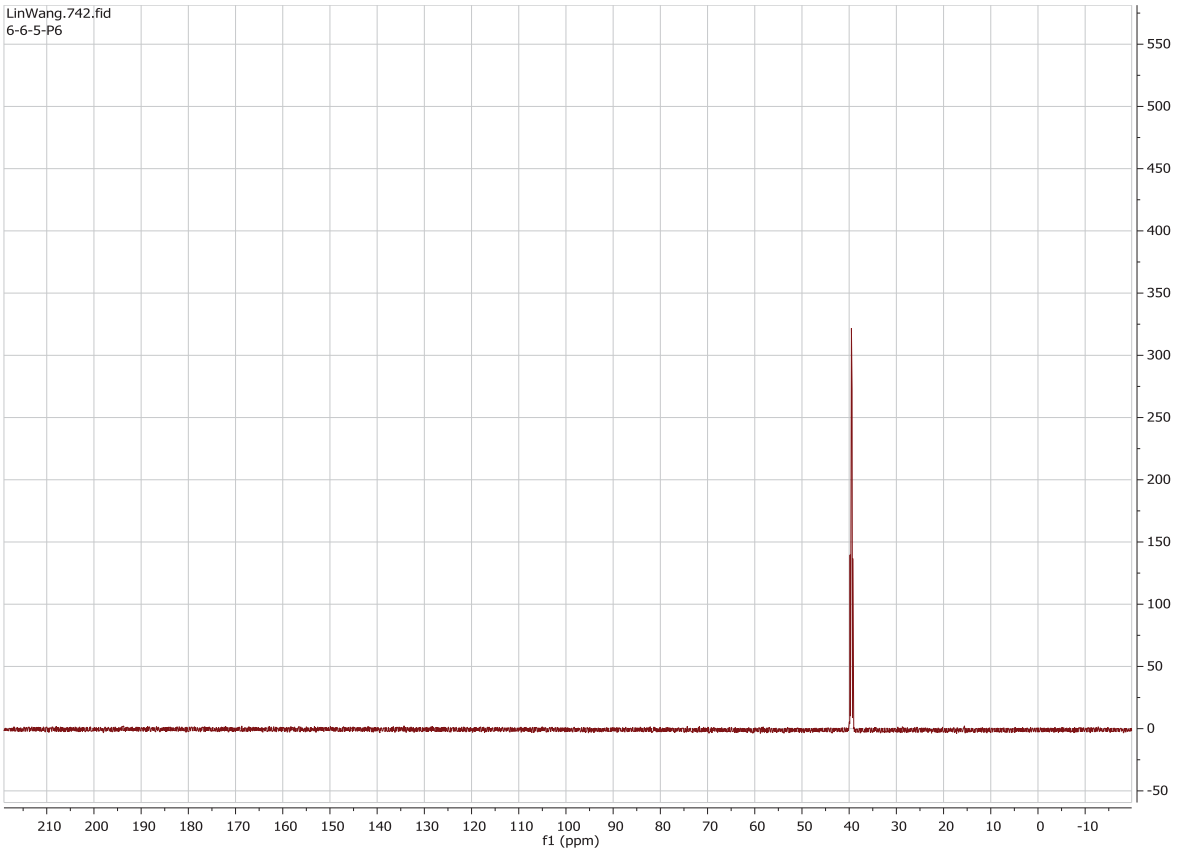

Fig. S26. ^{13}C NMR of Compound **3**

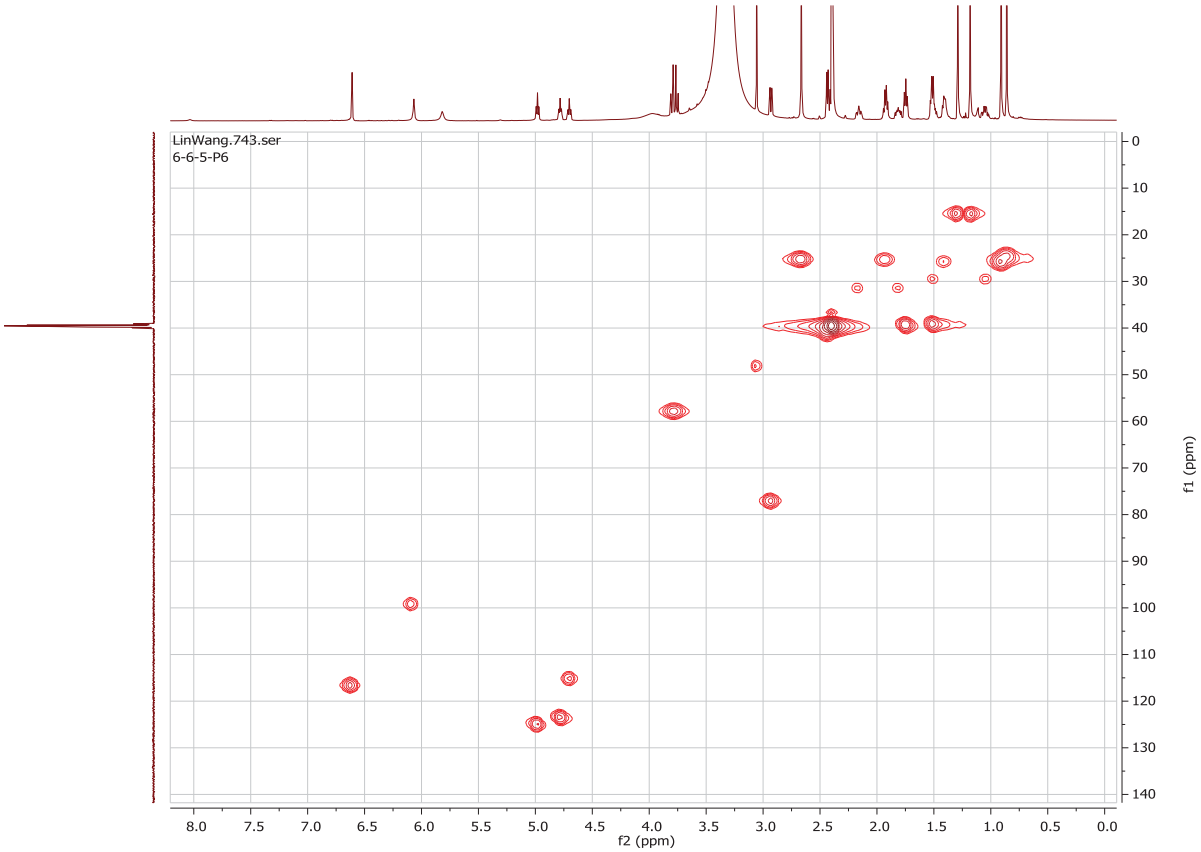

Fig. S27. ^{1}H-^{13}C HSQC of Compound **3**

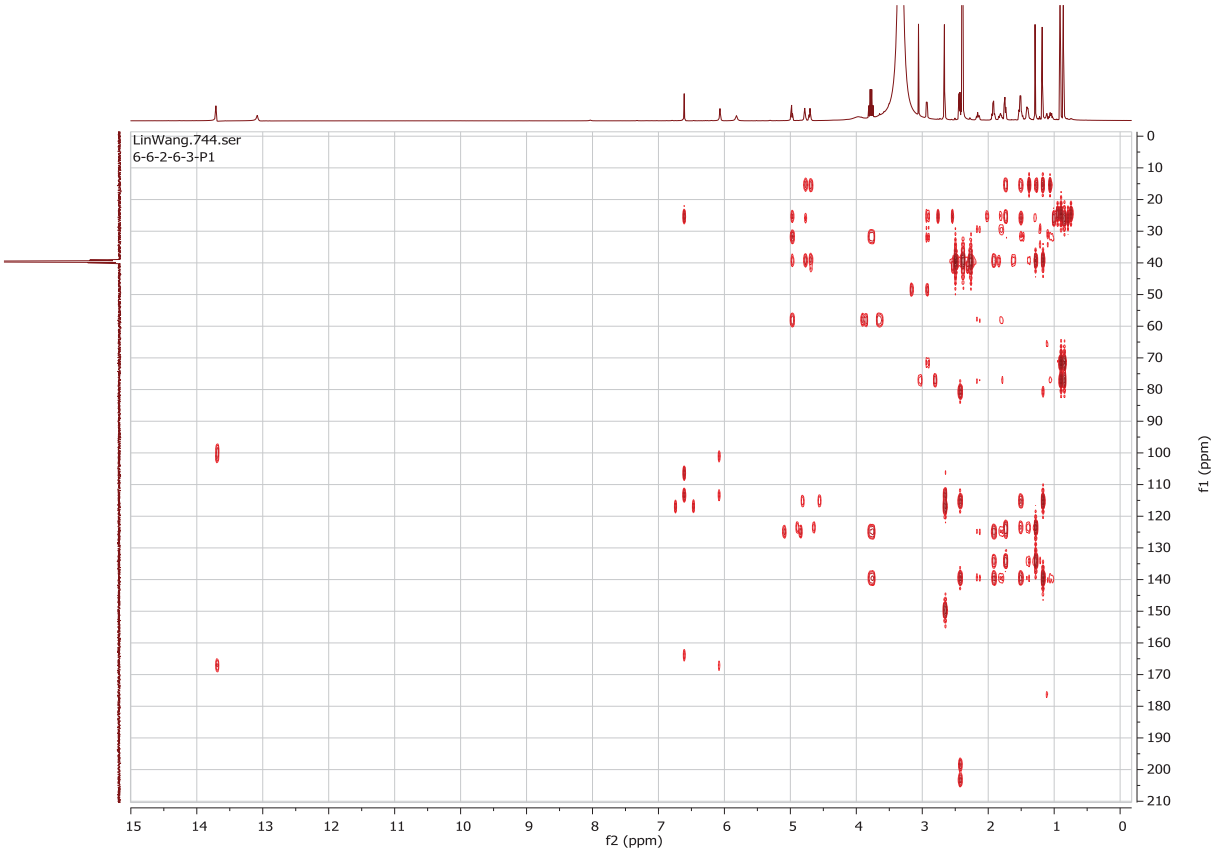

Fig. S28. ^{1}H-^{13}C HMBC of Compound **3**

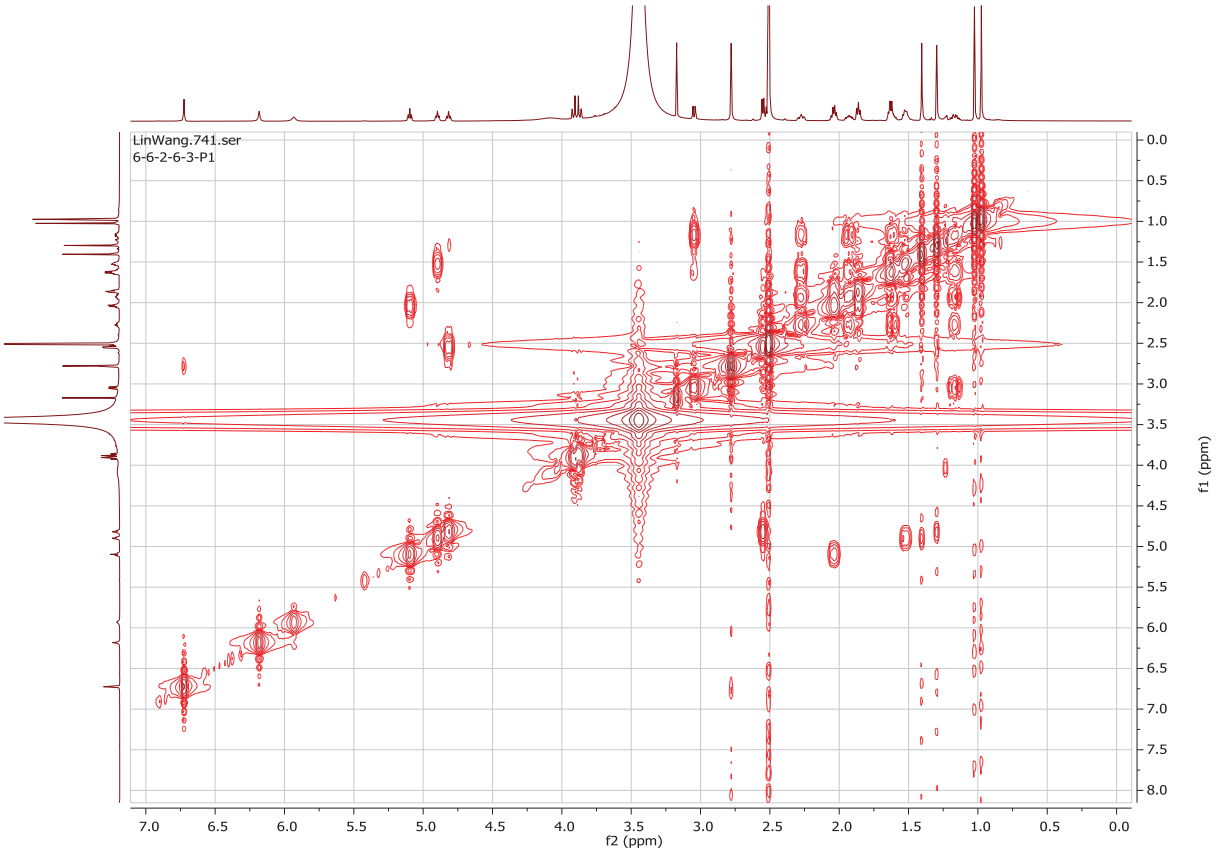

Fig. S29. ^{1}H-^{1}H COSY of Compound **3**

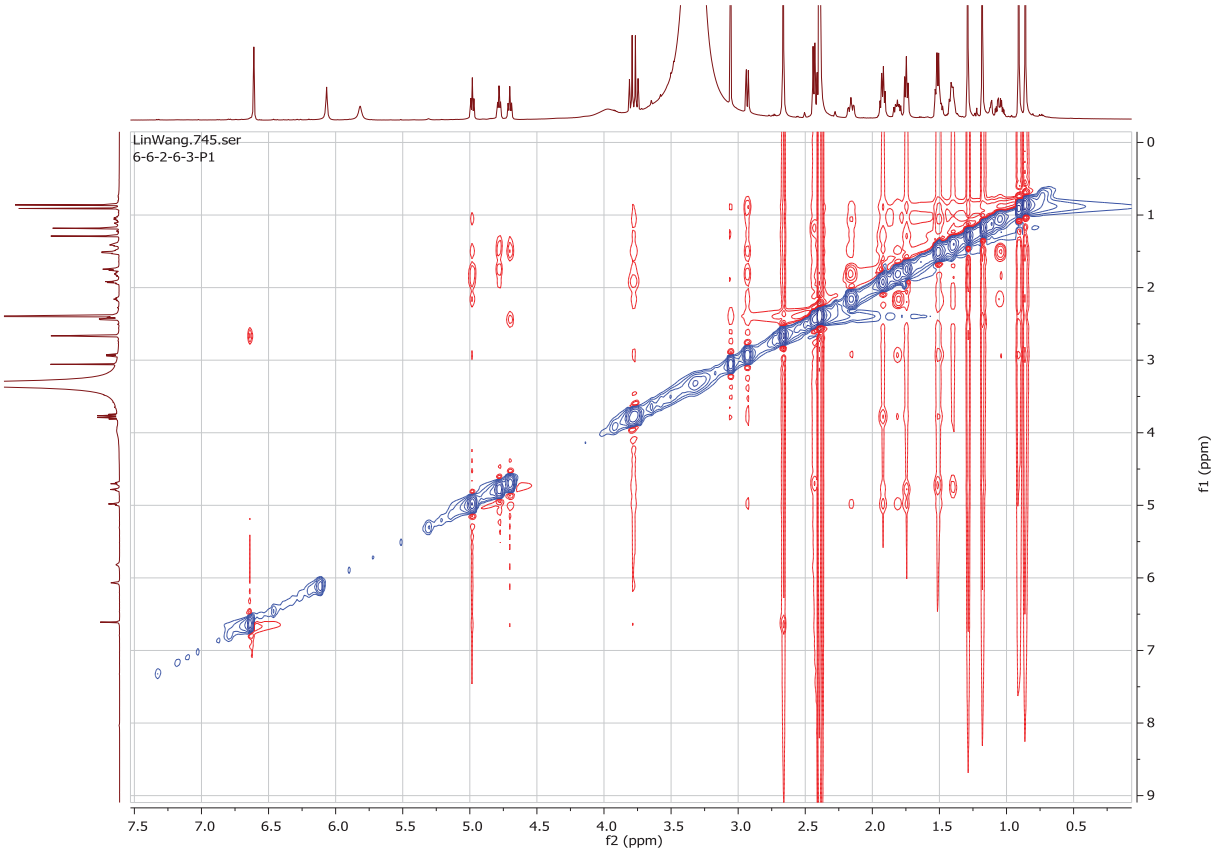

Fig. S30. ^{1}H-^{1}H ROESY of Compound **3**

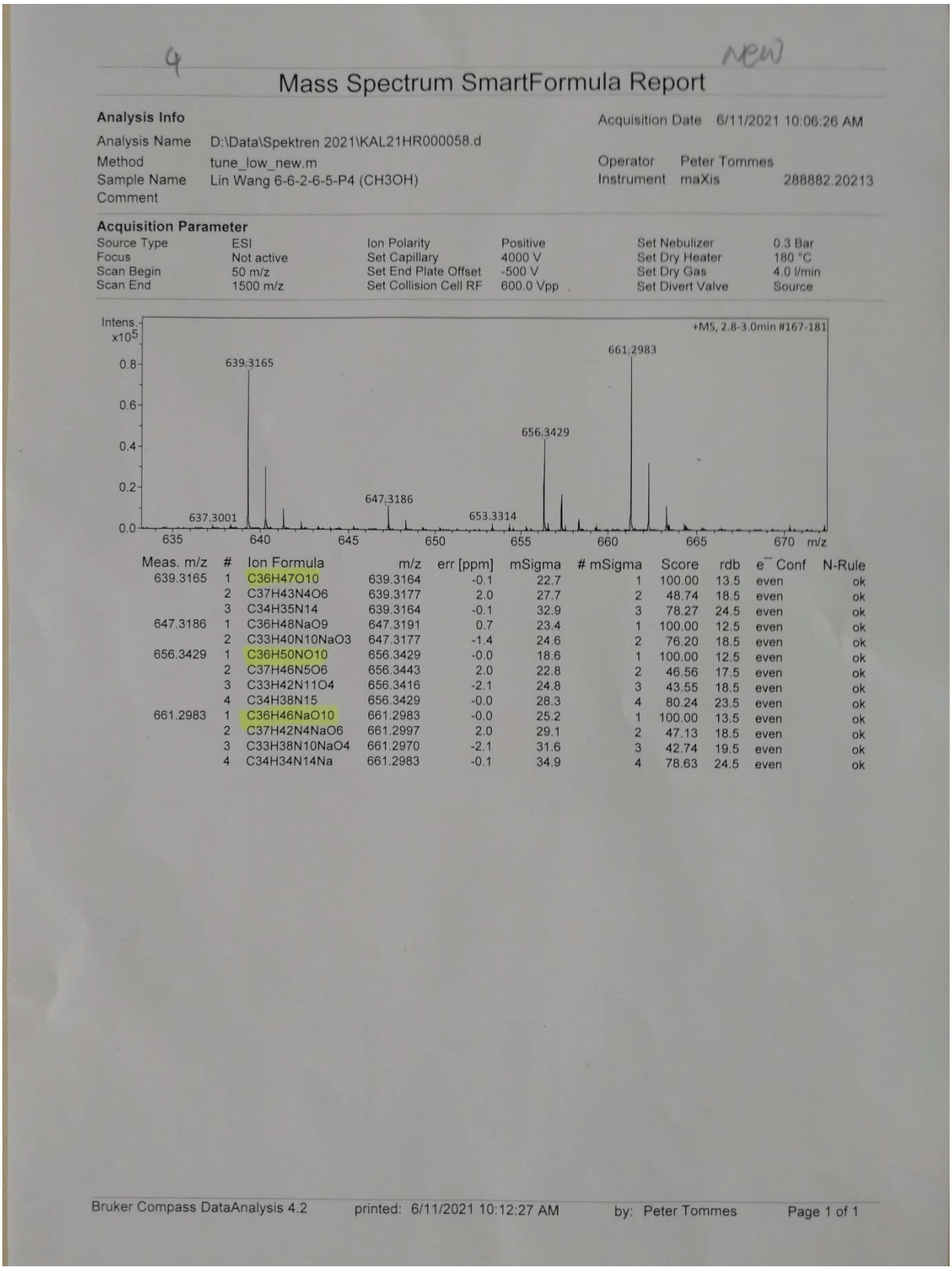

4 NEW

Mass Spectrum SmartFormula Report

Analysis Info

Analysis Name	D:\Data\Spektren 2021\KAL21HR000058.d	Acquisition Date	6/11/2021 10:06:26 AM
Method	tune_low_new.m	Operator	Peter Tommes
Sample Name	Lin Wang 6-6-2-6-5-P4 (CH3OH)	Instrument	maXis 288882.20213
Comment			

Acquisition Parameter

Source Type	ESI	Ion Polarity	Positive	Set Nebulizer	0.3 Bar
Focus	Not active	Set Capillary	4000 V	Set Dry Heater	180 °C
Scan Begin	50 m/z	Set End Plate Offset	-500 V	Set Dry Gas	4.0 l/min
Scan End	1500 m/z	Set Collision Cell RF	600.0 Vpp	Set Divert Valve	Source

Meas. m/z	#	Ion Formula	m/z	err [ppm]	mSigma	# mSigma	Score	rdb	e⁻ Conf	N-Rule
639.3165	1	C36H47O10	639.3164	-0.1	22.7	1	100.00	13.5	even	ok
	2	C37H43N4O6	639.3177	2.0	27.7	2	48.74	18.5	even	ok
	3	C34H35N14	639.3164	-0.1	32.9	3	78.27	24.5	even	ok
647.3186	1	C36H48NaO9	647.3191	0.7	23.4	1	100.00	12.5	even	ok
	2	C33H40N10NaO3	647.3177	-1.4	24.6	2	76.20	18.5	even	ok
656.3429	1	C36H50NO10	656.3429	-0.0	18.6	1	100.00	12.5	even	ok
	2	C37H46N5O6	656.3443	2.0	22.8	2	46.56	17.5	even	ok
	3	C33H42N11O4	656.3416	-2.1	24.8	3	43.55	18.5	even	ok
	4	C34H38N15	656.3429	-0.0	28.3	4	80.24	23.5	even	ok
661.2983	1	C36H46NaO10	661.2983	-0.0	25.2	1	100.00	13.5	even	ok
	2	C37H42N4NaO6	661.2997	2.0	29.1	2	47.13	18.5	even	ok
	3	C33H38N10NaO4	661.2970	-2.1	31.6	3	42.74	19.5	even	ok
	4	C34H34N14Na	661.2983	-0.1	34.9	4	78.63	24.5	even	ok

Bruker Compass DataAnalysis 4.2 printed: 6/11/2021 10:12:27 AM by: Peter Tommes Page 1 of 1

Fig. S31. HRESIMS of Compound **4**

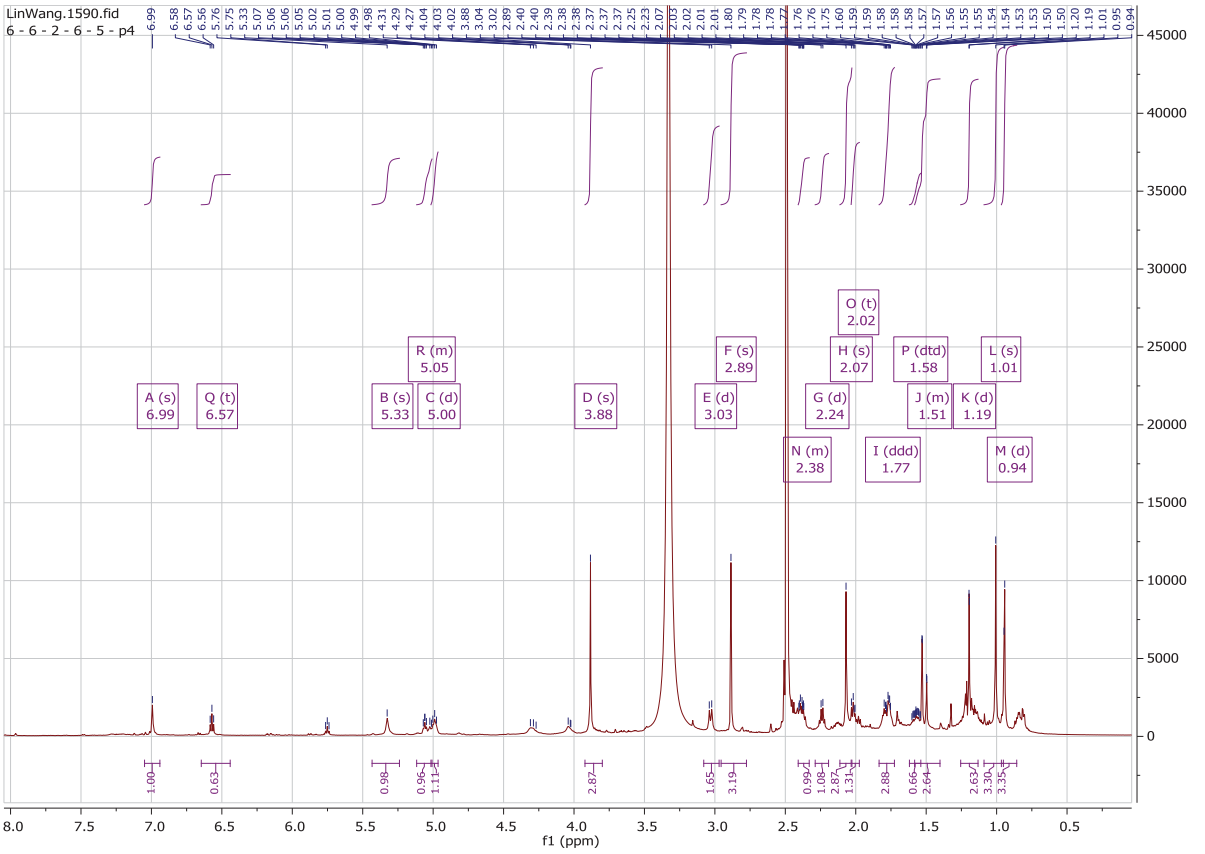

Fig. S32. ^{1}H NMR spectrum of Compound **4**

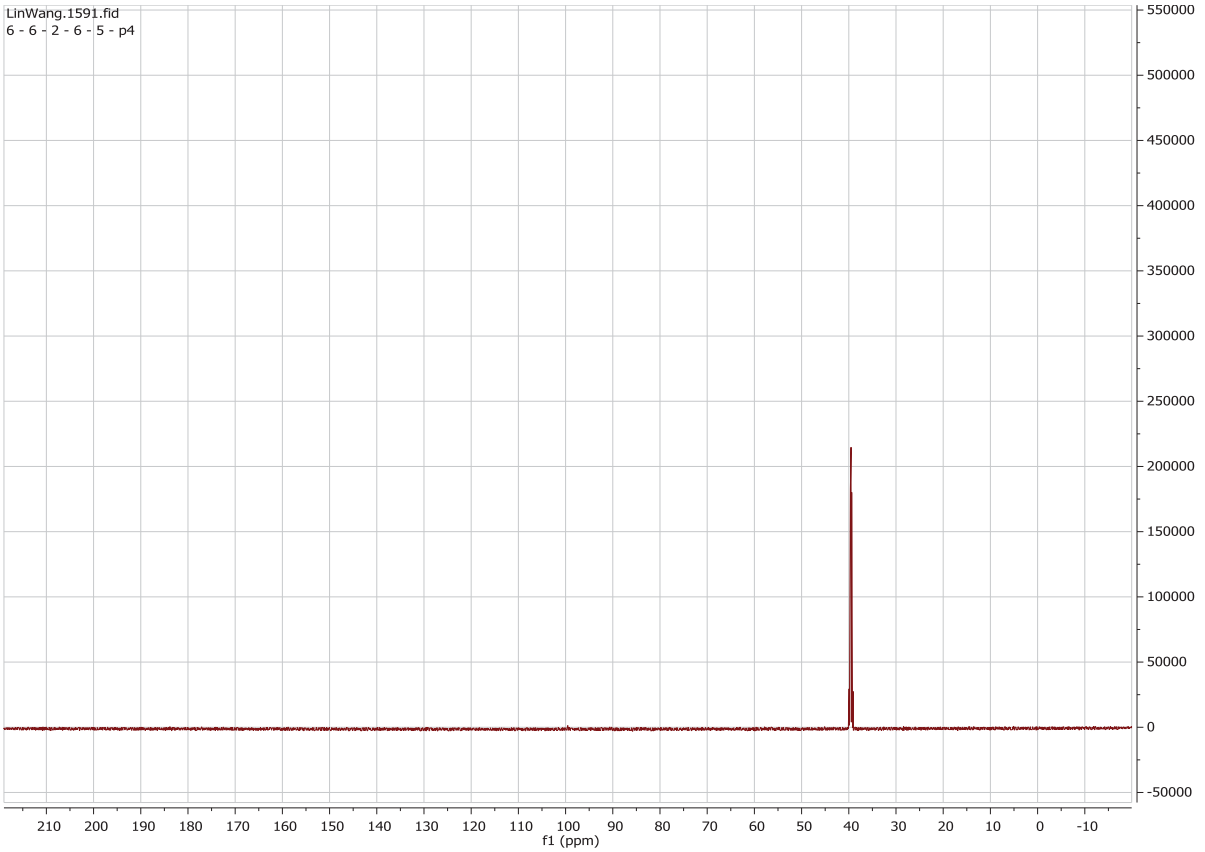

Fig. S33. ^{13}C NMR of Compound **4**

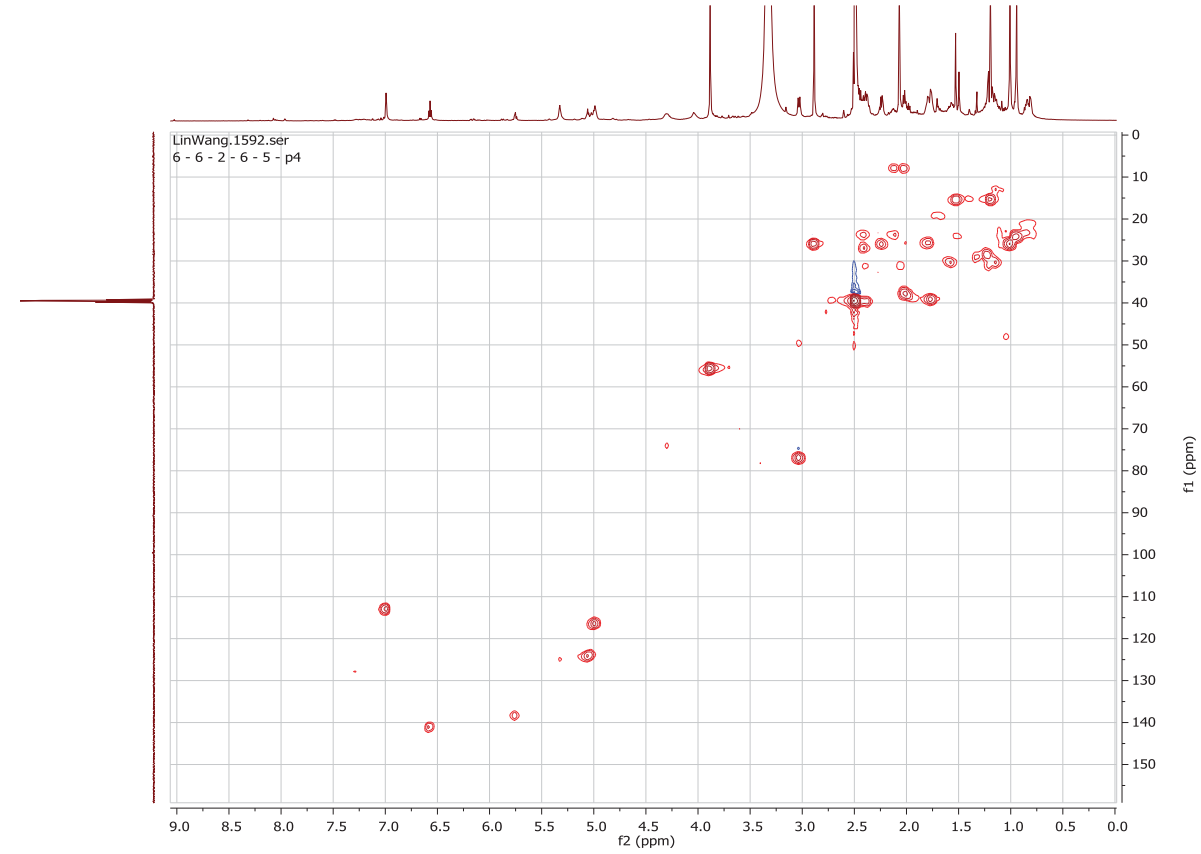

Fig. S34. ^{1}H-^{13}C HSQC of Compound **4**

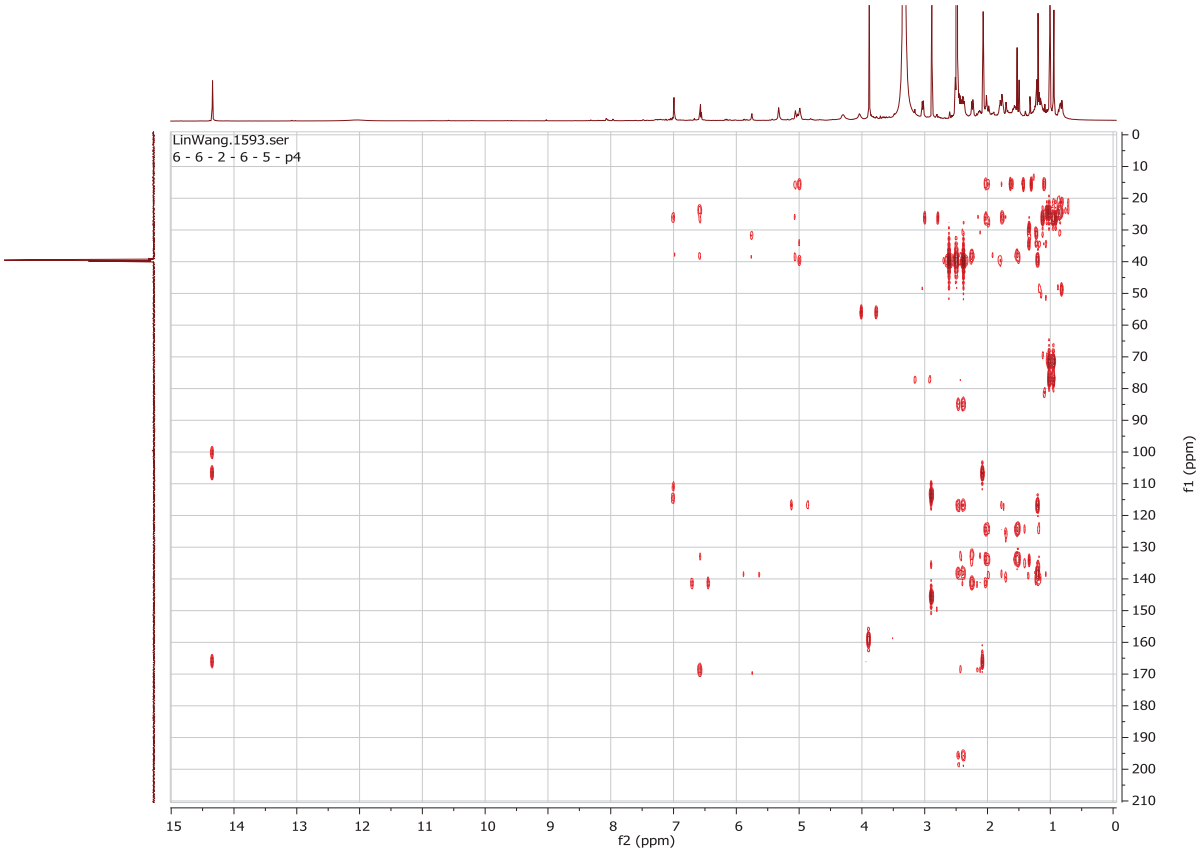

Fig. S35. ^{1}H-^{13}C HMBC of Compound **4**

Fig. S36. ^{1}H-^{1}H COSY of Compound **4**

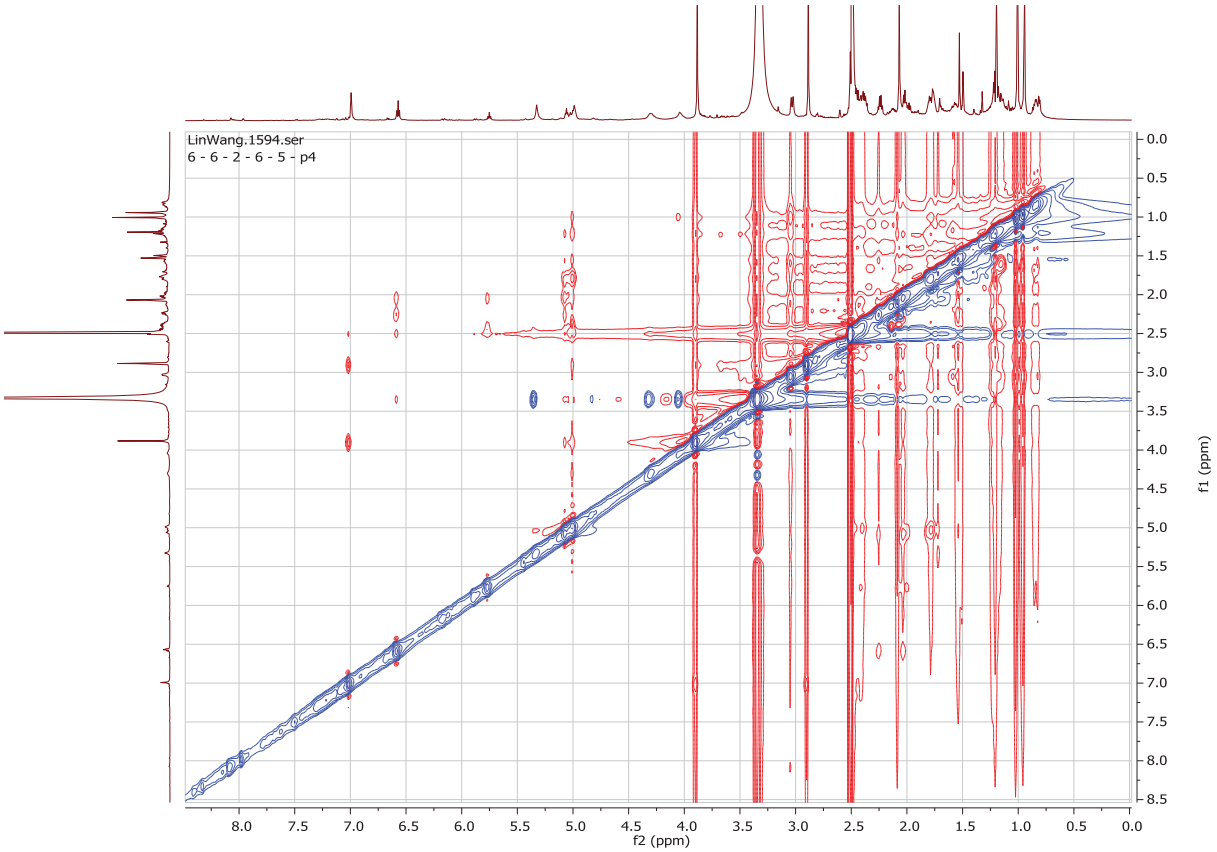

Fig. S37. ^{1}H-^{1}H ROESY of Compound **4**

5 new V

Mass Spectrum SmartFormula Report

Analysis Info Acquisition Date 6/7/2021 9:43:56 AM

Analysis Name	D:\Data\Spektren 2021\KAL21HR000054.d		
Method	tune_low_new.m	Operator	Peter Tommes
Sample Name	Lin Wang F6.7-R23-P2 (CH3OH)	Instrument	maXis 288882.20213
Comment	2,5 ul in 1 mkl		

Acquisition Parameter

Source Type	ESI	Ion Polarity	Positive	Set Nebulizer	0.3 Bar
Focus	Not active	Set Capillary	4000 V	Set Dry Heater	180 °C
Scan Begin	50 m/z	Set End Plate Offset	-500 V	Set Dry Gas	4.0 l/min
Scan End	1500 m/z	Set Collision Cell RF	600.0 Vpp	Set Divert Valve	Source

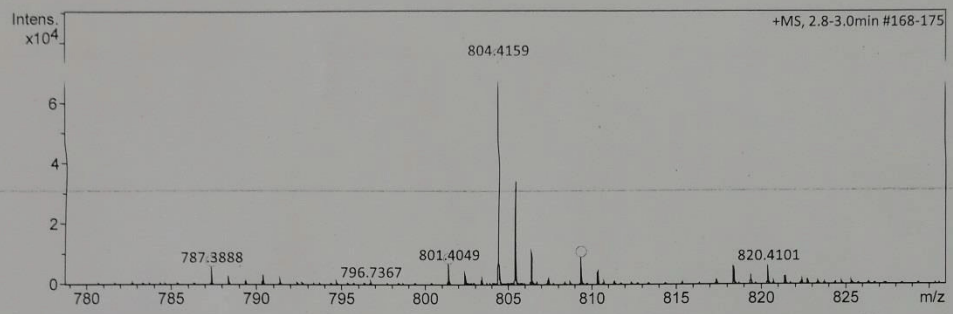

Meas. m/z	#	Ion Formula	m/z	err [ppm]	mSigma	# mSigma	Score	rdb	e⁻ Conf	N-Rule
787.3888	1	C55H51N2O3	787.3894	0.7	279.3	1	100.00	31.5	even	ok
	2	C42H59O14	787.3899	1.4	281.8	2	56.91	13.5	even	ok
	3	C40H47N14O4	787.3899	1.4	284.4	3	42.14	24.5	even	ok
	4	C39H51N10O8	787.3886	-0.3	284.8	4	60.98	19.5	even	ok
801.4049	1	C41H62NaO14	801.4032	-2.1	697.4	1	100.00	10.5	even	ok
	2	C43H61O14	801.4056	0.9	700.0	2	86.61	13.5	even	ok
	3	C42H58N4NaO10	801.4045	-0.4	701.3	3	72.62	15.5	even	ok
	4	C44H57N4O10	801.4069	2.6	704.1	4	11.67	18.5	even	ok
	5	C43H54N8NaO6	801.4059	1.2	705.4	5	16.35	20.5	even	ok
	6	C41H49N14O4	801.4056	0.9	705.8	6	16.98	24.5	even	ok
	7	C42H45N18	801.4069	2.6	710.2	7	2.07	29.5	even	ok
	8	C56H53N2O3	801.4051	0.3	724.1	8	0.11	31.5	even	ok
	9	C59H54NaO	801.4067	2.3	728.9	9	0.01	32.5	even	ok
804.4159	1	C42H62NO14	804.4165	0.8	5.1	1	100.00	12.5	even	ok
	2	C39H54N11O8	804.4151	-0.9	11.3	2	84.41	18.5	even	ok
	3	C38H58N7O12	804.4138	-2.6	14.5	3	33.42	13.5	even	ok
	4	C43H58N5O10	804.4178	2.4	14.9	4	36.14	17.5	even	ok
	6	C40H50N15O4	804.4165	0.8	17.9	6	78.91	23.5	even	ok
	7	C41H46N19	804.4178	2.4	28.1	7	27.33	28.5	even	ok
	8	C55H54N3O3	804.4160	0.1	77.8	8	16.48	30.5	even	ok
809.3713	1	C41H42N18Na	809.3732	2.4	20.2	1	46.93	29.5	even	ok
	2	C43H54N4NaO10	809.3732	2.4	21.1	2	45.65	18.5	even	ok
	3	C40H46N14NaO4	809.3719	0.7	23.4	3	100.00	24.5	even	ok
	4	C42H58NaO14	809.3719	0.7	29.1	4	87.18	13.5	even	ok
	5	C39H50N10NaO8	809.3705	-0.9	30.9	5	76.61	19.5	even	ok
	6	C55H50N2NaO3	809.3714	0.1	55.7	6	52.05	31.5	even	ok

Bruker Compass DataAnalysis 4.2 printed: 6/7/2021 9:50:01 AM by: Peter Tommes Page 1 of 1

Fig. S38. HRESIMS of Compound **5**

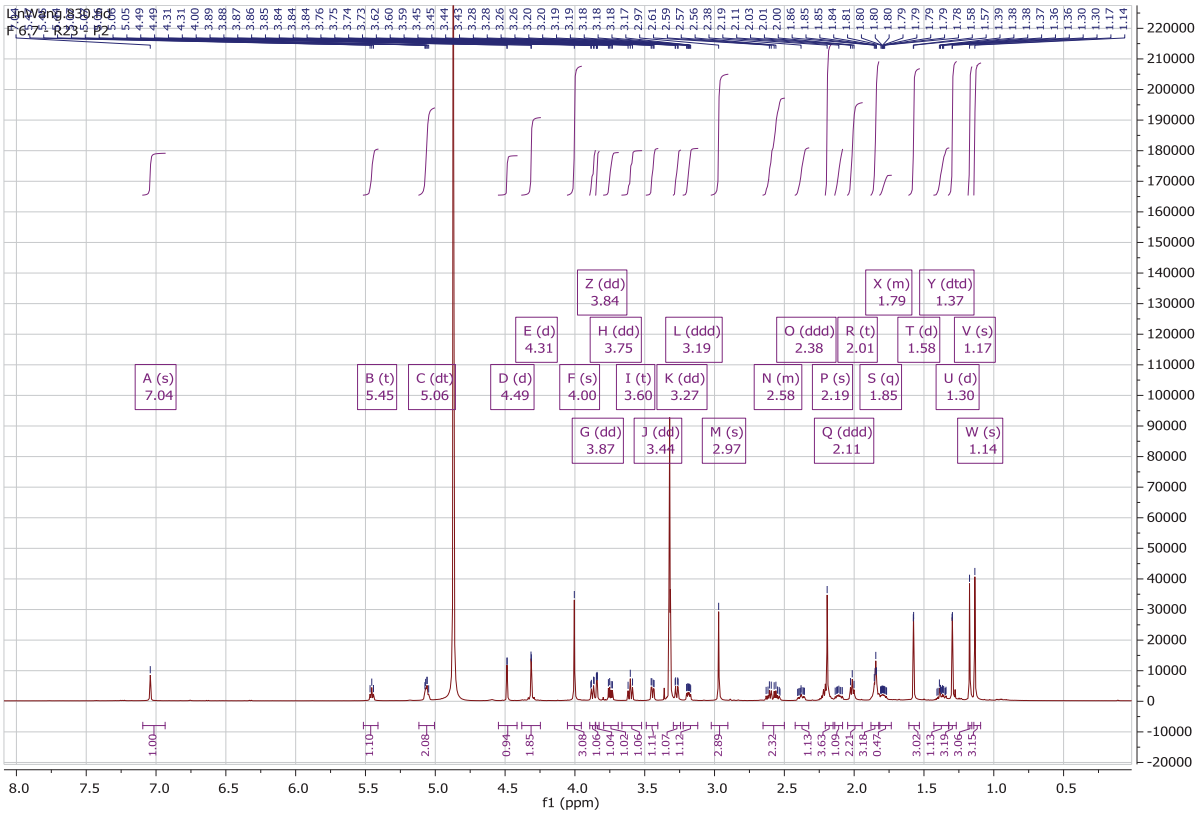

Fig. S39. [1]H NMR spectrum of Compound **5**

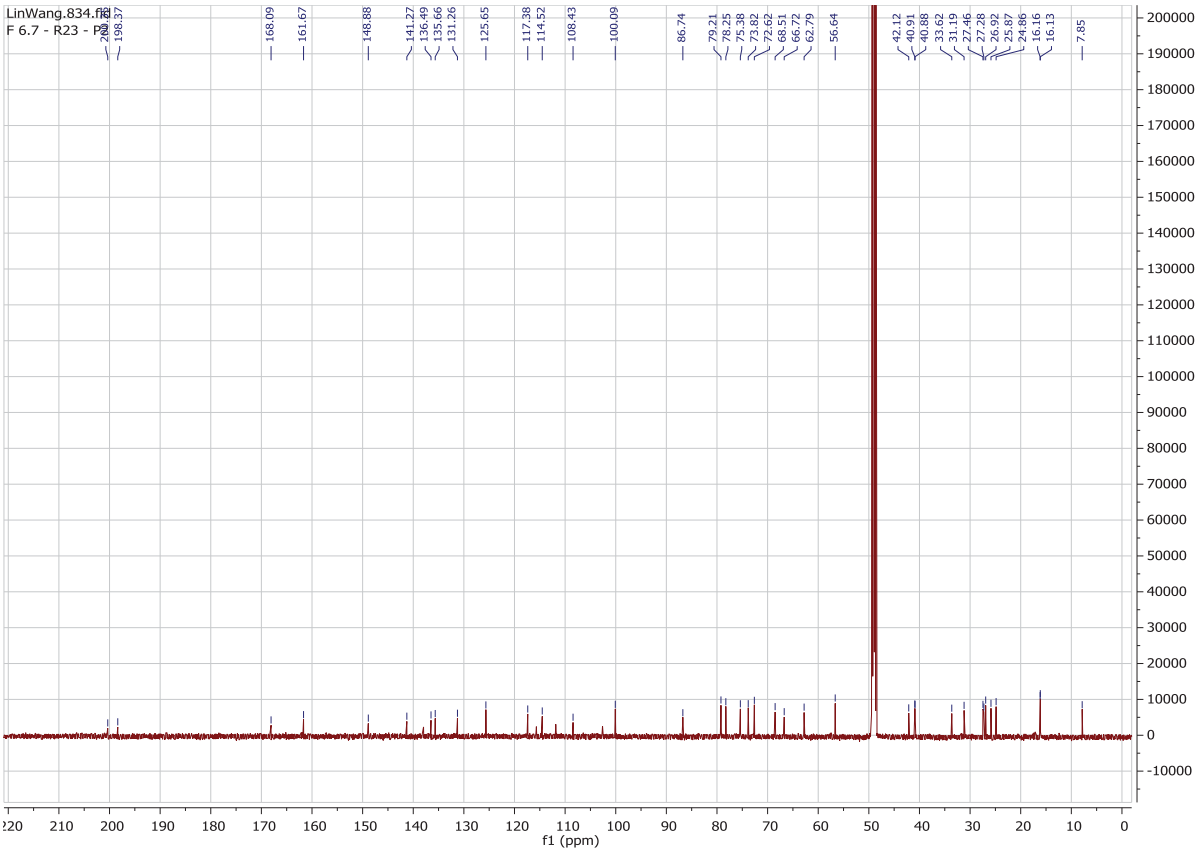

Fig. S40. [13]C NMR of Compound **5**

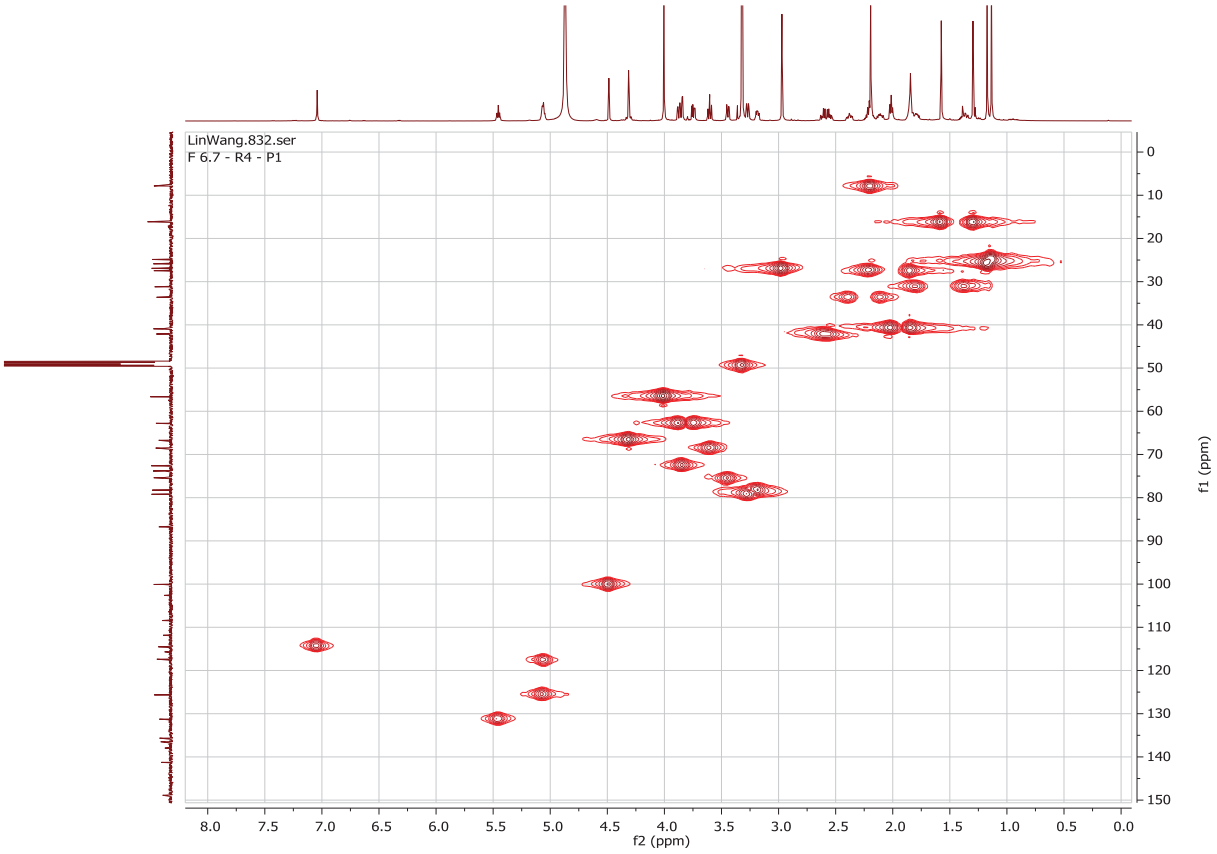

Fig. S41. ^{1}H-^{13}C HSQC of Compound **5**

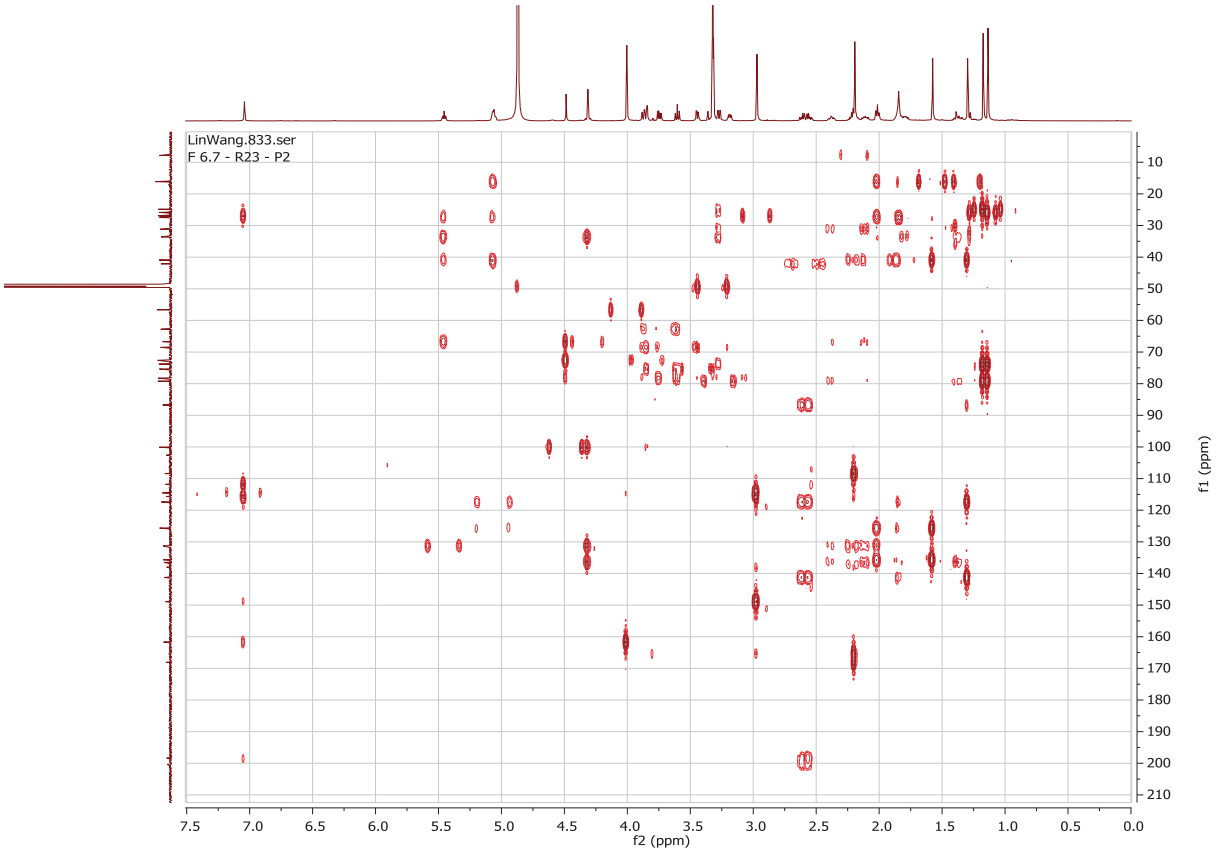

Fig. S42. ^{1}H-^{13}C HMBC of Compound **5**

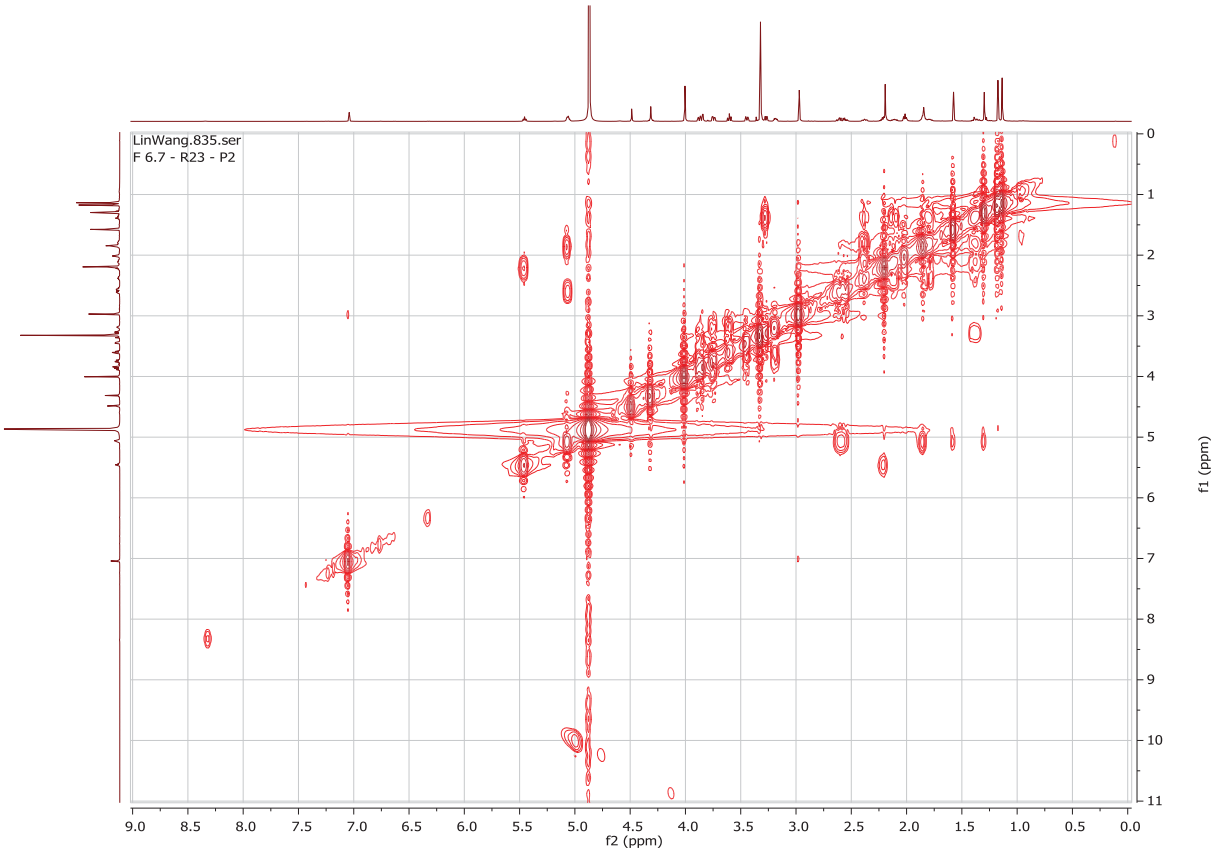

Fig. S43. ^{1}H-^{1}H COSY of Compound **5**

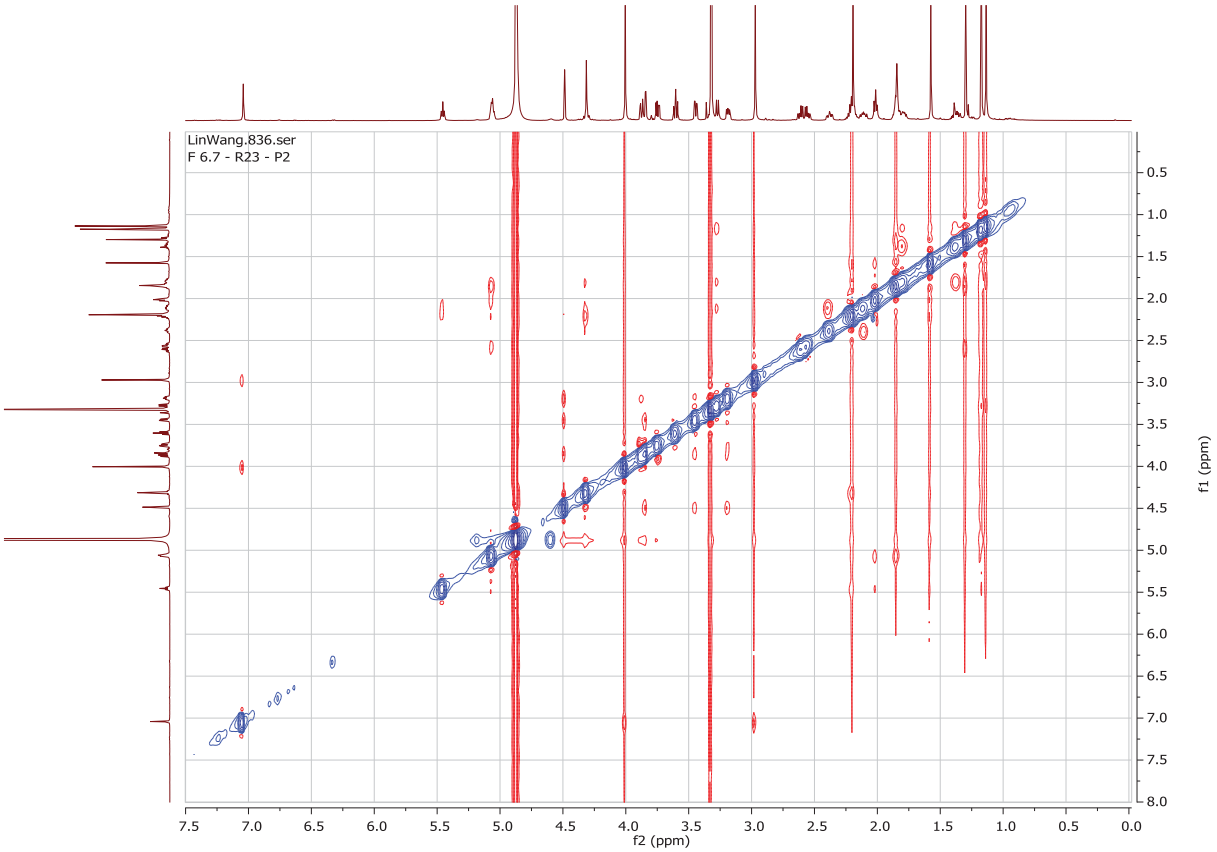

Fig. S44. ^{1}H-^{1}H ROESY of Compound **5**

6 New

Mass Spectrum SmartFormula Report

Analysis Info

Acquisition Date 6/7/2021 10:05:43 AM

Analysis Name	D:\Data\Spektren 2021\KAL21HR000055.d		
Method	tune_low_new.m	Operator	Peter Tommes
Sample Name	Lin Wang F6.7-R4-P1 (CH3OH)	Instrument	maXis 288882.20213
Comment	2 ul in 1 mkl		

Acquisition Parameter

Source Type	ESI	Ion Polarity	Positive	Set Nebulizer	0.3 Bar
Focus	Not active	Set Capillary	4000 V	Set Dry Heater	180 °C
Scan Begin	50 m/z	Set End Plate Offset	-500 V	Set Dry Gas	4.0 l/min
Scan End	1500 m/z	Set Collision Cell RF	600.0 Vpp	Set Divert Valve	Source

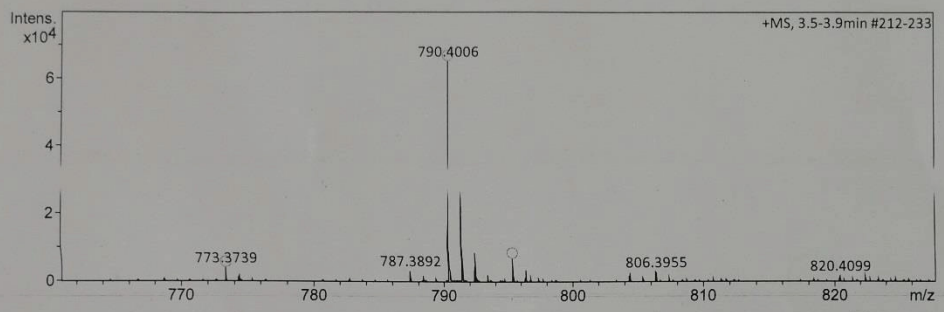

Meas. m/z	#	Ion Formula	m/z	err [ppm]	mSigma	# mSigma	Score	rdb	e⁻ Conf	N-Rule
773.3739	1	C41H57O14	773.3743	0.5	37.3	1	100.00	13.5	even	ok
	2	C38H49N10O8	773.3729	-1.2	41.2	2	67.93	19.5	even	ok
	3	C39H45N14O4	773.3743	0.5	43.4	3	84.87	24.5	even	ok
	4	C54H49N2O3	773.3738	-0.1	82.1	4	24.98	31.5	even	ok
790.4006	1	C41H60NO14	790.4008	0.3	1.4	1	100.00	12.5	even	ok
	2	C38H52N11O8	790.3995	-1.5	6.6	2	56.39	18.5	even	ok
	3	C42H56N5O10	790.4022	1.9	12.3	3	39.64	17.5	even	ok
	4	C39H48N15O4	790.4008	0.2	13.8	4	80.55	23.5	even	ok
	5	C40H44N19	790.4022	1.9	24.8	5	30.71	28.5	even	ok
	6	C54H52N3O3	790.4003	-0.4	76.6	6	12.21	30.5	even	ok
795.3560	1	C42H52N4NaO10	795.3576	1.9	16.0	1	52.92	18.5	even	ok
	2	C40H40N18Na	795.3576	1.9	19.4	2	49.71	29.5	even	ok
	3	C39H44N14NaO4	795.3562	0.2	21.0	3	100.00	24.5	even	ok
	4	C41H56NaO14	795.3562	0.3	24.4	4	92.22	13.5	even	ok
	5	C38H48N10NaO8	795.3549	-1.4	27.9	5	52.80	19.5	even	ok
	6	C54H48N2NaO3	795.3557	-0.4	55.0	6	38.41	31.5	even	ok

Bruker Compass DataAnalysis 4.2 printed: 6/7/2021 10:12:33 AM by: Peter Tommes Page 1 of 1

Fig. S45. HRESIMS of Compound **6**

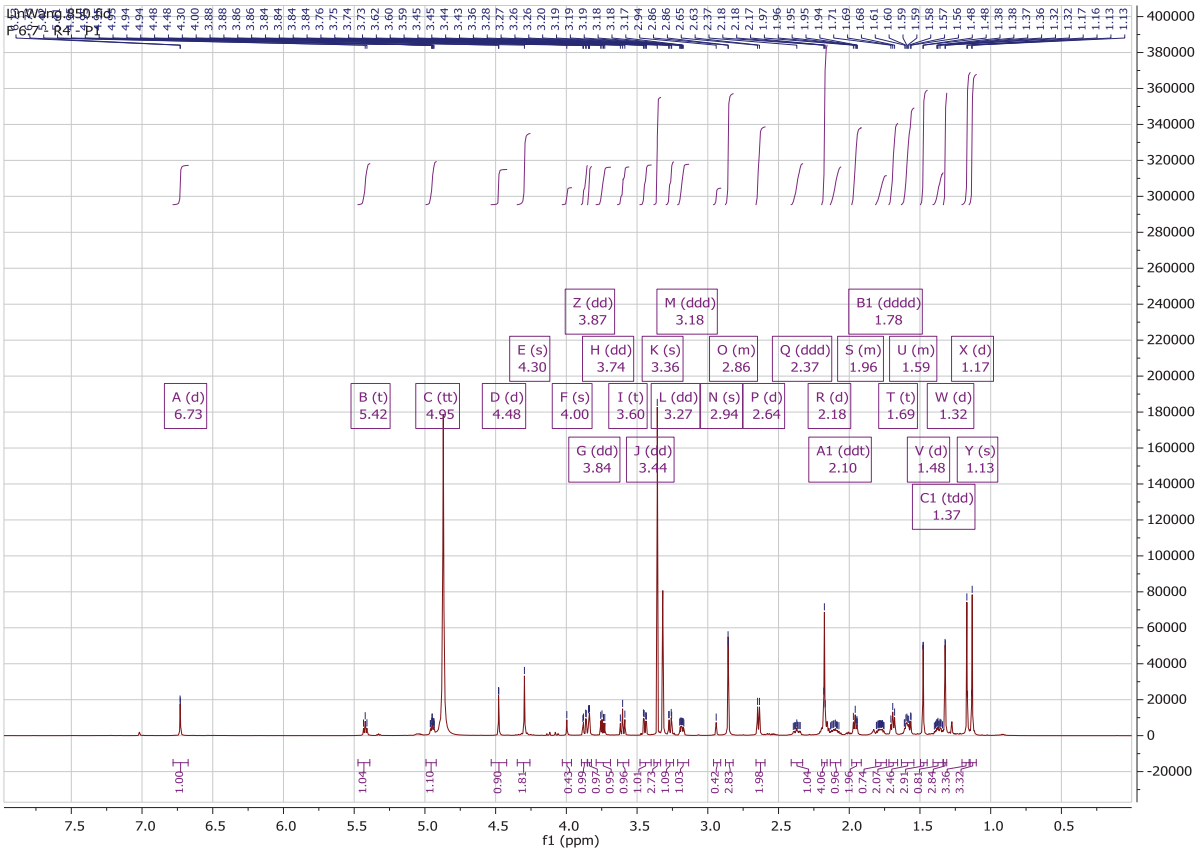

Fig. S46. [1]H NMR spectrum of Compound **6**

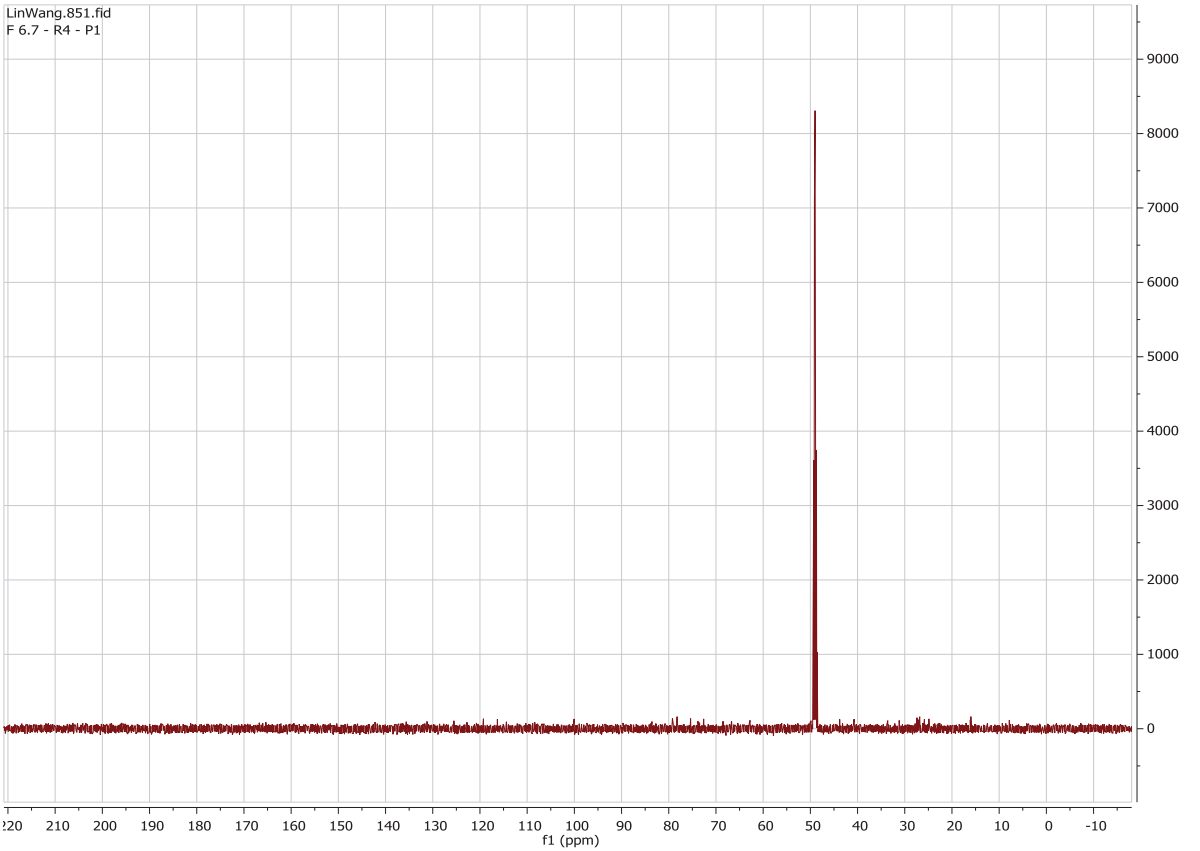

Fig. S47. [13]C NMR of Compound **6**

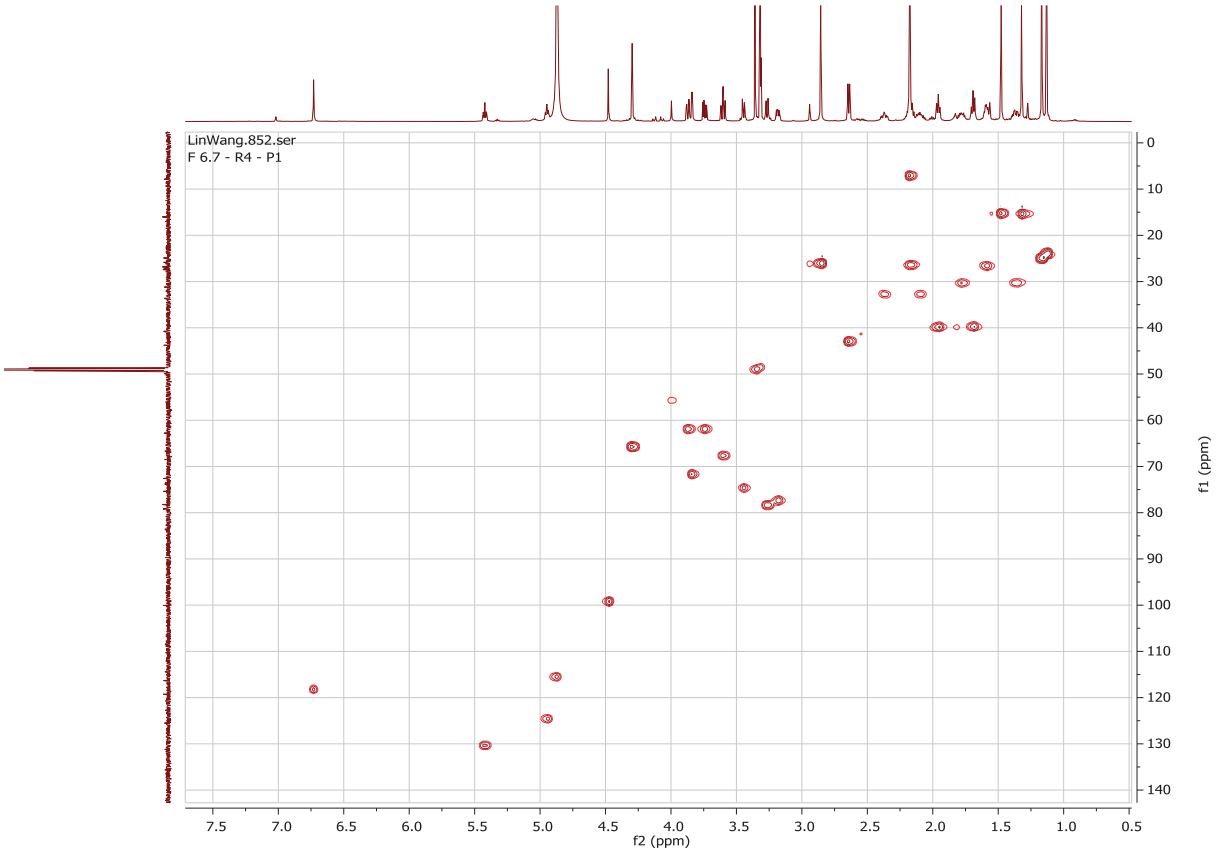

Fig. S48. ^{1}H-^{13}C HSQC of Compound **6**

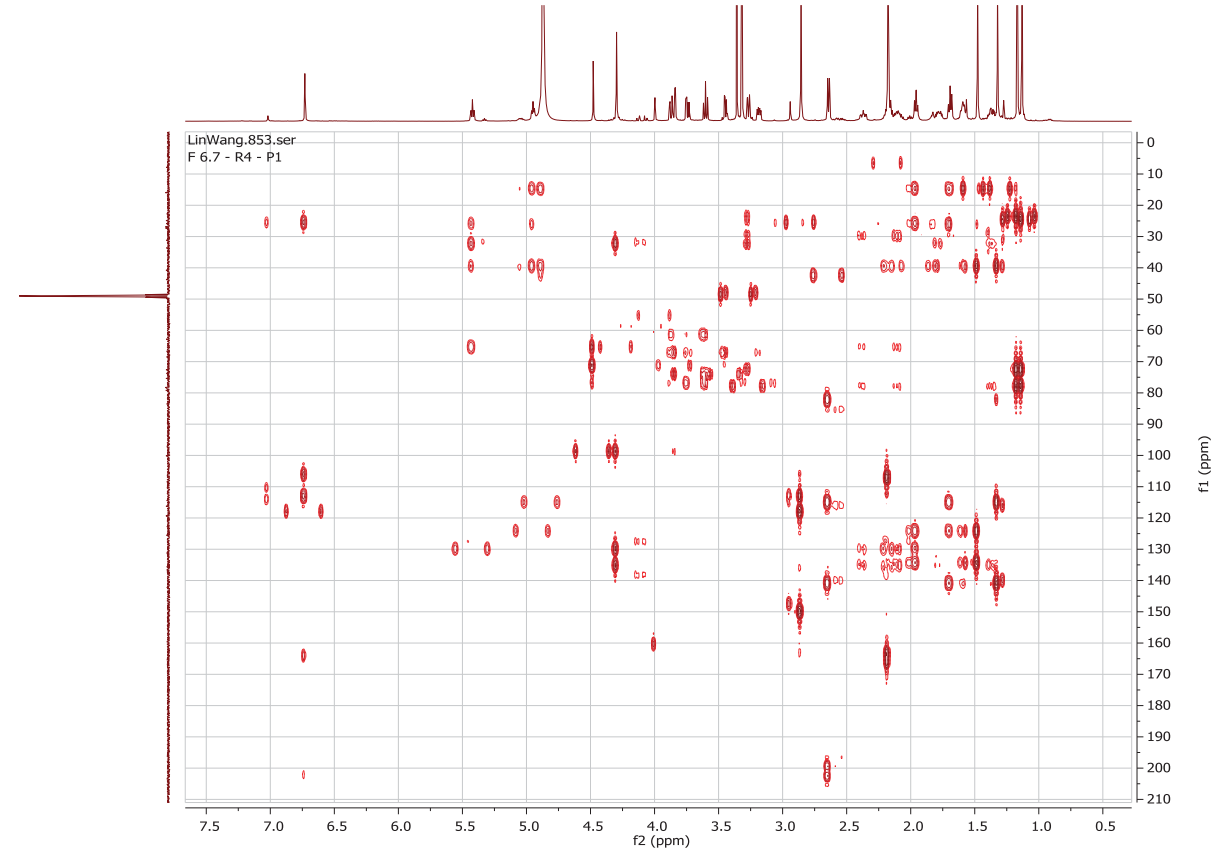

Fig. S49. ^{1}H-^{13}C HMBC of Compound **6**

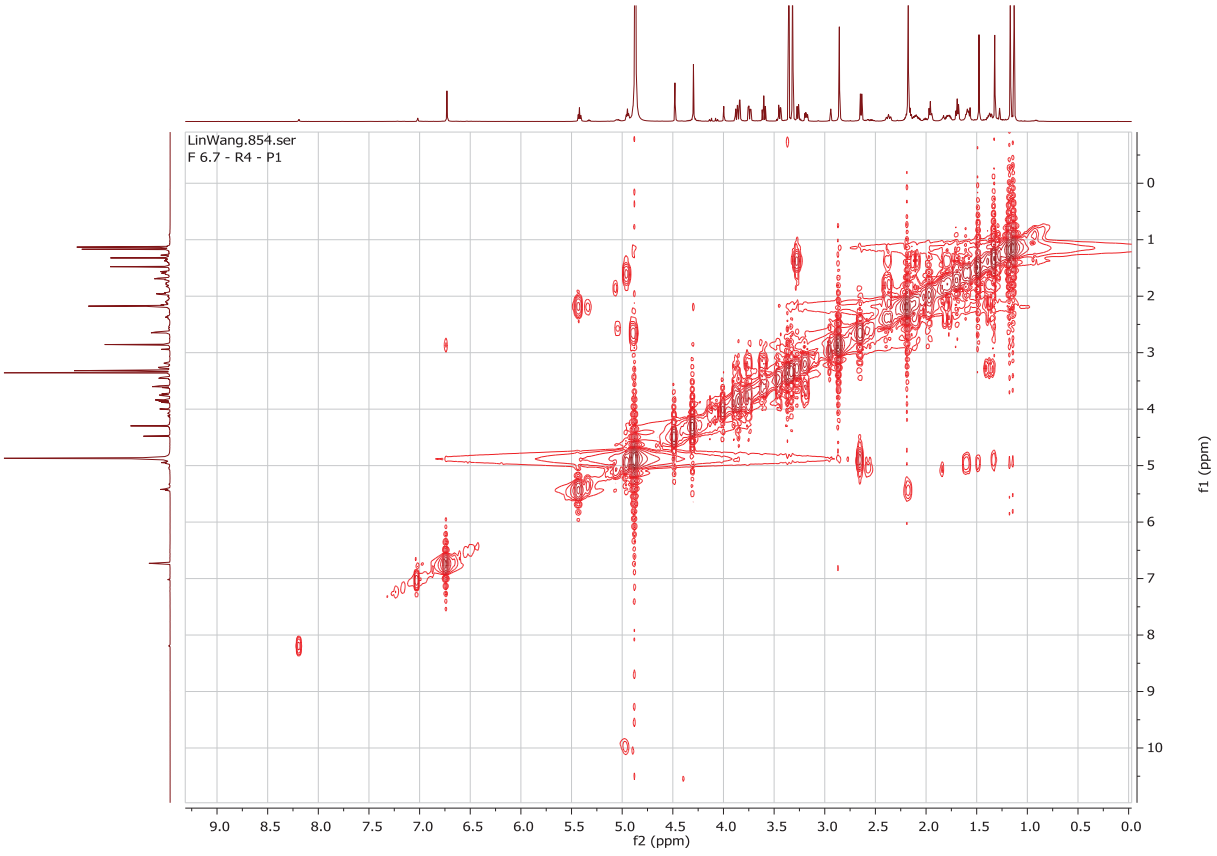

Fig. S50. ^{1}H-^{1}H COSY of Compound **6**

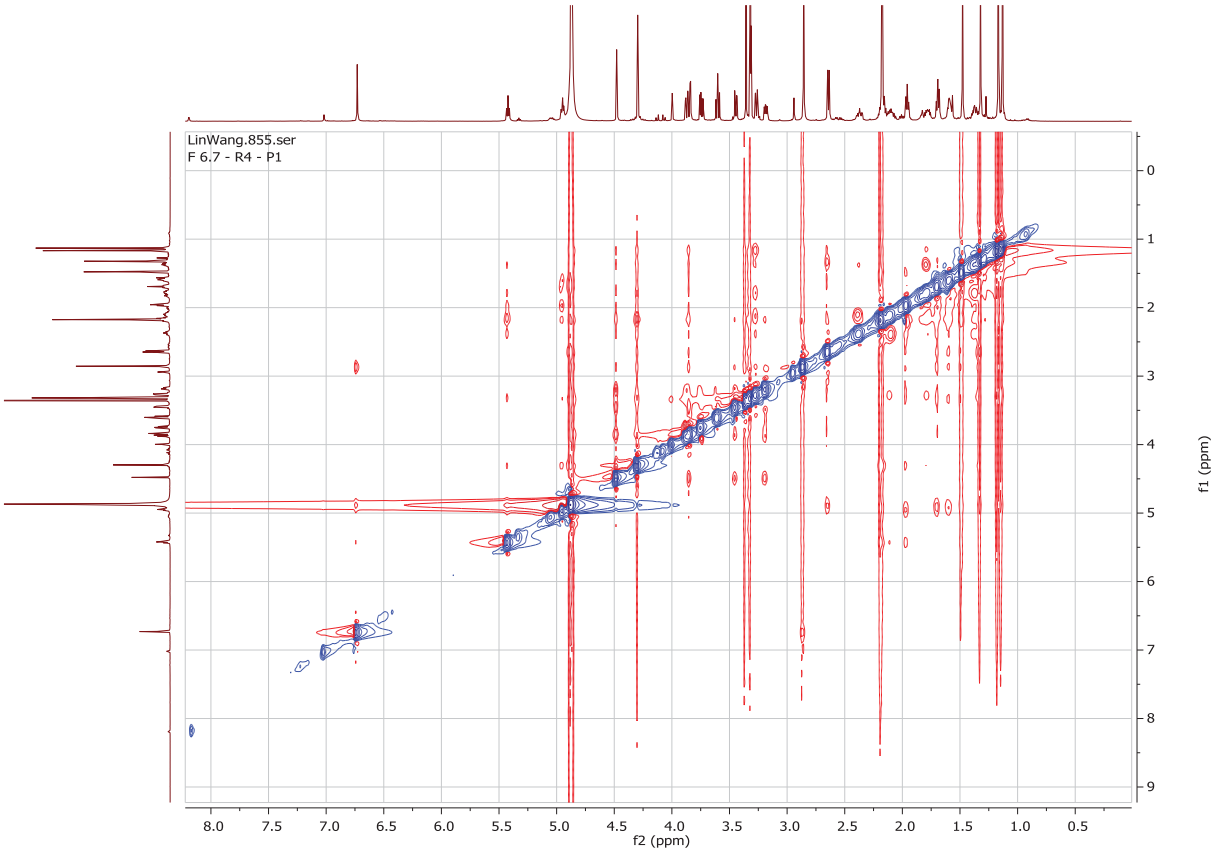

Fig. S51. ^{1}H-^{1}H ROESY of Compound **6**

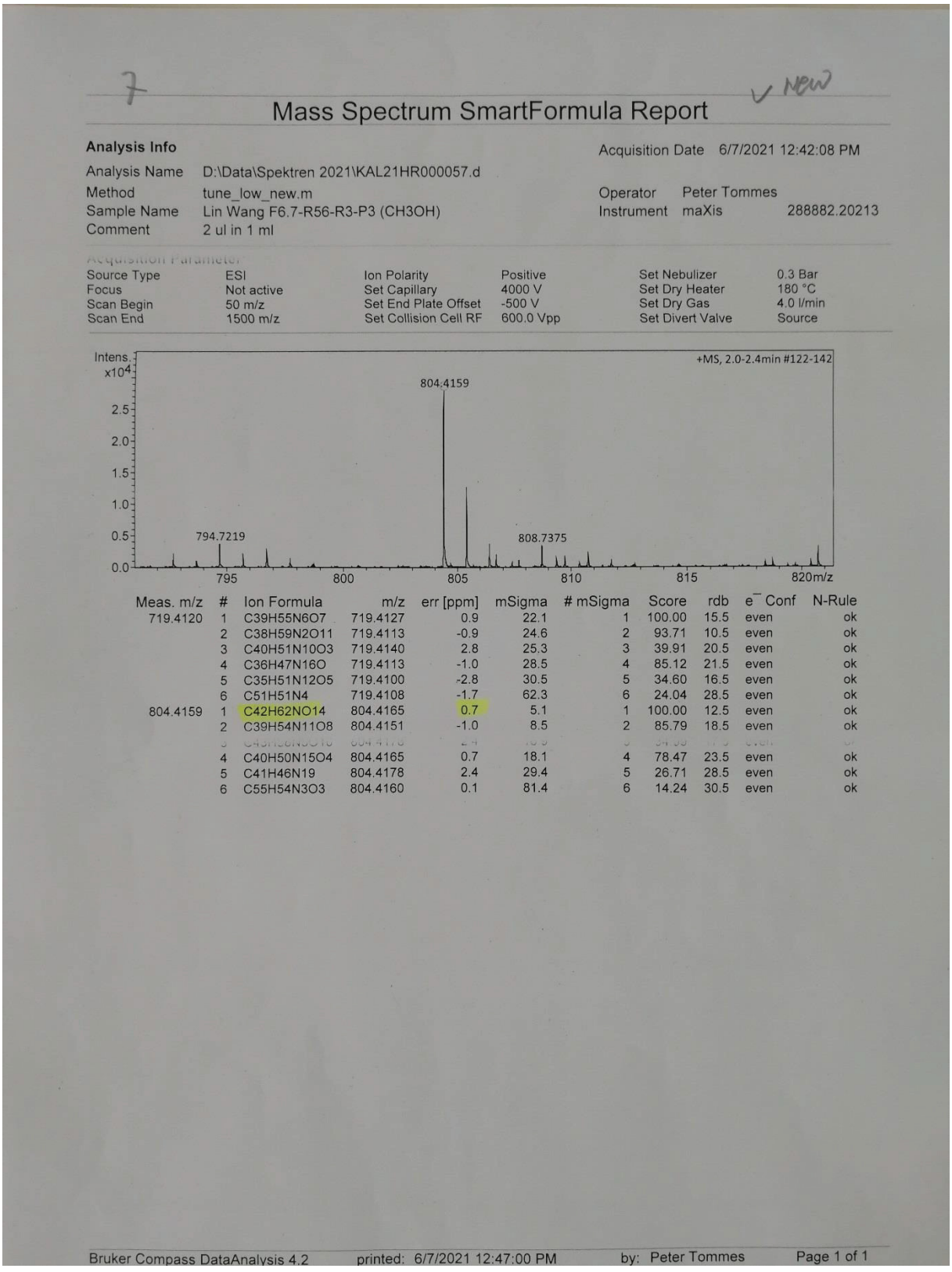

Fig. S52. HRESIMS of Compound **7**

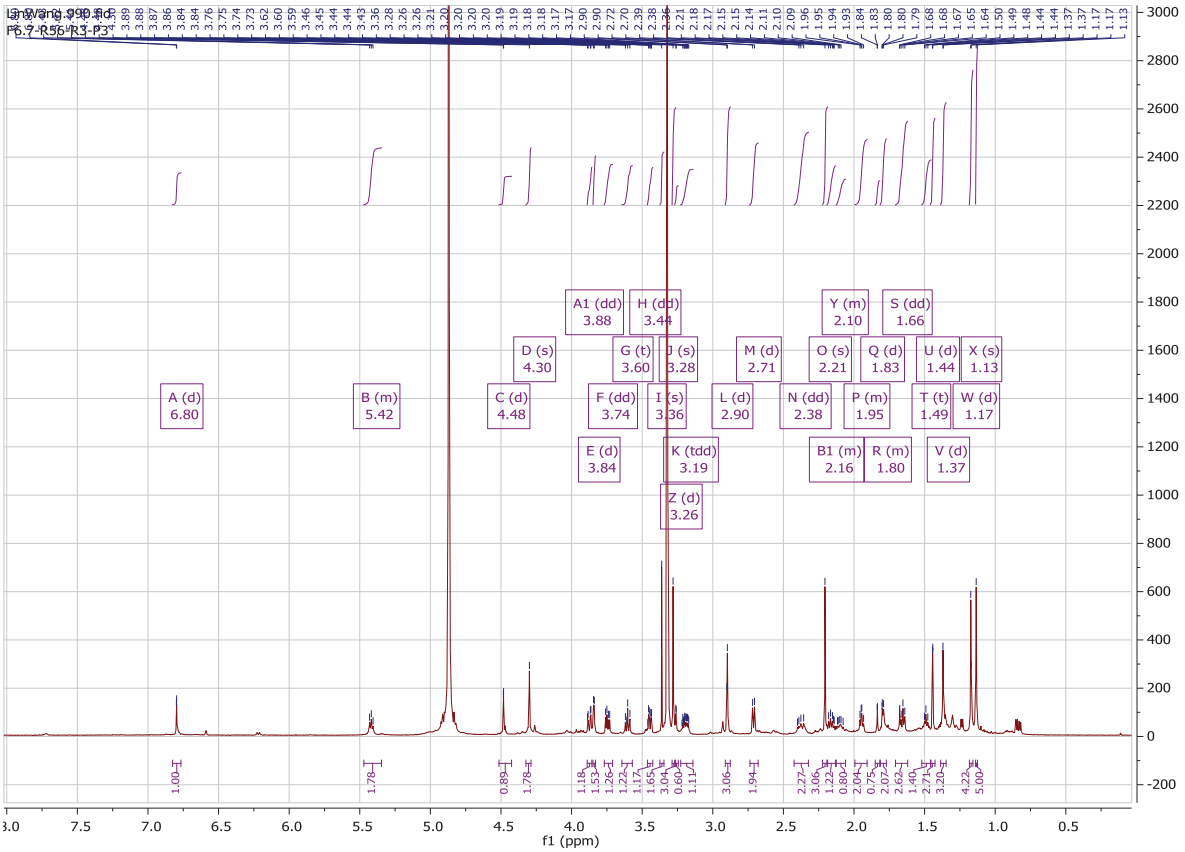

Fig. S53. ^{1}H NMR spectrum of Compound 7

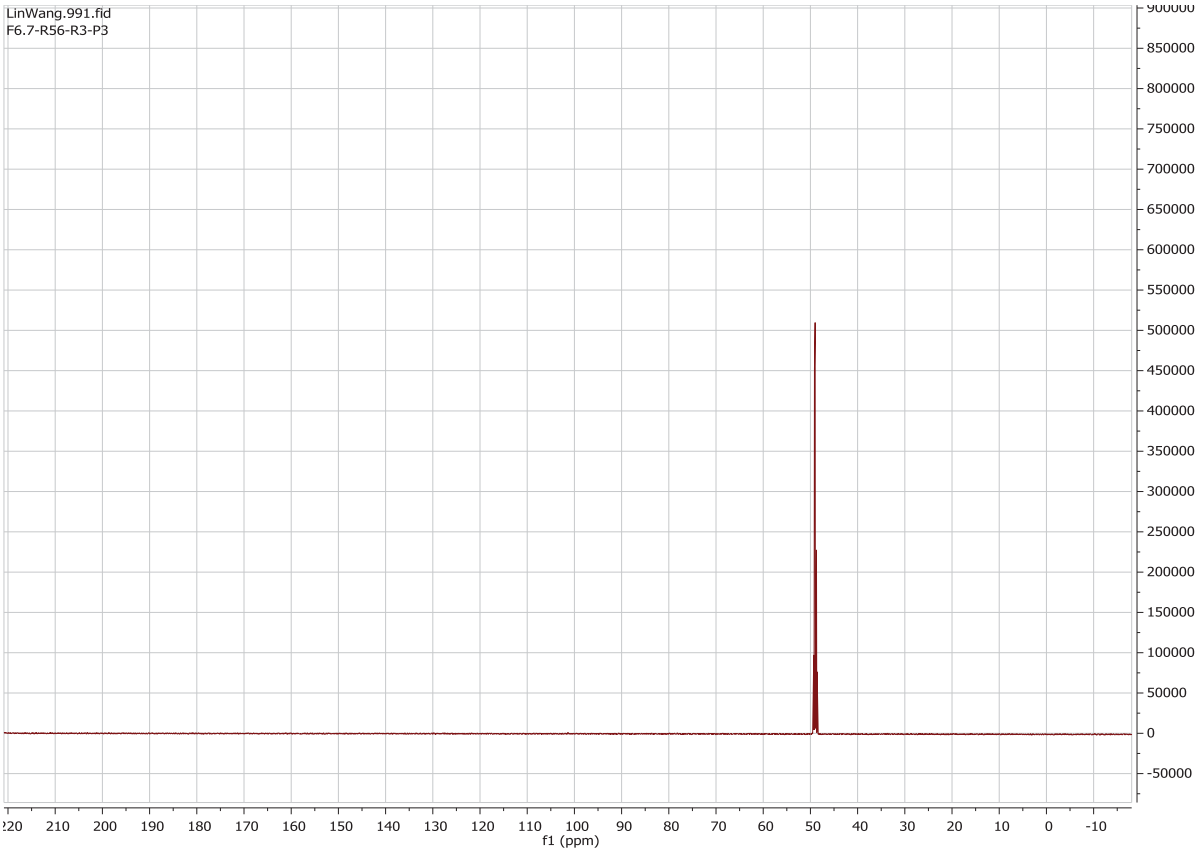

Fig. S54. ^{13}C NMR of Compound **7**

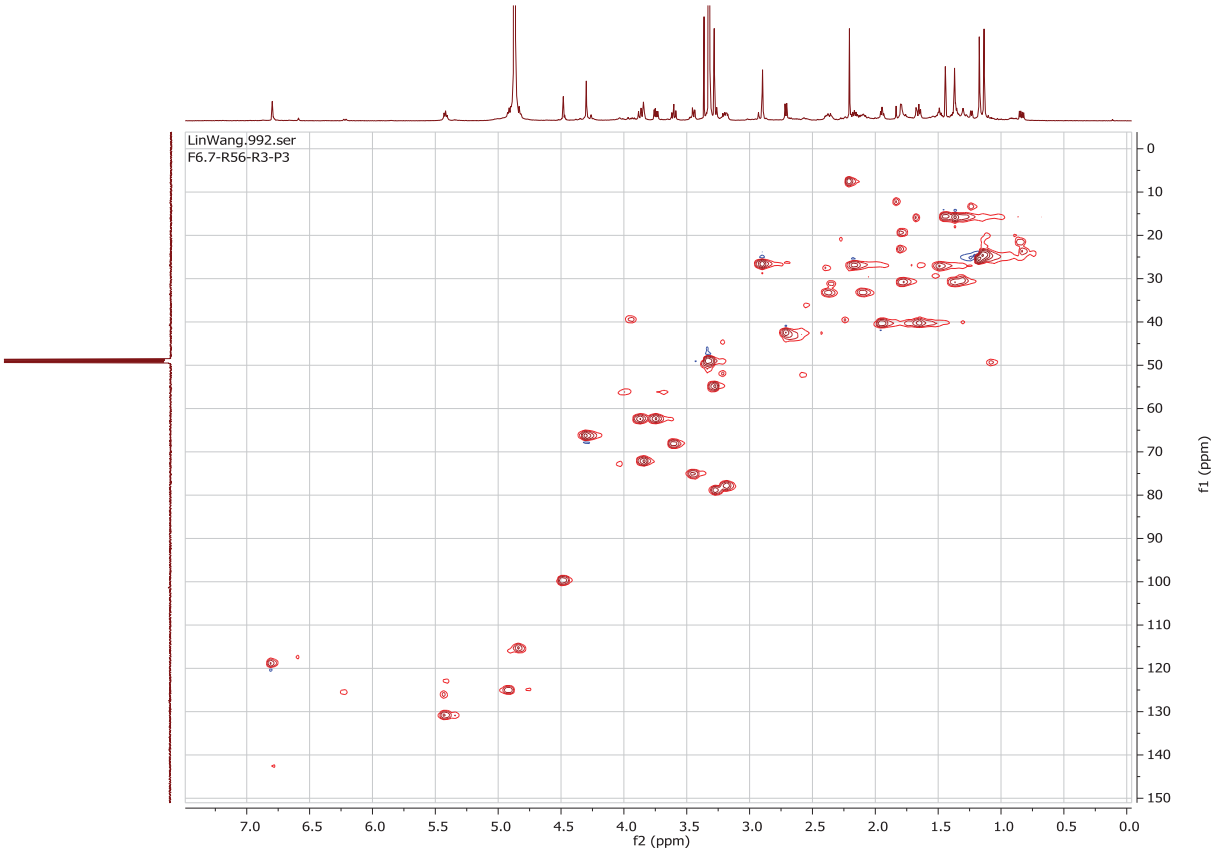

Fig. S55. ^{1}H-^{13}C HSQC of Compound **7**

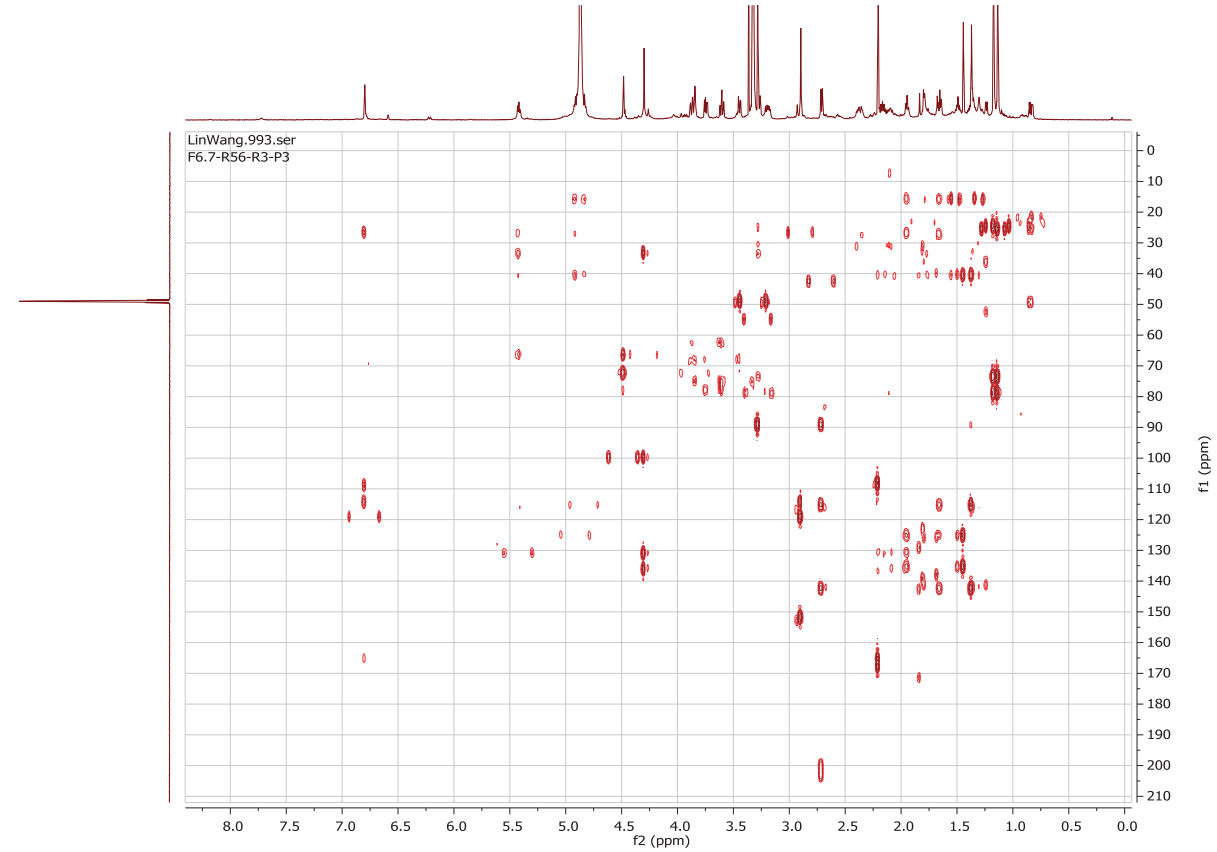

Fig. S56. ^{1}H-^{13}C HMBC of Compound **7**

Fig. S57. ^{1}H-^{1}H COSY of Compound **7**

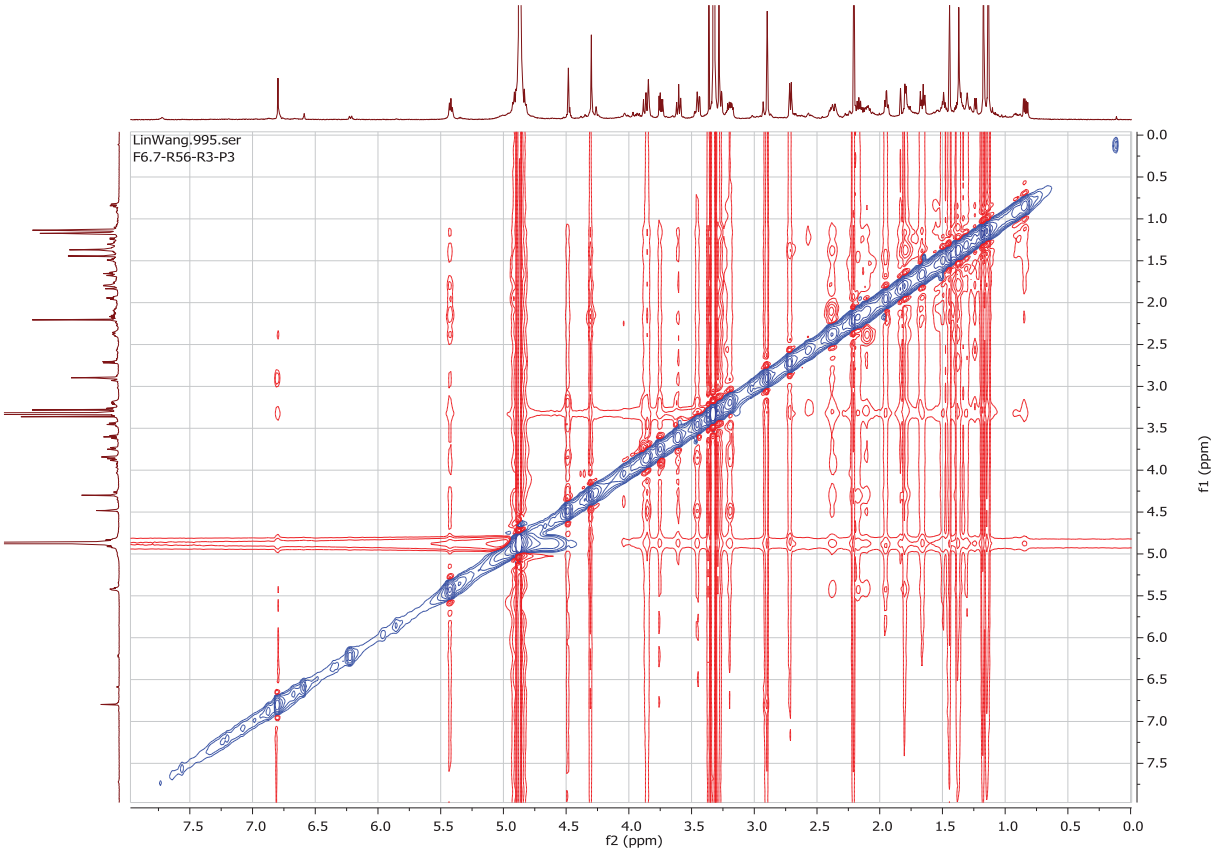

Fig. S58. ^{1}H-^{1}H ROESY of Compound **7**

8 NBW

Mass Spectrum SmartFormula Report

Analysis Info

Analysis Name	D:\Data\Spektren 2021\KAL21HR000059.d	Acquisition Date	6/11/2021 10:23:15 AM
Method	tune_low_new.m	Operator	Peter Tommes
Sample Name	Lin Wang F6.7-R23-P5.2 (CH3OH)	Instrument	maXis 288882.20213
Comment			

Acquisition Parameter

Source Type	ESI	Ion Polarity	Positive	Set Nebulizer	0.3 Bar
Focus	Not active	Set Capillary	4000 V	Set Dry Heater	180 °C
Scan Begin	50 m/z	Set End Plate Offset	-500 V	Set Dry Gas	4.0 l/min
Scan End	1500 m/z	Set Collision Cell RF	600.0 Vpp	Set Divert Valve	Source

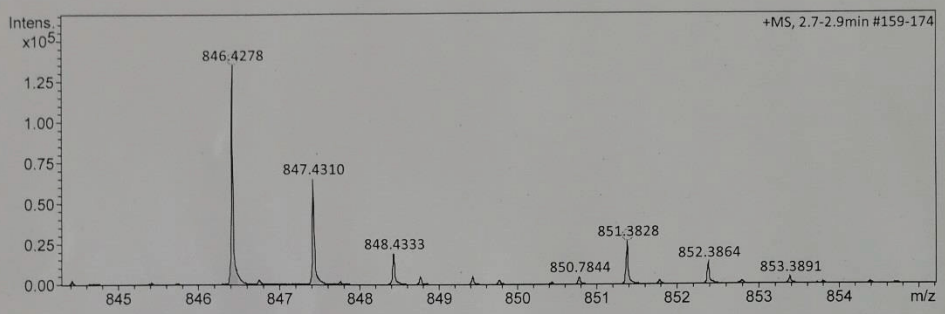

Meas. m/z	#	Ion Formula	m/z	err [ppm]	mSigma	# mSigma	Score	rdb	e⁻ Conf	N-Rule
846.4278	1	C44H64NO15	846.4270	-0.9	6.9	1	100.00	13.5	even	ok
	2	C45H60N5O11	846.4284	0.6	18.4	2	90.88	18.5	even	ok
	3	C42H52N15O5	846.4270	-0.9	18.6	3	79.35	24.5	even	ok
	4	C43H48N19O	846.4284	0.6	30.2	4	69.99	29.5	even	ok
	5	C57H56N3O4	846.4265	-1.5	83.9	5	7.80	31.5	even	ok
	6	C58H52N7	846.4279	0.0	96.0	6	8.80	36.5	even	ok
851.3828	1	C45H56N4NaO11	851.3838	1.1	6.1	1	79.48	19.5	even	ok
	2	C44H60NaO15	851.3824	-0.4	10.5	2	100.00	14.5	even	ok
	3	C42H48N14NaO5	851.3824	-0.4	12.0	3	96.79	25.5	even	ok
	4	C41H52N10NaO9	851.3811	-2.0	14.9	4	42.06	20.5	even	ok
	5	C43H44N18NaO	851.3838	1.1	18.5	5	63.00	30.5	even	ok
	6	C57H52N2NaO4	851.3819	-1.0	67.3	6	16.52	32.5	even	ok
	7	C58H48N6Na	851.3833	0.5	79.4	7	12.89	37.5	even	ok

Bruker Compass DataAnalysis 4.2 printed: 6/11/2021 10:27:52 AM by: Peter Tommes Page 1 of 1

Fig. S59. HRESIMS of Compound **8**

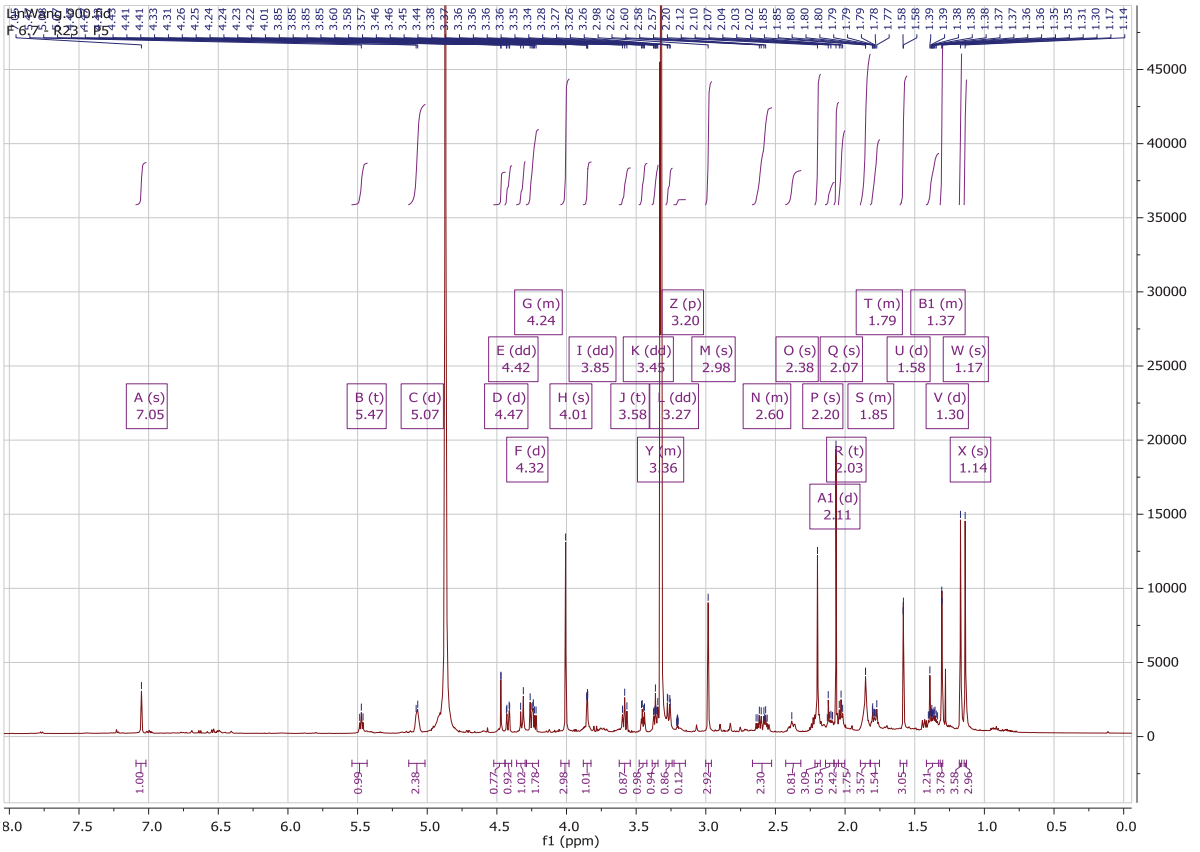

Fig. S60. ^{1}H NMR spectrum of Compound **8**

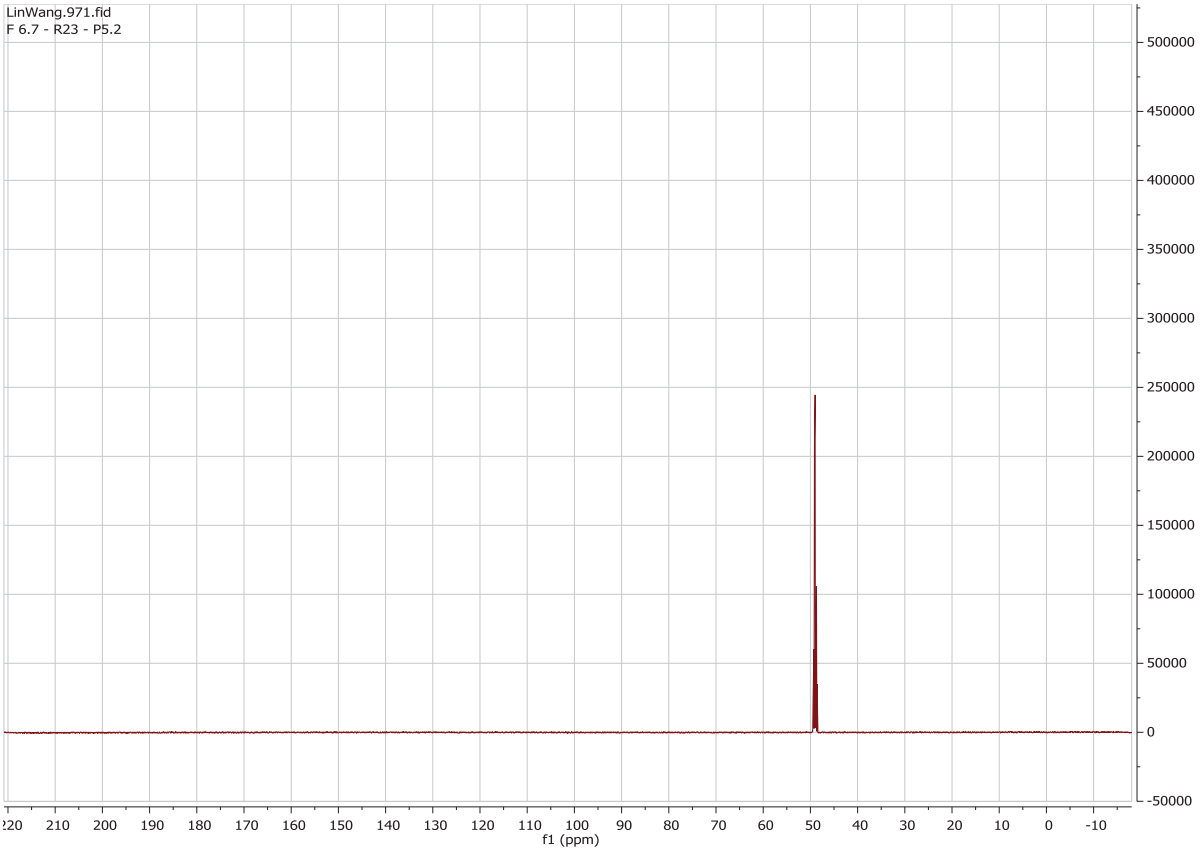

Fig. S61. ^{13}C NMR of Compound **8**

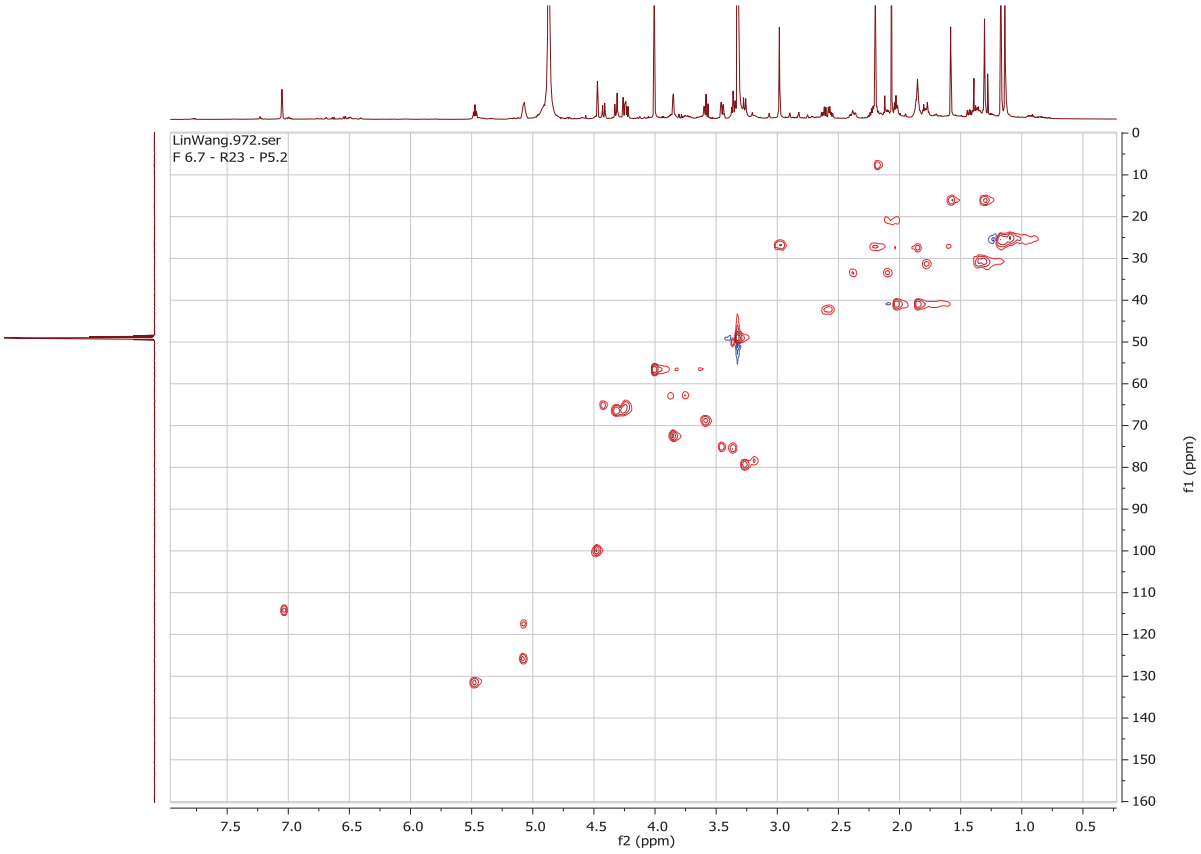

Fig. S62. ^{1}H-^{13}C HSQC of Compound **8**

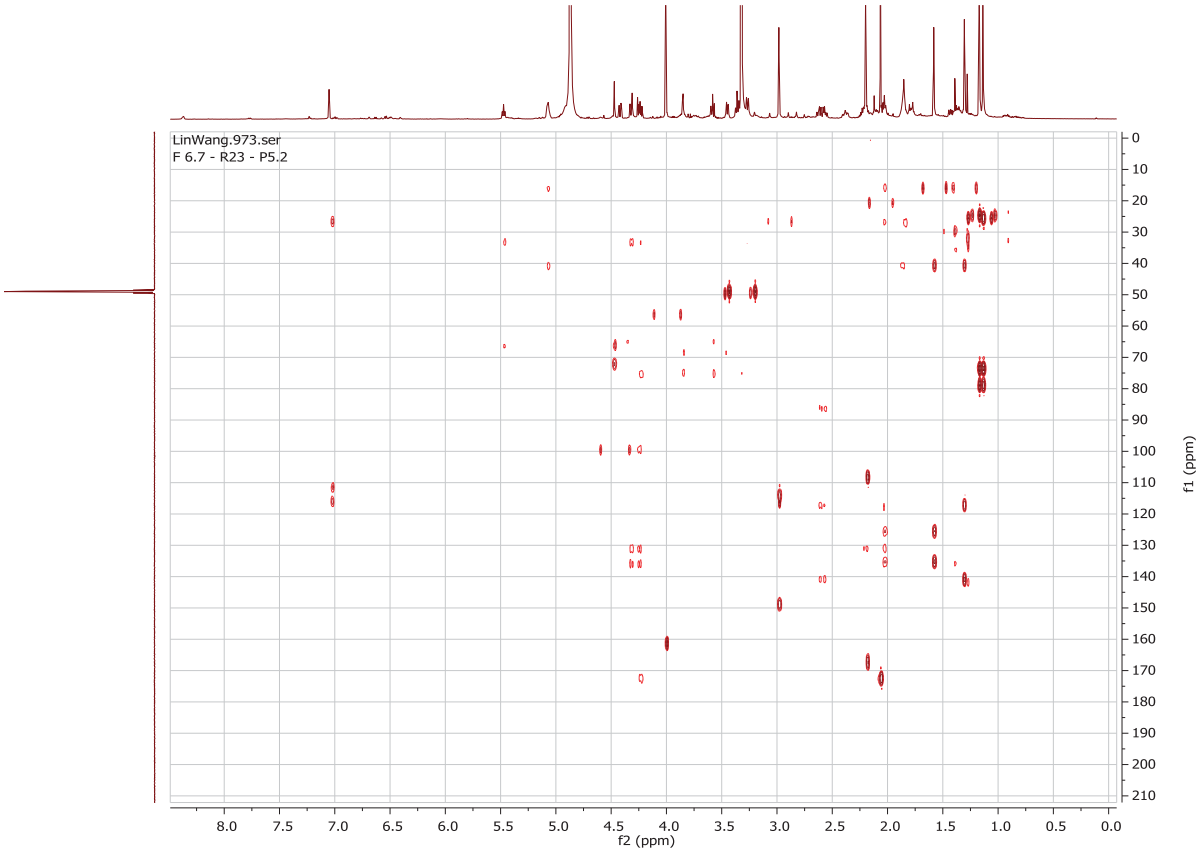

Fig. S63. ^{1}H-^{13}C HMBC of Compound **8**

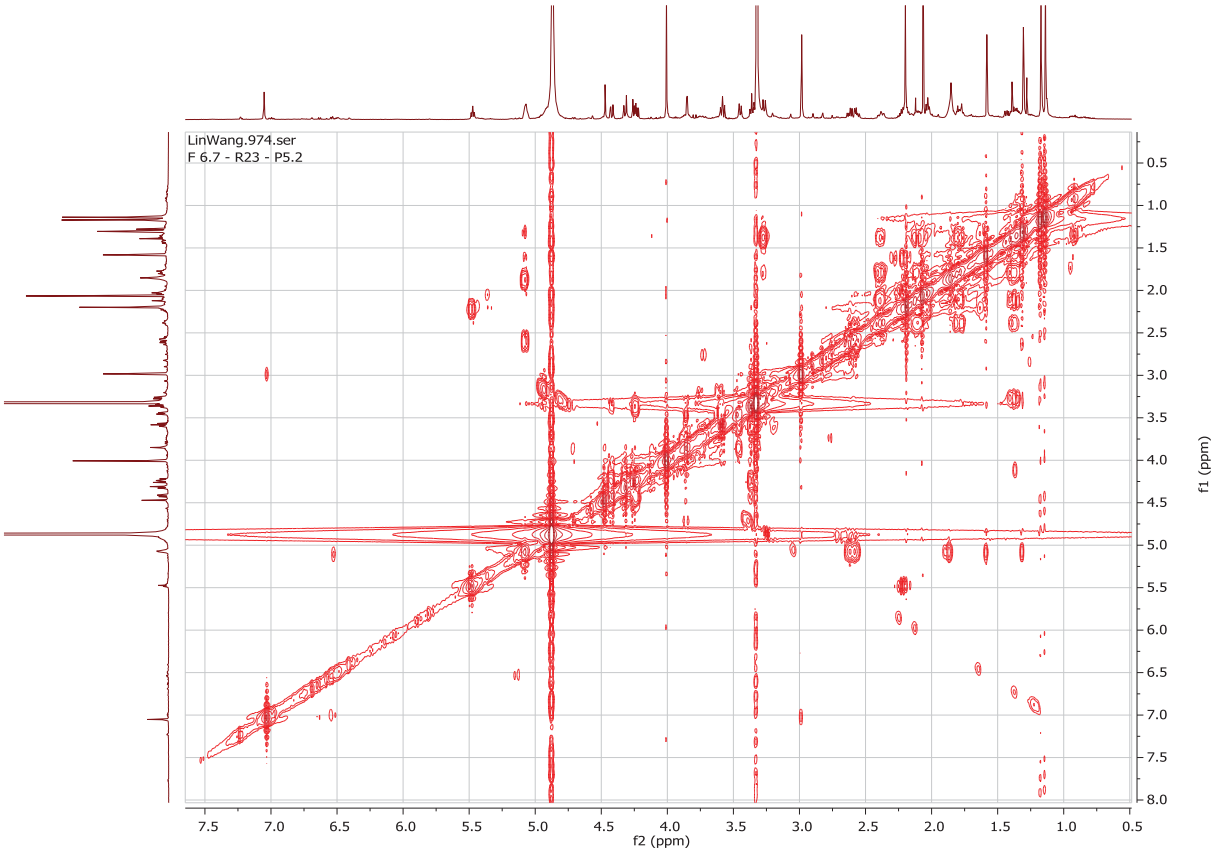

Fig. S64. ^{1}H-^{1}H COSY of Compound **8**

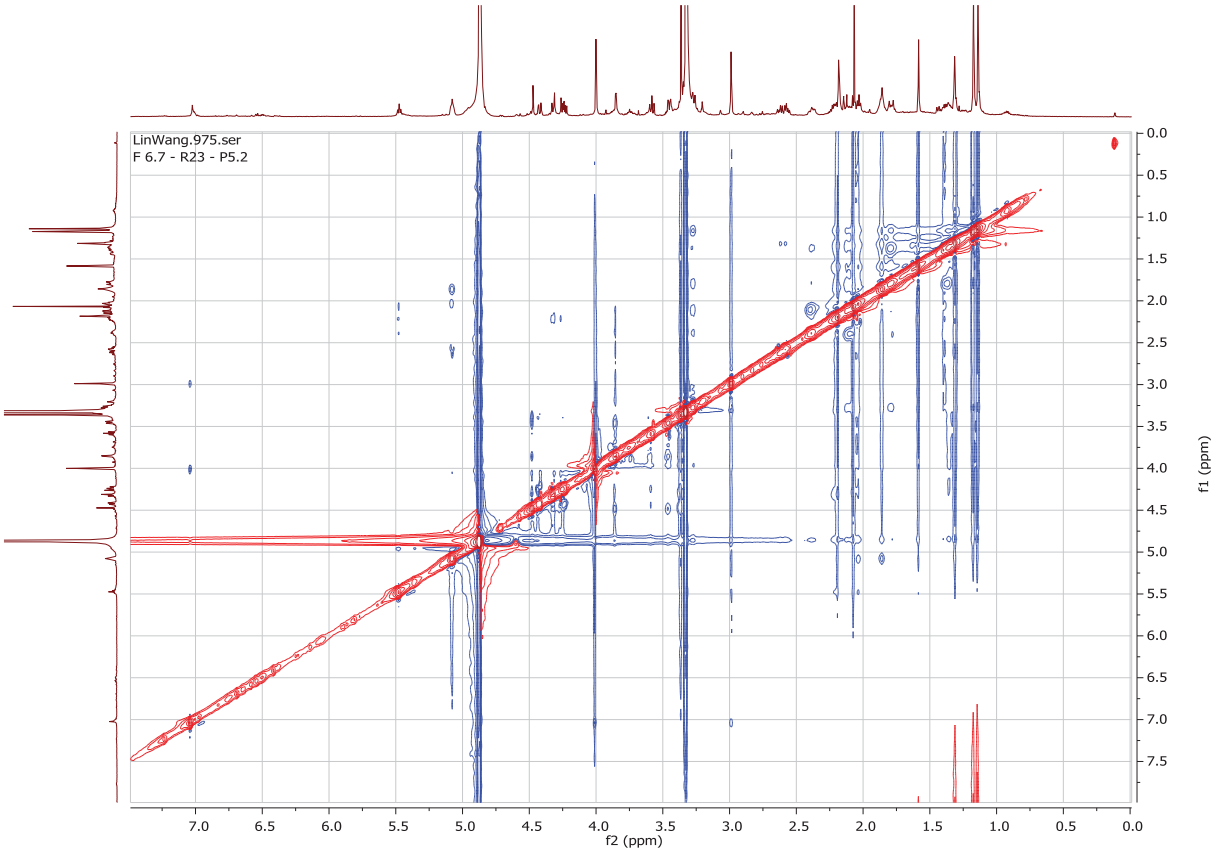

Fig. S65. ^{1}H-^{1}H ROESY of Compound **8**

Chapter 3 – Manuscript 2

Roseazine A with a 1,3-benzodioxole-2,5-diazabicyclo[2.2.1]heptane skeleton from endophytic fungus *Clonostachys rosea*

Overall contribution to the manuscript:

- Fermentation of fungal strain
- Compounds isolation
- Structure elucidation
- Determination of minimal inhibitory concentrations
- Manuscript writing

Roseazine A with a 1,3-benzodioxole-2,5-diazabicyclo[2.2.1]heptane skeleton from endophytic fungus *Clonostachys rosea*

Lin Wang [a], Tobias Heinen [b], Kristin Schwechel [a], Marian Frank [a], Huiqin Chen [c], Ying Gao [a], Christoph Janiak [b], Zhen Liu[d], Rainer Kalscheuer [a*]

a. Institute of Pharmaceutical Biology and Biotechnology, Heinrich Heine University Düsseldorf, Universitätsstrasse 1, 40225 Düsseldorf, Germany

b. Institute of Inorganic and Structural Chemistry, Heinrich Heine University Düsseldorf, Universitätsstrasse 1, 40225 Düsseldorf, Germany

c. Institute of Tropical Bioscience and Biotechnology, Chinese Academy of Tropical Agricultural Sciences, Haikou 571101, China.

d. Key Laboratory of Study and Discovery of Small Targeted Molecules of Hunan Province, School of Medicine, Hunan Normal University, Changsha 410013, China

[*]Corresponding author.

Rainer Kalscheuer: rainer.kalscheuer@hhu.de;

ABSTRACT

One unprecedented roseazine A (**1**), containing a 1,3-benzodioxole-2,5-diazabicyclo[2.2.1] heptane skeleton, one new crystal compound penicillither (**2**) together with five known compounds (**3**-**7**) were isolated from endophytic fungus *Clonostachys rosea*. Their structures were elucidated by a combination of different NMR spectroscopic and mass spectrometric analyses, as well as single crystal X-ray diffraction. Interestingly, compound **6** showed moderate activity against both wild type and methicillin-resistant *Staphylococcus aureus* with minimal inhibitory concentration of 25 μM, while compound **7** showed weak activity against *Mycobacterium tuberculosis* at 50 μM.

INTRODUCTION

Fungi are a potential abundant source of diverse natural products with interesting biological properties. Indeed, a large number of biologically active molecules have been discovered from endophytes in the last several decades. *Clonostachys rosea* is a fungus found widespread around the world and inhabits many diverse ecological niches, with the highest frequency in soil.[1] As biological activity in pharmaceutical and agrochemical applications.[2] Up to now, secondary metabolites reported from *C. rosea* have been found belonging to several chemical classes mainly including alkaloids,[3] polyketides[4-7] and terpenoids.[8] Many metabolites exhibit biological activities, such as antimicrobial[5], phytotoxic[4] and cytotoxic[8] activities. However, natural products containing piperazine connected with dioxolane or aromatic rings have been rarely reported from fungi so far. For example, chrysosporazine A, which was isolated from the marine derived fungus *Chrysosporium sp*. CMB-F214.[9], incorporates an unprecedented hexahydro-6H-pyrazino[1,2-b]isoquinolin-6-one scaffold and showed significant *in vitro* P-glycoprotein inhibitory activity in a cellular model. Another specific indole diketopiperazine alkaloid, chevalinulin A containing an unprecedented spiro-[bicycle[2.2.2]octane-diketopiperazine] skeleton, was obtained from deep sea cold-seep-derived fungus *Aspergillus*

chevalieri CS-122 and exhibited proangiogenic activity.[10] Based on the unique characterization and diversity of secondary metabolites fungi are capable to produce, we carried out chemical investigations on the fungus *C. rosea* and assessed antibacterial bioactivity of some secondary metabolites.

RESULTS AND DISCUSSION

An ethyl acetate crude extract was obtained from *C. rosea* cultured on solid rice medium. Different stationary phases like silica gel, Sephdex gel and ODS were used to chromatograph and yield the a new compound roseazine A (**1**) and a new crystal compound penicillither (**2**) together with five known compounds: arthriniumnin A (**3**), arthriniumnin C (**4**), trichalasin H (**5**), aspochalasin B (**6**) and aspochalasin I (**7**). Their chemical structures were elucidated by NMR spectroscopy, HRESIMS, single crystal X-ray diffraction and comparison with reported data (Fig. 1). [11-14]

Compound **1** was obtained as colorless powder. The positive HRESIMS analysis of **1** revealed a molecular formula of $C_{29}H_{28}N_2O_6$, indicating 17 degrees of unsaturation. Detailed analysis of its 1D and 2D NMR data collected in $CDCl_3$ allowed to establish fragments **1**A and**1**B for compound **1** (Fig. 2). The HMBC correlations from H-12 (δ_H 6.42) to C-8 (δ_C 150.0) and C-9 (δ_C 135.6), aromatic proton H-7 (δ_H 6.49) to C-6 (δ_C 128.3), C-8 and C-9 and another aromatic proton H-11 (δ_H 6.42) to C-6, C-9 and C-10 (δ_C 144.0) indicated the fragment 1A as benzo[1,3]dioxole and linked with a methoxy group by the HMBC correlation from H-29 (δ_H 3.85) to C-10.

The remaining ^{1}H NMR spectrum showed typical signals of ten aromatic protons at δ_H 7.52 (m, H-22/H-26), 7.46 (m, H-24), 7.39 (d, H-23/H-26), 7.35 (d, H-15/H-19), 7.34 (d, H-16/H-18), and 7.31 (m, H-17) (Table S1). The COSY correlations between H-22/H-23/H-24/H-25/H-26, and H-15/H-16/ H-17/H-18/H-19, together with key HMBC correlations from H-20 (δ_H 4.88) to C-21 (δ_C 140.5) and from H-15/H-19 to C-13 (δ_C 174.8) figured out two benzenes

connected with oxygenated methine and ketone. Additionally, the signals of HMBC correlations from H-3 (δ_H 4.81) to C-1 (δ_C 79.4) and C-5 (δ_C 61.2), from H-5 (δ_H 3.48) to C-1 and 3-C (δ_C 58.2), and from H-2 (δ_H 3.92) to C-1 allowed to form a piperazine ring and its linkage with these two aromatic rings through the HMBC correlations from H-5 to C-13, and H-20 to C-1. In addition, the HMBC correlations from H-28 (δ_H 2.21) to C-27(δ_C 169.9) confirmed presence of the ethanone group, while its attachment to the piperazine ring between C-2 and C-3 was revealed by ROESY correlations between H-28 and H-2.

Most importantly, the signals of HMBC correlations from H-4 (δ_H 3.34) to C-1 and C-3 demonstrated that a carbon bridge (C-4) was formed through crossing the piperazine ring at C-1 and C-3. Combining the piperazine which linked with the carbon bridge and two aromatic rings, this allowed identification of the structure as fragment **1B**.

Subsequently, the connection between fragments **1A** and **1B** via the bond of C-4−C-6 was established by the HMBC correlation from H-4 to C-6, and C-11 (δ_C 109.5). Thus, the planar structure of **1** was elucidated as roseazine A (Fig. 2+3), and detailed ^{1}H and ^{13}C NMR data are given in supporting Table 1. To further corroborate the proposed structure, a single crystal of **1** was obtained by slowly crystallizing in a solvent of mixture of methanol and DMSO at 4 °C. X-ray crystallographic analysis confirmed the structure of **1** and demonstrated its absolute configuration as C-1 (*S*), C-3 (*S*), C-4 (*R*), and C-20 (*S*) (Fig. 4).

Compound **2** was obtained as colorless powder and assigned the molecular formula $C_{17}H_{15}ClO_8$ by HRESIMS. The ^{1}H and ^{13}C NMR spectra (table 1) showed a good agreement with known compound methyl 3-chloroasterric acid. The proposed structure of **2** was supported by X-ray crystallographic analysis (Fig. 4) of a crystal obtained from crystallization of a solution in methanol after one month. But additional methyl ester was attached at acid group of **2** because of the reaction with solvent methanl.

Compounds **1**−**7** were evaluated for antimicrobial activity following the recommendations of the Clinical and Laboratory Standards Institute (CLSI).[16] Compounds **1**-**5** did not exhibit

antimicrobial activity, while compound **6** showed moderate activity against *Staphylococcus aureus* ATCC 29213 and *S. aureus* ATCC 700699 with a minimal inhibitory concentration (MIC) of 25 μM. Compound **7** displayed specific inhibitory activity against *Mycobacterium tuberculosis* strain H37Rv with MIC value of 50 μM (Table 2).

In conclusion, five known cytochalasin derivatives (**3**-**7**), one new chrysine E (**2**) and a new roseazine A (**1**) comprising a hitherto unprecedented 1,3-benzodioxole-2,5-diazabicyclo[2.2.1] heptane skeleton were isolated from the endophytic fungus *C. rosea*, enriching the diversity of secondary metabolites and scaffolds of natural products. Antibacterial activity screening revealed that compound **6** showed moderate activity against sensitive and methicillin-resistant strains of the gram-positive bacterium *S. aureus,* while compound **7** displayed some activity against *M. tuberculosis*. This work highlights the enormous potential of mother nature to create amazingly complex chemical scaffolds and adds to our knowledge of the diversity of natural products that might be useful in antibacterial drug discovery.

EXPERIMENTAL

General Experimental Procedure

The ^{1}H (600 MHz), ^{13}C (125 MHz) and 2D NMR spectra were recorded by Bruker Avance III, using TMS as an internal standard. Electrospray ionization mass spectra (ESI-MS) was measured by HP1100 Agilent Finnigan LCQ Deca XP Thermoquest mass spectrometer and high-resolution Electrospray ionization mass spectra (HRESIMS) were obtained by UHR-QTOF Maxis 4G mass spectrometer. Analytical HPLC was performed by Dionex P580 system with a photodiode array detector (UVD340S) while semi-preparative HPLC was using Knauer Azura system which equipped with Knauer Smartline UV Detector 2600 and EC 250/4.6 Nucleosil 120–5, C4 column (Macherey & Nagel). Stationary phases like silica gel 60M (0.04–0.063 mm) Merck MN and Sephadex LH-20 were used for column chromatography. Thin layer chromatography (TLC) was done using pre-coated silica gel 60 F254 plates (Merck) for

analysis of fractions by viewing under UV light at 254 and 366 nm or by spraying the plates with anisaldehyde reagent followed by heating. Distilled or spectral grade solvents were used for column chromatography and spectroscopic measurements, respectively.

Fungal Material and Fermentation

The endophytic fungus *C. rosea* was isolated from the plant *Conyza canadensis* collected in April 2018 in Beijing, P.R. China. The isolation of the fungal strain was achieved according to a standard procedure as described before.[17] The strain was identified as *Clonostachys rosea* according to DNA amplification and sequencing of the ITS region, which has been deposited in the GenBank database under accession number OL597994, and BLAST comparison with the nucleotide database at the National Center for Biotechnology Information. The strain was preserved under the designation CC-12GB in a cryogenic freezer (−80 °C) in the laboratory of R. Kalscheuer.

Extraction and Purification

The *C. rosea* strain was cultured on solid rice medium using twenty 1 L flasks each containing autoclaved 100 g rice and 110 mL water and statically incubated at 22 °C for 24 days. The fermented rice cultures were extracted by addition of 500 mL EtOAc for each flask twice. The combined extracts were combined and concentrated by rotary evaporation yielding a total of 39.2 g crude EtOAc extract. The crude extract was separated via silica gel vacuum liquid chromatography (VLC) with a stepwise elution with n-hexane / EtOAc (100:0, 80:20, 60:40, 40:60, 20:80, 0:100 v/v) and dichloroform / methanol (100:0, 60:40, 20:80, 0:100 v/v) as elution solvent with 1 L for each to give seven fractions (Fr.1-Fr.7). Fr.4 (3.7 g) was subjected to C-18 ODS chromatography and eluted with H_2O / MeOH (30%, 40%, 50%, 60%. 70%. 100% v/v) to obtained five sub-fractions (Fr.4.1- Fr.4.5). Afterwards, Fr.4.2 (2.0 g) was further fractioned by Sephadex LH-20 column with 2 L of MeOH to harvest five sub-fractions

(Fr.4.2.1- Fr.4.2.5). Fraction 4.2.2 (0.9 g) was further separated using VLC column with n-hexane / EtOAc (100:0, 60:40, 40:60, 20:80, 0:100 v/v) as elution solvent with 500 mL for each and collected five sub-fractions (Fr.4.2.2.1-Fr.4.2.2.5). Subsequently, semi-preparative HPLC was performed with a mixture of MeOH and H_2O to yield compound **1** (4.7 mg), **2** (3.5 mg), **3** (3.2 mg) and **4** (4.9 mg) from Fr.4.2.2.1. Compound **5** (10.2 mg), **6** (8.7 mg) and **7** (5.4 mg) were obtained from Fr.4.2.2.4 by semi-preparative HPLC with a mixture of MeOH and H_2O.

Roseazine A (**1**): Obtained as colorless powder, $[\alpha]_D^{25}$ -44.269 ($CHCl_3$);); UV (MeOH) λmax (nm): 212.2, 250.1; HRESIMS m/z 500.1947 $[M + H]^+$ (calcd for $C_{29}H_{28}N_2O_6$, 500.1947); ^1H and ^{13}C NMR data are given in Table 1.

Penicillither (**2**) Obtained as colorless powder, UV (MeOH) λ_{max} (nm): 218.2, 238.6, 317.1; HRESIMS m/z 397.0680 $[M + CH_3]^+$, calcd for $C_{17}H_{15}ClO_8$, 382.0455. ^1H and ^{13}C NMR data are given in Table 1.

Arthriniumnin A (**3**): Yellow amorphous powder, ESIMS m/z 448.3 $[M + H]^+$, formula with $C_{28}H_{33}NO_4$, ^{13}C NMR δ (ppm, in MeOH-d_4): 206.5, 172.2, 169.0, 142.4, 140.6, 137.5, 135.0, 133.3, 129.8, 128.4, 127.7, 126.3, 122.5, 87.1, 55.5, 50.9, 47.8, 42.6, 40.2, 38.5, 34.7, 34.0, 18.4, 16.6, 12.5, 11.1; ^1H NMR *J* Hz: 7.34, 7.28, 7.22, 6.74, 5.58, 5.57, 5.28, 3.67, 3.17, 2.91, 2.72, 2.35, 2.26, 2.26, 2.00, 1.94, 1.79, 1.75, 1.09, 0.99.

Arthriniumnin C (**4**): Yellow oil, ESIMS (m/z 463.3 $[M + H]^+$, formula with $C_{28}H_{33}NO_5$, ^{13}C NMR δ (ppm, in MeOH-d_4): 206.8, 172.3, 168.7, 141.3, 139.3, 136.8, 135.2, 132.3, 129.1, 128.0, 126.5, 121.4, 86.4, 54.7, 51.3, 47.6, 47.0 42.8, 35.2, 33.6, 19.7, 18.5, 14.0, 12.3; ^1H NMR *J* Hz: 7.58, 7.45, 7.42, 6.54, 5.88, 5.75, 5.21, 3.71, 3.42, 3.22, 3.00, 2.83, 2.35, 2.31, 2.26, 2.11, 1.99, 1.85, 1.62, 1.26, 1.17.

Trichalasin H (**5**): Yellow amorphous powder, ESIMS (m/z 402.2 $[M + H]^+$, formula with $C_{24}H_{35}NO_4$, ^{13}C NMR δ (ppm, in $CDCl_3$): 211.6, 173.1, 138.7, 127.4, 83.4, 81.3, 65.1, 63.9, 51.5, 51.1, 48.0, 42.5, 42.4, 38.7, 35.8, 34.7, 34.2, 24.6, 24.0, 23.8, 23.2, 21.3, 19.9, 13.3; ^1H

NMR *J* Hz: 5.43, 3.49, 3.38, 2.95, 2.77, 2.67, 2.54, 2.49, 2.43, 2.37, 2.32, 1.80, 1.71, 1.67, 1.48, 1.31, 1.18, 1.09, 1.07, 0.86, 0.85.

Aspochalasin B (**6**): Yellow oil, ESIMS (m/z 402.3 $[M + H]^+$, formula with $C_{24}H_{33}NO_4$, ^{13}C NMR δ (ppm, in MeOH-d_4): 206.1, 197.1, 174.7, 142.8, 139.6, 137.5, 128.6, 127.9, 125.6, 75.4, 70.7, 52.9, 49.9, 49.7, 48.7, 42.6, 40.93, 35.9, 33.1, 25.8, 24.2, 21.8, 20.1, 15.5, 14.2; ^1H NMR *J* Hz: 8.26, 6.40, 6.34, 5.42, 4.84, 3.18, 2.84, 2.58, 2.41, 1.89, 1.82, 1.78, 1.66, 1.29, 1.26, 0.93, 0.92.

Aspochalasin I (**7**): Yellow oil, ESIMS (m/z 418.3 $[M + H]^+$, formula with $C_{24}H_{35}NO_5$, ^{13}C NMR δ (in MeOH-d_4): 175.3, 169.3, 154.6, 141.6, 140.5, 125.2, 123.7, 120.5, 90.2, 79.2, 74.3, 53.5, 52.7, 49.6, 41.0, 40.7, 35.5, 28.4, 25.8, 24.1, 21.9, 19.7, 15.4, 14.2; ^1H NMR *J* Hz: 7.27, 6.16, 5.94, 5.27, 4.48, 3.84, 3.77, 3.23, 3.05, 2.90, 2.35, 2.15, 2.13, 1.77, 1.46, 1.39, 1.33, 1.27, 0.96, 0.95.

Single-crystal X-ray diffraction

For **1** and **2**, the single-crystal diffraction data was collected using a Rigaku XtaLAB Synergy S four-circle diffractometer with a Hybrid Pixel Array Detector and a PhotonJet X-ray source for Cu-Kα radiation (λ = 1.54184 Å) with a multilayer mirror monochromator. The data were collected under a cold nitrogen gas-stream at 100.0 (1) K using ω-scans. Data reduction and absorption correction were performed by CrysAlisPro.[18] Structures were solved by direct methods and refined with full-matrix least squares refinements on F2 using SHELXL[19] in OLEX2.[20] Crystal data and details on the structure refinement are given in Table SX (Supp. Info.). Amine- and Hydroxyl- hydrogen atom positions are freely refined with Uiso (H) = 1.2 Ueq. All hydrogen atoms were positioned geometrically and refined using riding models with Uiso (H) = 1.2·Ueq (CHarom./CH_2, aliph.) or 1.5·Ueq (CH_3). Graphics were drawn with the program Diamond.[21]

Microorganism Strains

Mueller Hinton broth was used to cultivate the *S. aureus* strains ATCC 25923 and ATCC 70669 at 37 °C. *M. tuberculosis* strain H37Rv was cultured at 37 °C aerobically in Middlebrook 7H9 medium supplemented with 0.5% glycerol, 0.05% tyloxapol and 10% (v/v) ADS enrichment, which is composed of 5% bovine serum albumin fraction V, 2% glucose, and 0.85% sodium chloride.

Determination of Minimal Inhibitory Concentration (MIC)

The antibacterial activity against strains of the gram-positive bacterium *S. aureus* were tested according to the Clinical and Laboratory Standards Institute (CLSI) (CLSI, 2018).[16] Pre-cultured bacteria were diluted to $OD_{600nm} \approx 0.1$ (corresponding to ca. 1×10^6 colony forming units/mL) and seeded into 96-well round bottom microtiter plates containing a two-fold serial dilution of the testing compounds at a concentration range from 0.78 μM-100 μM in a total volume of 100 μL. Moxifloxacin was used as positive control, while DMSO was employed as negative control. Plates was incubated at 37 °C aerobically for 16-20 hours. Next, 100 μg/mL resazurin was added to each well and plates were further incubated for 2-4 hours. Growth was measured through quantification of fluorescence of reduced resazurin by microplate reader (TECAN) (excitation 560 nm, emission 590 nm). All tests were repeated twice.

M. tuberculosis cells were incubated at 37°C in 7H9 medium at 80 rpm for four days. Afterwards, cells were seeded at density of 1×10^6 CFU/mL in 96-well round bottom microplate containing two-fold serial dilutions of testing compounds at a concentration range from 0.78-100 μM in a total volume of 100 μL. Rifamycin served as positive control and DMSO at a maximal concentration of 1% was used as solvent control. The plates were aerobically incubated at 37°C for 4 days and evaluated by microplate reader following the resazurin protocol as described above.

ASSOCIATED CONTENT

Supporting Information

The Supporting Information is available for detailed spectroscopic data; crystallographic data of **1** and **2**, NMR, and HRMS spectra for all isolated new compounds.

AUTHOR INFORMATION

Corresponding Author

Rainer Kalscheuer: rainer.kalscheuer@hhu.de

Notes

The authors declare no competing financial interest.

ACKNOWLEDGMENTS

We are grateful for the financial support from the China Scholarship Council, the Ministry of Education of China, for a doctoral scholarship awarded to L.W.. The Rigaku X-ray diffractometer was funded by the Deutsche Forschungsgemeinschaft (DFG, German Research Foundation) through project number 440366605.

REFERENCES

[1] Sun, Z. B.; Li, S. D.; Ren, Q.; Xu, J. L.; Lu, X.; Sun, M. H. Biology and applications of *Clonostachys rosea*. *J. Appl. Microbiol*. 2020, 3, 486-495.

[2] Han, P. P.; Zhang, X. P.; Xu, D.; Zhang, B. W.; Lai, D. W.; Zhou, L. G. Metabolites from *Clonostachys* Fungi and Their Biological Activities. *Journal of Fungi*. 2020, 6,229.

[3] Abdel-Wahab, N. M.; Harwoko, H.; Müller, W. E. G.; Hamacher, A.; Kassack, M. U.; Fouad, M. A.; Kamelb, M. S.; Lin, W. H.; Ebrahima, W.; Liu, Z.; Proksch, P. Cyclic heptapeptides from the soil-derived fungus *Clonostachys rosea*, *Bioorg. Med. Chem*. 2019, 27, 3954–3959.

[4] Supratman, U.; Suzuki, T.; Nakamura, T.; Yokoyama, Y.; Harneti, D.; Maharani, R.; Salam, S.; Abdullah, F. F.; Koseki, T.; Shiono, Y. New metabolites produced by endophyte *Clonostachys rosea* B5-2. *Nat. Prod. Res*. 2019, 35, 1525-1531.

[5] Zhai, M. M.; Qi, F. M.; Li, J.; Jiang, C. X.; Hou, Y.; Shi, Y. P.; Di, D. L.; Zhang, J. W.; Wu, Q. X. Isolation of secondary metabolites from the soil-derived fungus *Clonostachys rosea* YRS-06, a biological control agent, and evaluation of antibacterial activity. *J. Agric. Food Chem*. 2016, 64, 2298–2306.

[6] Ju, Y.M.; Juang, S. H.; Chen, K. J.; Lee, T. H. TMC-151 A monoacetate, a new polyketide from Bionectria ochroleuca. Z. *Natur forsch. B*. 2007, 62, 561–564.

[7] Okuda, T.; Kohno, J.; Kishi, N.; Asai, Y.; Nishio, M.; Komatsubara, S. Production of TMC-151, TMC-154 and TMC-171, a new class of antibiotics, is specific to '*Gliocladium roseum*' group. *Mycoscience* 2000, 41, 239–253.

[8] Dias, A. C. D. S.; Couzinet-Mossion, A.; Ruiz, N.; Lakhdar, F.; Etahiri, S.; Bertrand, S.; Ory, L.; Rousakis, C.; Pouchus, Y. F.; Nazih, E. H.; et al. Steroids from marine-derived fungi: Evaluation of antiproliferative and antimicrobial activities of eburicol. *Mar. Drugs* 2019, 17, 372.

[9] Elbanna, A. H.; Khalil, Z. G.; Bernhardt, P. V.; Capon, R. J. Chrysosporazines A–E: P-Glycoprotein Inhibitory Piperazines from an Australian Marine Fish Gastrointestinal Tract-Derived Fungus, *Chrysosporium sp*. CMB-F214. *Org. Lett*. 2019, 21, 8097−8100.

[10] Yan, L.H.; Li, P. H.; Li, X. M.; Yang S.Q.; Liu, K. C.; Wang, B. G.; Li, X. Chevalinulins A and B, Proangiogenic Alkaloids with a Spiro[bicyclo[2.2.2]octane-diketopiperazine] Skeleton from Deep-Sea Cold-Seep-Derived Fungus *Aspergillus chevalieri* CS-122. *Org. Lett*. 2022, 24, 2684−2688.

[11] Wang, J. F.; Wang, Z.; Ju, Z. R.; Wan, J. T.; Liao, S. R.; Lin, X. P, Zhang, T. Y, Zhou, X. F.; Chen, H.; Tu, Z. C.; Liu, Y. H. Cytotoxic Cytochalasins from Marine-Derived Fungus *Arthrinium arundinis*. *Planta Med*. 2015, 81, 160–166.

[12] Chen, L.; Liu, Y. T.; Song, B.; Zhang, H. W.; Ding, G.; Liu, X. Z.; Gu,Y. C.; Zou, Z. M. Stereochemical determination of new cytochalasans from the plant endophytic fungus Trichoderma gamsii. *Fitoterapia*. 2014, 96, 115–122.

[13] Wu, Z.; Zhang, X. T.; Anbari, W. H. A.; Zhang, M.; Chen, X.; Luo, Z. W.; Li, X. N.; Chen, C. M.; Liu, J. .; Wang, J. .; Zhu, H. C; Zhang Y. H. Amiaspochalasins A-H, Undescribed Aspochalasins with a C-21 Ester Carbonyl from *Aspergillus micronesiensis*. *J. Org. Chem*. 2019, 84, 5483−5491.

[14] Tailro, T.; Kazuo, S. Y.; Taisei, K.; Atsushi, M.; Haruo, S.; Yoichi, H. Selective Cytotoxicity and Stereochemistry of Aspochalasin D. *J. Antibiot*. 2001, 54, 379-381.

[15] Jongrungruangchok, S.; Aree, T.; Sureram, S.; Kittakoop, P. Crystal structure of 2-(2-carboxy-4-hydroxy-6-methoxyphenoxy)-3, 5-dichloro-6-hydroxy-4-methylbenzoic Acid 1-methyl ester. *Chinese J. Struct. Chem*. 2013, 32, 1742-1748.

[16] CLSI. Methods for dilution antimicrobial susceptibility tests for bacteria that grow aerobically. CLSI standard M07 11th ed. Wayne, PA: Clinical and Laboratory Standards Institute; 2018

[17] Kjer, J.; Debbab, A.; Aly, A. H.; & Proksch, P. Methods for isolation of marine-derived endophytic fungi and their bioactive secondary products. *Nature protocols*. 2010, 5, 479-490.

[18] CrysAlis PRO, Agilent Technologies Ltd, Yarnton, Oxfordshire, England, 2014.

[19] Sheldrick, G. M. Crystal Structure Refinement with SHELXL. *Acta Crystallographica C*. 2015, 71, 3-8.

[20] Dolomanov, O. V.; Bourhis, L. J.; Gildea, R. J.; Howard, J. A. K.; Puschmann, H. A Complete Structure Solution, Refinement and Analysis Program. *J. Appl. Crystallogr*. 2009, 42, 339-341.

[21] Brandenburg, K. Diamond Crystal and Molecular Structure Visualization, Version 4.6.6. Crystal Impact GbR, Bonn, Germany, 1997-2021.

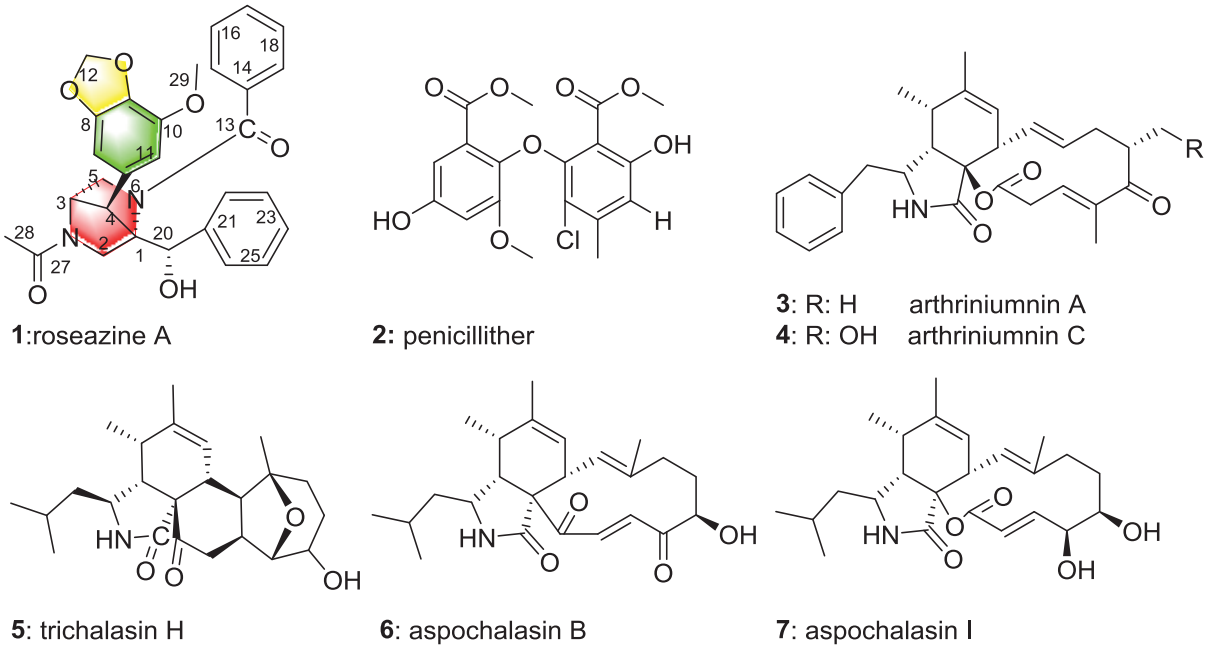

Figure 1: Structures of isolated compounds

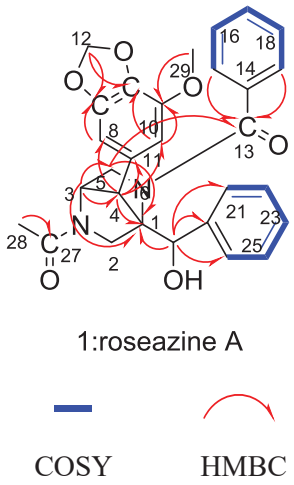

Figure 2. Key COSY and HMBC correlations of **1**.

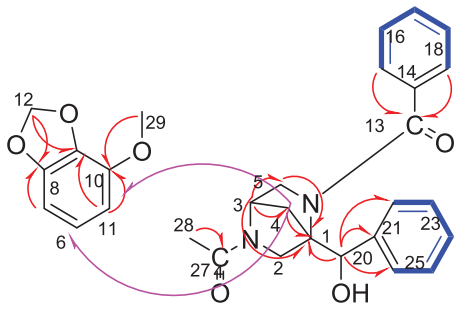

Figure 3. Key COSY and HMBC (red and purple arrows are for intra and inter-fragments **1A** and **1B**, respectively) correlations of compound **1**.

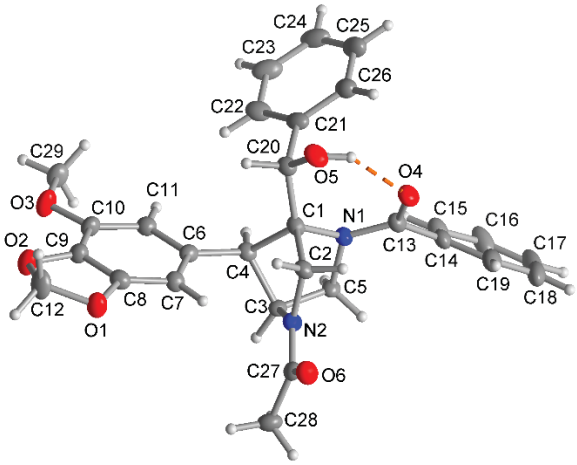

1

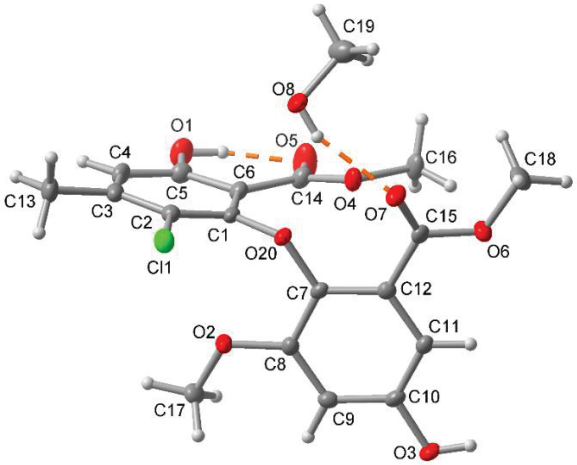

2

Figure 4. Molecular structures of **1** and **2** from single-crystal X-ray analysis (50% thermal ellipsoids, H atom with arbitrary radii). Compound **2** crystallized as a methanol solvate. The intramolecular hydrogen bonds and hydrogen bonds to the MeOH solvate are given as dashed oranges lines.

Table 1: ^{1}H and ^{13}C NMR data for compounds **1** (600, 125 MHz, δ in ppm, J in Hz).

Compound **1** ($CDCl_3$)		
Position	δ_C	δ_H (mult, J in Hz)
1	79.4	
2	57.0	3.92, d (11.74)
3	58.2	4.81, m
4	54.1	3.34, s
6	128.3	
7	102.9	6.49, d (1.95)
8	150.0	
9	135.6	
10	144.0	
11	109.5	6.42, d (1.69)
12	102.1	6.00, q
13	174.8	
14	135.5	
15	127.8	7.35, d (1.13)
16	129.2	7.34, d (1.67)
17	131.9	7.31, m
18	129.2	7.34, d (1.67)
19	128.7	7.35, d (1.13)
20	71.4	4.88, d (11.98)
21	140.5	
22	127.1	7.52, m
23	127.5	7.39, d (8.33)
24	127.5	7.46, m
25	128.7	7.39, d (8.33)
26	127.1	7.52, m
27	169.9	
28	22.5	2.21
29	57.1	3.85, d (0.73)

Table 2: Antibacterial effect of compounds **1**−**7** against a sensitive (ATCC 29213) and a methicillin-resistant (MRSA, ATCC 700699) strain of *Staphylococcus aureus* and against *M. tuberculosis* H37Rv.

Compound	**MIC** (μM)		
	S. aureus ATCC 29213	*S. aureus* ATCC 700699	*M. tuberculosis* H37Rv
1	n	n	n
2	50	100	
3	50	n	n
4	n	n	n
5	n	n	n
6	25	25	n
7	n	n	50

n: no activity (MIC >100 μM)

Graphic Abstract

Clonostachys rosea

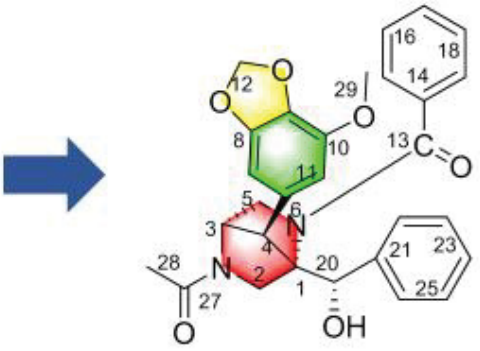

Supporting Information

Roseazine A with a 1,3-benzodioxole-2,5-diazabicyclo[2.2.1]heptane skeleton from endophytic fungus *Clonostachys rosea*

Lin Wang [a], Tobias Heinen [b], Kristin Schwechel [a], Marian Frank [a], Huiqin Chen [c], Ying Gao [a], Christoph Janiak [b], Zhen Liu[d], Rainer Kalscheuer [a*]

a. Institute of Pharmaceutical Biology and Biotechnology, Heinrich Heine University Düsseldorf, Universitätsstrasse 1, 40225 Düsseldorf, Germany

b. Institute of Inorganic and Structural Chemistry, Heinrich Heine University Düsseldorf, Universitätsstrasse 1, 40225 Düsseldorf, Germany

c. Institute of Tropical Bioscience and Biotechnology, Chinese Academy of Tropical Agricultural Sciences, Haikou 571101, China.

d. Key Laboratory of Study and Discovery of Small Targeted Molecules of Hunan Province, School of Medicine, Hunan Normal University, Changsha 410013, China

*Corresponding author.

Rainer Kalscheuer: rainer.kalscheuer@hhu.de;

CONTENT

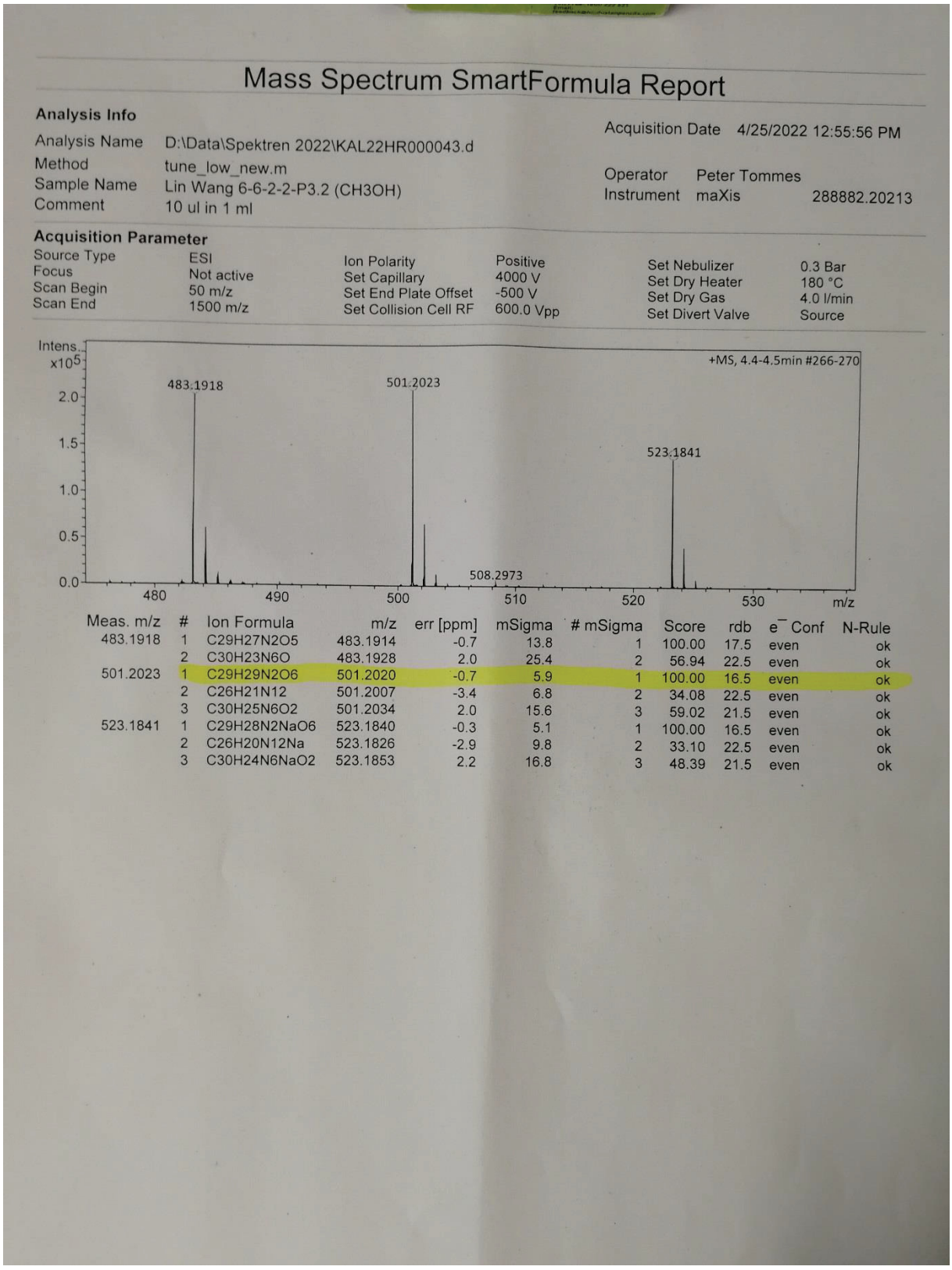

Mass Spectrum SmartFormula Report

Analysis Info

Analysis Name	D:\Data\Spektren 2022\KAL22HR000043.d	Acquisition Date	4/25/2022 12:55:56 PM
Method	tune_low_new.m	Operator	Peter Tommes
Sample Name	Lin Wang 6-6-2-2-P3.2 (CH3OH)	Instrument	maXis 288882.20213
Comment	10 ul in 1 ml		

Acquisition Parameter

Source Type	ESI	Ion Polarity	Positive	Set Nebulizer	0.3 Bar
Focus	Not active	Set Capillary	4000 V	Set Dry Heater	180 °C
Scan Begin	50 m/z	Set End Plate Offset	-500 V	Set Dry Gas	4.0 l/min
Scan End	1500 m/z	Set Collision Cell RF	600.0 Vpp	Set Divert Valve	Source

Meas. m/z	#	Ion Formula	m/z	err [ppm]	mSigma	# mSigma	Score	rdb	e⁻ Conf	N-Rule
483.1918	1	C29H27N2O5	483.1914	-0.7	13.8	1	100.00	17.5	even	ok
	2	C30H23N6O	483.1928	2.0	25.4	2	56.94	22.5	even	ok
501.2023	1	C29H29N2O6	501.2020	-0.7	5.9	1	100.00	16.5	even	ok
	2	C26H21N12	501.2007	-3.4	6.8	2	34.08	22.5	even	ok
	3	C30H25N6O2	501.2034	2.0	15.6	3	59.02	21.5	even	ok
523.1841	1	C29H28N2NaO6	523.1840	-0.3	5.1	1	100.00	16.5	even	ok
	2	C26H20N12Na	523.1826	-2.9	9.8	2	33.10	22.5	even	ok
	3	C30H24N6NaO2	523.1853	2.2	16.8	3	48.39	21.5	even	ok

Figure S1: HRESIMS of compound **1**

Figure S2: ^{1}H NMR of compound **1** in $CDCl_3$

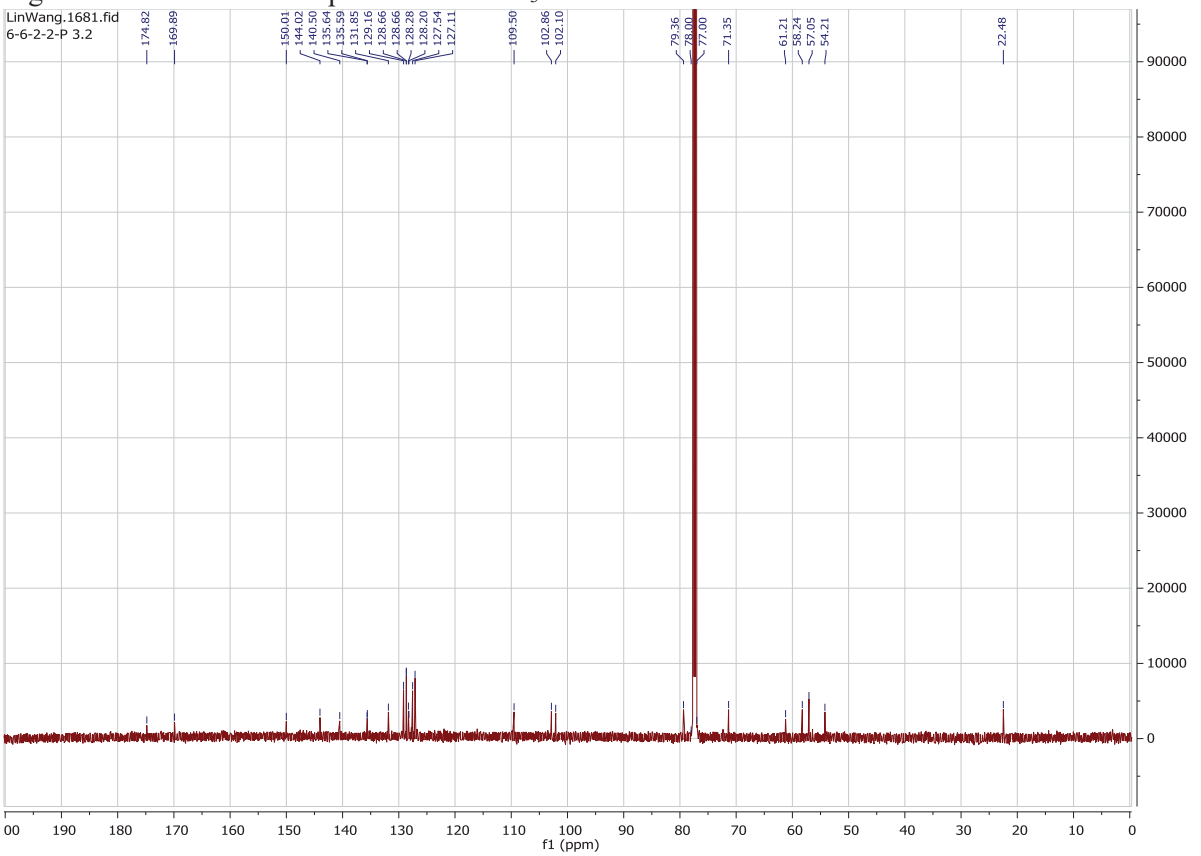

Figure S3: ^{13}C NMR of compound **1** in $CDCl_3$

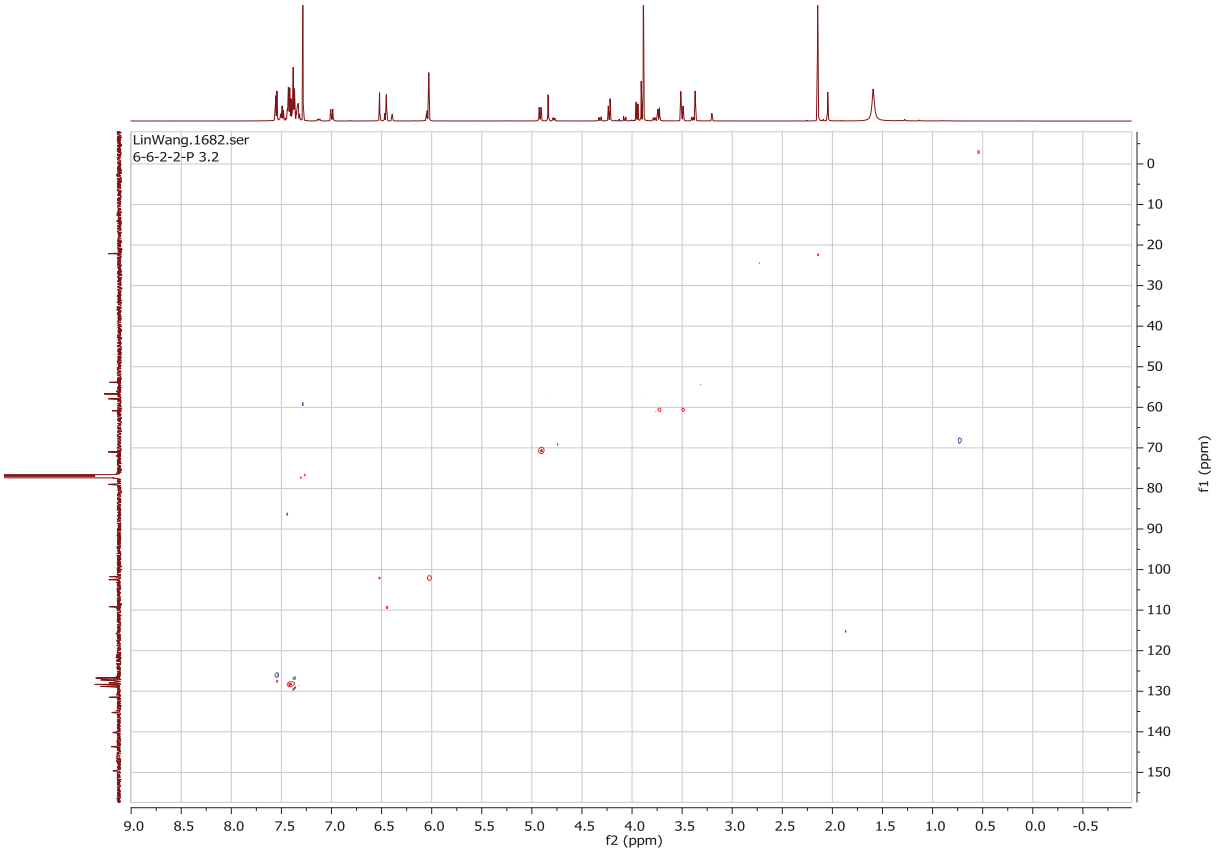

Figure S4: HSQC of compound **1** in $CDCl_3$

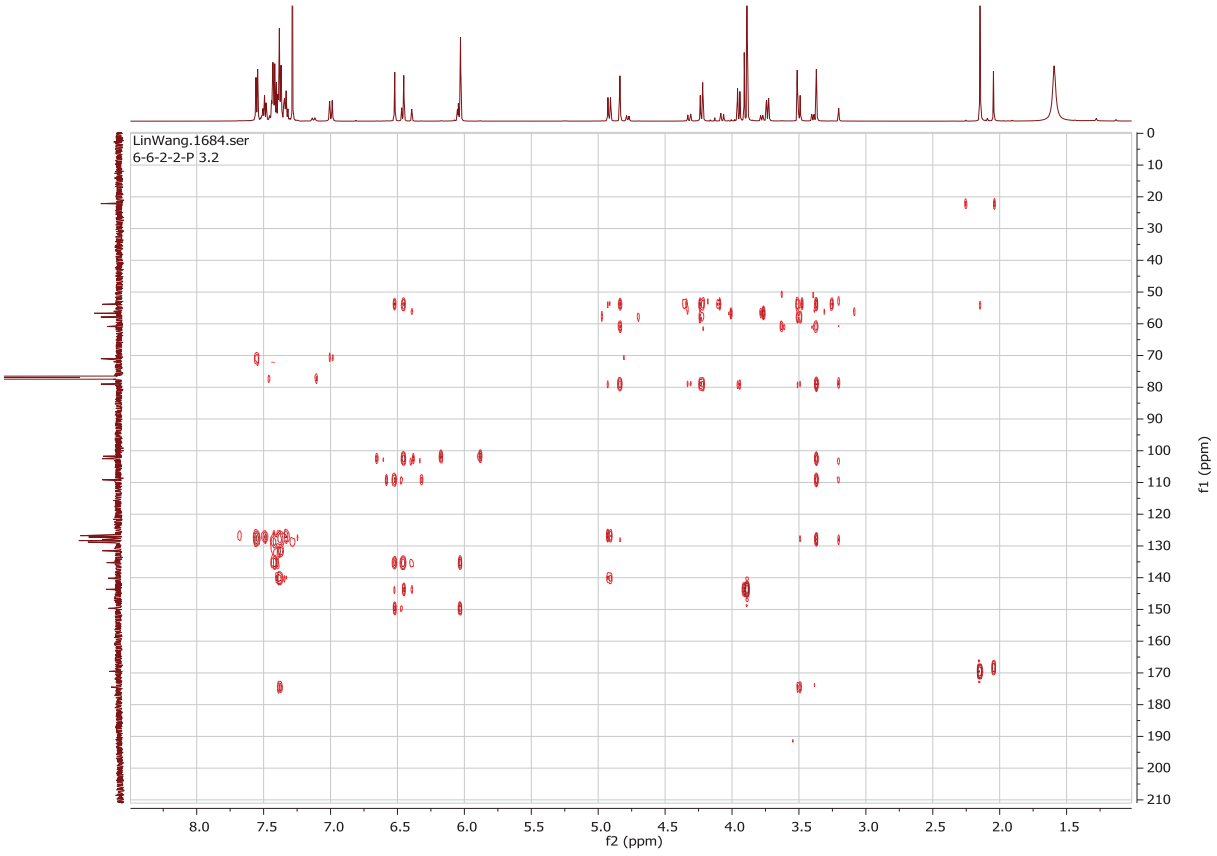

Figure S5: HMBC of compound **1** in $CDCl_3$

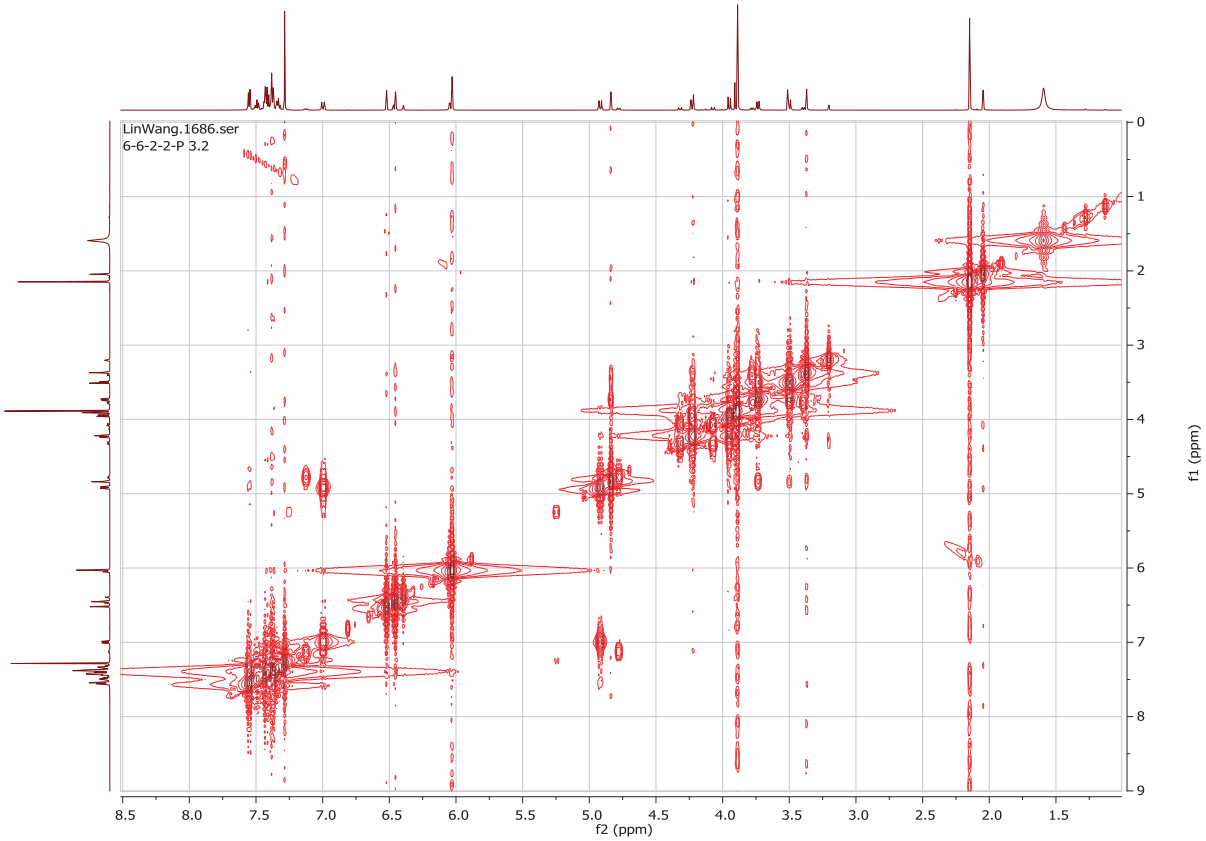

Figure S6: COSY of compound **1** in $CDCl_3$

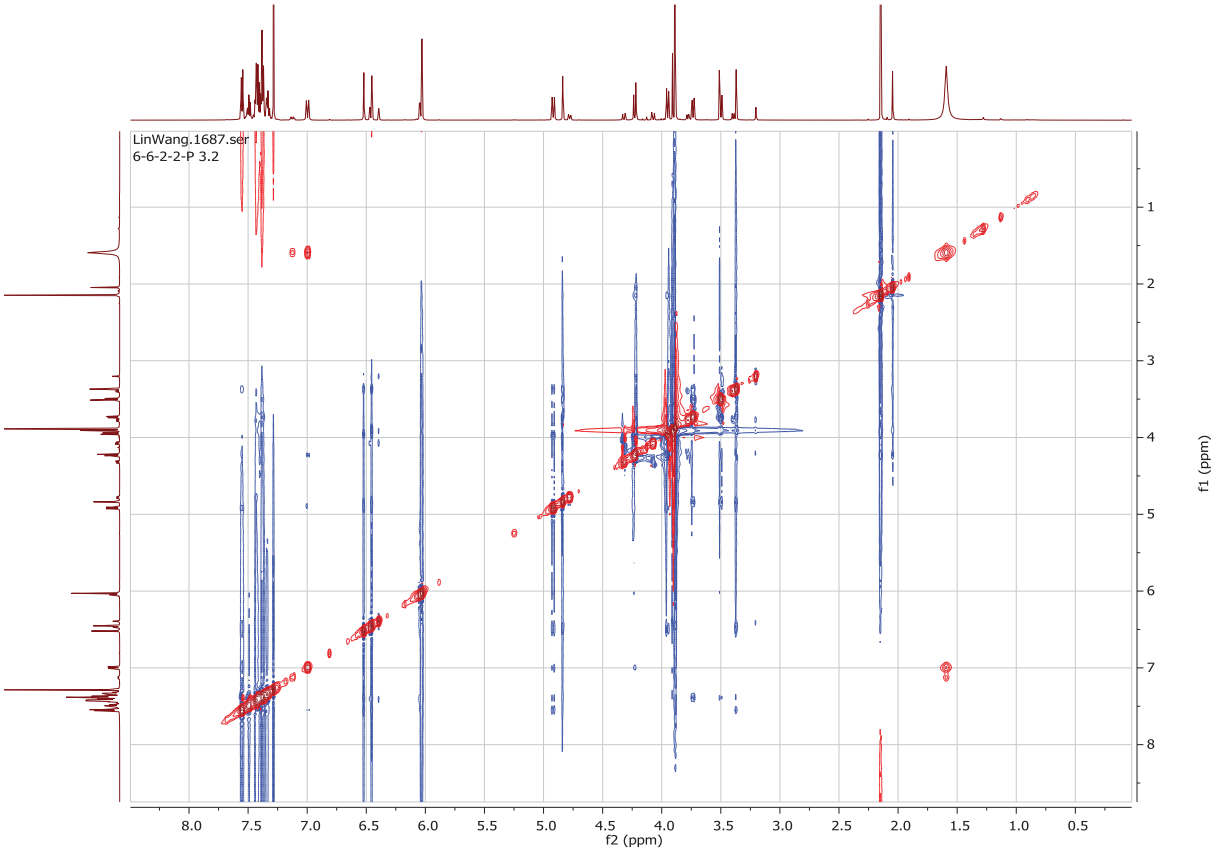

Figure S7: ROESY of compound **1** in $CDCl_3$

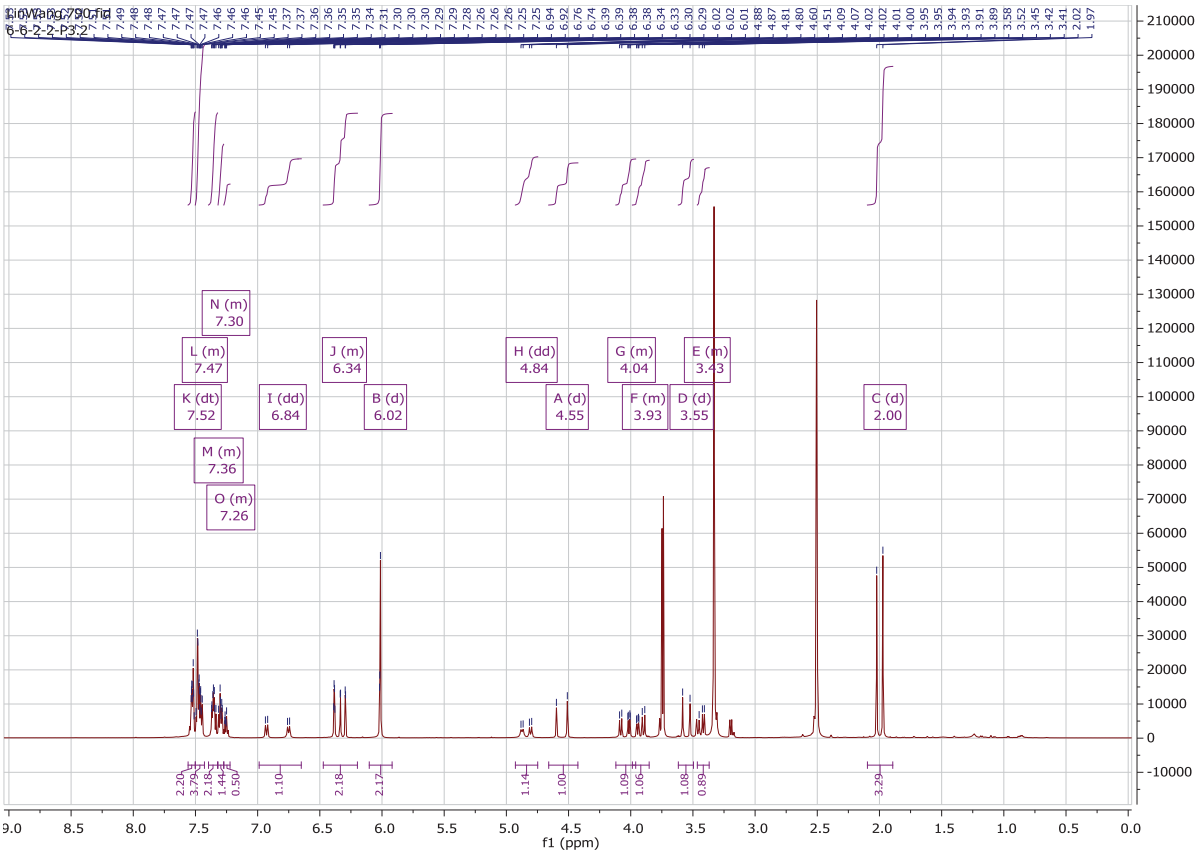

Figure S8: ^{1}H NMR of compound **1** in DMSO-d_6

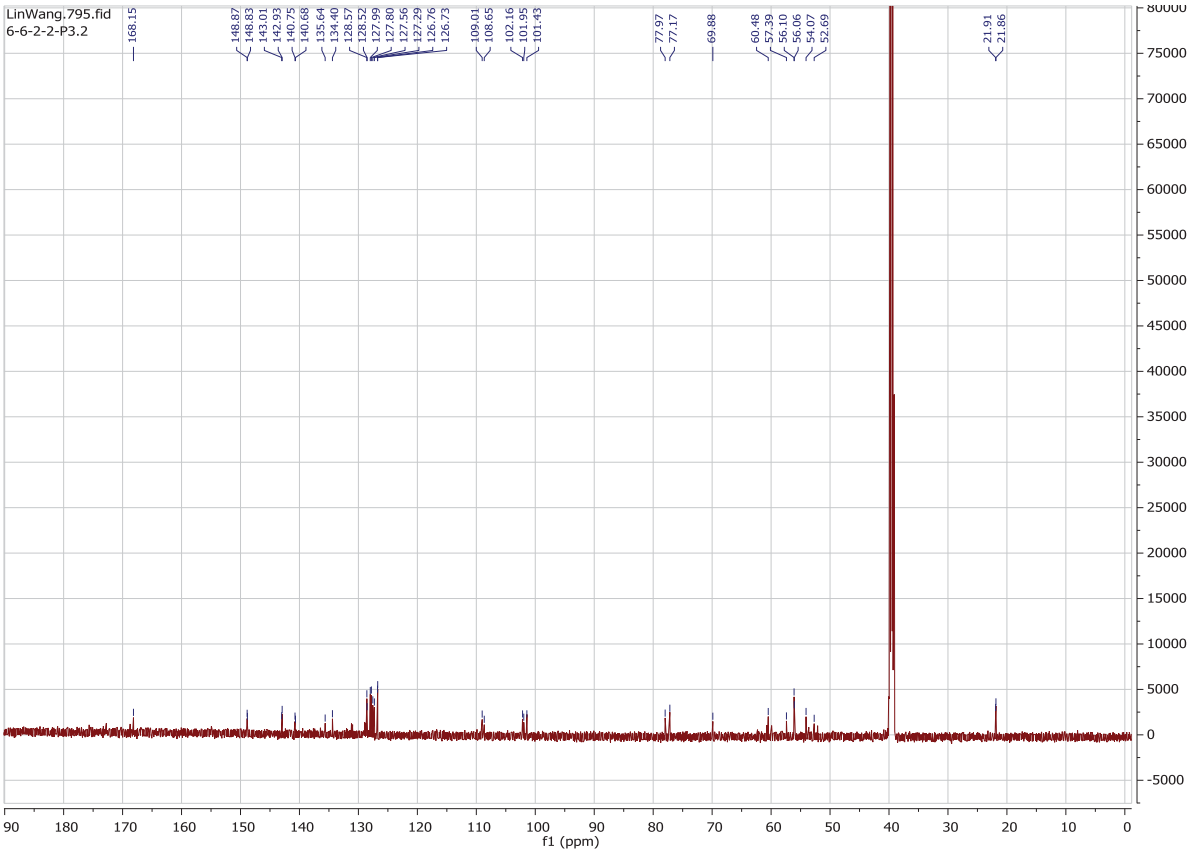

Figure S9: ^{13}C NMR of compound **1** in DMSO-d_6

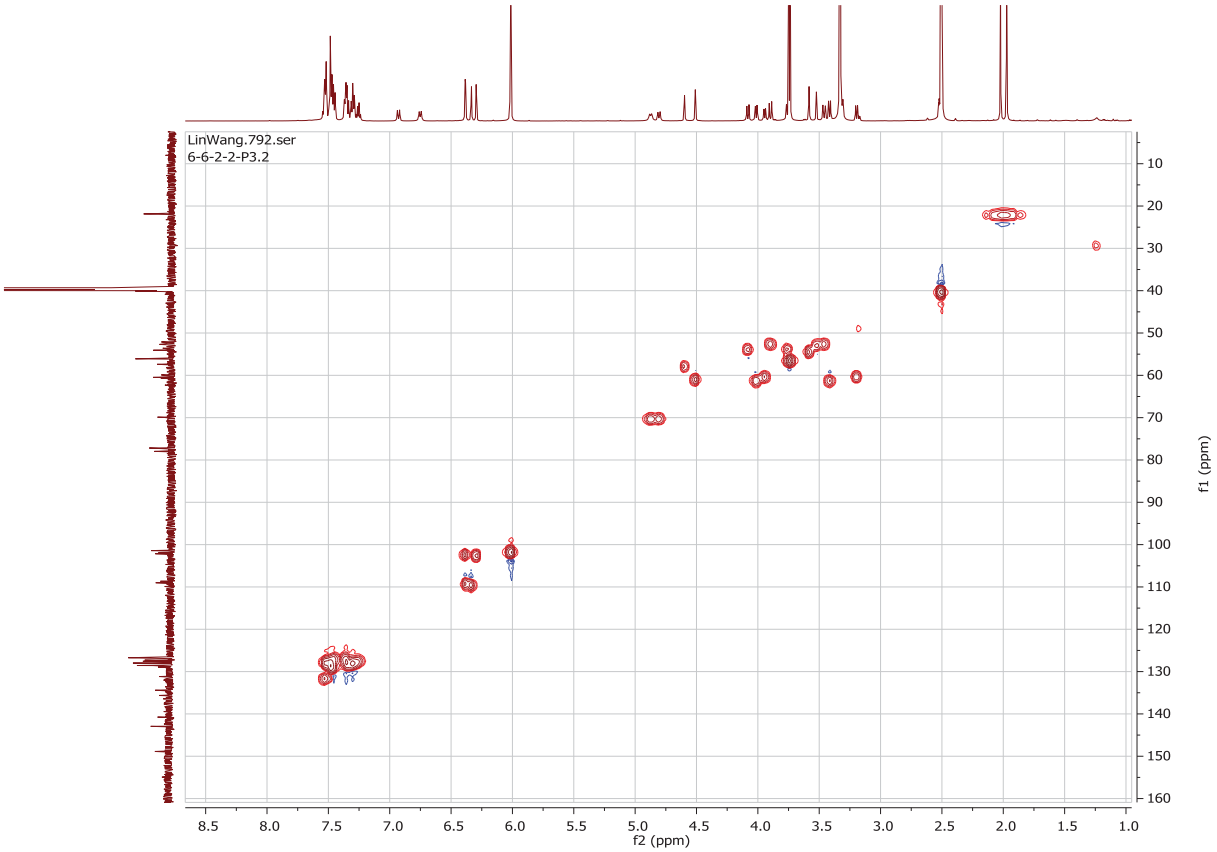

Figure S10: HSQC of compound **1** in DMSO-d_6

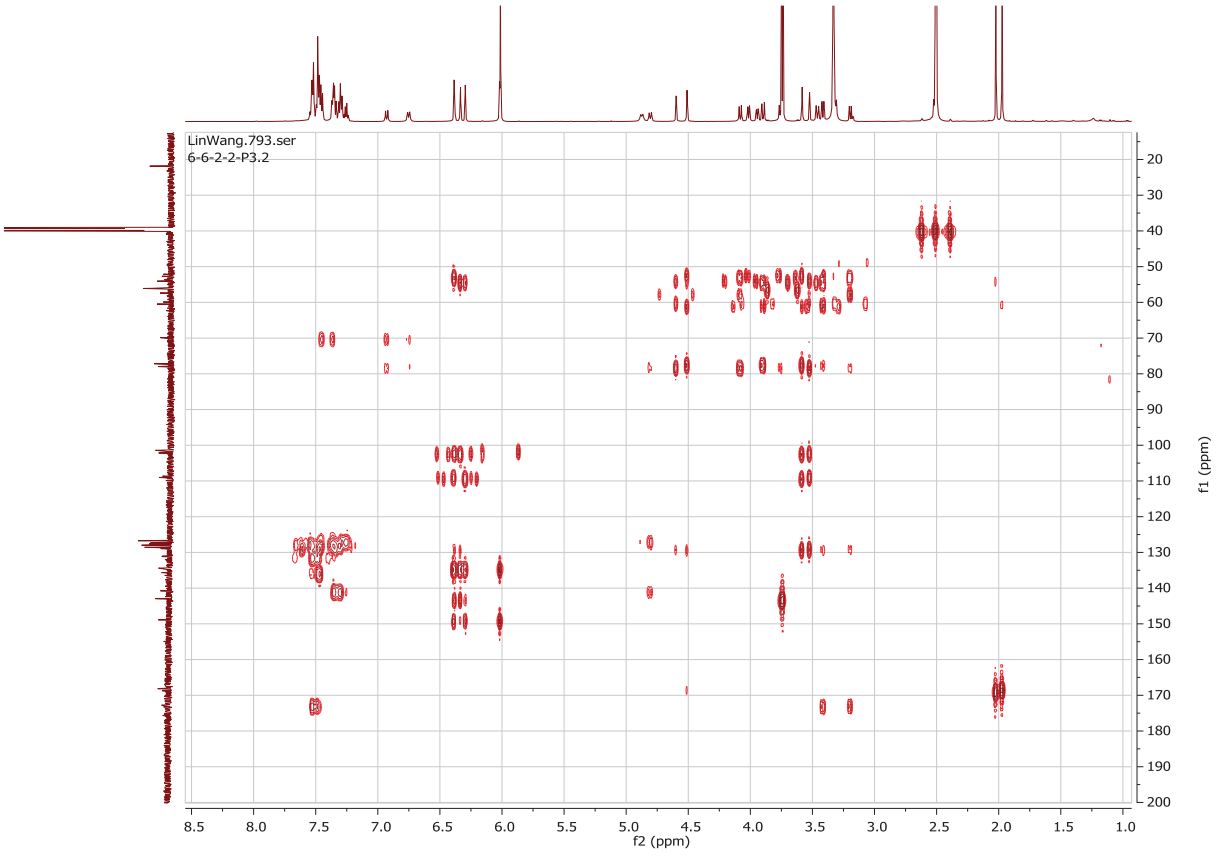

Figure S11: HMBC of compound **1** in DMSO-d_6

Figure S12: COSY of compound **1** in DMSO-d_6

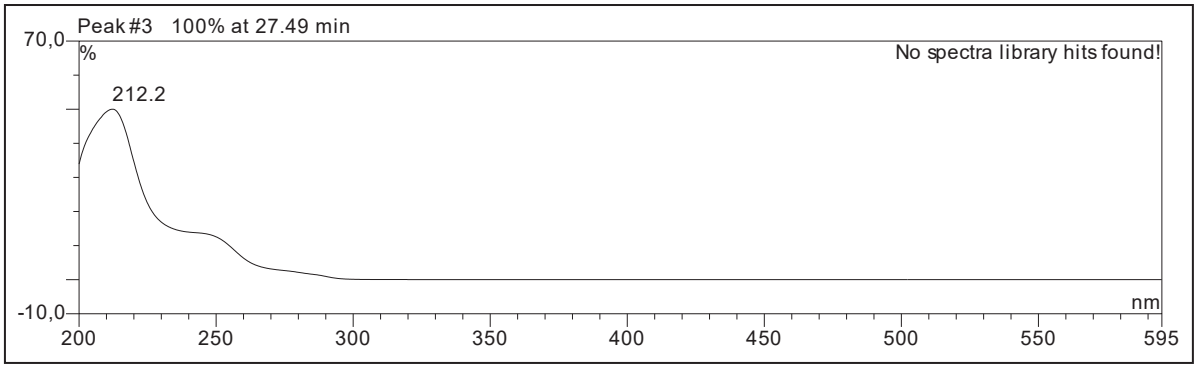

Figure S13: UV absorption of compound **1**

Crystallographic Tables ((Short version))

*Tabelle SX: Crystal data and structure refinement for **1** and **2**.*

Identification code	**1**	**2**
Empirical formula	$C_{29}H_{28}N_2O_6$	$C_{19}H_{21}ClO_9$
Formula weight [g/mol]	500.53	428.81
Temperature [K]	100.0(1)	100.0(1)
Crystal system	orthorhombic	monoclinic
Space group	$P2_12_12_1$	$P2_1/n$
a [Å]	6.01150(10)	11.12003(15)
b [Å]	44.6347(6)	14.7801(3)
c [Å]	9.11060(10)	11.80666(16)
α [°]	90	90
β [°]	90	91.2548(12)
γ [°]	90	90
Volume [Å^3]	2444.57(6)	1940.02(5)
Z	4	4
ρ_{calc} [g/cm^3]	1.360	1.468
μ [mm^{-1}]	0.785	2.206
F(000)	1056.0	896.0
Crystal size [mm^3]	0.13 × 0.03 × 0.02	0.65 × 0.53 × 0.36
Radiation	Cu K_α (λ = 1.54184)	Cu K_α (λ = 1.54184)
2Θ range for data collection [°]	7.924 to 158.018	9.59 to 158.276
Index ranges	-7 ≤ h ≤ 7, -56 ≤ k ≤ 56, -11 ≤ l ≤ 11	-11 ≤ h ≤ 14, -17 ≤ k ≤ 18, -15 ≤ l ≤ 12
Reflections collected	40796	14864
Independent reflections	5033 [R_{int} = 0.0580, R_{sigma} = 0.0326]	3897 [R_{int} = 0.0319, R_{sigma} = 0.0228]
Data/restraints/parameters	5033/0/339	3897/0/277
Goodness-of-fit on F^2	1.080	1.041
Final R indexes [I>=2σ (I)]	R_1 = 0.0539, wR_2 = 0.1453	R_1 = 0.0332, wR_2 = 0.0868
Final R indexes [all data]	R_1 = 0.0620, wR_2 = 0.1472	R_1 = 0.0342, wR_2 = 0.0875
Largest diff. peak/hole [e Å^{-3}]	0.38/-0.32	0.28/-0.22
Flack parameter	0.04(6)	-

((Long version))

Compound 1:

Crystal data

$C_{29}H_{28}N_2O_6$	D_x = 1.360 Mg m^{-3}
M_r = 500.53	Cu $K\square$ radiation, □ = 1.54184 Å
Orthorhombic, $P2_12_12_1$	Cell parameters from 23073 reflections
a = 6.0115 (1) Å	□ = 3.9–78.8°
b = 44.6347 (6) Å	□ = 0.79 mm^{-1}
c = 9.1106 (1) Å	T = 100 K
V = 2444.57 (6) Å^3	Needle, clear colourless
Z = 4	0.13 × 0.03 × 0.02 mm
F(000) = 1056	

Data collection

XtaLAB Synergy, Dualflex, HyPix diffractometer	4822 reflections with $I > 2\sigma(I)$
Detector resolution: 10.0000 pixels mm^{-1}	R_{int} = 0.058
ω scans	θ_{max} = 79.0°, θ_{min} = 4.0°
Absorption correction: gaussian *CrysAlis PRO* 1.171.41.92a (Rigaku Oxford Diffraction, 2020) Numerical absorption correction based on gaussian integration over a multifaceted crystal model Empirical absorption correction using spherical harmonics, implemented in SCALE3 ABSPACK scaling algorithm.	h = -7→7
T_{min} = 0.848, T_{max} = 1.000	k = -56→56
40796 measured reflections	l = -11→11
5033 independent reflections	

Refinement

Refinement on F^2	Hydrogen site location: mixed
Least-squares matrix: full	H atoms treated by a mixture of independent and constrained refinement
$R[F^2 > 2\sigma(F^2)]$ = 0.054	$w = 1/[\sigma^2(F_o^2) + (0.0865P)^2 + 1.5204P]$ where $P = (F_o^2 + 2F_c^2)/3$
$wR(F^2)$ = 0.147	$(\Delta/\sigma)_{max}$ = 0.001
S = 1.08	$\Delta\rho_{max}$ = 0.38 e Å^{-3}
5033 reflections	$\Delta\rho_{min}$ = -0.31 e Å^{-3}
339 parameters	Absolute structure: Flack x determined using 1844 quotients [(I+)-(I-)]/[(I+)+(I-)] (Parsons, Flack and Wagner, Acta Cryst. B69 (2013) 249-259).
0 restraints	Absolute structure parameter: 0.04 (6)
Primary atom site location: structure-invariant direct methods	

Special details

Geometry. All esds (except the esd in the dihedral angle between two l.s. planes) are estimated using the full covariance matrix. The cell esds are taken into account individually in the estimation of esds in distances, angles and torsion angles; correlations between esds in cell parameters are only used when they are defined by crystal symmetry. An approximate (isotropic) treatment of cell esds is used for estimating esds involving l.s. planes.

Fractional atomic coordinates and isotropic or equivalent isotropic displacement parameters (Å^2) for ***1***

	x	*y*	*z*	U_{iso}*/U_{eq}
C1	0.3609 (5)	0.62491 (6)	0.6127 (4)	0.0213 (6)
N1	0.4389 (5)	0.59585 (5)	0.5474 (3)	0.0212 (5)

O1	0.3088 (4)	0.75146 (5)	0.5751 (3)	0.0310 (6)
C2	0.1942 (6)	0.63727 (7)	0.4990 (4)	0.0233 (7)
H2A	0.082734	0.621999	0.470739	0.028*
H2B	0.117040	0.655357	0.535862	0.028*
N2	0.3454 (5)	0.64446 (6)	0.3759 (3)	0.0219 (5)
O2	0.5809 (4)	0.76729 (5)	0.7355 (3)	0.0315 (5)
C3	0.5756 (5)	0.63729 (6)	0.4204 (3)	0.0198 (6)
H3	0.694271	0.647767	0.363083	0.024*
O3	0.9026 (5)	0.72883 (5)	0.8654 (3)	0.0345 (6)
C4	0.5715 (5)	0.64451 (6)	0.5857 (3)	0.0200 (6)
H4	0.702187	0.634701	0.633686	0.024*
O4	0.1165 (4)	0.57088 (5)	0.5998 (3)	0.0274 (5)
C5	0.5968 (5)	0.60313 (6)	0.4260 (3)	0.0208 (6)
H5A	0.550503	0.593780	0.332282	0.025*
H5B	0.750471	0.596828	0.449861	0.025*
O5	0.0404 (4)	0.61922 (6)	0.7740 (3)	0.0294 (5)
C6	0.5673 (5)	0.67731 (7)	0.6285 (3)	0.0198 (6)
O6	0.0622 (4)	0.66085 (5)	0.2395 (3)	0.0302 (5)
C7	0.4151 (5)	0.69825 (6)	0.5704 (4)	0.0231 (6)
H7	0.305117	0.692543	0.500976	0.028*
C8	0.4334 (6)	0.72736 (7)	0.6191 (4)	0.0241 (6)
C9	0.5922 (6)	0.73674 (7)	0.7168 (4)	0.0241 (6)
C10	0.7471 (6)	0.71703 (7)	0.7734 (4)	0.0248 (6)
C11	0.7300 (6)	0.68698 (7)	0.7288 (4)	0.0237 (6)
H11	0.831639	0.672739	0.767583	0.028*
C12	0.3716 (7)	0.77521 (7)	0.6716 (5)	0.0369 (9)
H12A	0.257915	0.777850	0.749181	0.044*
H12B	0.385178	0.794230	0.616439	0.044*
C13	0.3024 (6)	0.57163 (7)	0.5405 (4)	0.0227 (6)
C14	0.3886 (6)	0.54459 (7)	0.4620 (4)	0.0253 (7)
C15	0.6035 (6)	0.53363 (7)	0.4857 (4)	0.0319 (8)
H15	0.704568	0.544272	0.546585	0.038*
C16	0.6674 (7)	0.50703 (8)	0.4191 (6)	0.0446 (11)
H16	0.811556	0.499127	0.437140	0.054*
C17	0.5234 (9)	0.49189 (8)	0.3266 (6)	0.0488 (12)
H17	0.569541	0.473801	0.280795	0.059*
C18	0.3134 (9)	0.50300 (8)	0.3008 (5)	0.0443 (11)
H18	0.216138	0.492844	0.235410	0.053*
C19	0.2433 (7)	0.52907 (8)	0.3704 (4)	0.0339 (8)
H19	0.096429	0.536295	0.355389	0.041*
C20	0.2737 (5)	0.62423 (7)	0.7699 (4)	0.0231 (6)

H20	0.296674	0.644903	0.809411	0.028*
C21	0.4016 (6)	0.60338 (7)	0.8727 (4)	0.0258 (7)
C22	0.6060 (6)	0.61196 (8)	0.9280 (4)	0.0305 (7)
H22	0.666412	0.630861	0.901348	0.037*
C23	0.7248 (7)	0.59328 (9)	1.0225 (4)	0.0369 (8)
H23	0.866180	0.599362	1.058321	0.044*
C24	0.6374 (8)	0.56603 (8)	1.0639 (4)	0.0388 (9)
H24	0.718081	0.553252	1.128116	0.047*
C25	0.4309 (8)	0.55741 (8)	1.0111 (4)	0.0391 (9)
H25	0.369766	0.538685	1.039968	0.047*
C26	0.3121 (7)	0.57585 (7)	0.9164 (4)	0.0307 (7)
H26	0.170297	0.569768	0.881307	0.037*
C27	0.2641 (6)	0.65763 (6)	0.2541 (4)	0.0239 (7)
C28	0.4279 (7)	0.66979 (8)	0.1430 (4)	0.0304 (7)
H28A	0.372678	0.665866	0.043662	0.046*
H28B	0.572241	0.659947	0.156245	0.046*
H28C	0.444907	0.691433	0.157213	0.046*
C29	1.0648 (6)	0.70869 (8)	0.9243 (4)	0.0315 (7)
H29A	1.151371	0.699895	0.844000	0.047*
H29B	0.989690	0.692723	0.979053	0.047*
H29C	1.164583	0.719656	0.990308	0.047*
H5	0.028 (8)	0.6018 (11)	0.744 (5)	0.038*

Atomic displacement parameters (Å^2) for ***1***

	U^{11}	U^{22}	U^{33}	U^{12}	U^{13}	U^{23}
C1	0.0184 (14)	0.0183 (13)	0.0271 (15)	0.0006 (11)	0.0008 (13)	0.0024 (11)
N1	0.0205 (12)	0.0200 (11)	0.0230 (12)	-0.0012 (10)	0.0031 (11)	-0.0001 (9)
O1	0.0320 (13)	0.0222 (10)	0.0388 (13)	0.0063 (9)	-0.0091 (11)	-0.0010 (10)
C2	0.0224 (16)	0.0224 (14)	0.0252 (16)	-0.0015 (12)	0.0016 (13)	0.0043 (12)
N2	0.0195 (13)	0.0235 (12)	0.0227 (12)	-0.0012 (10)	-0.0008 (11)	0.0020 (10)
O2	0.0338 (13)	0.0230 (11)	0.0379 (13)	0.0054 (10)	-0.0109 (12)	-0.0045 (9)
C3	0.0178 (14)	0.0233 (13)	0.0184 (13)	-0.0019 (11)	0.0006 (13)	0.0009 (11)
O3	0.0366 (14)	0.0279 (11)	0.0389 (13)	0.0056 (10)	-0.0197 (12)	-0.0067 (10)
C4	0.0134 (13)	0.0219 (13)	0.0247 (14)	0.0006 (11)	0.0011 (13)	0.0024 (11)
O4	0.0219 (12)	0.0280 (11)	0.0322 (13)	-0.0027 (9)	0.0037 (10)	0.0024 (9)
C5	0.0182 (14)	0.0240 (14)	0.0201 (13)	-0.0024 (11)	0.0033 (12)	-0.0005 (11)
O5	0.0186 (11)	0.0300 (11)	0.0396 (13)	0.0035 (9)	0.0075 (11)	0.0057 (10)
C6	0.0146 (13)	0.0243 (14)	0.0207 (13)	-0.0006 (11)	-0.0004 (12)	0.0012 (11)
O6	0.0253 (12)	0.0291 (11)	0.0361 (13)	0.0015 (9)	-0.0065 (11)	0.0030 (10)
C7	0.0185 (14)	0.0229 (14)	0.0278 (15)	0.0010 (11)	-0.0014 (13)	0.0007 (11)

C8	0.0219 (15)	0.0232 (14)	0.0272 (15)	0.0034 (12)	0.0019 (14)	0.0033 (12)
C9	0.0263 (16)	0.0224 (14)	0.0235 (14)	0.0018 (12)	-0.0030 (14)	-0.0007 (11)
C10	0.0251 (16)	0.0262 (14)	0.0230 (14)	0.0003 (12)	-0.0069 (14)	-0.0016 (12)
C11	0.0232 (15)	0.0237 (14)	0.0241 (14)	0.0023 (12)	0.0001 (13)	0.0018 (12)
C12	0.034 (2)	0.0215 (15)	0.055 (2)	0.0078 (14)	-0.0110 (19)	-0.0049 (15)
C13	0.0208 (15)	0.0213 (13)	0.0259 (16)	-0.0020 (11)	-0.0021 (13)	0.0031 (11)
C14	0.0297 (18)	0.0187 (13)	0.0274 (16)	-0.0043 (12)	0.0031 (14)	0.0025 (11)
C15	0.0284 (18)	0.0224 (15)	0.045 (2)	-0.0021 (13)	0.0034 (17)	0.0030 (14)
C16	0.037 (2)	0.0226 (16)	0.075 (3)	0.0002 (14)	0.019 (2)	0.0029 (18)
C17	0.065 (3)	0.0226 (16)	0.059 (3)	-0.0093 (18)	0.032 (2)	-0.0091 (17)
C18	0.062 (3)	0.0301 (18)	0.040 (2)	-0.0194 (19)	0.013 (2)	-0.0088 (16)
C19	0.038 (2)	0.0288 (16)	0.0353 (18)	-0.0105 (14)	0.0031 (17)	-0.0006 (14)
C20	0.0225 (15)	0.0214 (13)	0.0252 (15)	0.0024 (11)	0.0028 (13)	0.0024 (12)
C21	0.0313 (18)	0.0248 (14)	0.0212 (14)	0.0084 (13)	0.0047 (13)	0.0024 (11)
C22	0.0264 (17)	0.0360 (17)	0.0292 (16)	0.0060 (13)	0.0058 (15)	0.0061 (13)
C23	0.0309 (19)	0.053 (2)	0.0270 (17)	0.0137 (17)	0.0006 (16)	0.0045 (16)
C24	0.055 (3)	0.0381 (19)	0.0229 (16)	0.0206 (18)	0.0009 (17)	0.0046 (14)
C25	0.065 (3)	0.0239 (15)	0.0286 (17)	0.0070 (17)	0.001 (2)	0.0025 (13)
C26	0.041 (2)	0.0261 (15)	0.0246 (16)	0.0023 (14)	0.0007 (16)	0.0013 (13)
C27	0.0319 (17)	0.0181 (13)	0.0217 (15)	0.0003 (12)	-0.0027 (14)	-0.0014 (11)
C28	0.0328 (18)	0.0375 (17)	0.0209 (15)	0.0039 (14)	-0.0013 (15)	0.0049 (13)
C29	0.0302 (18)	0.0312 (16)	0.0331 (17)	0.0046 (14)	-0.0117 (17)	-0.0031 (13)

Geometric parameters (Å, º) for ***1***

C1—N1	1.502 (4)	C11—H11	0.9500
C1—C2	1.543 (4)	C12—H12A	0.9900
C1—C4	1.558 (4)	C12—H12B	0.9900
C1—C20	1.526 (4)	C13—C14	1.496 (5)
N1—C5	1.493 (4)	C14—C15	1.398 (5)
N1—C13	1.359 (4)	C14—C19	1.393 (5)
O1—C8	1.371 (4)	C15—H15	0.9500
O1—C12	1.428 (4)	C15—C16	1.388 (5)
C2—H2A	0.9900	C16—H16	0.9500
C2—H2B	0.9900	C16—C17	1.385 (7)
C2—N2	1.478 (4)	C17—H17	0.9500
N2—C3	1.477 (4)	C17—C18	1.377 (7)
N2—C27	1.348 (4)	C18—H18	0.9500
O2—C9	1.376 (4)	C18—C19	1.390 (6)
O2—C12	1.431 (4)	C19—H19	0.9500
C3—H3	1.0000	C20—H20	1.0000

C3—C4	1.540 (4)	C20—C21	1.528 (4)
C3—C5	1.531 (4)	C21—C22	1.382 (5)
O3—C10	1.362 (4)	C21—C26	1.399 (5)
O3—C29	1.431 (4)	C22—H22	0.9500
C4—H4	1.0000	C22—C23	1.395 (5)
C4—C6	1.515 (4)	C23—H23	0.9500
O4—C13	1.242 (4)	C23—C24	1.378 (6)
C5—H5A	0.9900	C24—H24	0.9500
C5—H5B	0.9900	C24—C25	1.386 (7)
O5—C20	1.421 (4)	C25—H25	0.9500
O5—H5	0.83 (5)	C25—C26	1.390 (5)
C6—C7	1.411 (4)	C26—H26	0.9500
C6—C11	1.406 (4)	C27—C28	1.513 (5)
O6—C27	1.229 (4)	C28—H28A	0.9800
C7—H7	0.9500	C28—H28B	0.9800
C7—C8	1.377 (4)	C28—H28C	0.9800
C8—C9	1.371 (5)	C29—H29A	0.9800
C9—C10	1.381 (4)	C29—H29B	0.9800
C10—C11	1.405 (4)	C29—H29C	0.9800
N1—C1—C2	104.2 (2)	O2—C12—H12B	110.2
N1—C1—C4	99.7 (2)	H12A—C12—H12B	108.5
N1—C1—C20	117.5 (2)	N1—C13—C14	117.0 (3)
C2—C1—C4	102.8 (2)	O4—C13—N1	123.0 (3)
C20—C1—C2	114.5 (3)	O4—C13—C14	119.9 (3)
C20—C1—C4	116.0 (3)	C15—C14—C13	121.9 (3)
C5—N1—C1	107.7 (2)	C19—C14—C13	118.1 (3)
C13—N1—C1	121.1 (3)	C19—C14—C15	119.9 (3)
C13—N1—C5	121.5 (3)	C14—C15—H15	120.4
C8—O1—C12	104.9 (3)	C16—C15—C14	119.2 (4)
C1—C2—H2A	111.6	C16—C15—H15	120.4
C1—C2—H2B	111.6	C15—C16—H16	119.6
H2A—C2—H2B	109.4	C17—C16—C15	120.7 (4)
N2—C2—C1	100.8 (3)	C17—C16—H16	119.6
N2—C2—H2A	111.6	C16—C17—H17	120.0
N2—C2—H2B	111.6	C18—C17—C16	120.1 (4)
C3—N2—C2	108.7 (2)	C18—C17—H17	120.0
C27—N2—C2	119.8 (3)	C17—C18—H18	119.9
C27—N2—C3	131.3 (3)	C17—C18—C19	120.1 (4)
C9—O2—C12	103.8 (3)	C19—C18—H18	119.9
N2—C3—H3	115.1	C14—C19—H19	120.0

N2—C3—C4	102.0 (2)	C18—C19—C14	120.0 (4)
N2—C3—C5	107.6 (2)	C18—C19—H19	120.0
C4—C3—H3	115.1	C1—C20—H20	105.8
C5—C3—H3	115.1	C1—C20—C21	114.5 (3)
C5—C3—C4	100.2 (2)	O5—C20—C1	111.5 (3)
C10—O3—C29	117.1 (3)	O5—C20—H20	105.8
C1—C4—H4	108.9	O5—C20—C21	112.6 (3)
C3—C4—C1	92.9 (2)	C21—C20—H20	105.8
C3—C4—H4	108.9	C22—C21—C20	120.1 (3)
C6—C4—C1	119.2 (2)	C22—C21—C26	118.8 (3)
C6—C4—C3	117.0 (2)	C26—C21—C20	121.0 (3)
C6—C4—H4	108.9	C21—C22—H22	119.5
N1—C5—C3	100.9 (2)	C21—C22—C23	121.0 (3)
N1—C5—H5A	111.6	C23—C22—H22	119.5
N1—C5—H5B	111.6	C22—C23—H23	119.9
C3—C5—H5A	111.6	C24—C23—C22	120.1 (4)
C3—C5—H5B	111.6	C24—C23—H23	119.9
H5A—C5—H5B	109.4	C23—C24—H24	120.3
C20—O5—H5	103 (3)	C23—C24—C25	119.4 (3)
C7—C6—C4	123.7 (3)	C25—C24—H24	120.3
C11—C6—C4	116.9 (3)	C24—C25—H25	119.6
C11—C6—C7	119.4 (3)	C24—C25—C26	120.7 (4)
C6—C7—H7	121.6	C26—C25—H25	119.6
C8—C7—C6	116.9 (3)	C21—C26—H26	120.0
C8—C7—H7	121.6	C25—C26—C21	119.9 (4)
O1—C8—C7	127.0 (3)	C25—C26—H26	120.0
C9—C8—O1	109.3 (3)	N2—C27—C28	118.1 (3)
C9—C8—C7	123.6 (3)	O6—C27—N2	119.9 (3)
O2—C9—C10	128.2 (3)	O6—C27—C28	121.9 (3)
C8—C9—O2	110.4 (3)	C27—C28—H28A	109.5
C8—C9—C10	121.1 (3)	C27—C28—H28B	109.5
O3—C10—C9	116.5 (3)	C27—C28—H28C	109.5
O3—C10—C11	126.7 (3)	H28A—C28—H28B	109.5
C9—C10—C11	116.8 (3)	H28A—C28—H28C	109.5
C6—C11—H11	118.9	H28B—C28—H28C	109.5
C10—C11—C6	122.1 (3)	O3—C29—H29A	109.5
C10—C11—H11	118.9	O3—C29—H29B	109.5
O1—C12—O2	107.4 (3)	O3—C29—H29C	109.5
O1—C12—H12A	110.2	H29A—C29—H29B	109.5
O1—C12—H12B	110.2	H29A—C29—H29C	109.5
O2—C12—H12A	110.2	H29B—C29—H29C	109.5

C1—N1—C5—C3	-6.2 (3)	C5—N1—C13—O4	-149.4 (3)
C1—N1—C13—O4	-7.5 (5)	C5—N1—C13—C14	33.0 (4)
C1—N1—C13—C14	174.9 (3)	C5—C3—C4—C1	-59.0 (2)
C1—C2—N2—C3	-1.2 (3)	C5—C3—C4—C6	175.9 (3)
C1—C2—N2—C27	-176.5 (3)	O5—C20—C21—C22	-154.2 (3)
C1—C4—C6—C7	-59.7 (4)	O5—C20—C21—C26	23.8 (4)
C1—C4—C6—C11	122.1 (3)	C6—C7—C8—O1	178.0 (3)
C1—C20—C21—C22	77.0 (4)	C6—C7—C8—C9	1.4 (5)
C1—C20—C21—C26	-105.1 (4)	C7—C6—C11—C10	-0.2 (5)
N1—C1—C2—N2	-68.4 (3)	C7—C8—C9—O2	175.1 (3)
N1—C1—C4—C3	53.8 (2)	C7—C8—C9—C10	0.0 (5)
N1—C1—C4—C6	177.1 (3)	C8—O1—C12—O2	19.2 (4)
N1—C1—C20—O5	-90.9 (3)	C8—C9—C10—O3	177.7 (3)
N1—C1—C20—C21	38.5 (4)	C8—C9—C10—C11	-1.5 (5)
N1—C13—C14—C15	45.8 (4)	C9—O2—C12—O1	-20.1 (4)
N1—C13—C14—C19	-138.5 (3)	C9—C10—C11—C6	1.6 (5)
O1—C8—C9—O2	-2.0 (4)	C11—C6—C7—C8	-1.3 (5)
O1—C8—C9—C10	-177.1 (3)	C12—O1—C8—C7	172.3 (4)
C2—C1—N1—C5	75.1 (3)	C12—O1—C8—C9	-10.7 (4)
C2—C1—N1—C13	-71.3 (3)	C12—O2—C9—C8	13.7 (4)
C2—C1—C4—C3	-53.3 (3)	C12—O2—C9—C10	-171.7 (4)
C2—C1—C4—C6	70.0 (3)	C13—N1—C5—C3	140.1 (3)
C2—C1—C20—O5	31.8 (4)	C13—C14—C15—C16	174.6 (3)
C2—C1—C20—C21	161.2 (3)	C13—C14—C19—C18	-176.9 (3)
C2—N2—C3—C4	-33.5 (3)	C14—C15—C16—C17	2.0 (6)
C2—N2—C3—C5	71.4 (3)	C15—C14—C19—C18	-1.0 (5)
C2—N2—C27—O6	-7.3 (4)	C15—C16—C17—C18	-0.6 (7)
C2—N2—C27—C28	168.9 (3)	C16—C17—C18—C19	-1.6 (6)
N2—C3—C4—C1	51.6 (2)	C17—C18—C19—C14	2.4 (6)
N2—C3—C4—C6	-73.4 (3)	C19—C14—C15—C16	-1.1 (5)
N2—C3—C5—N1	-64.5 (3)	C20—C1—N1—C5	-157.0 (3)
O2—C9—C10—O3	3.6 (5)	C20—C1—N1—C13	56.5 (4)
O2—C9—C10—C11	-175.6 (3)	C20—C1—C2—N2	161.9 (2)
C3—N2—C27—O6	178.7 (3)	C20—C1—C4—C3	-179.0 (2)
C3—N2—C27—C28	-5.1 (5)	C20—C1—C4—C6	-55.7 (4)

C3—C4—C6—C7	50.7 (4)	C20—C21—C22—C23	179.8 (3)
C3—C4—C6—C11	-127.4 (3)	C20—C21—C26—C25	-179.4 (3)
O3—C10—C11—C6	-177.6 (3)	C21—C22—C23—C24	-1.0 (6)
C4—C1—N1—C5	-30.8 (3)	C22—C21—C26—C25	-1.4 (5)
C4—C1—N1—C13	-177.3 (3)	C22—C23—C24—C25	-0.1 (6)
C4—C1—C2—N2	35.3 (3)	C23—C24—C25—C26	0.4 (6)
C4—C1—C20—O5	151.3 (2)	C24—C25—C26—C21	0.4 (6)
C4—C1—C20—C21	-79.3 (3)	C26—C21—C22—C23	1.8 (5)
C4—C3—C5—N1	41.6 (3)	C27—N2—C3—C4	141.0 (3)
C4—C6—C7—C8	-179.4 (3)	C27—N2—C3—C5	-114.1 (3)
C4—C6—C11—C10	178.1 (3)	C29—O3—C10—C9	-179.7 (3)
O4—C13—C14—C15	-131.9 (3)	C29—O3—C10—C11	-0.6 (5)
O4—C13—C14—C19	43.8 (5)		

Compound 2·MeOH

Crystal data

$C_{18}H_{17}ClO_8 \cdot CH_4O$	$F(000) = 896$
$M_r = 428.81$	$D_x = 1.468$ Mg m^{-3}
Monoclinic, $P2_1/n$	Cu $K\alpha$ radiation, $\lambda = 1.54184$ Å
$a = 11.12003$ (15) Å	Cell parameters from 11971 reflections
$b = 14.7801$ (3) Å	$\theta = 3.0$–$78.6°$
$c = 11.80666$ (16) Å	$\mu = 2.21$ mm^{-1}
$\beta = 91.2548$ (12)°	$T = 100$ K
$V = 1940.02$ (5) Å^3	Block, clear orange
$Z = 4$	0.65 × 0.53 × 0.36 mm

Data collection

XtaLAB Synergy, Dualflex, HyPix diffractometer	3897 independent reflections
Radiation source: micro-focus sealed X-ray tube, PhotonJet (Cu) X-ray Source	3757 reflections with $I > 2\sigma(I)$
Mirror monochromator	$R_{int} = 0.032$
Detector resolution: 10.0000 pixels mm^{-1}	$\theta_{max} = 79.1°$, $\theta_{min} = 4.8°$
ω scans	$h = -11\rightarrow14$

Absorption correction: gaussian *CrysAlis PRO* 1.171.41.92a (Rigaku Oxford Diffraction, 2020) Numerical absorption correction based on gaussian integration over a multifaceted crystal model Empirical absorption correction using spherical harmonics, implemented in SCALE3 ABSPACK scaling algorithm.	k = -17□18
T_{min} = 0.075, T_{max} = 1.000	l = -15□12
14864 measured reflections	

Refinement

Refinement on F^2	Hydrogen site location: mixed
Least-squares matrix: full	H atoms treated by a mixture of independent and constrained refinement
$R[F^2 > 2\sigma(F^2)]$ = 0.033	$w = 1/[\sigma^2(F_o^2) + (0.0445P)^2 + 0.9842P]$ where $P = (F_o^2 + 2F_c^2)/3$
$wR(F^2)$ = 0.088	$(\Delta/\sigma)_{max} < 0.001$
S = 1.04	$\Delta\rho_{max}$ = 0.28 e Å^{-3}
3897 reflections	$\Delta\rho_{min}$ = -0.22 e Å^{-3}
277 parameters	Extinction correction: *SHELXL2017*/1 (Sheldrick 2017), $Fc^*=kFc[1+0.001xFc^2\lambda^3/\sin(2\theta)]^{-1/4}$
0 restraints	Extinction coefficient: 0.0036 (2)
Primary atom site location: structure-invariant direct methods	

Special details

Geometry. All esds (except the esd in the dihedral angle between two l.s. planes) are estimated using the full covariance matrix. The cell esds are taken into account individually in the estimation of esds in distances, angles and torsion angles; correlations between esds in cell parameters are only used when they are defined by crystal symmetry. An approximate (isotropic) treatment of cell esds is used for estimating esds involving l.s. planes.

*Fractional atomic coordinates and isotropic or equivalent isotropic displacement parameters (Å^2) for **2**·MeOH*

	x	y	z	U_{iso}*/U_{eq}
Cl1	0.40755 (3)	0.22742 (2)	0.15750 (3)	0.02224 (11)
O20	0.15964 (8)	0.27264 (6)	0.12518 (8)	0.0153 (2)
O3	-0.12945 (9)	0.43326 (7)	0.44492 (8)	0.0200 (2)
O6	-0.19197 (8)	0.19537 (7)	0.15881 (8)	0.0208 (2)
O4	-0.01675 (8)	0.33316 (7)	-0.01707 (8)	0.0210 (2)
O2	0.24018 (8)	0.41943 (7)	0.24641 (8)	0.0212 (2)
O7	-0.01077 (9)	0.13731 (7)	0.12281 (8)	0.0216 (2)

O1	0.23263 (10)	0.50201 (8)	-0.16254 (9)	0.0286 (3)
O8	0.15135 (9)	0.13769 (8)	-0.05391 (9)	0.0261 (2)
O5	0.01785 (10)	0.45728 (9)	-0.11810 (11)	0.0402 (3)
C11	-0.10035 (11)	0.31711 (9)	0.30576 (11)	0.0159 (3)
H11	-0.177723	0.292510	0.318917	0.019*
C6	0.18347 (12)	0.38600 (9)	-0.02533 (11)	0.0177 (3)
C7	0.08731 (11)	0.31421 (9)	0.20454 (10)	0.0148 (3)
C12	-0.02613 (12)	0.27770 (9)	0.22498 (11)	0.0150 (3)
C10	-0.06067 (12)	0.39192 (9)	0.36631 (10)	0.0160 (3)
C15	-0.07163 (12)	0.19628 (9)	0.16325 (11)	0.0163 (3)
C9	0.05293 (12)	0.42797 (9)	0.34817 (11)	0.0165 (3)
H9	0.079888	0.479059	0.390438	0.020*
C1	0.23054 (11)	0.32380 (9)	0.05516 (11)	0.0154 (3)
C3	0.43407 (12)	0.35471 (10)	-0.00537 (12)	0.0194 (3)
C5	0.26666 (13)	0.43698 (10)	-0.08805 (12)	0.0207 (3)
C18	-0.24619 (14)	0.11844 (11)	0.10134 (14)	0.0272 (3)
H18A	-0.223112	0.118519	0.021705	0.041*
H18B	-0.333938	0.122347	0.105786	0.041*
H18C	-0.218209	0.062415	0.137644	0.041*
C13	0.56672 (12)	0.33504 (11)	0.00003 (14)	0.0264 (3)
H13A	0.596608	0.341491	0.078318	0.040*
H13B	0.608987	0.377692	-0.048638	0.040*
H13C	0.581042	0.273099	-0.026059	0.040*
C2	0.35324 (12)	0.30721 (9)	0.06148 (11)	0.0167 (3)
C8	0.12685 (11)	0.38919 (9)	0.26820 (11)	0.0163 (3)
C14	0.05505 (12)	0.39659 (10)	-0.05606 (12)	0.0211 (3)
C17	0.27526 (13)	0.50463 (10)	0.29359 (12)	0.0216 (3)
H17A	0.353363	0.522417	0.263816	0.032*
H17B	0.281569	0.499501	0.376262	0.032*
H17C	0.214917	0.550447	0.273074	0.032*
C4	0.38917 (12)	0.42067 (10)	-0.07741 (12)	0.0216 (3)
H4	0.443307	0.455623	-0.120581	0.026*
C16	-0.14320 (12)	0.34324 (12)	-0.04616 (13)	0.0267 (3)
H16A	-0.158976	0.318992	-0.122298	0.040*
H16B	-0.164915	0.407480	-0.044508	0.040*
H16C	-0.191312	0.310065	0.008643	0.040*
C19	0.06413 (15)	0.10592 (13)	-0.13361 (14)	0.0340 (4)
H19A	0.102167	0.095542	-0.206566	0.051*
H19B	0.000219	0.151136	-0.142990	0.051*
H19C	0.029655	0.049118	-0.106410	0.051*
H8	0.1181 (19)	0.1489 (15)	0.0041 (19)	0.041*

H3	-0.198 (2)	0.4084 (15)	0.4474 (18)	0.041*
H1	0.154 (2)	0.5017 (15)	-0.1631 (18)	0.041*

*Atomic displacement parameters (Å²) for **2**·MeOH*

	U^{11}	U^{22}	U^{33}	U^{12}	U^{13}	U^{23}
Cl1	0.01696 (17)	0.0249 (2)	0.02478 (18)	0.00193 (12)	-0.00176 (12)	0.00342 (12)
O20	0.0150 (4)	0.0159 (5)	0.0153 (4)	0.0000 (3)	0.0047 (3)	-0.0011 (3)
O3	0.0198 (5)	0.0224 (5)	0.0179 (5)	0.0013 (4)	0.0057 (4)	-0.0049 (4)
O6	0.0163 (4)	0.0206 (5)	0.0255 (5)	-0.0032 (4)	0.0003 (4)	-0.0057 (4)
O4	0.0127 (4)	0.0299 (6)	0.0205 (5)	0.0000 (4)	-0.0003 (4)	0.0052 (4)
O2	0.0155 (4)	0.0247 (5)	0.0237 (5)	-0.0055 (4)	0.0042 (4)	-0.0088 (4)
O7	0.0213 (5)	0.0175 (5)	0.0265 (5)	-0.0016 (4)	0.0085 (4)	-0.0048 (4)
O1	0.0263 (5)	0.0304 (6)	0.0291 (6)	-0.0001 (5)	0.0042 (4)	0.0130 (5)
O8	0.0204 (5)	0.0349 (6)	0.0233 (5)	-0.0025 (4)	0.0075 (4)	-0.0097 (4)
O5	0.0241 (6)	0.0457 (8)	0.0507 (7)	0.0038 (5)	-0.0019 (5)	0.0267 (6)
C11	0.0147 (6)	0.0187 (7)	0.0144 (6)	0.0008 (5)	0.0021 (5)	0.0015 (5)
C6	0.0155 (6)	0.0202 (7)	0.0176 (6)	0.0010 (5)	0.0034 (5)	-0.0016 (5)
C7	0.0147 (6)	0.0185 (6)	0.0114 (5)	0.0027 (5)	0.0018 (4)	0.0005 (5)
C12	0.0167 (6)	0.0153 (6)	0.0131 (6)	0.0011 (5)	-0.0002 (5)	0.0010 (5)
C10	0.0185 (6)	0.0183 (7)	0.0113 (6)	0.0038 (5)	0.0020 (5)	0.0011 (5)
C15	0.0166 (6)	0.0186 (7)	0.0140 (6)	-0.0018 (5)	0.0036 (5)	0.0020 (5)
C9	0.0189 (6)	0.0164 (6)	0.0142 (6)	0.0009 (5)	-0.0012 (5)	-0.0011 (5)
C1	0.0156 (6)	0.0168 (6)	0.0139 (6)	-0.0019 (5)	0.0038 (5)	-0.0035 (5)
C3	0.0160 (6)	0.0210 (7)	0.0213 (6)	-0.0025 (5)	0.0033 (5)	-0.0060 (5)
C5	0.0229 (7)	0.0206 (7)	0.0187 (6)	-0.0008 (6)	0.0025 (5)	0.0009 (5)
C18	0.0237 (7)	0.0248 (8)	0.0329 (8)	-0.0075 (6)	-0.0017 (6)	-0.0084 (6)
C13	0.0151 (6)	0.0322 (8)	0.0320 (8)	-0.0028 (6)	0.0038 (6)	-0.0012 (6)
C2	0.0163 (6)	0.0169 (7)	0.0168 (6)	0.0003 (5)	0.0009 (5)	-0.0022 (5)
C8	0.0145 (6)	0.0196 (7)	0.0146 (6)	-0.0004 (5)	0.0000 (5)	0.0008 (5)
C14	0.0176 (6)	0.0267 (8)	0.0191 (6)	0.0028 (5)	0.0030 (5)	0.0025 (5)
C17	0.0220 (6)	0.0199 (7)	0.0228 (7)	-0.0055 (5)	0.0018 (5)	-0.0028 (5)
C4	0.0193 (6)	0.0237 (7)	0.0222 (7)	-0.0050 (6)	0.0070 (5)	-0.0006 (6)
C16	0.0125 (6)	0.0429 (9)	0.0246 (7)	0.0007 (6)	-0.0014 (5)	0.0059 (6)
C19	0.0304 (8)	0.0429 (10)	0.0284 (8)	0.0096 (7)	-0.0040 (6)	-0.0085 (7)

*Geometric parameters (Å, º) for **2**·MeOH*

Cl1—C2	1.7352 (14)	C12—C15	1.4897 (18)
O20—C7	1.3911 (15)	C10—C9	1.3919 (18)
O20—C1	1.3803 (16)	C9—H9	0.9500

O3—C10	1.3605 (16)	C9—C8	1.3891 (18)
O3—H3	0.85 (2)	C1—C2	1.3867 (18)
O6—C15	1.3381 (16)	C3—C13	1.5035 (18)
O6—C18	1.4487 (17)	C3—C2	1.3982 (19)
O4—C14	1.3208 (18)	C3—C4	1.380 (2)
O4—C16	1.4478 (16)	C5—C4	1.386 (2)
O2—C8	1.3670 (16)	C18—H18A	0.9800
O2—C17	1.4278 (17)	C18—H18B	0.9800
O7—C15	1.2082 (17)	C18—H18C	0.9800
O1—C5	1.3513 (18)	C13—H13A	0.9800
O1—H1	0.87 (2)	C13—H13B	0.9800
O8—C19	1.4166 (19)	C13—H13C	0.9800
O8—H8	0.80 (2)	C17—H17A	0.9800
O5—C14	1.2243 (19)	C17—H17B	0.9800
C11—H11	0.9500	C17—H17C	0.9800
C11—C12	1.4016 (18)	C4—H4	0.9500
C11—C10	1.3836 (19)	C16—H16A	0.9800
C6—C1	1.4144 (19)	C16—H16B	0.9800
C6—C5	1.4149 (19)	C16—H16C	0.9800
C6—C14	1.4740 (18)	C19—H19A	0.9800
C7—C12	1.3979 (18)	C19—H19B	0.9800
C7—C8	1.4042 (19)	C19—H19C	0.9800
C1—O20—C7	120.52 (10)	H18A—C18—H18B	109.5
C10—O3—H3	110.4 (14)	H18A—C18—H18C	109.5
C15—O6—C18	115.59 (11)	H18B—C18—H18C	109.5
C14—O4—C16	115.83 (11)	C3—C13—H13A	109.5
C8—O2—C17	117.39 (10)	C3—C13—H13B	109.5
C5—O1—H1	105.5 (14)	C3—C13—H13C	109.5
C19—O8—H8	108.3 (15)	H13A—C13—H13B	109.5
C12—C11—H11	120.1	H13A—C13—H13C	109.5
C10—C11—H11	120.1	H13B—C13—H13C	109.5
C10—C11—C12	119.86 (12)	C1—C2—Cl1	118.90 (10)
C1—C6—C5	117.47 (12)	C1—C2—C3	121.66 (13)
C1—C6—C14	125.22 (12)	C3—C2—Cl1	119.43 (10)
C5—C6—C14	117.10 (12)	O2—C8—C7	115.88 (11)
O20—C7—C12	118.89 (12)	O2—C8—C9	123.69 (12)
O20—C7—C8	122.02 (11)	C9—C8—C7	120.43 (12)
C12—C7—C8	119.03 (12)	O4—C14—C6	115.38 (12)
C11—C12—C15	118.03 (12)	O5—C14—O4	121.98 (13)
C7—C12—C11	120.27 (12)	O5—C14—C6	122.54 (13)

C7—C12—C15	121.70 (12)	O2—C17—H17A	109.5
O3—C10—C11	122.26 (12)	O2—C17—H17B	109.5
O3—C10—C9	117.30 (12)	O2—C17—H17C	109.5
C11—C10—C9	120.44 (12)	H17A—C17—H17B	109.5
O6—C15—C12	110.85 (11)	H17A—C17—H17C	109.5
O7—C15—O6	123.07 (12)	H17B—C17—H17C	109.5
O7—C15—C12	126.08 (12)	C3—C4—C5	121.34 (13)
C10—C9—H9	120.0	C3—C4—H4	119.3
C8—C9—C10	119.94 (12)	C5—C4—H4	119.3
C8—C9—H9	120.0	O4—C16—H16A	109.5
O20—C1—C6	123.41 (11)	O4—C16—H16B	109.5
O20—C1—C2	116.44 (12)	O4—C16—H16C	109.5
C2—C1—C6	120.02 (12)	H16A—C16—H16B	109.5
C2—C3—C13	121.41 (13)	H16A—C16—H16C	109.5
C4—C3—C13	120.28 (13)	H16B—C16—H16C	109.5
C4—C3—C2	118.31 (12)	O8—C19—H19A	109.5
O1—C5—C6	122.85 (13)	O8—C19—H19B	109.5
O1—C5—C4	116.31 (13)	O8—C19—H19C	109.5
C4—C5—C6	120.82 (13)	H19A—C19—H19B	109.5
O6—C18—H18A	109.5	H19A—C19—H19C	109.5
O6—C18—H18B	109.5	H19B—C19—H19C	109.5
O6—C18—H18C	109.5		
O20—C7—C12—C11	178.94 (11)	C1—O20—C7—C8	-40.30 (17)
O20—C7—C12—C15	-0.61 (18)	C1—C6—C5—O1	-176.13 (12)
O20—C7—C8—O2	0.74 (18)	C1—C6—C5—C4	5.3 (2)
O20—C7—C8—C9	-178.85 (11)	C1—C6—C14—O4	-10.8 (2)
O20—C1—C2—Cl1	-1.69 (16)	C1—C6—C14—O5	172.75 (15)
O20—C1—C2—C3	179.94 (11)	C5—C6—C1—O20	177.22 (11)
O3—C10—C9—C8	-179.40 (11)	C5—C6—C1—C2	-7.16 (19)
O1—C5—C4—C3	-178.84 (13)	C5—C6—C14—O4	163.80 (12)
C11—C12—C15—O6	26.28 (16)	C5—C6—C14—O5	-12.7 (2)
C11—C12—C15—O7	-152.92 (13)	C18—O6—C15—O7	-0.23 (19)
C11—C10—C9—C8	0.49 (19)	C18—O6—C15—C12	-179.47 (11)
C6—C1—C2—Cl1	-177.61 (10)	C13—C3—C2—Cl1	2.98 (18)
C6—C1—C2—C3	4.0 (2)	C13—C3—C2—C1	-178.66 (13)
C6—C5—C4—C3	-0.2 (2)	C13—C3—C4—C5	176.76 (13)
C7—O20—C1—C6	-63.13 (16)	C2—C3—C4—C5	-3.1 (2)
C7—O20—C1—C2	121.10 (13)	C8—C7—C12—C11	1.71 (19)
C7—C12—C15—O6	-154.16 (12)	C8—C7—C12—C15	-177.83 (12)
C7—C12—C15—O7	26.6 (2)	C14—C6—C1—O20	-8.2 (2)

C12—C11—C10—O3	179.40 (12)	C14—C6—C1—C2	167.40 (13)
C12—C11—C10—C9	-0.48 (19)	C14—C6—C5—O1	8.9 (2)
C12—C7—C8—O2	177.88 (12)	C14—C6—C5—C4	-169.66 (13)
C12—C7—C8—C9	-1.71 (19)	C17—O2—C8—C7	168.82 (12)
C10—C11—C12—C7	-0.63 (19)	C17—O2—C8—C9	-11.61 (19)
C10—C11—C12—C15	178.93 (11)	C4—C3—C2—Cl1	-177.13 (10)
C10—C9—C8—O2	-178.93 (12)	C4—C3—C2—C1	1.2 (2)
C10—C9—C8—C7	0.6 (2)	C16—O4—C14—O5	-3.9 (2)
C1—O20—C7—C12	142.57 (12)	C16—O4—C14—C6	179.62 (12)

*Hydrogen-bond geometry (Å, º) for **2**·MeOH*

D—H···*A*	*D*—H	H···*A*	*D*···*A*	*D*—H···*A*
O8—H8···O7	0.80 (2)	2.03 (2)	2.7871 (14)	156 (2)
O3—H3···O8^{i}	0.85 (2)	1.81 (2)	2.6539 (15)	176 (2)
O1—H1···O5	0.87 (2)	1.74 (2)	2.5439 (16)	151 (2)

Symmetry code: (i) *x*-1/2, -*y*+1/2, *z*+1/2.

Chapter 4 – Manuscript 3

Studies on the Antibacterial Activity of the Natural Product Pestalotic acid A against Methicillin-Resistant *Staphylococcus aureus*

Overall contribution to the manuscript:

- Fermentation of fungal strain
- "OSMAC" approach assay
- Compounds isolation
- Structure elucidation
- Determination of minimal inhibitory concentrations
- Determination of cytotoxicity and therapeutic index
- Determination of time-kill curves and hemolysis assay *in vitro*
- Determination of single step resistance frequency
- Membrane Potential assay
- Propidium iodide internalization
- Manuscript writing

Studies on the Antibacterial Activity of the Natural Product Pestalotic acid A against Methicillin-Resistant *Staphylococcus aureus*

Lin Wang,[a] **Kristin Schwechel**,[a] **Tobias Heinen**,[b] **Lasse van Geelen**,[a] **Christoph Janiak**,[b] **Zhen Liu**,[c] **Rainer Kalscheuer**[a, *]

[a] Institute of Pharmaceutical Biology and Biotechnology, Heinrich Heine University, Universitätsstr. 1, 40225 Düsseldorf, Germany.

[b] Institute of Inorganic and Structural Chemistry, Heinrich Heine University, Universitätsstr. 1, 40225 Düsseldorf, Germany.

[c] Key Laboratory of Study and Discovery of Small Targeted Molecules of Hunan Province, School of Medicine, Hunan Normal University, Changsha 410013, China.

[*]Corresponding author.

Rainer kalscheuer: E-mail: rainer.kalscheuer@hhu.de

Abstract

Bacterial infections remain a major cause of mortality and morbidity worldwide. Despite highly specific intervention measurements and policies, the rate of infections is still high due to the emergence of antibiotic–resistant bacteria. This study describes the isolation of pestalotic acid A (**1**) and pestaloside A (**9**) from solid rice culture of the endophytic fungus *Pestalotiopsis chamaeropis* as well as of the derivatives pestalotic acid B-G (**2**-**8**), which were produced during supplementation of the rice medium with 3.5% sodium iodide. Notably, pestalotic acid G (**8**) and pestaloside A (**9**) were identified as new natural compounds, and their structures were elucidated by 1D and 2D NMR spectra and HRESIMS. Additionally, we determined absolute configuration of the known compound pestalotic acid C (**3**) by X-ray diffraction. Bioactivity studies showed that both pestalotic acid A and G exhibited potent antibacterial activity against methicillin-resistant *Staphylococcus aureus* ATCC 700699 (MRSA) with MIC_{90} values of 6.25 μM. The strong bactericidal killing effects combined with low cytotoxicity suggests pestalotic acid A as promising candidate for further preclinical development. Mode of action studies indicated that pestalotic acid A might impair the integrity of the cell membrane of MRSA.

Key words: *Pestalotiopsis chamaeropis, Pestalotic acid, antibacterial activity, MRSA, integrity of cell membrane, OSMAC*

Introduction

When Alexander Fleming discovered the first antibiotic penicillin in 1928, it was a milestone of chemical therapy and dawn of the "antibiotic era". Truly, penicillin was a miracle drug as previously fatal infections could be cured. However, penicillin resistance occurred only a few years after its introduction and became a significant problem until now.[1] Currently, infections caused by antibiotic-resistant strains of *Staphylococcus aureus*, such as methicillin-resistant *S. aureus* (MRSA), have reached epidemic proportions globally[2] and are predicted to be the leading cause of death in the near future unless effective counter measures are taken very soon.[3] These infections not only severely compromise human health, but also represent a high burden on healthcare systems and require an excessive consumption of resources.[4] Despite this urgent medical need, however, the latest discovery of a new antibiotic class that found widely use in clinical market were lipopeptides in 1987. Since then, a continuous lack of innovation in this field today has led to few novel antibiotic candidates in the drug discovery pipeline.[5, 6] As a consequence, more and more bacterial infections are becoming hard to treat. Especially the lack of antibiotics against multi-drug resistant bacteria, such as MRSA, is seriously complicating clinical treatment.

It is well known that fungi remain one of the most important resources for the discovery of new bioactive compounds[7]. Historically, the drug discovery from microorganisms supplied diverse important drugs, such as the antibiotic penicillin, the immunosuppressant cyclosporine and the anti-hypercholesterolemic agent lovastatin.[8] Thus, antibiotic development from fungi is considered an potent resource to identify novel chemical scaffolds. In our study, the endophytic fungus *Pestalotiopsis chamaeropis*, which has been isolated from the plant *Aster subulatus Michx*, was subjected to a "one strain many compounds" (OSMAC) approach to induce silent gene cluster and expand diversity of the produced secondary metabolites. Pestalotic acid derivates were isolated and found to exhibit strong antibacterial potency against MRSA. Initial characterization of the biologically activity is described, pointing toward the

impairment of structural integrity of the bacterial cell wall and/or the cytoplasmic membrane as the potential mode of action.

Results and discussion

Secondary metabolites from fungi play an indispensable role in drug discovery. Following this line, we have isolated from the plant *Aster subulatus* (Michx.) an endophytic fungus, which was identified as *Pestalotiopsis chamaeropis* with 100% identity by BLAST search of the internal transcribed spacer (ITS) sequence in comparison with the nucleotide database of the National Center for Biotechnology Information (NCBI). Next, we fermented *P. chamaeropis* at a large-scale on solid rice medium and extracted the obtained biomass using ethyl acetate to study the profile of the produced secondary metabolites. From the ethyl acetate extract, pestalotic acid A (compound **1**) and pestaloside A (compound **9**) were isolated using different chromatographic steps as described in detail in the Material & Methods section. Since we observed antibacterial activity of pestalotic acid A during preliminary explorative screenings, a modification of the culture conditions was implemented to potentially expand the diversity of compounds. For this, 3.5% sodium iodide was supplemented to standard rice medium. This approach was first described by Zeeck and co-workers[9] and was referred to as "one strain many compounds" (OSMAC), which triggers expression of silent biosynthetic gene clusters and results in unlocking of the fungal chemical diversity. This might allow the discovery of novel molecules of both medical and biotechnological interest.[10] In the present study, the described OSMAC approach yielded compounds **2**-**8** (Figure 1), which were not found in the extract obtained from the non-supplemented rice medium. Notably, from the secondary metabolites we isolated from *P. chamaeropis*, compounds **8** and **9** were identified as new natural products as described in detail below, while all other isolated molecules were identified as known natural compounds based on comparison of their spectroscopic data with the literature.

Compound **8** was obtained as colorless oil, suggested with a molecular formula of $C_{23}H_{32}O_8$ by HRESIMS. The analysis of ^{13}C NMR at δ_C 195.8, 179.2 (179.9), 172.3, 171.9, 160.4 (160.5), 123.5 (123.6), 101.9 (102.5), 37.9, 35.6, 29.0-23.1 and ^{1}H NMR at δ_H 6.91, 4.87, 1.45-1.27 suggested compound **8** had good agreement with co-isolated known compound **6** from position 1-11', except for the terminal residue. While the HMBC correlations from H-17' (δ_H 4.87) to C-14' (δ_C 195.5), and from H-16' (δ_H 4.87) to C-12'((δ_C 35.1) and C-13' (δ_C 71.1) evident the presence of ketone and hydroxyl group. Thus, the structure of **8** was elucidated as pestalotic acid H with the structure as drawn in figure 1 and the ^{1}H NMR and ^{13}C NMR data are given at table 1.

Compound **9** was obtained as colorless oil with the molecular formula of $C_{20}H_{30}O_7$ determined by HRESIMS. The ^{1}H NMR correlations revealed two aromatic protons at δ_H 6.92 (d, H-3) and δ_H 6.72 (d, H-4), two olefinic protons at δ_H 6.51 (dt, H-7) and δ_H 6.24 (dt, H-8), an oxygenated methylene at δ_H 4.67 (m, H-8), together with the COSY correlations between H-9/H-10/H-11/H-12/H-13 figured out the **9** has similar aglycone with known compound pestaloside.[11] The remaining NMR signals in **9** included additional five oxygenated methynes (CH-15 to 19 at δ_H 5.28, 4.10, 3.91, 3.18, 3.76) and an methyl group (CH_3-20, δ_H 1.26), suggesting an additional pyranoside unit in **9**, which were supported by COSY correlations between H-15/H-16/H-17/H-18/H-19 and the HMBC correlations from H-20 (δ_H 1.26) to C-18 (δ_C 73.8) and C-15 (δ_C 100.8). Furthermore, the HMBC correlations from H-15 (δ_H 5.27) to C-16 (δ_C 71.4) and C-2 (δ_C 150.4) indicated the pyranoside residue was connected on the position of C-2. Further hydrolysis was implemented and identified the pyranose residue as α- L-Rhamnose by determination of specific optical rotation with the value of $[\alpha]_D^{25}$ -6.990 (Methanol). Thus, the structure of **9** was elucidated as pestaloside A with the structure as shown in figure 2 and the corresponding ^{1}H NMR and ^{13}C NMR data are given in table 1.

Compound **3** was obtained as colorless powder with the molecular formula of $C_{21}H_{30}O_7$ as determined by HRESIMS. The ^{1}H NMR δH (*J* Hz): 7.56 (7.49), 7.45 (7.39), 4.88 (4.80), 3.79, 3.02, 2.94 (2.82), 2.05 (1.99), 1.89, 1.61, 1.41, 1.17 and ^{13}C NMR δC: 194.7, 179.7 (179.3), 170.1, 167.8, 160.3 (159.8), 123.2, 102.4 (101.5), 93.5, 78.4 (78.3), 68.5 (68.2), 39.1, 38.8, 37.8 (37.7), (29.4, 29.2, 29.0, 28.9, 28.7), 25.6 (25.3), 23.4 (23.3), 23.2 (23.1) suggested a structure of the known compound pestalotic acid C. However, the absolute configuration has not previously been described. In the present study, high-quality crystals of compound **3** were obtained in methanol by slow solvent evaporation, enabling us to corroborate the structure and to demonstrate that the absolute configuration is 4 (S), 4' (R), 13'(R) employing X-ray diffraction. Furthermore, due to presence of a double bond between the furan-dione ring and the dihydrofuran ring, the NMR spectra revealed interconversion of *E*- and *Z*-isomers of compounds **1**-**8** occurred at the ratio of approximately 1:1.

Pestalotic acid derivatives exhibit significant activity against gram-positive bacteria. Minimal inhibitory concentrations (MICs) of compounds **1**-**9** were determined against gram-positive bacteria including MRSA, vancomycin-resistant *Enterococcus faecium*, *Enterococcus faecalis, Streptococcus pneumonia*, and *Mycobacterium tuberculosis* as well as against the fungus *Candida albicans* following CLSI guidelines.[12] Various pestalotic acid derivates exhibited significant activity against gram-positive bacteria, especially MRSA, but no effects could be observed against *C. albicans* and *M. tuberculosis* (Table 2). Interestingly, compound **1** and **7**, which both contain the same unsubstituted decanoyl side chain, showed the strongest antibacterial activity against MRSA with MIC_{90} values of 6.25 μM. However, hydroxylation, esterification, or hydroformylation negatively affected antibacterial activity as compounds **2**-**6** exhibited significantly higher MIC_{90} values in the range of ≥100 μM. If position 10 was substituted by a methyl group like in compound **7**, no significant effects could be observed in our assays. Due to their strongest antibacterial activity, promising compounds **1** and **7** were

further evaluated.

Disc diffusion test and growth–kinetics. Disc diffusion test is an alternative culture-based microbiology assay used in drug discovery to determine the susceptibility of compounds on bacteria. The results showed that compound **1** could inhibit the growth of MRSA and form a clear zone around the disk with similar size compared to the positive control (Supporting information Figure 1). In addition, growth-kinetics also demonstrated impaired growth at the concentration of 6.25 μM after 22 hours incubation with compound **1** (Supporting information Figure 2), which is consistent with the MIC.

Cytotoxicity and therapeutic index. To determine the general cytotoxic effects of compounds **1** and **7**, the human THP-1 monocytic cell line, the human MRC-5 lung fibroblast cell line, the human CLS-54 lung carcinoma cell line, and the human H4 brain neuroglioma cell line were exposed to the compounds at a concentration range from 0.78-100 μM. Compound **7** showed a substantial level of cytotoxicity to all tested cell lines. However, compound **1** exhibited cytotoxicity only against HEK293 cells at 50 μM (Figure 3a). Furthermore, compound **1** displayed no hemolytic activity against sheep erythrocytes even at high concentrations up to 100 μM (Figure 5). The selectivity index was determined through the quotient of the observed cytotoxic concentration (IC_{50}) and the MIC_{90} resulting in an SI value $\geq$ 10 for compound **1** (Table 3), making this compound a promising drug lead candidate.

In vitro time-killing kinetic. Time-killing curves monitor bacterial viability and are routinely used to evaluate the effect of antimicrobials over time. MRSA was treated with compound **1** at 4-fold MIC. After 24 hours incubation, bacterial viability was strongly reduced from 10^8 to 10^4 CFU/mL (Figure 4). This indicated compound **1** has strong bactericidal characteristics and further mode of action studies were carried out.

Mutant isolation and mode of action studies. Characterization of spontaneously resistant mutants might be informative with respect to predicting the mode of action of an antibacterial compound. Toward this end, different densities of MRSA cells were plated out on solid media containing different concentrations of compound **1** and incubated for 48 hours. This resulted in the isolation of three mutants when 4-fold MIC was used. Mutants displayed significant resistance to compound **1** with MIC values of 50 μM (Supporting information Table 1).

With regard to the potential antibacterial mechanism of compound **1**, we hypothesized that it could target the cell membrane based on its lipophilic structure containing a long decanoyl side chain that could possibly incorporate into the phospholipid bilayers. Thus, a fluorescence approach was employed to determine potential impact on membrane potential. The probe 3,3'-diethyloxacarbocyanine iodide (DiOC2(3)) was used to monitor membrane potential in both wild-type and resistant bacterial cells suspended in PBS buffer. DiOC2(3) is a green fluorescent dye that accumulates within cells in a charge-dependent manner, shifting its fluorescence spectrum from green to red due to dye stacking in presence of an energized membrane. A decrease in the ratio of red/green fluorescence is indicative of depolarization of membrane potential. When wild-type cells of MRSA were treated with compound **1**, a dose-dependent decrease in the membrane potential was observed, reaching an effect at high concentration comparable to the inophore CCCP that was used as positive control in this assay. In contrast, membrane potential remained in a polarized state in cells treated with the negative control moxifloxacin, which is a bactericidal drug that inhibits DNA replication by targeting DNA gyrase but is not directly impairing membrane function (Figure 6). These findings suggest that compound **1** is able to depolarize the bacterial membrane, an effect that is known to result in killing of bacterial cells.

Since membrane depolarization can occur both in presence or absence of concomitant impairment of structural integrity of the membrane, a propidium iodide (PI) internalization assay was used to test the leakage of cell membrane. Red fluorescence occurs when PI can enter

cells through damaged or permeabilized membranes allowing binding to double-stranded DNA, while intact cell membranes are impermeable for this dye.[13] MRSA cells were pre-treated with PI and subsequently exposed on the 4-fold MIC of compounds. PI fluorescence increased after 40 mins incubation with compound **1**, which occurred with a marked delay compared to the positive control lysostaphin. However, in spontaneously resistant mutants, PI uptake was not detectable leading to the conclusion that corruption of the membrane integrity might be the mode of action (Figure 7). The molecular nature of the mutations present in the spontaneous resistant mutants is not known yet, but the resistance mechanism could be related to reduced uptake of the compound, upregulation of drug efflux pumps, or alteration of membrane composition or receptor proteins in the membrane that are necessary for interaction with compound **1**. To exclude that resistant occurs through metabolism or decomposition, compound **1** was determined by LC-MS measurements in extracts obtained from bacterial culture supernatants of wild-type and mutants. However, no significant differences between wild-type and resistant mutants could be detected (Supporting information Figure 3), ruling out metabolism or decomposition as a relevant mechanism involved in resistance to compound **1**.

CONCLUSIONS

We discovered new natural products with significant antimicrobial activity against MRSA using the "OSMAC" approach employing the endophytic fungus *P. chamaeropis*. Nine natural compounds were obtained, with isolation of pestalotic acid H and pestaloside A being reported for the first time. High-quality crystals allowed elucidation of the absolute configuration of the previously reported compound pestalotic acid C by X-ray diffraction. While the production of secondary metabolites was triggered by supplementation of sodium iodide to the medium, none of the isolated compounds was found to be halogenated, indicating that sodium iodide was not simply fed into secondary biosynthetic pathways as a precursor. Pestalotic acid derivatives exhibited various degrees of antibacterial activity against MRSA and allowed limited structure-

activity relationship (SAR) studies. Further functional characterization of the most active compound pestalotic acid A (**1**) revealed a promising therapeutic window. Assays determining membrane potential and membrane integrity are supportive of the membrane being the target of pestalotic acid A explaining the strong bactericidal effect. In contrast, lack of hemolytic activity demonstrated that pestalotic acid A is not a generally membrane-active molecule but specifically targets the bacterial cell membrane. Consequently, pestalotic acid A is a promising lead candidate for discovery of antibacterial agents that likely targets on the bacterial membrane.

Materials and methods

General experiments

HPLC analysis was performed with a Dionex UltiMate 3000 system through an UltiMate 3000 pump and a photodiode array UV routine at channel 235, 254, 280 and 340 nm (DAD 3000 RS,) on Eurospher 100-10C18 column (125×4 mm, L×ID, Knauer, Germany). Semipreparative HPLC was done with a Merck Hitachi Chromaster HPLC system (UV detector 5410; pump 5110; column Eurospher 100-10C18, 300 8 mm, Knauer, Germany) performed by mixtures of MeCN-H_2O with flow rate at 5 mL/min. Merck MN silica gel 60 M (0.04–0.063 mm) and Sephadex LH-20 were used for column chromatography. Thin-layer chromatography (TLC) analysis was performed on silica gel 60 F254 TLC plates, and visualized under UV detection at 254 and 366 nm or by spraying the plates with anisaldehyde reagent followed by heating (Macherey-Nagel, Germany). 1D and 2D NMR spectra were recorded on a Bruker ARX 600 NMR spectrometer through TMS as an internal standard. ESI and HRESIMS spectra were obtained employing an Agilent Finnigan LCQ Deca and a UHR-QTOF maXis 4G (Bruker Daltonics), respectively. Jasco P-2000 polarimeter was used to measure optical rotations in Methanol solvent.

Fungal material and fermentation

The fungal strain *P. chamaeropis* was isolated from the plant *Aster subulatus* (Michx.) collected in April 2018 in Beijing, P.R. China. Identification was performed by determination of the internal transcribed spacer (ITS) sequence and nucleotide BLAST search in the NCBI database following standard molecular biology protocols for fungi as described previously.[14] The accession number of the internal transcribed spacer (ITS) sequence in GenBank is ON556592. The fungal strain is stored as glycerol-agar aliquots in a -80 °C freezer in our laboratory at the Institute of Pharmaceutical Biology and Biotechnology, Heinrich-Heine University, Duesseldorf, Germany.

Chemical section: "OSMAC" approach and isolation

P. chamaeropis was aerobically grown on solid rice medium in fifteen Erlenmeyer flasks each containing 100 g rice and 110 mL water at 22 °C. After two weeks of fermentation, rice cultures were extracted with 500 mL EtOAc for each flask and soaked overnight, which was repeated twice until the color of EtOAc extract became light. The combined extracts were dried by rotary evaporation to yield 15.8 g of dried crude EtOAc extract. The crude EtOAc extract was fractionated via vacuum liquid chromatography (VLC) with silica gel using *n*-hexane / EtOAc and dichloroform / methanol (V/V) as mobile phase with mixtures from 100:0, 80:20, 60:40, 40:60, 20:80, 0:100, respectively, and resulted in nine fractions (Fr.1-Fr.9). Fraction 9 (1.9 g) was further separated by Sephadex LH-20 column eluted with dichloroform / methanol = 1:1 (V/V) to gain six sub-fractions (Fr.9-1 – Fr.9-6). Fraction 9-6 (312 mg) was chromatographed on an ODS RP column and eluted using a gradient elution of methanol / H_2O (V/V) from 40:60, 50:50, 60:40, 70:30, 80:20, 90:10, 100:0 to yield four sub-fractions (Fr.9-6-1 – Fr.9-6-4). Sub-fraction 9-6-3 (103 mg) was separated by semi-preparative HPLC with a mixture of MeOH-H_2O to obtain compound **9** (3.5 mg). Same routine was used to obtain sub-fraction Fr.8-2-4, and semi-preparative HPLC was used to harvest compound **1** (5.2 mg) by a mixture of MeOH-H_2O as mobile phase.

Based on the interesting compound **1**, **"**OSMAC" was carried out using 3.5% sodium chloride, sodium fluoride, sodium bromide, sodium iodide, ammonium nitrate, L-rhamnose, zinc sulfate, magnesium nitrate or ferric sulfate, respectively, which were added to rice medium. Furthermore, we performed a co-culture of *P. chamaeropis* with *Bacillus subtilis* on regular rice medium. All small-scale fermentation conditions were incubated at 22 °C for two weeks. Plain rice medium served as blank control. Interestingly, HPLC spectra showed significant change in the secondary metabolite profile during cultivation on rice medium supplemented with sodium iodide with loss of the main peak and enrichment of pestalotic acid derivatives. Next, large scale fermentation using sodium iodide-supplemented rice medium was carried out to obtain 18.5 g crude extract, which showed inhibitory activity against MRSA at a concentration of 100 μg/ml. Crude extract was fractionated via vacuum liquid chromatography (VLC) as well as with silica gel using *n*-hexane / EtOAc from 100:0, 80:20,70:30, 60:40, 50:50, 40:60, 30: 70, 20:80, 0:100 to obtain four fractions (Fr.1-Fr4). Fraction 2 (4.1 g) was further chromatographed with ODS column using MeOH / H_2O (V/V) from 30:70, 50:50, 60:40, 70:30, 80:20, 90:10, 100:0 to obtain six sub-fractions (Fr.V2-R1~ Fr.V2-R6). Fraction V2-R2 (189 mg) was separated by semi-preparative HPLC with a mixture of MeCN-H_2O to obtain compound **2** (5.1 mg), compound **3** (3.8 mg), compound **4** (3.2 mg) and compound **5** (7.0 mg). Fraction V2-R4 (125 mg) was separated by semi-preparative HPLC as well using mobile phase MeCN-H_2O mixture to harvest compound **6** (2.3 mg) and compound **7** (4.5 mg). Compound **8** (4.7 mg) was obtained using a similar method by semi- preparative HPLC.

Pestalotic acid A (**1**): colorless powder; $[\alpha]_D^{25}$ -225.736 (CH_3OH); UV (MeOH) λ_{max} (nm): 214.7, 313.3, 322.2; HRESIMS *m/z*: 382,1989 $[M + H]^+$ (calcd for $C_{21}H_{30}O_6$, 378.2042); ^1H NMR in $CDCl_3$:7.83 (7.81), 7.50 (7.40), 4.89, 2.96, 2.84, 1.99, 1.60, 1.28, 0.90; ^{13}C NMR in $CDCl_3$: 198.2 (197.1), 181.7 (181.0), 172.5, 170.8, 163.6 (163.3), 123.4, 104.3 (103.6), 94.9 (94.5), 80.7 (80.3), 38.7 (38.6), 36.7 (36.6), 33.1 (33.0), 30.7(30.6), 25.0 (24.9), 23.7, 23.3

(23.2), 14.4

Pestalotic acid B (**2**): colorless oil; $[\alpha]_D^{25}$ -234.198 (CH_3OH); UV (MeOH) λ_{max} (nm): 235.2, 301.7, 344.9; ESI-MS *m/z*: 382,1989 [M + H]+ (calcd for $C_{21}H_{30}O_7$ 394.1992); ^1H NMR in $CDCl_3$: 7.55 (7.48), 7.45 (7.39), 4.87 (4.79), 3.02, 2.95, 2.82, 2.07, 1.63, 1.29, 0.93; ^{13}C NMR in $CDCl_3$: 196.9 (149.6), 179.5, 170.3, 168.2, 160.5, 123.4, 102.6 (101.7), 93.8, 73.5 (73.4), 38.1, 37.7, 36.4, 30.0, 25.3, 24.1, 23.4, 9.9.

Pestalotic acid C (**3**): colorless powder; $[\alpha]_D^{25}$ -205.878 (CH_3OH); UV (MeOH) λ_{max} (nm): 233.7, 316.5, 342.8; HRESIMS *m/z*: 382,1989 [M + H]+ (calcd for $C_{21}H_{30}O_7$ 394.1992); ^1H NMR in $CDCl_3$: 7.56 (7.49), 7.45 (7.39), 4.88 (4.80), 3.79, 3.02, 2.94 (2.82), 2.05 (1.99), 1.89, 1.61, 1.44 (1.41), 1.17; ^{13}C NMR in $CDCl_3$: 196.7 (194.8), 173.0 (172.3), 170.6, 167.6, 160.0, 123.5, 101.8, 78.8, 68.4, 39.3, 38.0, 35.6, 29.0, 23.6, 23.5.

Pestalotic acid D (**4**): colorless oil; $[\alpha]_D^{25}$ -196.631 (CH_3OH); UV (MeOH) λ_{max} (nm): 215.0, 305.7, 318.0; ESIMS *m/z*: 382,1989 [M + H]+ (calcd for $C_{21}H_{28}O_7$ 392.1835); ^1H NMR in $CDCl_3$: 7.53 (7.49), 7.45 (7.41), 4.87, 3.20, 2.90 (2.80), 2.40, 2.13, 2.20, 1.99 (1.90), 1.61, 1.25, 1.04; ^{13}C NMR in $CDCl_3$: 211.6, 196.1(194.3), 179.9, 172.6, 170.4, 160.5, 123.5, 101.9, 90.2, 77.4, 43.0, 37.6, 35.9, 30.0, 28.8, 23.3.

Pestalotic acid E (**5**): colorless oil; $[\alpha]_D^{25}$ -223.639 (CH_3OH); UV (MeOH) λ_{max} (nm): 236.1, 302.1, 347.6; ESIMS *m/z*: 382,1989 [M + H]+ (calcd for $C_{21}H_{30}O_7$ 392.1835); ^1H NMR in $CDCl_3$: 7.55 (7.48), 7.45 (7.41), 4.88, 3.18, 2.98 (2.80), 2.40, 2.13, 2.00 (1.91), 1.60, 1.52, 1.23, 1.14; ^{13}C NMR in $CDCl_3$: 209.6, 194.1(193.0), 179.6, 173.0, 170.1, 160.1, 123.8, 101.4, 93.0, 78.4, 43.7, 38.0, 36.5, 29.9, 28.7, 23.6, 23.3.

Pestalotic acid F (**6**): colorless oil; $[\alpha]_D^{25}$ -191.176 (CH_3OH); UV (MeOH) λ_{max} (nm): 235.1, 302.6, 345.2; ESIMS *m/z*: 382,1989 [M + H]+ (calcd for $C_{23}H_{32}O_8$ 436.2097); ^1H NMR in $CDCl_3$: 7.54 (7.49), 7.45 (7.44), 4.88, 4.04, 3.01, 2.83, 2.02, 1.91, 1.61, 1.40, 1.29, 1.24; ^{13}C NMR in $CDCl_3$: 196.7(194.2), 179.5 (179.2), 170.1, 167.9, 160.2 (159.3), 123.4 (123.2), 102.3 (101.4), 94.0 (93.6), 78.4, 62.9, 37.1, 36.8, 36.5, 29.2, 27.7, 23.6, 23.2, 22.6.

Pestalotic acid G (**7**): colorless oil; $[\alpha]_D^{25}$ -121.416 (CH_3OH); UV (MeOH) λ_{max} (nm): 231.7, 304.9, 344.6; HRESIMS *m/z*: 382,1989 [M + H]+ (calcd for $C_{22}H_{32}O_6$ 392.2199); ^1H NMR in $CDCl_3$: 7.55 (7.50), 7.43 (7.42), 4.89, 3.71, 2.99, 2.81, 1.99 (1.91), 1.61, 1.42, 1.23,0.88; ^{13}C NMR in $CDCl_3$: 196.8(194.6), 179.4, 170.5, 170.0, 160.3, 123.7 (123.5), 102.7 (102.2), 94.1, 79.1 (78.4), 52.5, 38.5 (38.3), 36.5 (36.2), 29.8, 29.6, 24.4, 23.0, 14.5.

Pestalotic acid H (**8**): colorless oil; $[\alpha]_D^{25}$ -9.614(CH_3OH); UV (MeOH) λ_{max} (nm): 214.5, 320.7, 307.7; HRESIMS *m/z*: 382,1989 [M + H]+ (calcd for $C_{23}H_{32}O_8$ 436.2097); ^1H NMR and ^{13}C NMR data see table 1.

Pestaloside A (**9**): colorless oil; $[\alpha]_D^{25}$ -15.547 (CH_3OH); UV (MeOH) λ_{max} (nm): 238.6, 317.1; HRESIMS *m/z*: 382,1989 [M + CH_3]+ (calcd for $C_{20}H_{30}O_7$, 382.1992); ^1H NMR and ^{13}C NMR data see table 2.

Hydrolysis

Compound **9** (2.0 mg) was hydrolyzed with 2N HCl (2.0 mL) at 90 °C for 4 h as previously described.[15] After cooling, the solution was extracted with chloroform (5 mL) and H_2O twice. The water phase containing the sugar was examined using specific optical rotation analysis with $[\alpha]_D^{25}$ -6.990 (Methanol) which had a good agreement with reference[16] and identified the sugar as α, L-rhamnose.

Biological section: Characterization of active substances

Antibacterial characterization.

Nosocomial bacterial strains were incubated aerobically in a Mueller Hinton broth at 37 °C including *Staphylococcus aureus* (MSSA strain ATCC 25923, MRSA/VISA strain ATCC 700699, MRSA strain), *Enterococcus faecalis* (ATCC 29212, ATCC 51299 (gentamycin-resistant)), *Enterococcus faecium* (ATCC 35667, ATCC 700221 (vancomycin-resistant)), *Escherichia coli* ATCC 25922. *Candida albicans* was steadily grow in YPD medium (yeast

extract 10 g/L, peptone 20 g/L, D-glucose 20 g/L) at 37 °C. *Mycobacterium tuberculosis* H37Rv strain was grown aerobically in a Middlebrook 7H9 medium supplemented with 0.05% (v/v) tyloxapol, 0.5% (v/v) glycerol and 10% (v/v) ADS (5% w/v, bovine serum albumin fraction V; 2% w/v, glucose; 0.85% w/v, sodium chloride) at 37 °C, 5% CO_2 in a humidified atmosphere.

Determination of minimal inhibitory concentration (MIC).

The biological activity of compounds **1-9** was tested against both Gram-positive bacteria, including *S. aureus, E. faecalis*, and *E. faecium*, the Gram-negative bacterium *E. coli*, and the fungus *C. albicans* using the recommendations of the Clinical and Laboratory Standards Institute (CLSI, 2018)[12]. Briefly, bacteria were pre-cultured in Mueller-Hinton (MH) broth at 37 °C shaking at 180 rpm. The optical density was adjusted to OD_{600} nm ~ 0.1 (1×10^6 CFU/mL) and 5×10^5 CFU/well were seeded into 96 well round bottom microtiter plates containing the testing compounds at a concentration range from 0.78 – 100 μM in a total volume of 100 μL. 2% DMSO was used as solvent control, while moxifloxacin was employed as positive control. Subsequently, the plates were aerobically incubated at 37 °C overnight. MICs were determined by Tecan Pro-2000 plate reader employing the resazurin assay at excitation wavelength 540 nm and emission wavelength 590 nm. All tests were duplicated twice.

C. albicans cells were incubated in YPD broth in glass flask at 37°C shaking at 180 rpm overnight to harvest the cells in the yeast form. Afterwards, cells were seeded in 96-well round bottom microtiter plates with a density of 1×10^6 CFU/mL, which contained the testing compounds at concentrations ranging from 0.78 – 100 μM in a total volume of 100 μL. The plates were incubated at 37°C overnight. 2% DMSO was used as negative control, while hygromycin B served as positive control.[17] The readout was performed with the resazurin assay as above.

M. tuberculosis cells were incubated in 7H9 medium at 37°C shaking at 80 rpm for five days. Afterwards, the cell density was adjusted to 1×10^6 CFU/mL and $2\text{x}10^5$ CFU were seeded

in 96 well round bottom microplate which containing two fold serial dilutions of compounds (1-10) at concentrations ranging from 0.78-100 μM in a total volume of 100 μL. Rifampicin was used as positive control, DMSO at a maximal concentration of 2% was used as solvent control. Next, the plates were incubated at 37°C for 5 days at 37 °C, 5% CO_2, in a humidified atmosphere. Readout was performed following the resazurin protocol as described above.

Disc diffusion assay

Disc diffusion is one of the classical methods for susceptibility testing, which is broadly used in clinical diagnostic as well as in research.[18] The disk diffusion method was used according to recommendation of EUCAST Disk Diffusion Test Methodology.[19] *S. aureus* and *Candida albicans* cells were pre-cultured. Afterwards, cell suspension were adjusted to a concentration of 1-2 x 10^8 CFU/mL and used to inoculate Mueller-Hinton agar plated using 100 μL culture aliquots. Subsequently, sterile filter discs containing 5 μL of the testing compounds at 10 mM were placed onto the surface of the agar plate. DMSO served as negative control, moxifloxacin and hygromycin B were used as positive control for MRSA and *Candida albicans*, respectively. The plates were incubated overnight, and the diameter of the resulting inhibitions zones were evaluated by caliper.

Determination of growth kinetics

MRSA strain was inoculated in Mueller-Hinton broth and diluted to an $OD_{600\ nm} = 0.1$. The cells were seeded into 96-well microtiter plates containing different concentrations of testing compound. Mueller-Hinton broth with DMSO was used as growth control, moxifloxacin was used as positive control. Microtiter plates were incubated in a Tecan Infinite 200pro plate reader at 37 °C shaking and $OD_{600\ nm}$ was measured for 24 h every 30 min.

Determination of cytotoxicity and therapeutic index.

Cytotoxicity studies were conducted as described previously[20] to evaluate the therapeutic index of compounds. Human cell lines THP-1 (human monocytic leukemia cell line), CLS-54

(human lung carcinoma cell line) and H4 (human brain neuroglioma cell line) were cultured in RPMI 1640 medium containing 10% fetal bovine serum (FBS), while HEK293 (human embryonic kidney cells) and HUH7 cells (human liver cell line) were cultivated using an EMEM medium supplemented with 2 mM L-glutamine, 1 mM sodium pyruvate, 1% (v/v) non-essential amino acids and 10% (v/v) FBS. All cells were cultured at 37 °C in a humidified atmosphere with 5% CO_2. Afterwards, cells were adjusted to a density of 2 x 10^5 cells/mL and seeded into 96-well flat-bottom microtiter plates in a total volume of 100 μL containing two-fold serial dilutions of compounds at a final concentration range from 0.78-100 μM. 2% (v/v) DMSO was used as solvent control, uninoculated medium was treated as blank control, moxifloxacin was employed as positive control. Subsequently, plates were incubated at 37 °C with 5% CO_2 for 48 hours. Subsequently, fluorescence was evaluated after addition of 10 μL of resazurin solution (100 μg/mL) and 2-4 hours of further incubation. All tests were duplicated twice.

Determination of time-kill kinetics

Time-killing kinetic was performed for compound **1** against MRSA. An overnight culture was adjusted to a concentration of approx. 5 x 10^8 CFU/mL and subsequently split into three aliquots. One aliquot was incubated with testing compound **1** at 4-fold MIC, another culture contained 4-fold MIC of moxifloxacin as positive control, and the third aliquot was cultured with the solvent control. After 0, 3, 6, 9 and 24 h incubation, 100 μL culture aliquots were taken and plated on MH agar plates. CFU were counted after an overnight incubation at 37°C. In order to avoid the potential degradation of compound, after 6 hours of incubation the cultures were centrifuged at 4,000 rpm for 10 min to remove the medium and replace it with an equal volume of fresh medium containing the compound at the initial concentration.

Determination of hemolytic activity

Hemolytic activity was tested following a published standard protocol.[21] Briefly, defibrinated sheep red blood cells (RBC) were washed twice with PBS and centrifuged at 3,000 rpm, 10 min at 4 °C. Afterwards, 100 μL of 8% RBC suspension in PBS was treated with compound **1** at different concentrations ranging from 1.56-100 μM and incubated at 37 °C for 1 hour. The mixtures were collected in 1.5-ml centrifugation tubes and centrifuged at 3,000 rpm for 3 min. The supernatant was transferred to a new 96-well microtiter plate, and hemoglobin release was measured in a Tecan Infinite 200pro plate reader by absorption at 540 nm. 2% Triton X-100 was used as positive control and PBS was used as negative control.

Measurement of membrane potential

MRSA cells were grown in Mueller-Hinton broth to an OD_{600} of 0.5. Afterwards, the cells were washed with PBS and centrifuged at 5,000g for 5 min. Cells were incubated in 30 μM DiOC2(3) for 15 min for dye uptake in the dark. Subsequently, cells were transferred to a 96-well black wall plate and measured 10 min for baseline determination at excitation wavelength 488 nm, emission wavelength 530 nm for green and excitation wavelength 488 nm, emission wavelength 630 nm for red fluorescence. Cells were treated with different concentration of compound and measured for another 30 min. Carbonyl cyanide m-chlorophenyl hydrazine (CCCP) was employed as positive control, 12.5 μM of moxifloxacin and DMSO served as negative controls. Ratios of red and green fluorescence were calculated to quantify membrane potential.

Resistant mutant isolation

A MRSA culture was adjusted to different OD_{600nm} of 0.2, 0.4, 0.6, 1.0 and 1.2. 10 μL of each cell suspension was used to inoculate a 12-well microtiter plate containing different concentrations of testing compound including 2- and 4-fold MIC in 1 ml of MH agar in each well. The plate was incubated at 37 °C for 72 hours and three colonies were isolated from the

well containing compound **1** at 4-MIC named M3.0, M3.1, and M3.2 respectively. Subsequently, the MIC for these three colonies was determined as described above.

Propidium iodide internalization assay.

The propidium iodide (PI) internalization assay was performed as previously described.[22] Briefly, pre-cultures of MRSA parental strain and spontaneous resistant mutants in Mueller-Hinton broth were washed and diluted to OD_{600nm} = 0.4–0.5. The cell suspension was incubated with 7.5 μg/mL PI for 10 min at 37 °C. Afterwards, the suspension was transferred to a black walled 96-well plate and certain concentrations of testing compounds were added. Lysostophin was employed as a positive control while moxifloxacin and DMSO served as negative control, only PBS was used as background control. The baseline fluorescence at excitation wavelength 535 nm and emission wavelength 617 nm were established for 10 min before the addition of compounds. Subsequently, the fluorescence intensity of the PI dye was measured for another 2 h by Tecan Infinite-2000 plate reader every 5 min.

LC-MS assay

MRSA and spontaneous resistant mutants were pre-cultured to an OD_{600nm} of 0.5. The cells were then treated with compound at 200 μM concentration and incubated at 37 °C for 4 hours. Then, the culture was centrifuged at 5,000 rpm for 10 min and the supernatant was harvested. An external standard method was established for quantifying the content of compound using LC-MS.

ASSOCIATED CONTENT

Supporting Information

AUTHOR'S INFORMATION

Lin Wang E-mail: liwan103@hhu.de

Kristin Schwechel E-mail: Kristin.Schwechel@hhu.de

Tobias Heinen E-mail: heinent@uni-duesseldorf.de

Lasse van Geelen E-mail: Lasse.Geelen@hhu.de

Christopher Janiak E-mail: Janiak@hhu.de

Zhen Liu E-mail: zhenferizi0@sina.com

Rainer Kalscheuer E-mail: rainer.kalscheuer@hhu.de

Funding

This work was financially supported by the China Scholarship Council, the Ministry of Education of China, for a doctoral scholarship awarded to L.W. The Rigaku X-ray diffractometer was funded by the Deutsche Forschungsgemeinschaft (DFG, German Research Foundation) through project number 440366605.

DECLARATION OF COMPETING INTEREST

The authors declare that there is no conflict of interests for the publication of this artical.

Reference

[1] Chambers HFDeleo, F. R. Waves of resistance: *Staphylococcus aureus* in the antibiotic era. Nat Rev Microbiol. 2009; 7, 629641.

[2] Grundmann. H, Aires-de-Sousa. M, Boyce. J, Tiemersma. E. Emergence and resurgence of meticillin-resistant Staphylococcus aureus as a public-health threat. Lancet. 2006; 368:874–85.

[3] Review on Antimicrobial Resistance (London). Grande-Bretagne. Antimicrobial resistance: tackling a crisis for the health and wealth of nations: Review on Antimicrobial Resistance; 2014.

[4] Cosgrove S. E, Carmeli. Y. The impact of antimicrobial resistance on health and economic

outcomes. Clin Infect Dis. 2003; 36: 1433–1437.

[5] World Health Organization - WHO. *Antibacterial agents in clinical development: an analysis of the antibacterial clinical development pipeline, including tuberculosis*.2017

[6] Theuretzbacher, U. Resistance drives antibacterial drug development. *Curr Opin Pharmacol*; 2011, 11, 433–438.

[7] An Z, editor. Handbook of industrial mycology. CRC Press; Aug, 30, 2004.

[8] Kock J.L.F, Strauss, T, Pohl C.H, Smith D.P., Botes P.J, Pretorius E.E, Tepeny T, Sebolai O, Botha A, Nigam S. Bioprospecting for novel oxylipins in fungi: the presence of 3-hydroxy oxylipins in Pilobolus. Antonie van Leeuwenhoek, 2001; 1, 93-99.

[9] Bode H. B, Bethe B, Höfs, R, Zeeck A. Big effects from small changes: possible ways to explore nature's chemical diversity. *ChemBioChem*. 2002; 7, 619–627.

[10] Romano S, Jackson S. A, Patry S, Dobson A D. Extending the "one strain many compounds"(OSMAC) principle to marine microorganisms. Marine drugs. 2018; 17, 244.

[11] Lee J.C, Yang X, Schwartz M, Strobel G, Clardy J. The relationship between an endangered North American tree and an endophytic fungus. *Chem. Biol*. 1995; 2, 721-727.

[12] CLSI. Methods for dilution antimicrobial susceptibility tests for bacteria that grow aerobically. CLSI standard M07 11th ed. Wayne, PA: Clinical and Laboratory Standards Institute; 2018.

[13] Rosenberg M, Azevedo N.F, Ivask, A. Propidium iodide staining underestimates viability of adherent bacterial cells. *Sci Rep*. 20199; 9, 6483.

[14] Kjer J, Debbab A, Aly AH, Proksch P. Methods for isolation of marine-derived endophytic fungi and their bioactive secondary products. *Nat Protoc*. 2010; 5, 479–490.

[15] Elnaggar M.S, Ebrahim W, Mándi A, Kurtán T, Müller W.E, Kalscheuer R, Singab A, Lin W, Liu Z, Proksch P. Hydroquinone derivatives from the marine-derived fungus *Gliomastix sp*. *RSC advances*. 2017; 49, 30640-30649.

[16] Hudson, C. S, Yanovsky E. Indirect measurements of rotatory of some alpha and beta forms of the sugars by means solubility experiments. *J. Am. Chem. Soc.* 1917; 39, 1013-1038.

[17] Gao Y, Wang L, Kalscheuer R, Liu Z, Proksch P. Antifungal polyketide derivatives from the endophytic fungus *aplosporella javeedii*. *Bioorg Med Chem*. 2020; 28, 115456.

[18] Jonasson E, Matuschek E, Kahlmeter G. The EUCAST rapid disc diffusion method for antimicrobial susceptibility testing directly from positive blood culture bottles. *J. Antimicrob. Chemother*. 2020; 4, 968-978.

[19] EUCAST. Antimicrobial susceptibility testing EUCAST disk diffusion method. Version 6.0, 2017.

[20] Rehberg N, Sommer G A, Drießen D, Kruppa M, Adeniyi E. T, Chen S, Wang L, Wolf K, Tasch B. O. A, Ioerger T. R, Zhu K, Müller T. J. J, Kalscheuer R. Nature-inspired (di) azine-bridged bisindole alkaloids with potent antibacterial in vitro and in vivo efficacy against methicillin-resistant *Staphylococcus aureus*. *J. Med. Chem*. 2020; 21, 12623-12641.

[21] Meier D, Hernández M.V, van Geelen L, Muharini R, Proksch P, Bandow J.E, Kalscheuer R.The plant-derived chalcone Xanthoangelol targets the membrane of Gram-positive bacteria. *Bioorg. Med. Chem*. 2019; 23, 115151.

[22] Hu Y, Amin M. N, Padhee S, Wang R. E, Qiao Q, Bai G, Li Y, Mathew A, Cao C, Cai J. Lipidated peptidomimetics with improved antimicrobial activity. *ACS Med. Chem. Lett*. 2012; 3, 683-686.

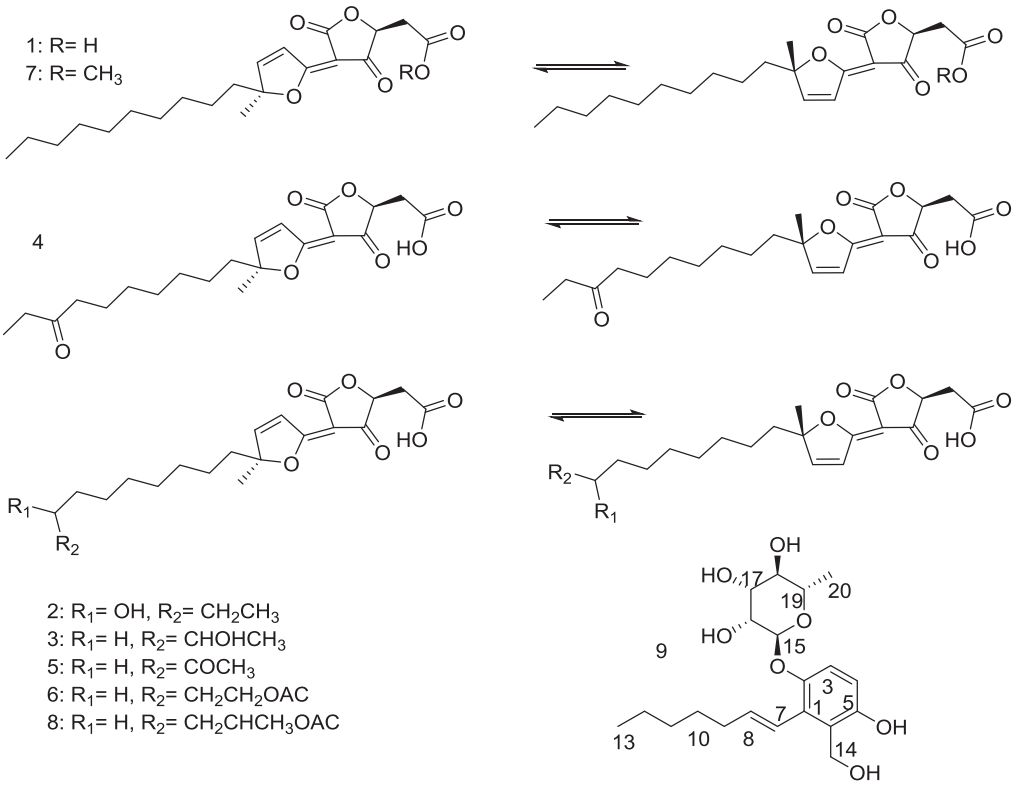

Figure 1: Structure of compounds **1-9**

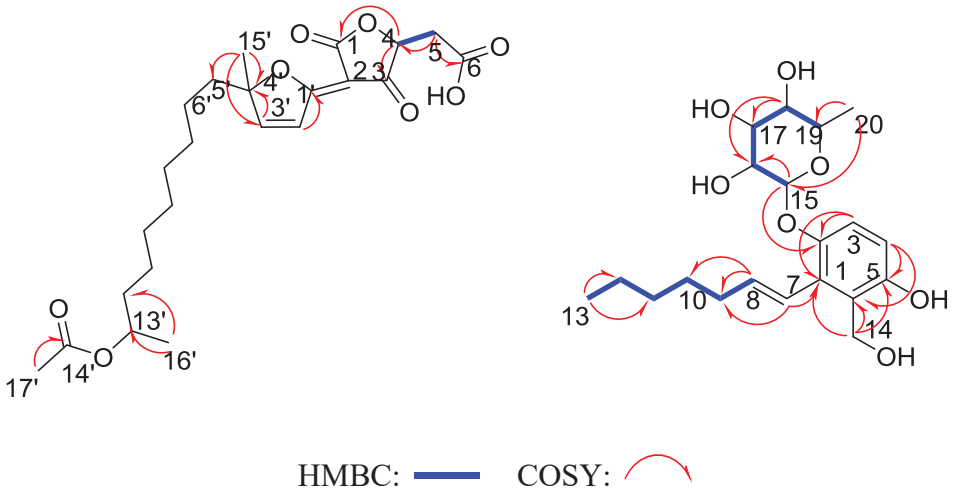

Figure 2: Key correlations of new compounds **8** and **9**

Table 1: ^{1}H and ^{13}C NMR data for **8** and **9** (600, 125 MHz, TMS, δ in ppm, J in Hz).

Compound **8** ($CDCl_3$)			Compound **9** ($MeOH\text{-}d_4$)		
Position	δ_C	δ_H (mult, J in Hz)	Position	δ_C	δ_H (mult, J in Hz)
1	171.9		1	129.2	
2			2	150.4	
4	195.8		3	115.7	6.91, d, (8.59)
4	78.4	4.87, m	4	116.2	6.71 (d, (10.07)
5	35.6	2.83	5	150	
6	172.3		6	128.4	
1’	179.4		7	124.5	6.51 (dt)
	180		8	138.3	6.25 (dt)
2’	123.5	7.55, d (6.82)	9	34.8	2.26 (m)
	123.6	7.50, d (5.61)	10	29.8	1.51
3’	160.4	7.45, d (5.61)	11	32.6	1.39
	160.5	7.41, dd (1.22, 1.25)	12	23.6	1.36
4’	101.9		13	14.3	0.94
	102.5		14	57.5	4.67
5’	37.9	2.02, s	15	100.8	5.27 (d, (1.80)
		1.90, td	16	71.4	4.08, dd (1.96, 1.84)
6’	23.8	1.23, m	17	72.6	3.90, dd (4.40,5.10)
7’-11’	23-29	1.23, m	18	73.8	3.46, d (8.97)
12’	35.1	1.23, m	19	70.2	3.75, d (5.56,5.80)
13’	71.1	4.87, m	20	17.8	1.26, d (4.85)
14’	171.8				
15’	23.2	1.61, s			
16’	20	1.19, dt			
17’	21.3	2.04, s			

Table 2: Minimal inhibitory concentration of compounds **1-9**.

Strains	MIC (μM)								
	1	**2**	**3**	**4**	**5**	**6**	**7**	**8**	**9**
S. aureus ATCC 29213	12.5	n	n	n	n	n	12.5	n	n
S. aureus ATCC 700699	6.25	n	n	n	n	100	6.25	n	n
E. faecalis ATCC 29212	50	n	n	n	n	n	100	n	n
E. faecalis ATCC 51299	25	n	n	n	n	n	50	n	n
E. faecium ATCC 35667	25	n	n	n	n	100	50	n	n
E. faecium ATCC 700221	25	n	n	n	n	n	12.5	n	n
E. coli ATCC 25922	n	n	n	n	n	n	100	n	n
S. pneumonia ATCC 49619	n	n	n	n	n	n	n	n	n
Candida albicans	n	n	n	n	n	n	n	n	n
M. tuberculosis H37Rv	n	n	n	n	n	n	n	n	n

n, not active (MIC >100 μM).

Table 3: Selective therapeutic index of compounds **1** and **7**.

	IC_{50} (μM)		SI	
Human cell lines	1	7	1	7
HEK-293:	45.5	18.6	7.28	3
HUH-7:	>100	41.1	>10	6.6
THP-1:	42.0	7.8	6.72	1.3
CLS-54:	45.6	0.71	7.29	0.1
H-4:	>100	22.5	>10	3.6

$MICs_{90}$: 6.25 μM and 6.2 μM for compounds **1** and **7**, respectively;

SI= IC_{50}/MIC_{90}.

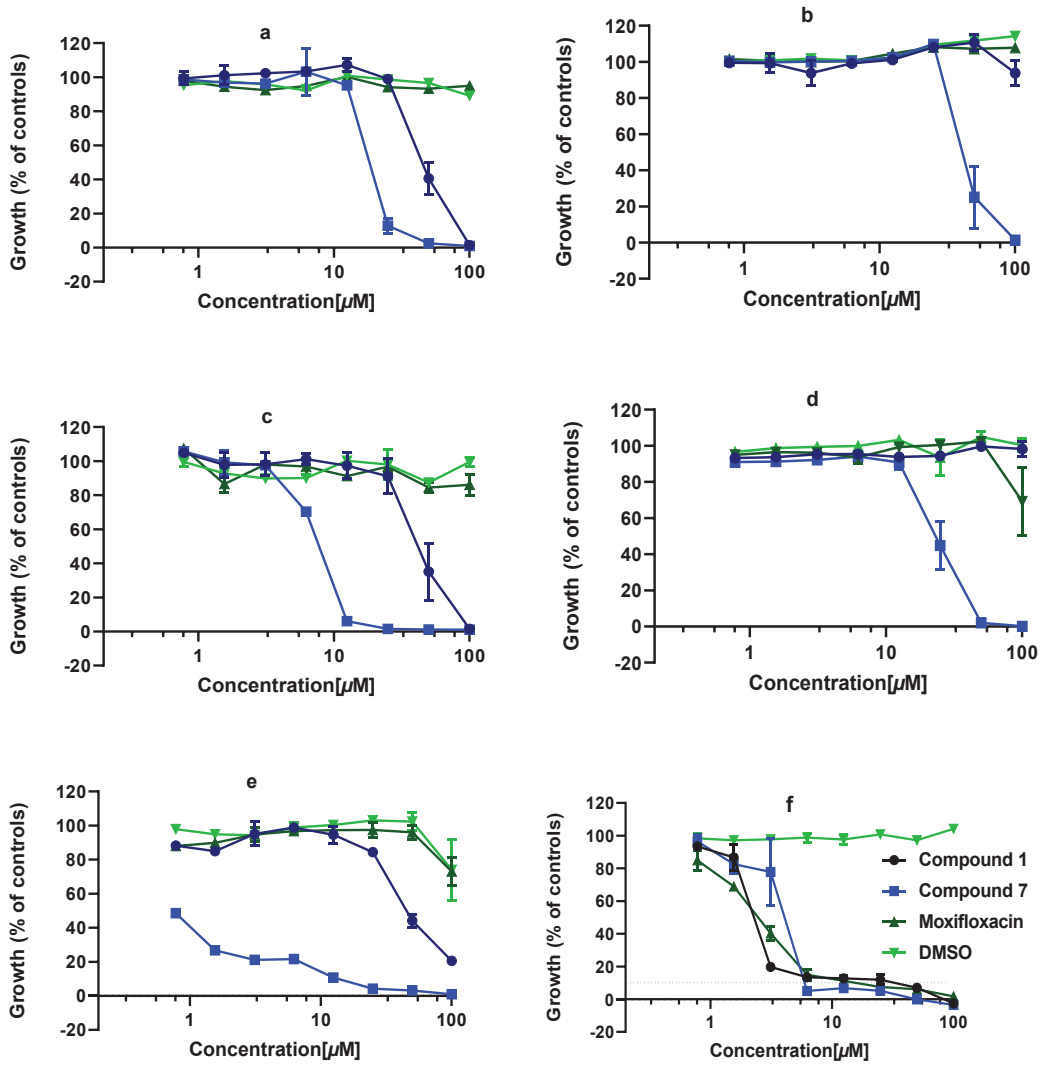

Figure 3: Cytotoxicity of compounds **1** and **7** against different human cell lines. Cell viability after treatment was determined by measuring metabolic activity employing resazurin reduction assay. a: HEK-293; b: HUH-7; c: THP-1; d: H-4; e: CLS-54. f: Antibacterial dose-response of compounds **1** and **7** against to MRSA cells.

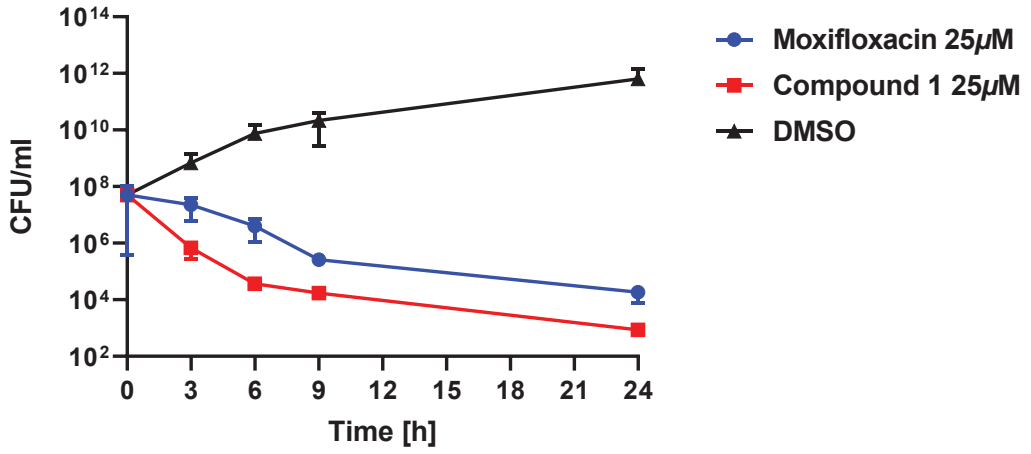

Figure 4: Time-kill kinetics of compound **1** (pestalotic acid A). Initial cell density was 10^8 CFU/mL. Cells were treated with compounds at the indicated concentrations for 24 hours. Aliquots taken at different time points after addition of compounds were serially diluted and plated on solid media for colony forming unit (CFU) counting.

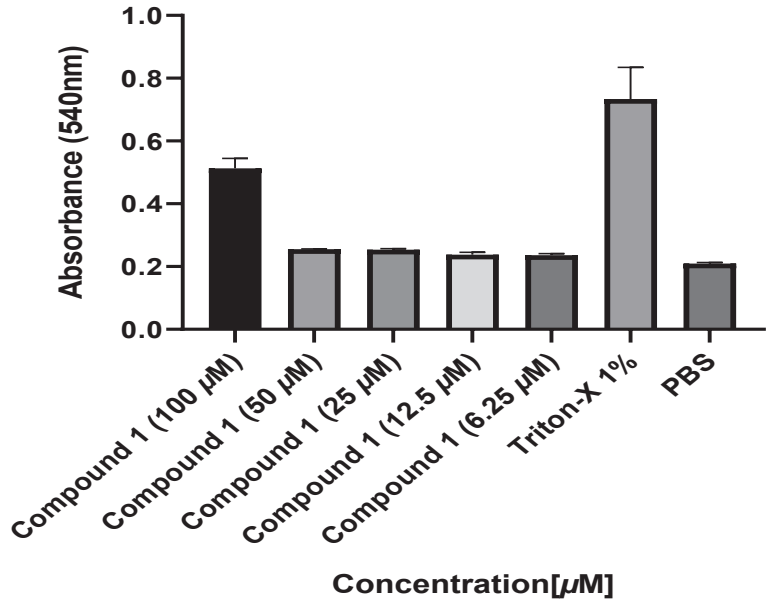

Figure 5: Hemolytic activity of compound **1** (pestalotic acid A). Defibrinated sheep red blood cells were treated at the indicated concentrations. Release of hemoglobin in cell-free supernatants was quantified by measuring absorbance at 540 nm. Triton-X (1%) and PBS were used as positive or negative control, respectively.

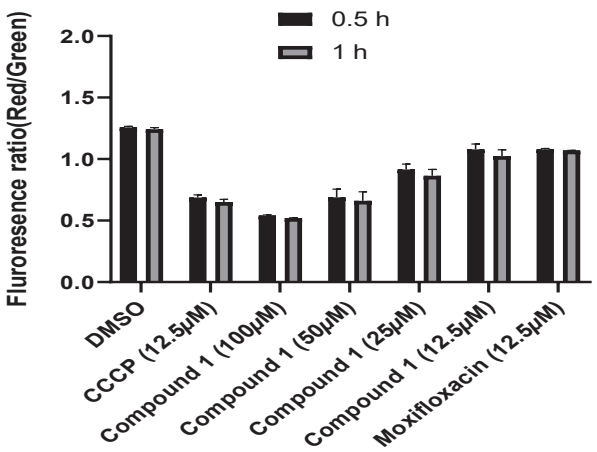

Figure 6: Influence of compound **1** (pestalotic acid A) on membrane potential in MRSA cells. Membrane potential after treatment at different concentrations was determined using DiOC2(3) by quantification of the ratio of red and green fluorescence. Reduced red fluorescence is indicative of membrane depolarization.

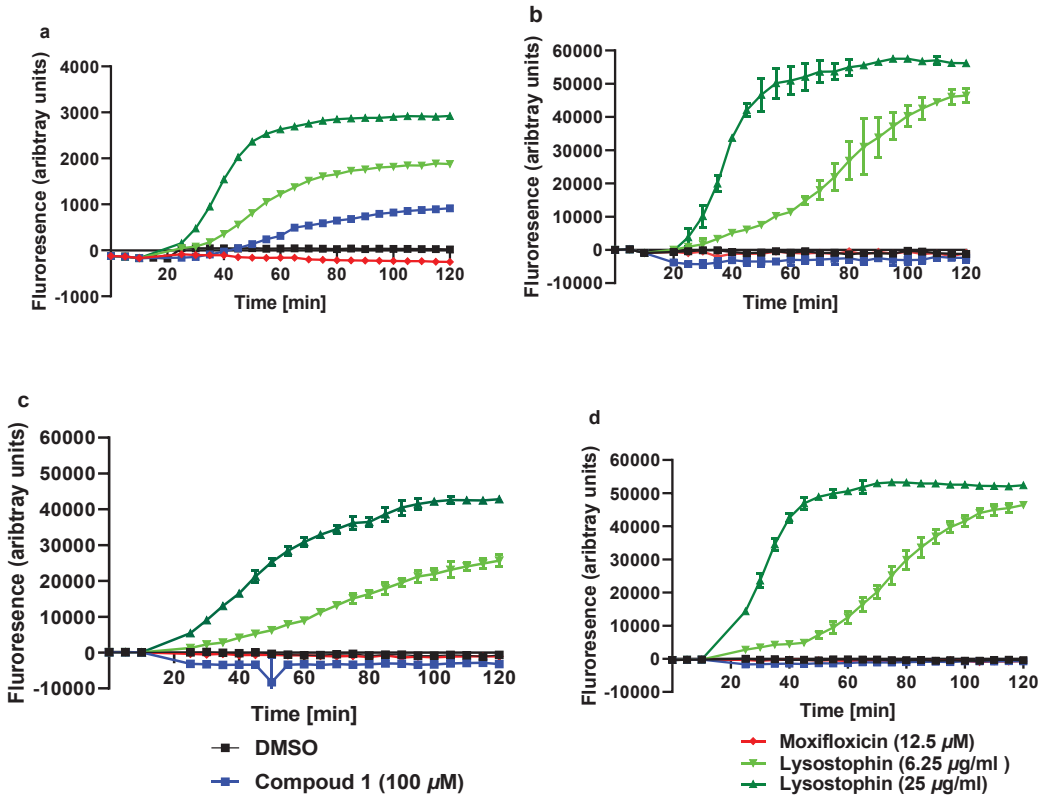

Figure 7: Propidium iodide internalization assay to asses impact of compound 1 (pestalotic acid A) on membrane integrity in wild-type and spontaneous resistant mutants cells of MRSA. a: Wild-type MRSA; b: Spontaneous resistant mutant 3.0; c: Spontaneous resistant mutant 3.1; d: Spontaneous resistant mutant 3.2.

Graphic Abstract

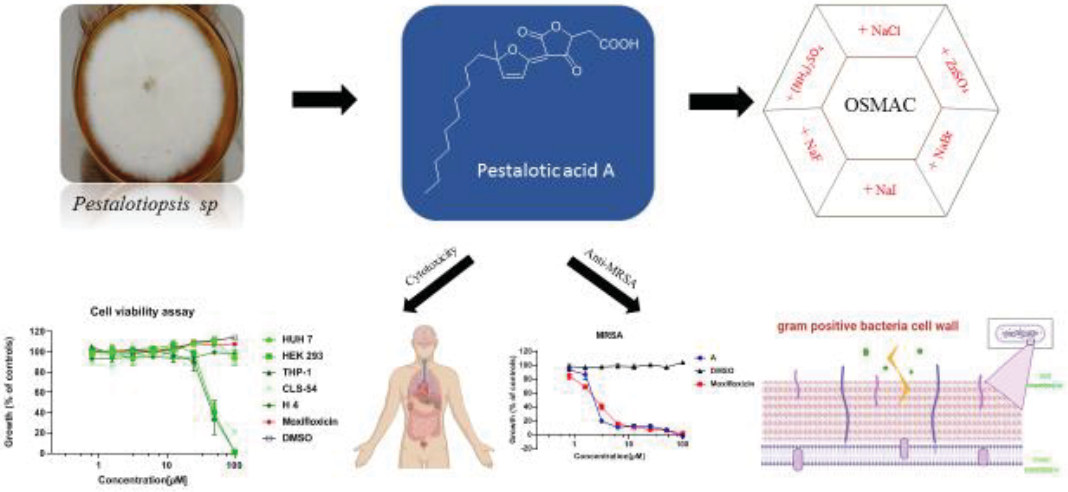

Supporting Information

Studies on the Antibacterial Activity of the Natural Product Pestalotic acid A against Methicillin-Resistant *Staphylococcus aureus*

Lin Wang,[a] Kristin Schwechel,[a] Tobias Heinen,[b] Lasse van Geelen,[a] Christoph Janiak,[b] Zhen Liu,[c] Rainer Kalscheuer[a, *]

[a] Institute of Pharmaceutical Biology and Biotechnology, Heinrich Heine University, Universitätsstr. 1, 40225 Düsseldorf, Germany.

[b] Institute of Inorganic and Structural Chemistry, Heinrich Heine University, Universitätsstr. 1, 40225 Düsseldorf, Germany.

[c] Key Laboratory of Study and Discovery of Small Targeted Molecules of Hunan Province, School of Medicine, Hunan Normal University, Changsha 410013, China.

[*]Corresponding author.

Rainer kalscheuer: E-mail rainer.kalscheuer@hhu.

CONTENT

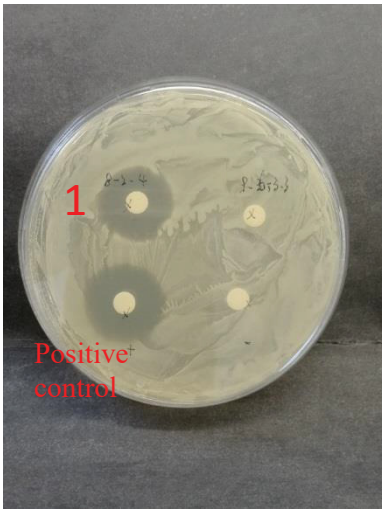

Figure S1: Disc Diffusion testing for compound **1**

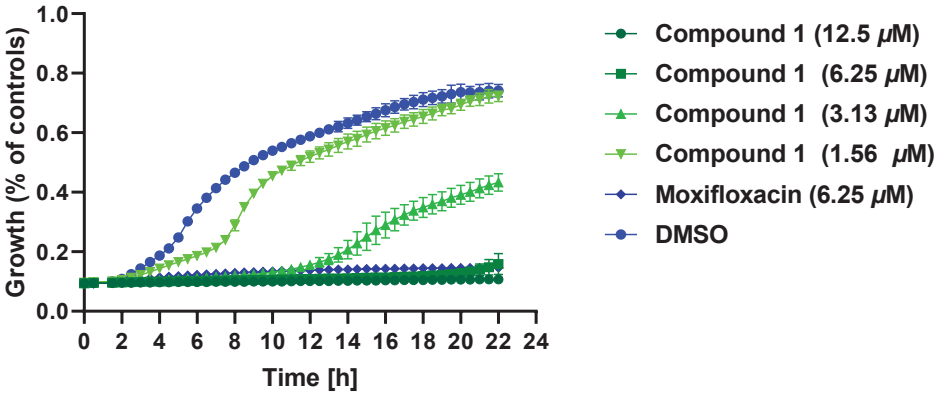

Figure S2: Growth kinetics of compound **1**

Table S1: Minimal inhibitory concentration of compound **1** treated with wild type and resistant mutants

Strains	MIC_{90} (μM)
Mu3.0	50
Mu3.1	50
Mu3.2	50
Sensitive type	6.25

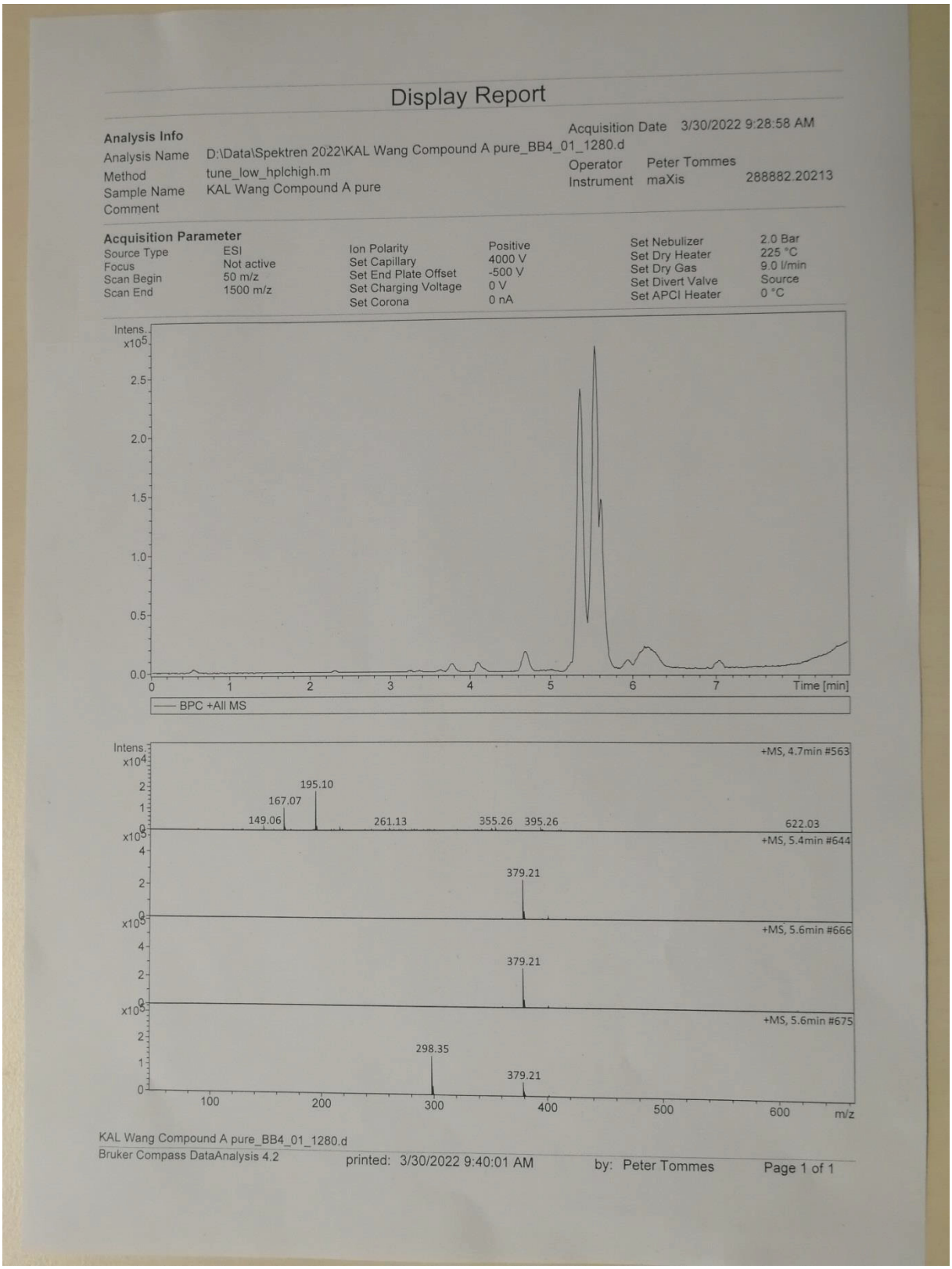

Figure S3: LC-MS of compound **1**

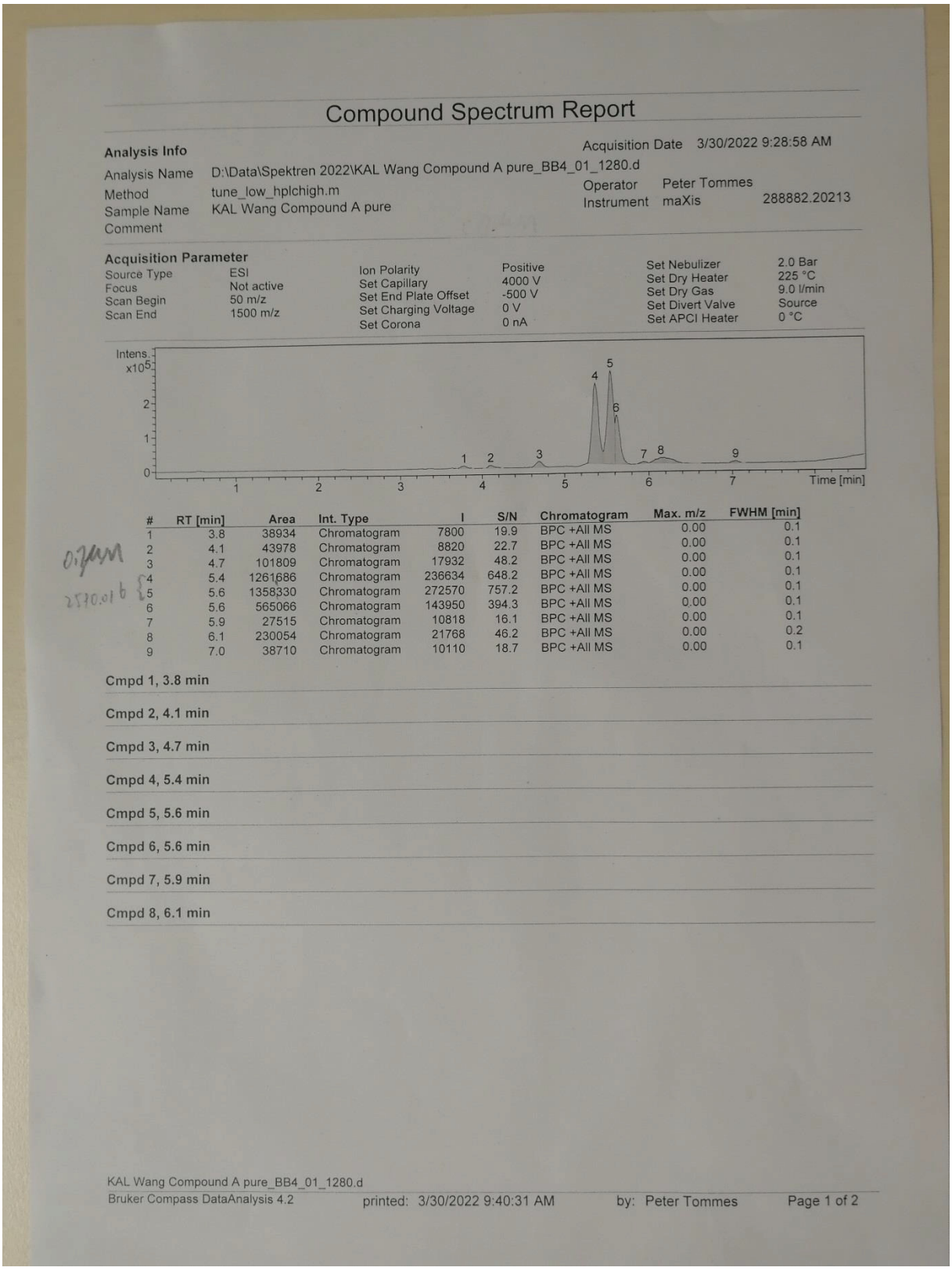

Compound Spectrum Report

Analysis Info

Analysis Name	D:\Data\Spektren 2022\KAL Wang Compound A pure_BB4_01_1280.d	Acquisition Date	3/30/2022 9:28:58 AM
Method	tune_low_hplchigh.m	Operator	Peter Tommes
Sample Name	KAL Wang Compound A pure	Instrument	maXis 288882.20213
Comment			

Acquisition Parameter

Source Type	ESI	Ion Polarity	Positive	Set Nebulizer	2.0 Bar
Focus	Not active	Set Capillary	4000 V	Set Dry Heater	225 °C
Scan Begin	50 m/z	Set End Plate Offset	-500 V	Set Dry Gas	9.0 l/min
Scan End	1500 m/z	Set Charging Voltage	0 V	Set Divert Valve	Source
		Set Corona	0 nA	Set APCI Heater	0 °C

#	RT [min]	Area	Int. Type	I	S/N	Chromatogram	Max. m/z	FWHM [min]
1	3.8	38934	Chromatogram	7800	19.9	BPC +All MS	0.00	0.1
2	4.1	43978	Chromatogram	8820	22.7	BPC +All MS	0.00	0.1
3	4.7	101809	Chromatogram	17932	48.2	BPC +All MS	0.00	0.1
4	5.4	1261686	Chromatogram	236634	648.2	BPC +All MS	0.00	0.1
5	5.6	1358330	Chromatogram	272570	757.2	BPC +All MS	0.00	0.1
6	5.6	565066	Chromatogram	143950	394.3	BPC +All MS	0.00	0.1
7	5.9	27515	Chromatogram	10818	16.1	BPC +All MS	0.00	0.1
8	6.1	230054	Chromatogram	21768	46.2	BPC +All MS	0.00	0.2
9	7.0	38710	Chromatogram	10110	18.7	BPC +All MS	0.00	0.1

Cmpd 1, 3.8 min

Cmpd 2, 4.1 min

Cmpd 3, 4.7 min

Cmpd 4, 5.4 min

Cmpd 5, 5.6 min

Cmpd 6, 5.6 min

Cmpd 7, 5.9 min

Cmpd 8, 6.1 min

KAL Wang Compound A pure_BB4_01_1280.d
Bruker Compass DataAnalysis 4.2 printed: 3/30/2022 9:40:31 AM by: Peter Tommes Page 1 of 2

Figure S4: LC-MS of compound **1** with integral area at 0.1 μM

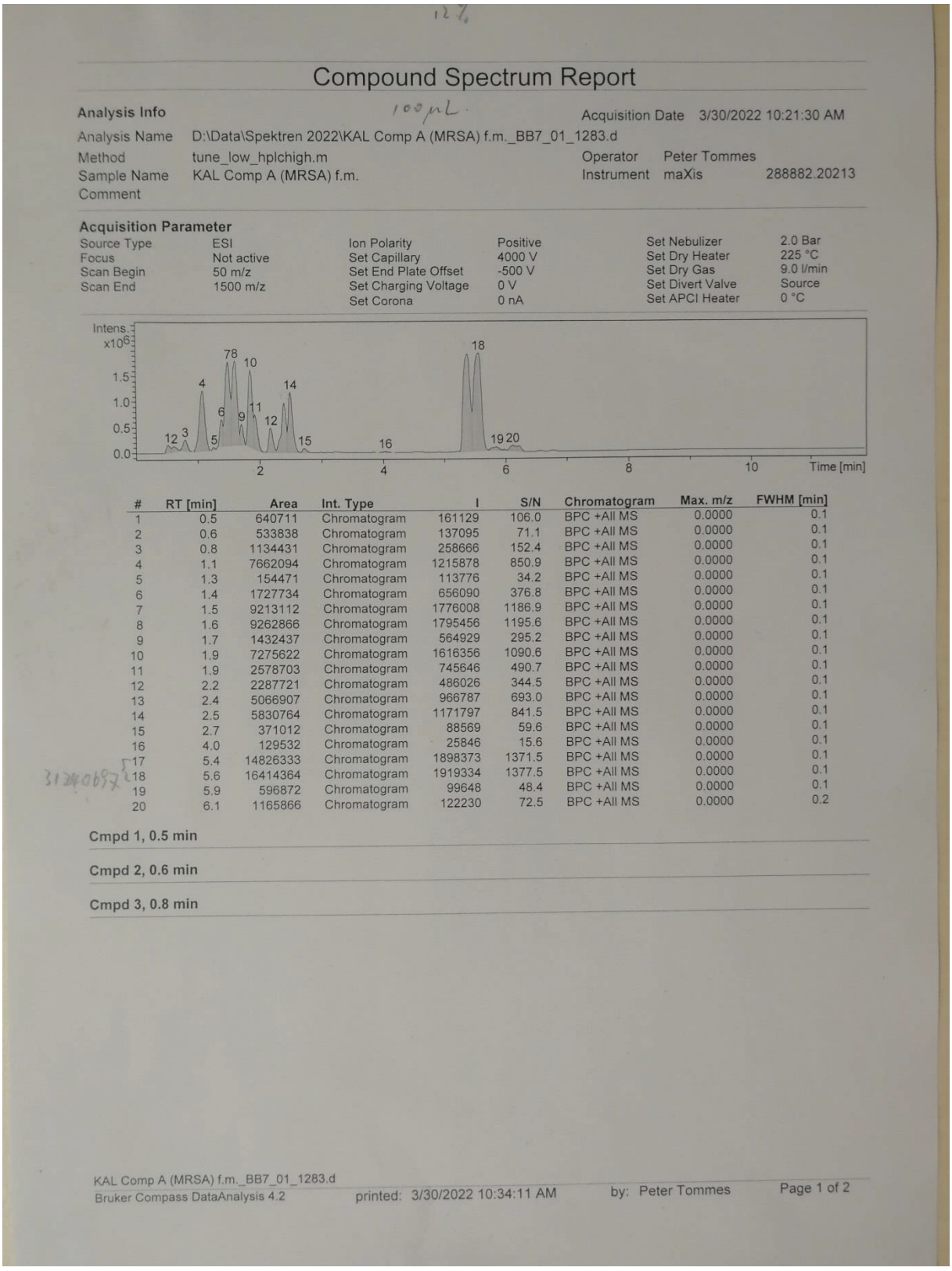

12%

Compound Spectrum Report

Analysis Info 100µL

Analysis Name	D:\Data\Spektren 2022\KAL Comp A (MRSA) f.m._BB7_01_1283.d	Acquisition Date	3/30/2022 10:21:30 AM
Method	tune_low_hplchigh.m	Operator	Peter Tommes
Sample Name	KAL Comp A (MRSA) f.m.	Instrument	maXis 288882.20213
Comment			

Acquisition Parameter

Source Type	ESI	Ion Polarity	Positive	Set Nebulizer	2.0 Bar
Focus	Not active	Set Capillary	4000 V	Set Dry Heater	225 °C
Scan Begin	50 m/z	Set End Plate Offset	-500 V	Set Dry Gas	9.0 l/min
Scan End	1500 m/z	Set Charging Voltage	0 V	Set Divert Valve	Source
		Set Corona	0 nA	Set APCI Heater	0 °C

#	RT [min]	Area	Int. Type	I	S/N	Chromatogram	Max. m/z	FWHM [min]
1	0.5	640711	Chromatogram	161129	106.0	BPC +All MS	0.0000	0.1
2	0.6	533838	Chromatogram	137095	71.1	BPC +All MS	0.0000	0.1
3	0.8	1134431	Chromatogram	258666	152.4	BPC +All MS	0.0000	0.1
4	1.1	7662094	Chromatogram	1215878	850.9	BPC +All MS	0.0000	0.1
5	1.3	154471	Chromatogram	113776	34.2	BPC +All MS	0.0000	0.1
6	1.4	1727734	Chromatogram	656090	376.8	BPC +All MS	0.0000	0.1
7	1.5	9213112	Chromatogram	1776008	1186.9	BPC +All MS	0.0000	0.1
8	1.6	9262866	Chromatogram	1795456	1195.6	BPC +All MS	0.0000	0.1
9	1.7	1432437	Chromatogram	564929	295.2	BPC +All MS	0.0000	0.1
10	1.9	7275622	Chromatogram	1616356	1090.6	BPC +All MS	0.0000	0.1
11	1.9	2578703	Chromatogram	745646	490.7	BPC +All MS	0.0000	0.1
12	2.2	2287721	Chromatogram	486026	344.5	BPC +All MS	0.0000	0.1
13	2.4	5066907	Chromatogram	966787	693.0	BPC +All MS	0.0000	0.1
14	2.5	5830764	Chromatogram	1171797	841.5	BPC +All MS	0.0000	0.1
15	2.7	371012	Chromatogram	88569	59.6	BPC +All MS	0.0000	0.1
16	4.0	129532	Chromatogram	25846	15.6	BPC +All MS	0.0000	0.1
17	5.4	14826333	Chromatogram	1898373	1371.5	BPC +All MS	0.0000	0.1
18	5.6	16414364	Chromatogram	1919334	1377.5	BPC +All MS	0.0000	0.1
19	5.9	596872	Chromatogram	99648	48.4	BPC +All MS	0.0000	0.1
20	6.1	1165866	Chromatogram	122230	72.5	BPC +All MS	0.0000	0.2

Cmpd 1, 0.5 min

Cmpd 2, 0.6 min

Cmpd 3, 0.8 min

Figure S5: LC-MS of compound **1** with integral area treated with MRSA cells

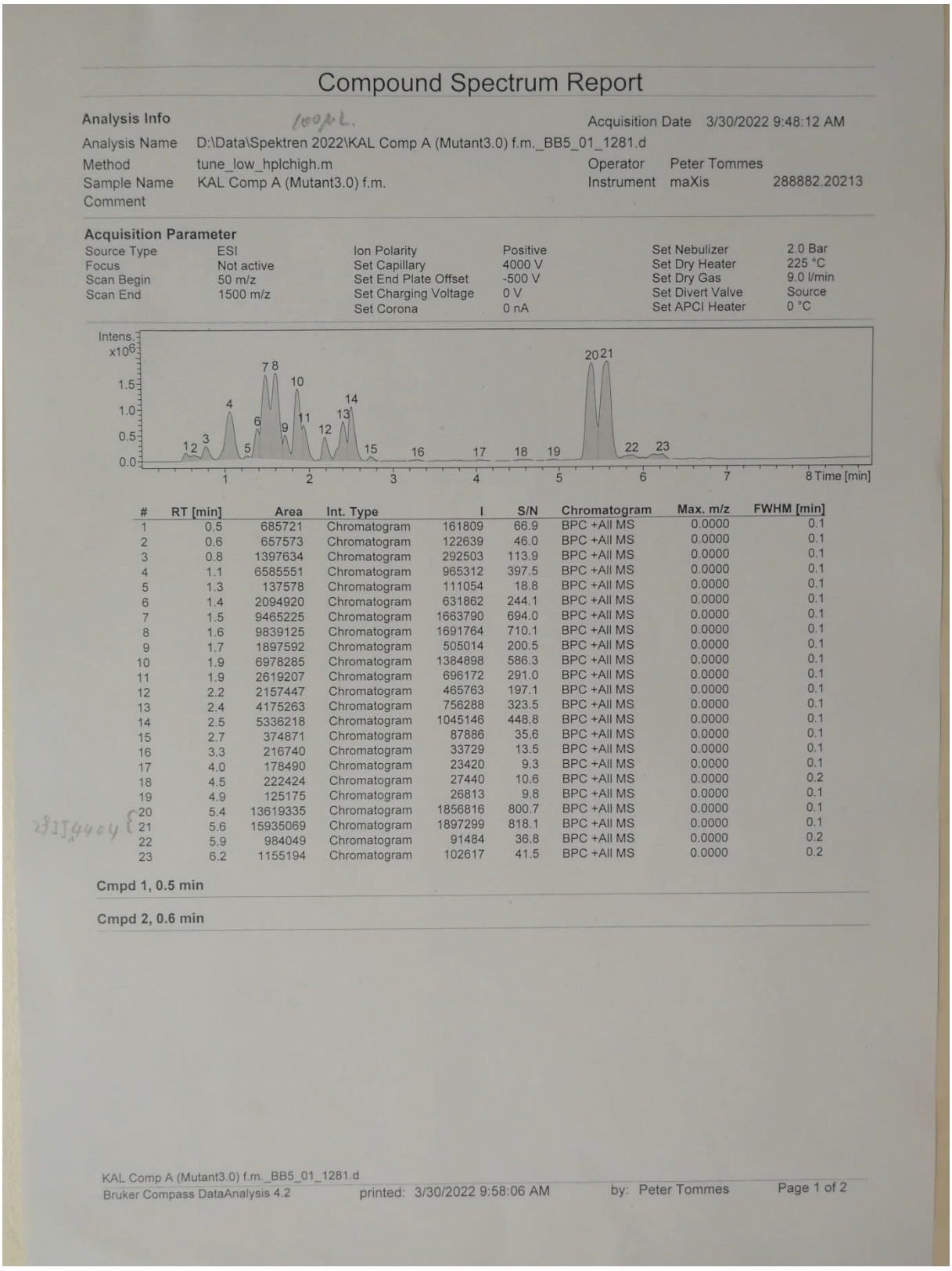

Compound Spectrum Report

Analysis Info 100pL. Acquisition Date 3/30/2022 9:48:12 AM

Analysis Name	D:\Data\Spektren 2022\KAL Comp A (Mutant3.0) f.m._BB5_01_1281.d		
Method	tune_low_hplchigh.m	Operator	Peter Tommes
Sample Name	KAL Comp A (Mutant3.0) f.m.	Instrument	maXis 288882.20213
Comment			

Acquisition Parameter

Source Type	ESI	Ion Polarity	Positive	Set Nebulizer	2.0 Bar
Focus	Not active	Set Capillary	4000 V	Set Dry Heater	225 °C
Scan Begin	50 m/z	Set End Plate Offset	-500 V	Set Dry Gas	9.0 l/min
Scan End	1500 m/z	Set Charging Voltage	0 V	Set Divert Valve	Source
		Set Corona	0 nA	Set APCI Heater	0 °C

#	RT [min]	Area	Int. Type	I	S/N	Chromatogram	Max. m/z	FWHM [min]
1	0.5	685721	Chromatogram	161809	66.9	BPC +All MS	0.0000	0.1
2	0.6	657573	Chromatogram	122639	46.0	BPC +All MS	0.0000	0.1
3	0.8	1397634	Chromatogram	292503	113.9	BPC +All MS	0.0000	0.1
4	1.1	6585551	Chromatogram	965312	397.5	BPC +All MS	0.0000	0.1
5	1.3	137578	Chromatogram	111054	18.8	BPC +All MS	0.0000	0.1
6	1.4	2094920	Chromatogram	631862	244.1	BPC +All MS	0.0000	0.1
7	1.5	9465225	Chromatogram	1663790	694.0	BPC +All MS	0.0000	0.1
8	1.6	9839125	Chromatogram	1691764	710.1	BPC +All MS	0.0000	0.1
9	1.7	1897592	Chromatogram	505014	200.5	BPC +All MS	0.0000	0.1
10	1.9	6978285	Chromatogram	1384898	586.3	BPC +All MS	0.0000	0.1
11	1.9	2619207	Chromatogram	696172	291.0	BPC +All MS	0.0000	0.1
12	2.2	2157447	Chromatogram	465763	197.1	BPC +All MS	0.0000	0.1
13	2.4	4175263	Chromatogram	756288	323.5	BPC +All MS	0.0000	0.1
14	2.5	5336218	Chromatogram	1045146	448.8	BPC +All MS	0.0000	0.1
15	2.7	374871	Chromatogram	87886	35.6	BPC +All MS	0.0000	0.1
16	3.3	216740	Chromatogram	33729	13.5	BPC +All MS	0.0000	0.1
17	4.0	178490	Chromatogram	23420	9.3	BPC +All MS	0.0000	0.1
18	4.5	222424	Chromatogram	27440	10.6	BPC +All MS	0.0000	0.2
19	4.9	125175	Chromatogram	26813	9.8	BPC +All MS	0.0000	0.1
20	5.4	13619335	Chromatogram	1856816	800.7	BPC +All MS	0.0000	0.1
21	5.6	15935069	Chromatogram	1897299	818.1	BPC +All MS	0.0000	0.1
22	5.9	984049	Chromatogram	91484	36.8	BPC +All MS	0.0000	0.2
23	6.2	1155194	Chromatogram	102617	41.5	BPC +All MS	0.0000	0.2

Cmpd 1, 0.5 min

Cmpd 2, 0.6 min

Figure S6: LC-MS of compound **1** with integral area treated with resistant mutant 3.0

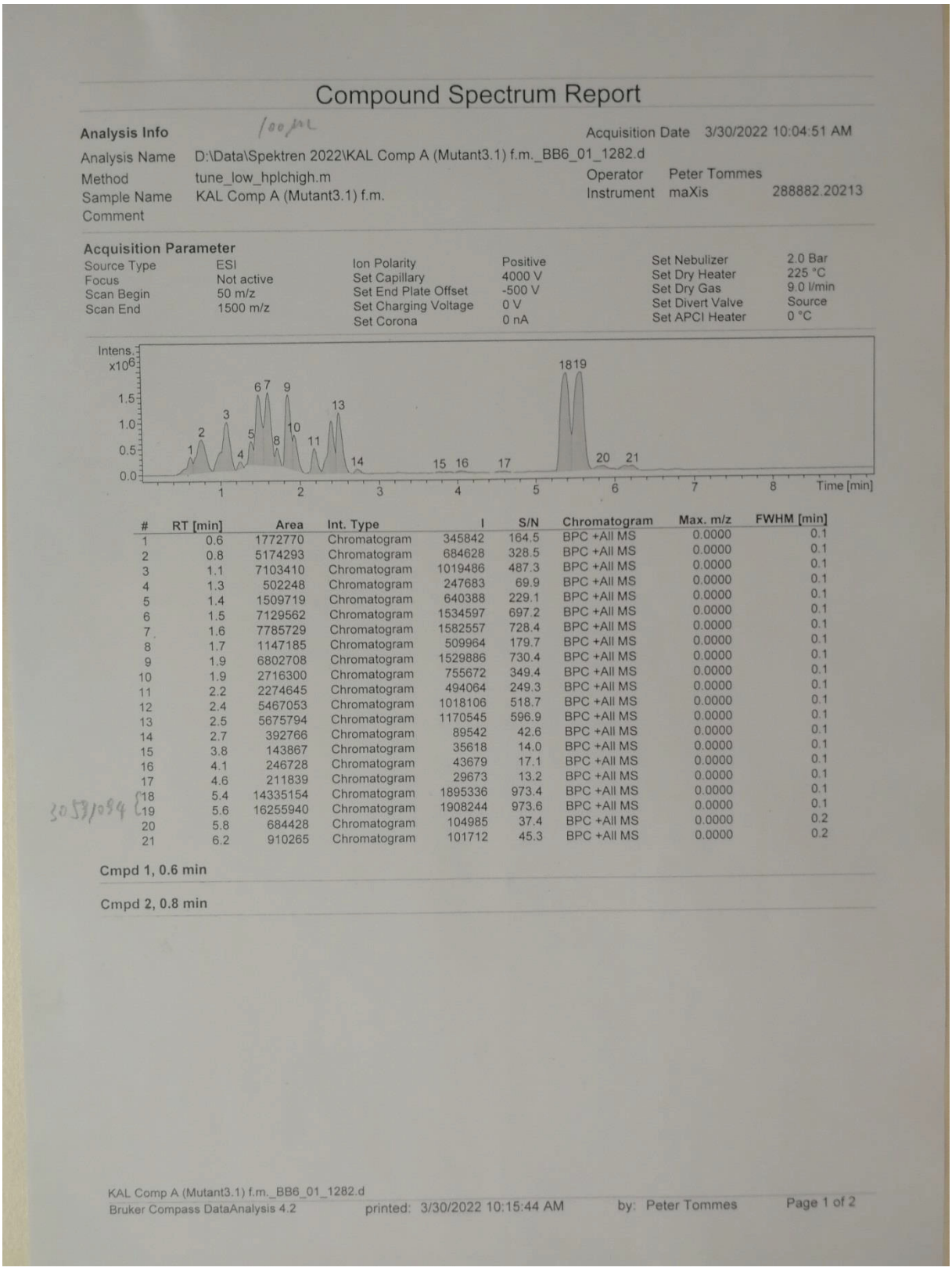

Compound Spectrum Report

Analysis Info 100µL

Acquisition Date 3/30/2022 10:04:51 AM

Analysis Name	D:\Data\Spektren 2022\KAL Comp A (Mutant3.1) f.m._BB6_01_1282.d		
Method	tune_low_hplchigh.m	Operator	Peter Tommes
Sample Name	KAL Comp A (Mutant3.1) f.m.	Instrument	maXis 288882.20213
Comment			

Acquisition Parameter

Source Type	ESI	Ion Polarity	Positive	Set Nebulizer	2.0 Bar
Focus	Not active	Set Capillary	4000 V	Set Dry Heater	225 °C
Scan Begin	50 m/z	Set End Plate Offset	-500 V	Set Dry Gas	9.0 l/min
Scan End	1500 m/z	Set Charging Voltage	0 V	Set Divert Valve	Source
		Set Corona	0 nA	Set APCI Heater	0 °C

#	RT [min]	Area	Int. Type	I	S/N	Chromatogram	Max. m/z	FWHM [min]
1	0.6	1772770	Chromatogram	345842	164.5	BPC +All MS	0.0000	0.1
2	0.8	5174293	Chromatogram	684628	328.5	BPC +All MS	0.0000	0.1
3	1.1	7103410	Chromatogram	1019486	487.3	BPC +All MS	0.0000	0.1
4	1.3	502248	Chromatogram	247683	69.9	BPC +All MS	0.0000	0.1
5	1.4	1509719	Chromatogram	640388	229.1	BPC +All MS	0.0000	0.1
6	1.5	7129562	Chromatogram	1534597	697.2	BPC +All MS	0.0000	0.1
7	1.6	7785729	Chromatogram	1582557	728.4	BPC +All MS	0.0000	0.1
8	1.7	1147185	Chromatogram	509964	179.7	BPC +All MS	0.0000	0.1
9	1.9	6802708	Chromatogram	1529886	730.4	BPC +All MS	0.0000	0.1
10	1.9	2716300	Chromatogram	755672	349.4	BPC +All MS	0.0000	0.1
11	2.2	2274645	Chromatogram	494064	249.3	BPC +All MS	0.0000	0.1
12	2.4	5467053	Chromatogram	1018106	518.7	BPC +All MS	0.0000	0.1
13	2.5	5675794	Chromatogram	1170545	596.9	BPC +All MS	0.0000	0.1
14	2.7	392766	Chromatogram	89542	42.6	BPC +All MS	0.0000	0.1
15	3.8	143867	Chromatogram	35618	14.0	BPC +All MS	0.0000	0.1
16	4.1	246728	Chromatogram	43679	17.1	BPC +All MS	0.0000	0.1
17	4.6	211839	Chromatogram	29673	13.2	BPC +All MS	0.0000	0.1
18	5.4	14335154	Chromatogram	1895336	973.4	BPC +All MS	0.0000	0.1
19	5.6	16255940	Chromatogram	1908244	973.6	BPC +All MS	0.0000	0.1
20	5.8	684428	Chromatogram	104985	37.4	BPC +All MS	0.0000	0.2
21	6.2	910265	Chromatogram	101712	45.3	BPC +All MS	0.0000	0.2

30531084

Cmpd 1, 0.6 min

Cmpd 2, 0.8 min

Figure S7: LC-MS of compound **1** with integral area treated with resistant mutant 3.1

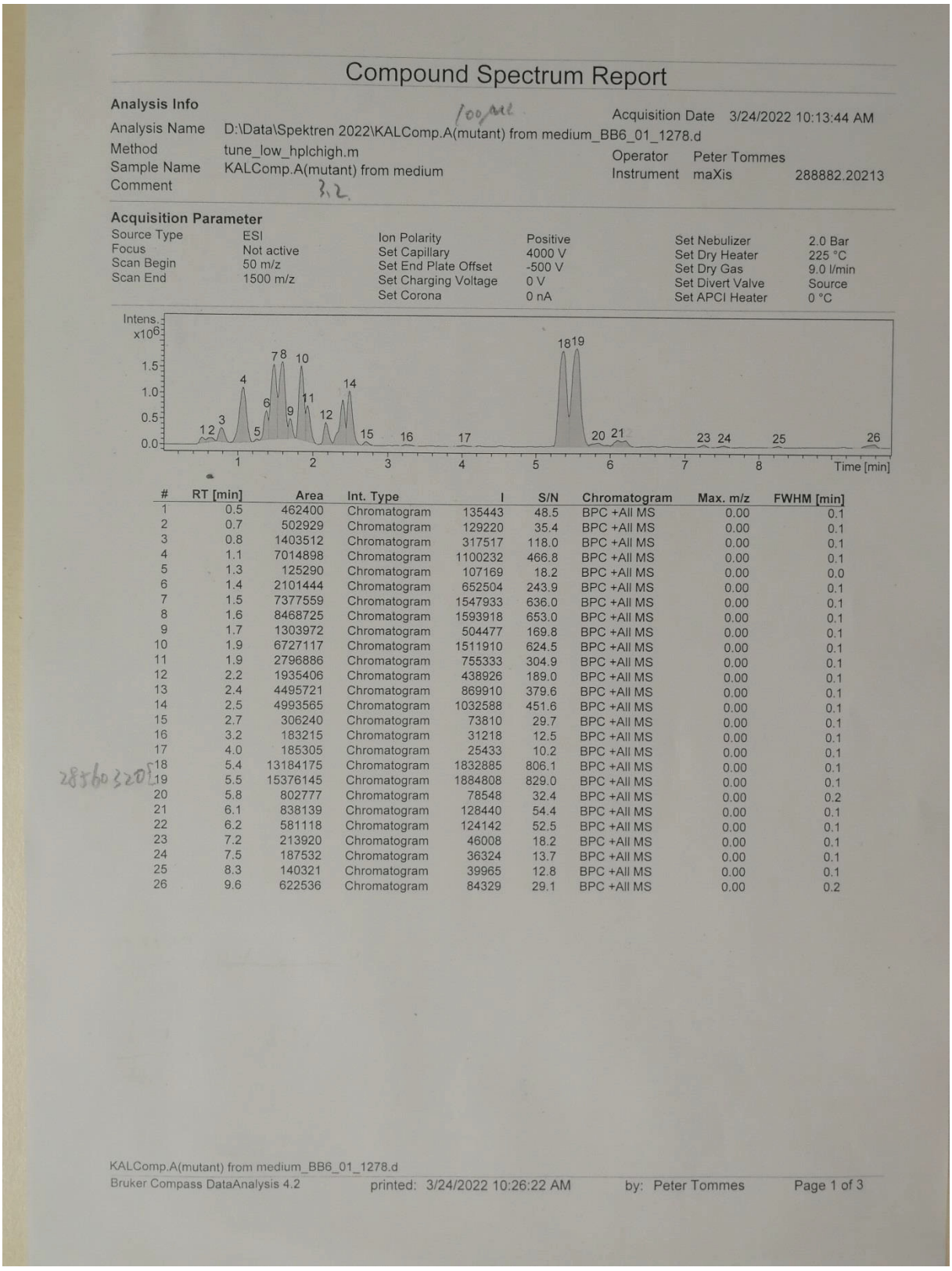

Compound Spectrum Report

Analysis Info

Analysis Name	D:\Data\Spektren 2022\KALComp.A(mutant) from medium_BB6_01_1278.d	Acquisition Date	3/24/2022 10:13:44 AM
Method	tune_low_hplchigh.m	Operator	Peter Tommes
Sample Name	KALComp.A(mutant) from medium	Instrument	maXis 288882.20213
Comment			

Acquisition Parameter

Source Type	ESI	Ion Polarity	Positive	Set Nebulizer	2.0 Bar
Focus	Not active	Set Capillary	4000 V	Set Dry Heater	225 °C
Scan Begin	50 m/z	Set End Plate Offset	-500 V	Set Dry Gas	9.0 l/min
Scan End	1500 m/z	Set Charging Voltage	0 V	Set Divert Valve	Source
		Set Corona	0 nA	Set APCI Heater	0 °C

#	RT [min]	Area	Int. Type	I	S/N	Chromatogram	Max. m/z	FWHM [min]
1	0.5	462400	Chromatogram	135443	48.5	BPC +All MS	0.00	0.1
2	0.7	502929	Chromatogram	129220	35.4	BPC +All MS	0.00	0.1
3	0.8	1403512	Chromatogram	317517	118.0	BPC +All MS	0.00	0.1
4	1.1	7014898	Chromatogram	1100232	466.8	BPC +All MS	0.00	0.1
5	1.3	125290	Chromatogram	107169	18.2	BPC +All MS	0.00	0.0
6	1.4	2101444	Chromatogram	652504	243.9	BPC +All MS	0.00	0.1
7	1.5	7377559	Chromatogram	1547933	636.0	BPC +All MS	0.00	0.1
8	1.6	8468725	Chromatogram	1593918	653.0	BPC +All MS	0.00	0.1
9	1.7	1303972	Chromatogram	504477	169.8	BPC +All MS	0.00	0.1
10	1.9	6727117	Chromatogram	1511910	624.5	BPC +All MS	0.00	0.1
11	1.9	2796886	Chromatogram	755333	304.9	BPC +All MS	0.00	0.1
12	2.2	1935406	Chromatogram	438926	189.0	BPC +All MS	0.00	0.1
13	2.4	4495721	Chromatogram	869910	379.6	BPC +All MS	0.00	0.1
14	2.5	4993565	Chromatogram	1032588	451.6	BPC +All MS	0.00	0.1
15	2.7	306240	Chromatogram	73810	29.7	BPC +All MS	0.00	0.1
16	3.2	183215	Chromatogram	31218	12.5	BPC +All MS	0.00	0.1
17	4.0	185305	Chromatogram	25433	10.2	BPC +All MS	0.00	0.1
18	5.4	13184175	Chromatogram	1832885	806.1	BPC +All MS	0.00	0.1
19	5.5	15376145	Chromatogram	1884808	829.0	BPC +All MS	0.00	0.1
20	5.8	802777	Chromatogram	78548	32.4	BPC +All MS	0.00	0.2
21	6.1	838139	Chromatogram	128440	54.4	BPC +All MS	0.00	0.1
22	6.2	581118	Chromatogram	124142	52.5	BPC +All MS	0.00	0.1
23	7.2	213920	Chromatogram	46008	18.2	BPC +All MS	0.00	0.1
24	7.5	187532	Chromatogram	36324	13.7	BPC +All MS	0.00	0.1
25	8.3	140321	Chromatogram	39965	12.8	BPC +All MS	0.00	0.1
26	9.6	622536	Chromatogram	84329	29.1	BPC +All MS	0.00	0.2

Figure S8: LC-MS of compound **1** with integral area treated with resistant mutant 3.2

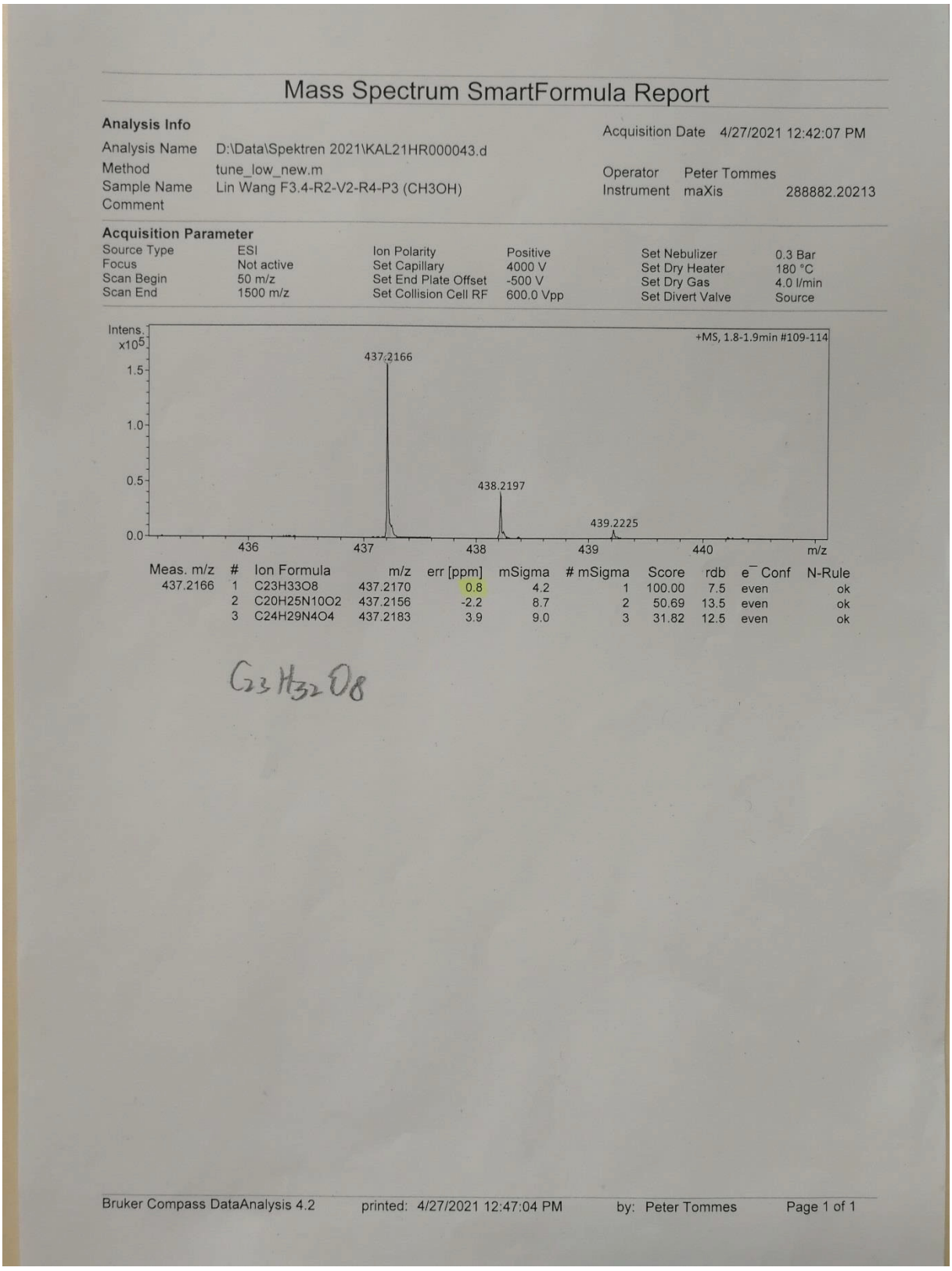

Mass Spectrum SmartFormula Report

Analysis Info

Acquisition Date 4/27/2021 12:42:07 PM

Analysis Name	D:\Data\Spektren 2021\KAL21HR000043.d		
Method	tune_low_new.m	Operator	Peter Tommes
Sample Name	Lin Wang F3.4-R2-V2-R4-P3 (CH3OH)	Instrument	maXis 288882.20213
Comment			

Acquisition Parameter

Source Type	ESI	Ion Polarity	Positive	Set Nebulizer	0.3 Bar
Focus	Not active	Set Capillary	4000 V	Set Dry Heater	180 °C
Scan Begin	50 m/z	Set End Plate Offset	-500 V	Set Dry Gas	4.0 l/min
Scan End	1500 m/z	Set Collision Cell RF	600.0 Vpp	Set Divert Valve	Source

Meas. m/z	#	Ion Formula	m/z	err [ppm]	mSigma	# mSigma	Score	rdb	e⁻ Conf	N-Rule
437.2166	1	C23H33O8	437.2170	0.8	4.2	1	100.00	7.5	even	ok
	2	C20H25N10O2	437.2156	-2.2	8.7	2	50.69	13.5	even	ok
	3	C24H29N4O4	437.2183	3.9	9.0	3	31.82	12.5	even	ok

$C_{23}H_{32}O_8$

Bruker Compass DataAnalysis 4.2 printed: 4/27/2021 12:47:04 PM by: Peter Tommes Page 1 of 1

Figure S9: HREISMS of compound **8**

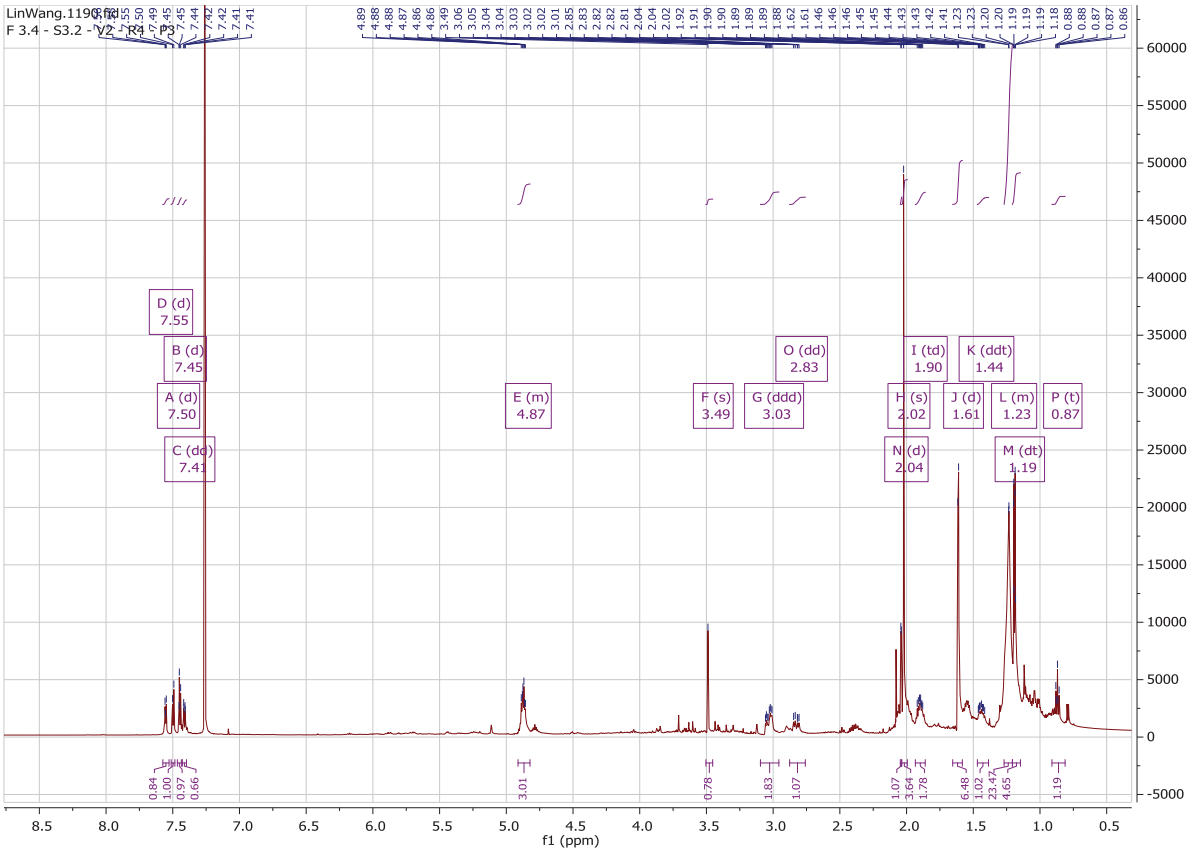

Figure S10 : ^{1}H NMR of compound **8**

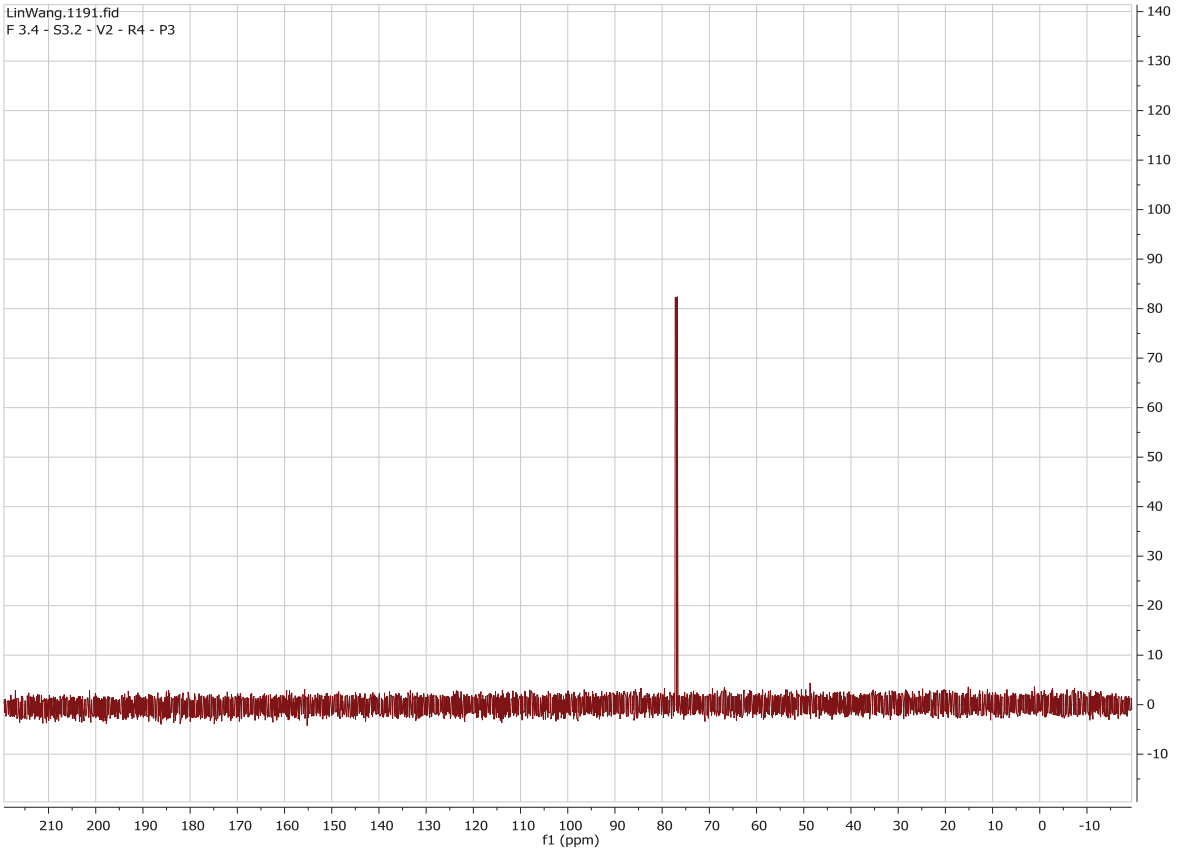

Figure S11: ^{13}C NMR of compound **8**

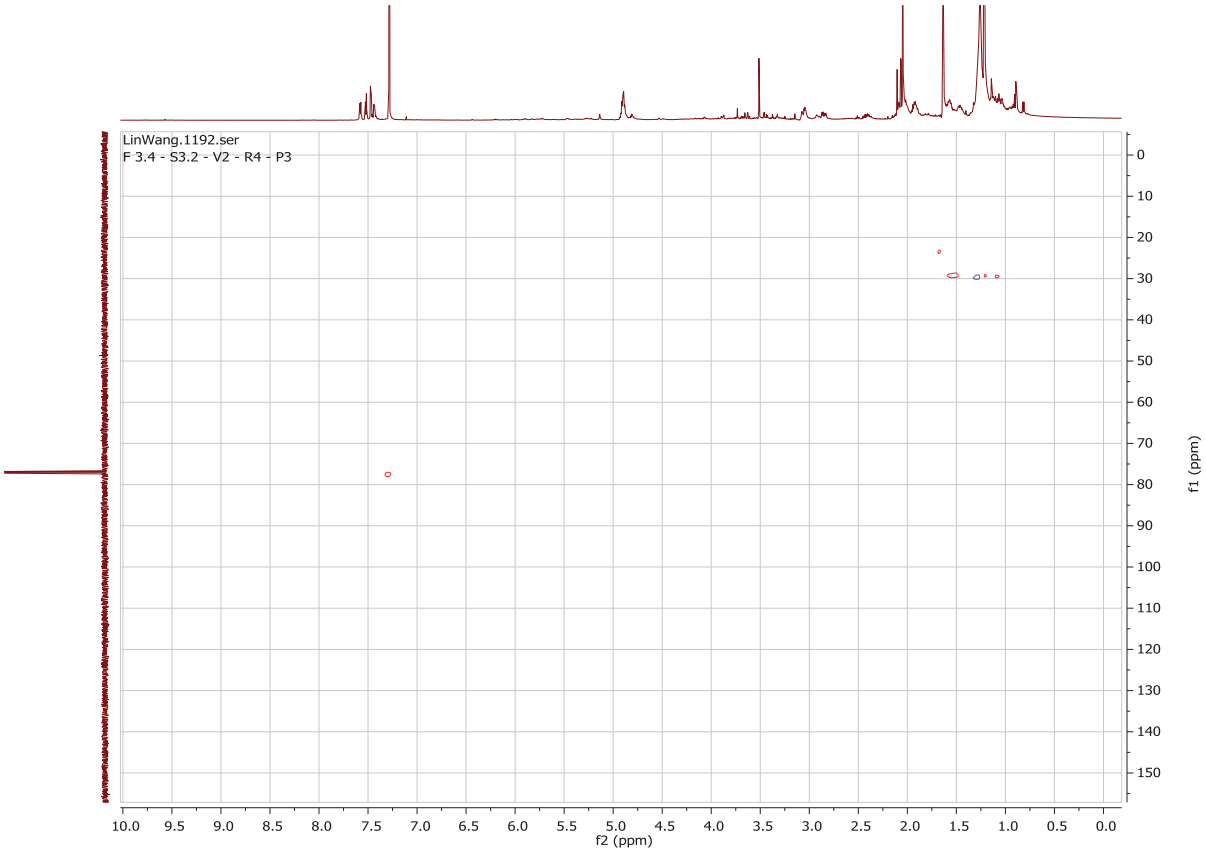

Figure S12: HSQC of compound **8**

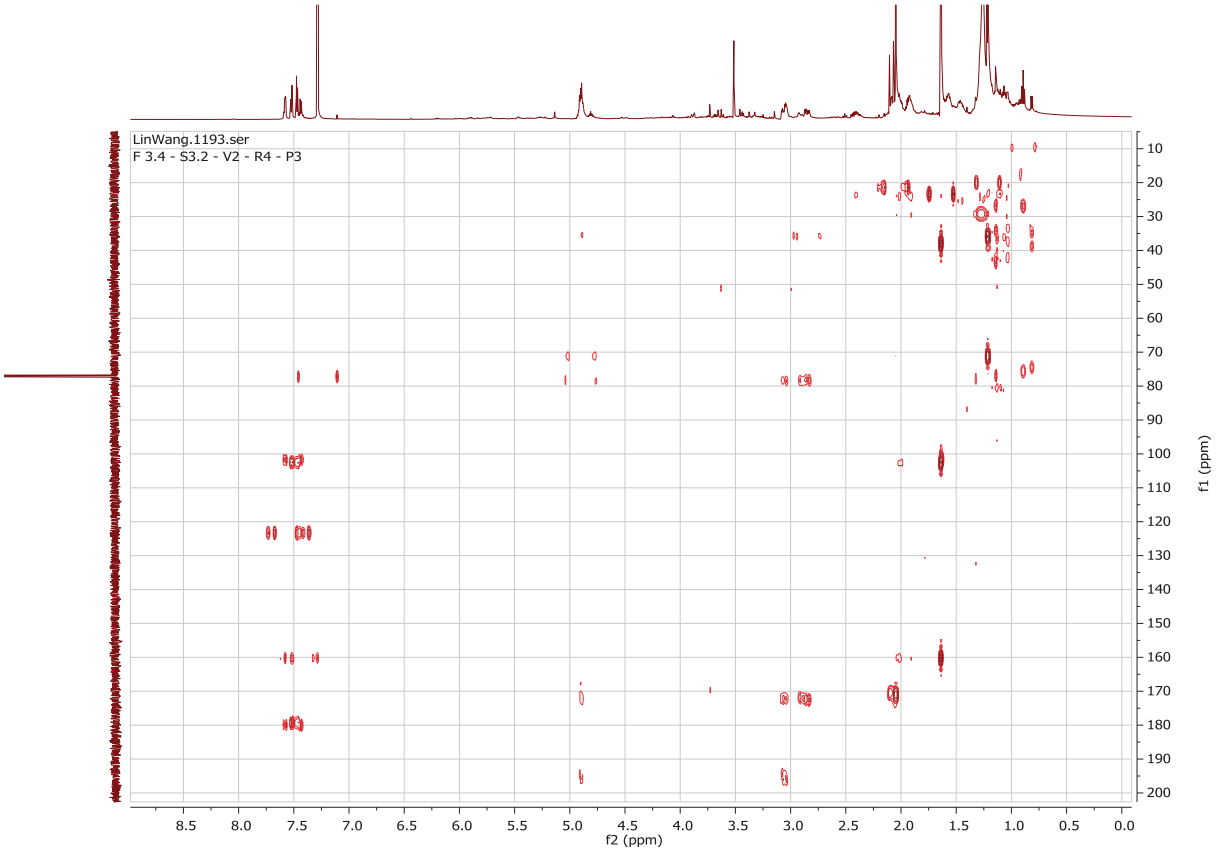

Figure S13: HMBC of compound **8**

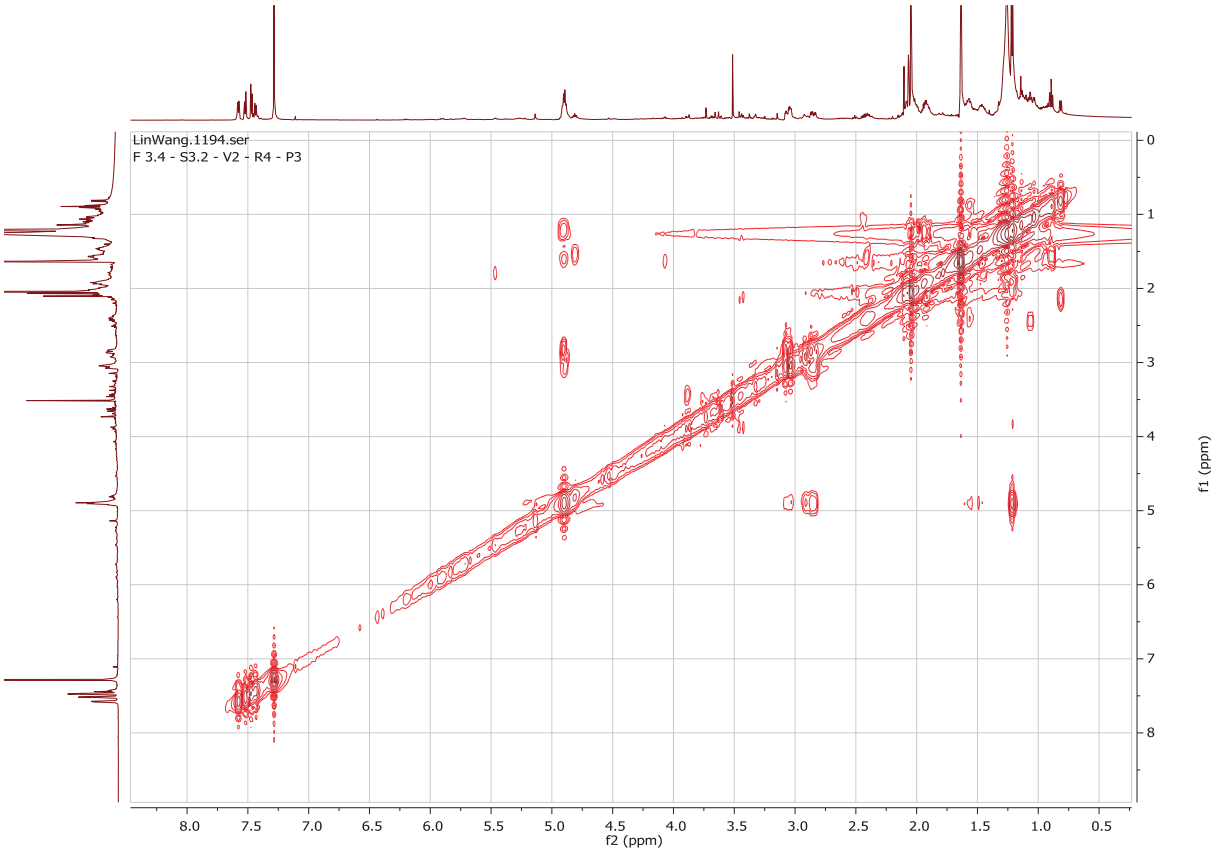

Figure S14: COSY of compound **8**

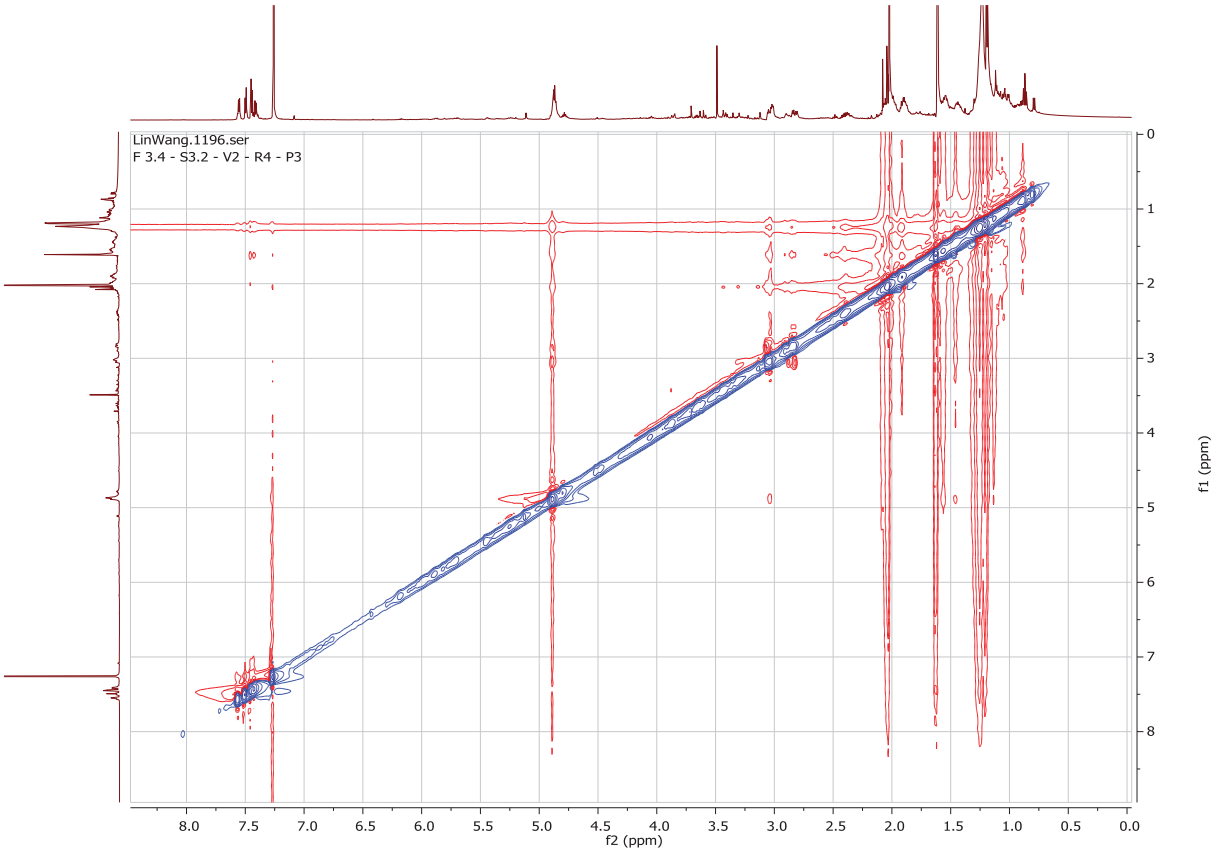

Figure S15: ROESY of compound **8**

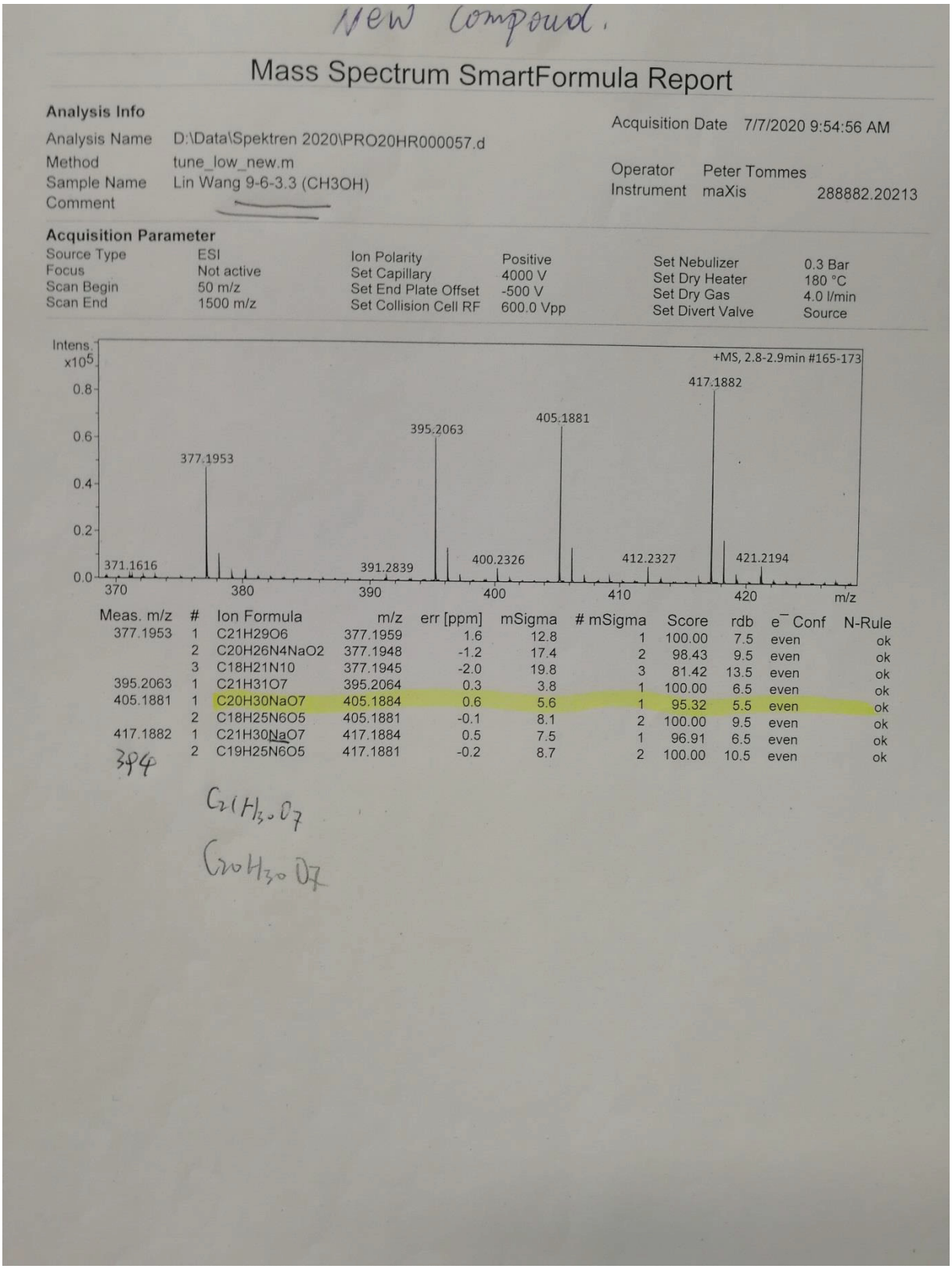

Figure S16: HREISMS of compound **9**

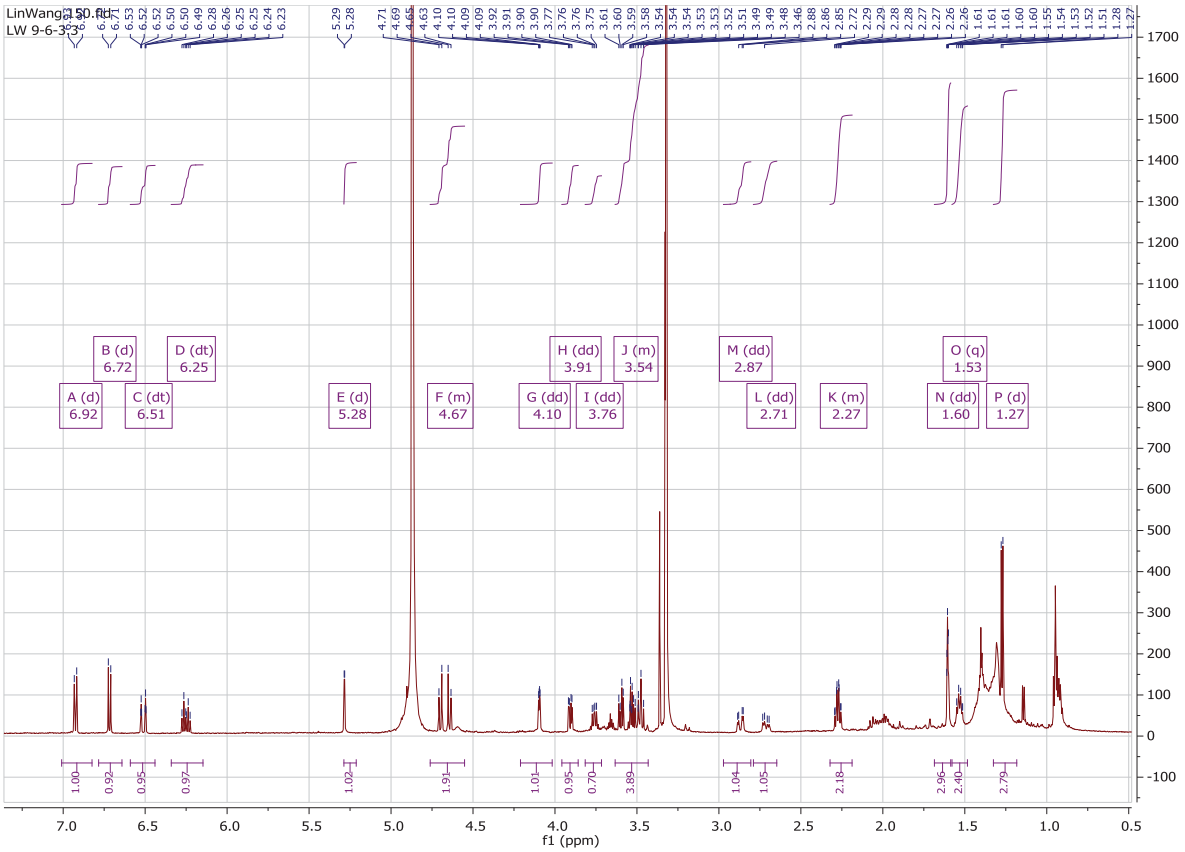

Figure S17: ^{1}H NMR of compound **9**

Figure S18: ^{13}C NMR of compound **9**

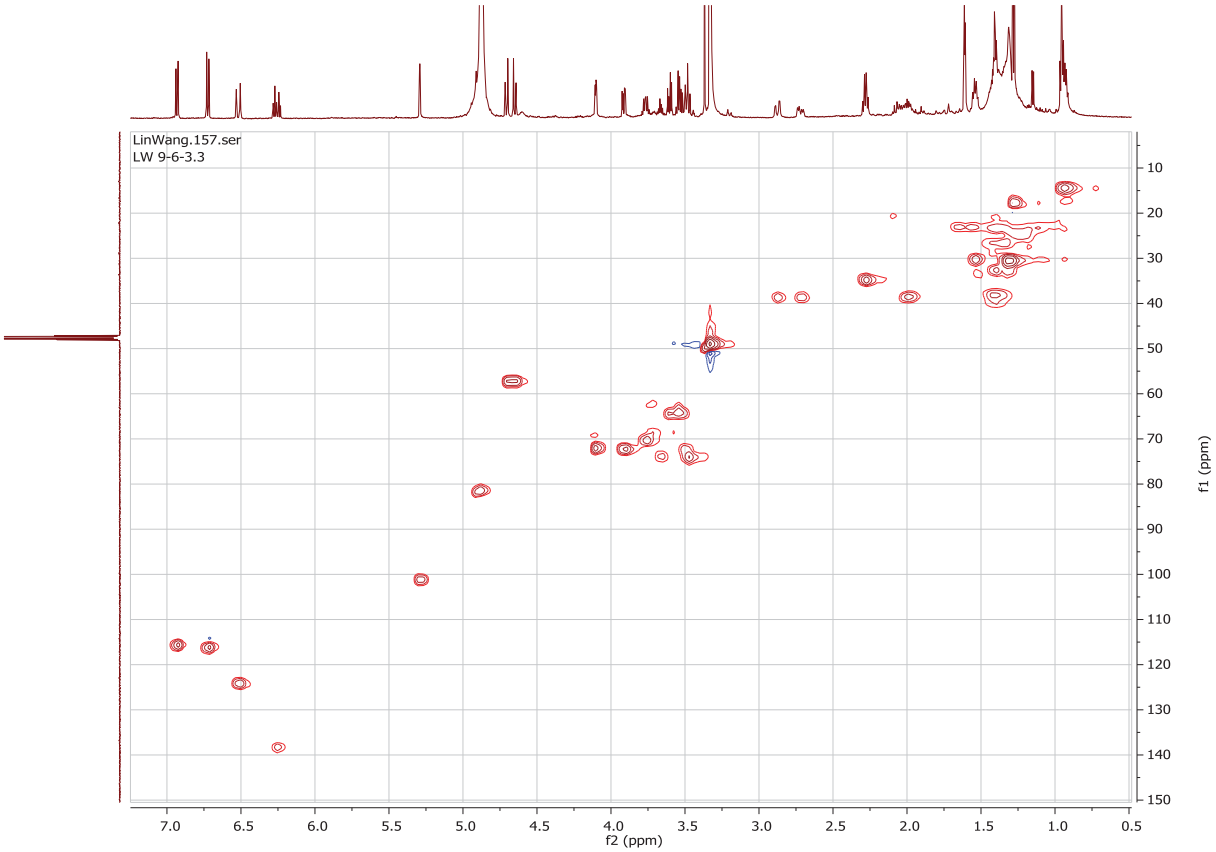

Figure S20: HSQC of compound **9**

Figure S21: HMBC of compound **9**

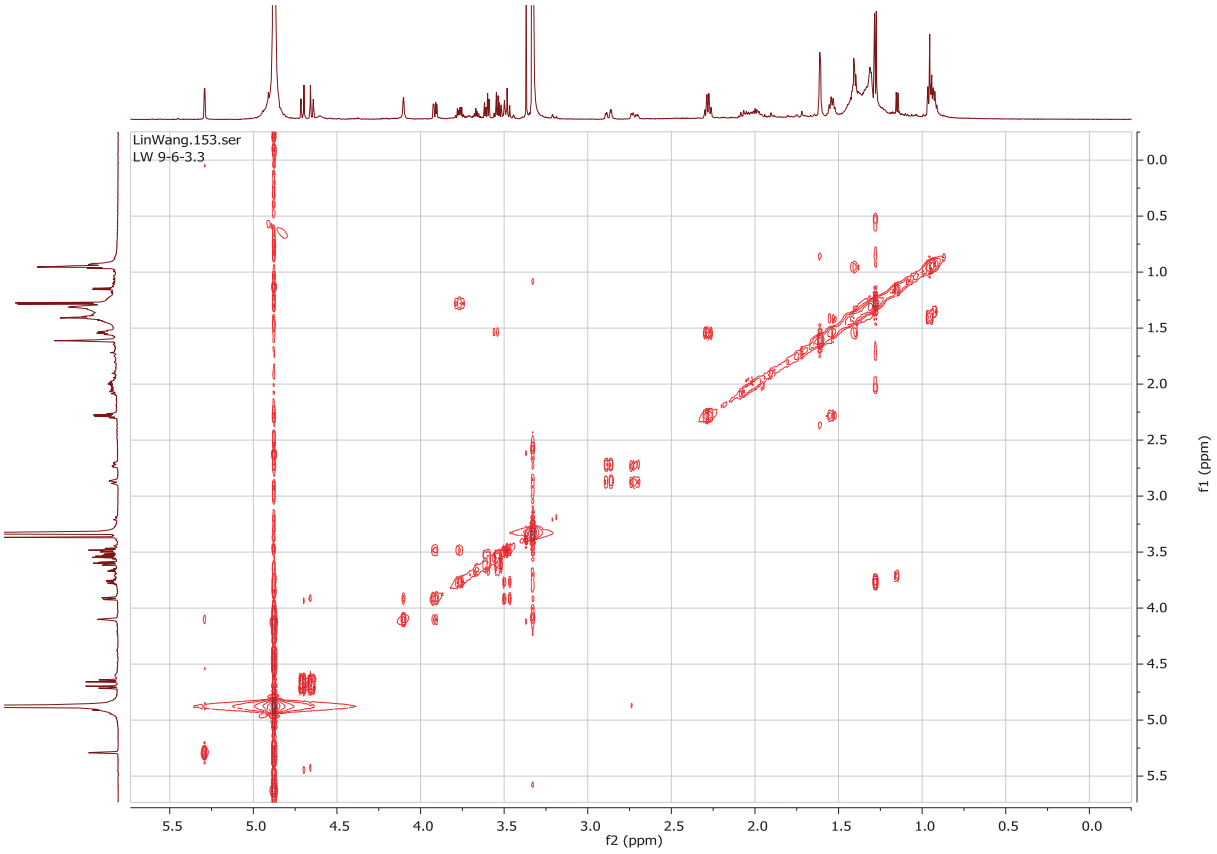

Figure S22: COSY of compound **9**

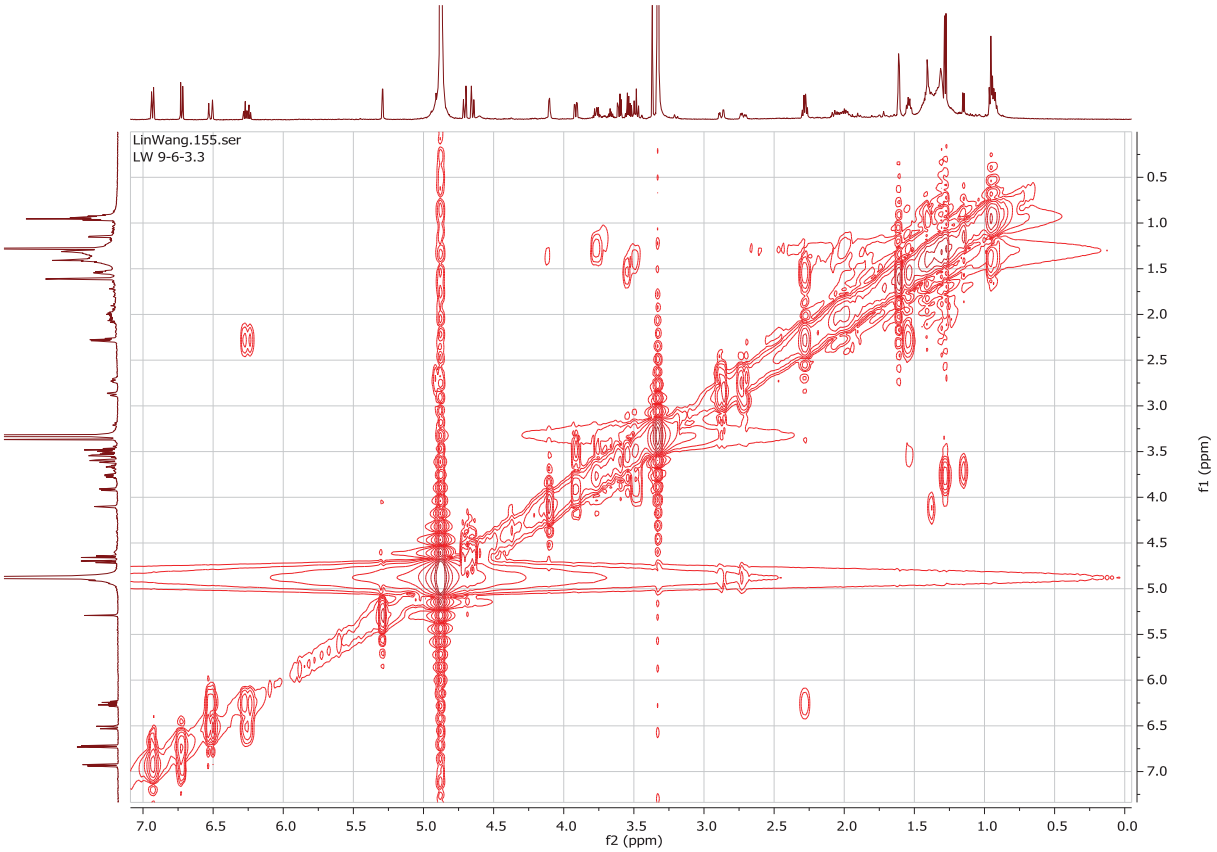

Figure S23: ROESY of compound **9**

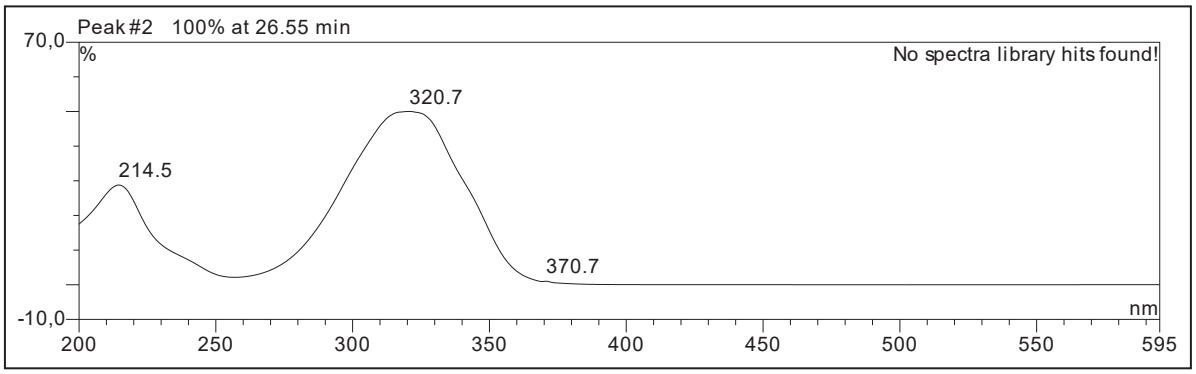

Figure S24: UV absorption of compound **8**

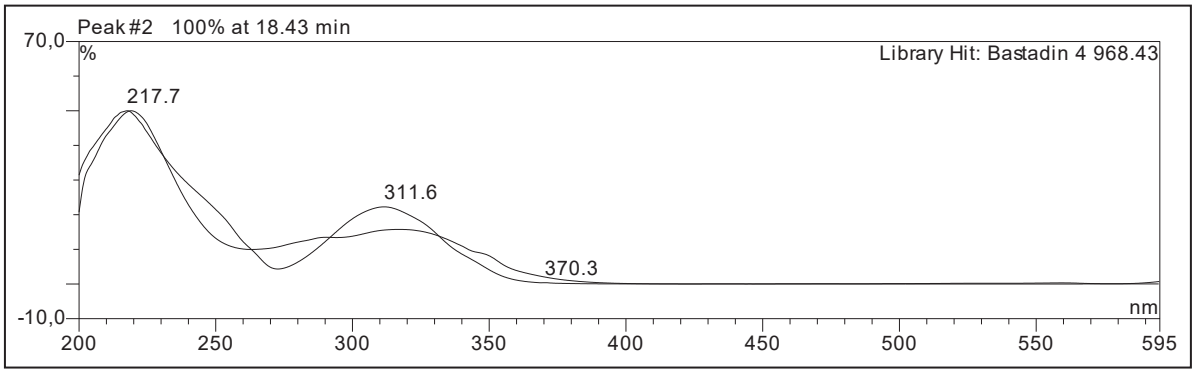

Figure S25: UV absorption of compound **9**

Chapter 5 – Publication Manuscript 4

Antifungal polyketide derivatives from the endophytic fungus *Aplosporella javeedii*

Published in Bioorganic & Medicinal Chemistry

Impact factor: 3.073 (2019)

Overall contribution to the Publication manuscript:

- Determination of minimal inhibitory concentrations (Gram-positive bacteria and *Candida albicans*)
- Evaluation of cytotoxicity and therapeutic index
- Determination of time-kill kinetic
- Draft writing

Bioorganic & Medicinal Chemistry 28 (2020) 115456

Contents lists available at ScienceDirect

Bioorganic & Medicinal Chemistry

journal homepage: www.elsevier.com/locate/bmc

Antifungal polyketide derivatives from the endophytic fungus *Aplosporella javeedii*

Ying Gao[a], Lin Wang[a], Rainer Kalscheuer[a], Zhen Liu[a,*], Peter Proksch[a,b,*]

[a] Institute of Pharmaceutical Biology and Biotechnology, Heinrich Heine University Düsseldorf, Universitätsstrasse 1, 40225 Düsseldorf, Germany
[b] Hubei Key Laboratory of Natural Products Research and Development, College of Biological and Pharmaceutical Sciences, China Three Gorges University, Yichang 443002, People's Republic of China

ARTICLE INFO

Keywords:
Aplosporella javeedii
Polyketides
Antifungal activity
Antibacterial activity

ABSTRACT

Six new polyketides aplojaveediins A–F (1–6) were isolated from the endophytic fungus *Aplosporella javeedii* associated with the host plant *Orychophragmus violaceus* (Brassicaceae). The structures of the new metabolites were elucidated by analysis of their NMR and MS data. Compound 1 exhibited antifungal activity against the hyphae form of *Candida albicans* strain ATCC 24433 in the agar plate diffusion assay and the microbroth dilution assay. The kinetic of killing of *C. albicans* cells for compound 1 was considerably faster than that of the positive control hygromycin B. Compounds 1 and 6 also exhibited moderate antibacterial activities against sensitive (ATCC 29213) and drug-resistant (ATCC 700699) strains of *Staphylococcus aureus*.

1. Introduction

Endophytic fungi are firmly established as sources of new bioactive metabolites and have been shown to accumulate diverse groups of compounds such as alkaloids, terpenoids, steroids, phenols, quinones, xanthones, and peptides.[1,2,3,4,5] Due to this pronounced chemical diversity, endophytic fungi represent an important potential source of new medicinal and biotechnological agents. During our ongoing research on new bioactive secondary metabolites from endophytic fungi,[6,7] *Aplosporella javeedii* was isolated from stem tissue of *Orychophragmus violaceus* (L.) O. E. Schul (*Brassicaceae*) collected around Beijing. *O. violaceus* is an edible wild herb as well as a medicinal plant that is used in Traditional Chinese Medicine (TCM).[8,9] It is recorded in the TCM literature for dissipating swelling and for treating unknown pyrogenic infections.[10] In recent years, researchers also reported hepatoprotective effects for this plant.[11] *A. javeedii* is a member of the fungal family *Aplosporellaceae* and is usually associated with canker and dieback disease of woody plants. It was first isolated and identified from wood sections of *Celtis africana* Burm.f. (*Cannabaceae*) and *Searsia lancea* (L.f.) F.A. Barkley (*Anacardiaceae*) in South Africa in 2013.[12] Other records are from China and came from woody trees of the *Fabaceae*, *Cupressaceae*,[13] *Rhamnaceae*,[14] and *Moraceae*.[15] To our best knowledge, this is the first record of *A. javeedii* from a host plant of the *Brassicaceae*. Until now, there are no reports on secondary metabolites of *A. javeedii* which prompted us to investigate this fungus. When grown on solid rice medium *A. javeedii* yielded six new polyketides (1–6) (Fig. 1). In this paper, we report the isolation and structure elucidation of these polyketides, as well as their antifungal and antibacterial activities.

2. Results and discussion

Compound 1 was obtained as colorless crystals, with UV absorptions at λ_{max} 208, 220 and 298 nm. Its molecular formula was established as $C_{12}H_{18}O_3$ on the basis of prominent pseudomolecular ion peaks at *m/z* 223.1332 $[M+H]^+$ and 221.1178 $[M-H]^+$ in the HRESIMS spectrum, indicating five degrees of unsaturation. The ^{1}H NMR data of 1 (Table 1) showed one aldehyde proton at δ_H 10.01 (s, H-7), one aromatic proton at δ_H 6.24 (s, H-5), one aromatic methyl group at δ_H 1.99 (s, Me-8). The ^{13}C NMR data of 1 (Table 1) displayed one aldehyde carbon at δ_C 194.1 (C-7) and six aromatic carbons at δ_C 165.2 (C-2), 165.0 (C-6), 147.9 (C-4), 112.7 (C-1), 110.2 (C-5), and 110.1 (C-3). The HMBC correlations (Fig. 2) from H-7 to C-1, C-2, and C-6, from Me-8 to C-2, C-3, and C-4, and from H-5 to C-1, C-3, and C-6 established the presence of a pentasubstituted benzene ring with an aldehyde group and a methyl group at C-1 and C-3, respectively. The remaining NMR data are characteristic signals of a *n*-pentyl chain, which was further confirmed by the COSY correlations between H_2-9 (δ_H 2.80)/H_2-10 (δ_H 1.61), H_2-10/H_2-11 (δ_H 1.35), H_2-12 (δ_H 1.36)/Me-13 (δ_H 0.91) as well as by the HMBC correlations from Me-13 to C-11 (δ_C 32.7) and C-12 (δ_C 23.5). In addition,

* Corresponding authors at: Institute of Pharmaceutical Biology and Biotechnology, Heinrich Heine University Düsseldorf, Universitätsstrasse 1, 40225 Düsseldorf, Germany (P. Proksch).
E-mail addresses: zhenfeizi0@sina.com (Z. Liu), proksch@uni-duesseldorf.de (P. Proksch).

https://doi.org/10.1016/j.bmc.2020.115456
Received 19 January 2020; Accepted 16 March 2020
Available online 25 March 2020
0968-0896/

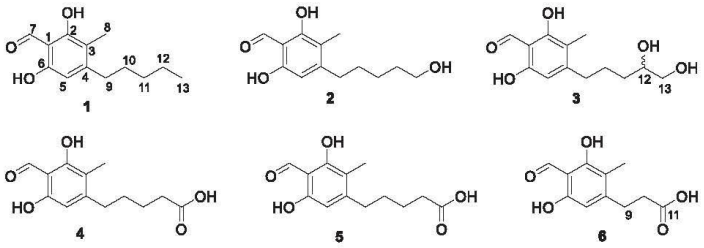

Fig. 1. Structures of new polyketides isolated from *A. javeedii*.

Table 1
^{1}H and ^{13}C NMR data for compounds **1**–**3** in methanol-d_4.

NO.	1[a]		2[a]		3[b]	
	δ_C, type	δ_H (J in Hz)	δ_C, type	δ_H (J in Hz)	δ_C, type[c]	δ_H (J in Hz)
1	112.7, C		112.7, C		112.7, C	
2	165.2, C		165.3, C		165.3, C	
3	110.1, C		110.1, C		110.1, C	
4	147.9, C		147.8, C		147.6, C	
5	110.2, CH	6.24, s	110.3, CH	6.25, s	110.3, CH	6.26, s
6	165.0, C		165.3, C		165.2, C	
7	194.1, C	10.01, s	194.1, C	10.03, s	194.2, C	10.05, s
8	7.1, CH_3	1.99, s	7.1, CH_3	1.99, s	7.1, CH_3	1.99, s
9	32.5, CH_2	2.80, m	32.5, CH_2	2.82, m	32.5, CH_2	2.88, ddd (13.9, 9.5, 6.1) 2.81, ddd (13.9, 9.3, 6.2)
10	33.7, CH_2	1.61, m	33.8, CH_2	1.64, m	30.0, CH_2	1.80, m 1.67, m
11	32.7, CH_2	1.35, m	26.7, CH_2	1.44, m	34.0, CH_2	1.59, m 1.43, m
12	23.5, CH_2	1.36, m	33.4, CH_2	1.56, m	72.9, CH	3.59, m
13	14.3, CH_3	0.91, t (6.9)	62.8, CH_2	3.55, t (6.4)	67.4, CH_2	3.45, dd (11.1, 4.8) 3.42, dd (11.1, 6.3)

[a] Recorded at 300 (^{1}H) and 75 MHz (^{13}C).
[b] Recorded at 600 (^{1}H) and 150 MHz (^{13}C).
[c] Data extracted from HSQC and HMBC spectra.

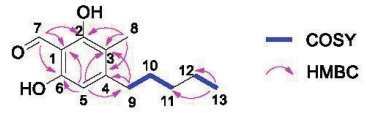

Fig. 2. COSY and key HMBC correlations for compound **1**.

the HMBC correlations from H-5 to C-9 (δ_C 32.5) and from H_2-9 to C-3, C-4, and C-5 indicated the location of the *n*-pentyl chain at C-4. The substitution of two hydroxy group at C-2 and C-6 of the benzene ring was suggested by the chemical shifts of C-2 and C-6 as well as the molecular formula of **1**. Thus, compound **1** was determined as 2,6-dihydroxy-3-methyl-4-pentylbenzaldehyde, for which the trivial name aplojaveediin A is proposed.

The molecular formula of **2** was determined as $C_{13}H_{18}O_4$ by the HRESIMS data, containing an additional oxygen atom when compared to **1**. The NMR data of **2** (Table 1) were similar to those of compound **1** except for the replacement of signals of the terminal methyl group in the side chain by signals of an oxygenated methylene resonating at δ_C 62.8 (C-13) and δ_H 3.55 (2H, t, J = 6.4 Hz, H_2-13). The COSY correlations between H_2-13/H_2-12 (δ_H 1.56), H_2-12/H_2-11 (δ_H 1.44), H_2-11/H_2-10 (δ_H 1.64), H_2-10/H_2-9 (δ_H 2.82) together with the HMBC correlations from H_2-13 to C-11 (δ_C 26.7) and C-12 (δ_C 33.4) indicated the location of a hydroxy group at C-13 in the side chain of **2**. Detailed analysis of the 2D NMR spectra of **2** revealed that the remaining substructure of **2** was identical to that of **1**. Thus, the structure of **2** was elucidated as shown.

Compound **3** has the molecular formula $C_{13}H_{18}O_5$ as deduced from the HRESIMS data, containing an additional oxygen atom when compared to **2**. Comparison of the NMR data of **2** and **3** (Table 1) suggested that they are structurally similar. The major difference is the observation of an additional oxygenated methine at δ_C 72.9 (C-12) and δ_H 3.59 (H-12) in **3**. Besides, the protons of the oxygenated methylene at C-13 appeared as two dd peaks in **3** instead of two triplet peaks in **2**. The above finding suggested the attachment of an additional hydroxy group at C-12, which was further confirmed by the COSY correlations between H_2-13/H-12/H_2-11/H_2-10/H_2-9. Due to the limited amount, the absolute configuration at C-12 of **3** was not determined.

Aplojaveediin D (**4**) was found to have the molecular formula $C_{13}H_{16}O_5$ on the basis of the HRESIMS data, accounting for six degrees of unsaturation. Its ^{1}H NMR data (Table 2) were similar to those of **1** but lacked signals of the terminal methyl group in the side chain. Meanwhile, the ^{13}C NMR spectrum of **4** exhibited the signal of one additional carbonyl carbon at δ_C 178.0 (C-13). The HMBC correlations from H_2-12 (δ_H 2.32, t, J = 6.5 Hz) to C-13, C-11 (δ_C 25.9), and C-10 (δ_C 33.3), together with the COSY correlations between H_2-12/H_2-11 (δ_H 1.67) and between H_2-10 (δ_H 1.66)/H_2-9 (δ_H 2.84) indicated a terminal carboxylic acid group in the side chain that replaced the methyl substituent of compound **1**. The remaining substructure of **4** was

Table 2
^{1}H and ^{13}C NMR data for compounds **4**–**6** in methanol-d_4.

NO.	4[a]		5[a]		6[b]	
	δ_C, type	δ_H (J in Hz)	δ_C, type	δ_H (J in Hz)	δ_C, type	δ_H (J in Hz)
1	112.8, C		112.7, C		112.7, C	
2	165.3, C		165.3, C		165.4, C	
3	110.1, C		110.2, C		110.2, C	
4	147.5, C		147.3, C		147.2, C	
5	110.2, CH	6.26, s	110.3, CH	6.25, s	110.1, CH	6.28, s
6	164.8, C		165.0, C		165.2, C	
7	194.2, C	10.04, s	194.1, C	10.02, s	194.3, C	10.07, s
8	7.1, CH_3	1.99, s	7.1, CH_3	1.99, s	7.1, CH_3	1.97, s
9	32.2, CH_2	2.84, t (7.0)	32.1, CH_2	2.83, t (7.3)	28.9, CH_2	3.10, t (7.8)
10	33.3, CH_2	1.66, m	33.2, CH_2	1.65, m	41.2, CH_2	2.46, t (7.8)
11	25.9, CH_2	1.67, m	25.7, CH_2	1.67, m	181.8, C	
12	35.0, CH_2	2.32, t (6.5)	34.4, CH_2	2.36, t (7.0)		
13	178.0, C		175.7, C			
13-OMe			52.0, CH_3	3.65, s		

[a] Recorded at 300 (^{1}H) and 75 MHz (^{13}C).
[b] Recorded at 600 (^{1}H) and 150 MHz (^{13}C).

identical to that of **1** as confirmed by detailed analysis of the 2D NMR spectra of **4**.

Compound **5** exhibited the molecular formula $C_{14}H_{18}O_5$ as determined by the HRESIMS data. The ^1H and ^{13}C NMR data of **5** were similar to those of **4** (Table 2). Analysis of the 2D NMR spectra revealed that both compounds shared the same benzene ring core structure. Compound **5** was identified as the C-13*O*-methyl derivative of **4**, as evident from the presence of an additional methoxy group at δ_H 3.65 (3H, s) and δ_C 52.0, together with the HMBC correlations from the protons of this additional methoxy group and H_2-12 (δ_H 2.36, t, J = 7.0 Hz) to the carbonyl carbon at δ_C 175.7 (C-13), and from H_2-12 to C-10 (δ_C 33.2) and C-11 (δ_C 25.7). Compound **5** could already be detected in the HPLC chromatogram of the crude fungal extract which argues for **5** being a natural product and not an artefact arising from **4** in the presence of MeOH. Moreover, incubation of **4** in MeOH for several days at room temperature failed to yield **5**.

The molecular formula of aplojaveediin F (**6**) was established as $C_{11}H_{12}O_5$ from the HRESIMS data, requiring six degrees of unsaturation. Comparison of the NMR data (Table 2) indicated compound **6** to be closely related to compound **4** except for that the side chain of **6** lacked two methylene groups when compared to **4**. The HMBC correlations from H_2-10 (δ_H 2.46, t, J = 7.8 Hz) to C-11 (δ_C 181.8) and C-4 (δ_C 147.2), and from H_2-9 (δ_H 3.10, t, J = 7.8 Hz) to C-11, C-3, C-4 and C-5 as well as the COSY correlations between H_2-10 and H_2-9 indicated the presence of a *n*-propanoic acid side chain at C-4 in **6**. Thus, the structure of **6** was elucidated as shown.

Compounds **1**–**6** were tested for their antibacterial activity against a panel of bacterial strains. Compound **1** exhibited moderate antibacterial activity against the sensitive *Staphylococcus aureus* strain ATCC 29213, the methicillin-resistant and vancomycin intermediate sensitive (MRSA/VISA) *S. aureus* strain ATCC 700699 and *Bacillus subtilis* (ATCC 169) with minimal inhibitory concentrations (MICs) of 50, 50 and 25 μM, respectively. Compound **6** also exhibited moderate antibacterial activity against *S. aureus* ATCC 29213 and ATCC 700699 with MICs of 25 and 50 μM, respectively. No or only a very weak antibacterial effect was observed for compounds **1** and **6** against the other tested bacterial strains (Table S1). Compounds **2**–**5** showed no antibacterial activity.

In addition, compounds **1**–**6** were tested for their antifungal activity against *Candida albicans* grown in the yeast or the hyphae form. While compounds **2**–**6** were inactive, compound **1** exhibited antifungal activity against the hyphae form of *C. albicans* strain ATCC 24433 with an inhibition diameter of 8 mm in the agar plate diffusion assay at a concentration of 1 mM. The compound was also active against the yeast *Saccharomyces cerevisiae* resulting in an inhibition diameter of 18 mm (Fig. S44). The MIC of compound **1** against the hyphae form of *C. albicans* strain ATCC 24433 in liquid medium was 100 μM as determined by the microbroth dilution assay. Moreover, compound **1** showed no substantial cytotoxicity against the three tested human cell lines (HUH7, THP-1, CLS-54) up to a concentration of 100 μM (Fig. 3). As an extension of the antifungal assay, a time-kill assay was performed (Fig. 4). Incubation of cells of the hyphae form of *Candida albicans* strain ATCC 24,433 with compound **1** at 400 μM (=4-fold MIC) resulted in a rapid decrease of viability by 3.5-log over a period of 6 h, after which a plateau was reached. In contrast, the positive control hygromycin B (474 μM = 4-fold MIC), which has antifungal activity against *C. candida*,[16,17] exhibited only a largely static growth inhibitory effect (Fig. 4). This finding highlights the fungicidal property of compound **1**. When comparing the antifungal activity of compounds **1**–**6**, it is obvious that addition of polar groups to the side chain (**2**–**5**) as well as shortening of the side chain (**6**) weakens the antifungal activity, which might be due to hindered uptake by the fungus. Based on its fungicidal activity and lack of cytotoxicity against human cells, compound **1** could be a promising candidate for the development of new antifungal agents.

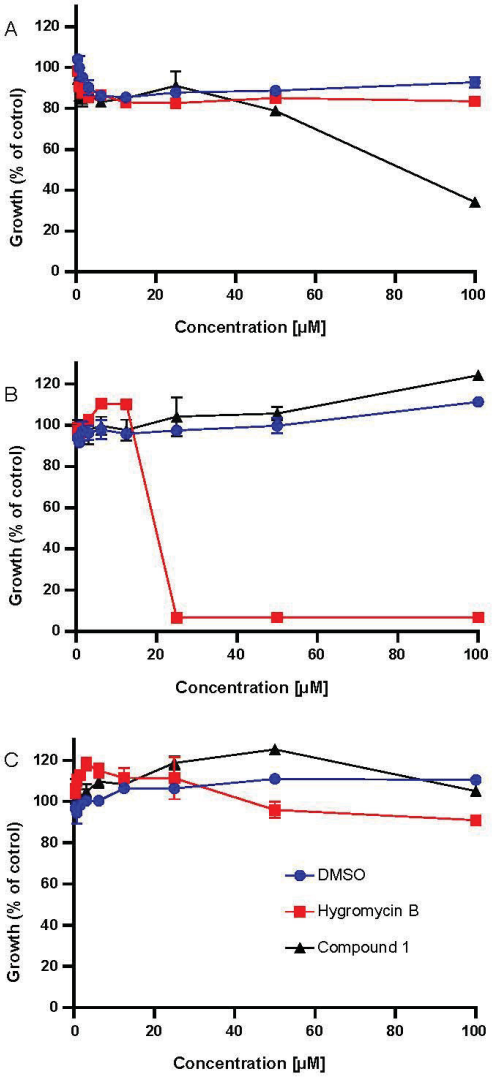

Fig. 3. Evaluation of cytotoxicity of compound **1** against different human cell lines. (A) Effect against the human liver cell line HUH7, (B) the human lung epithelial cell line CLS-54, and (C) the human monocytic leukemia cell line THP-1. DMSO was used as solvent control, the antifungal compound hygromycin B as reference. Data represent means from two replicates ± standard error.

3. Experimental

3.1. General experimental procedures

Optical rotations were measured with a Perkin-Elmer-241 MC polarimeter. NMR spectra were recorded at 25 °C on Bruker ARX 300 or 600 NMR spectrometers. Chemical shifts were referenced to the solvent residual peaks. Mass spectra (ESI) were recorded with a Finnigan LCQ

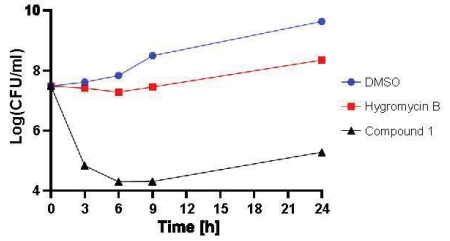

Fig. 4. Time-kill curve of compound **1** (400 μM, black) against the hyphae form of *Candida albicans* strain ATCC 24433. The antifungal compound hygromycin B (474 μM, red) was used as positive control; DMSO (blue) was used as the solvent control. Colony forming units (CFU) were quantified after the indicated time points of incubation. The medium was replaced after 6 h incubation with fresh medium containing compounds at the initial concentration to avoid effects by potential compound degradation.

Deca mass spectrometer while HRESIMS were recorded with a UHR-QTOF maXis 4G (Bruker Daltonics) mass spectrometer. HPLC analysis was performed with a Dionex UltiMate-3400SD system with a LPG-3400SD pump and a photodiode array detector (DAD 3000RS). The analytical column (125 × 4 mm) was prefilled with Eurosphere-10 C_{18} (Knauer, Germany). Semi-preparative HPLC was performed using a Merck Hitachi HPLC System (UV detector L7400; pump L7100; Eurosphere-100 C_{18}, 300 × 8 mm, Knauer, Germany). Normal phase column chromatography included Merck MN silica gel 60 M (0.04–0.063 mm) or Sephadex LH-20. TLC plates precoated with silica gel F_{254} (Merck, Germany) were used to monitor fractions following column chromatography with UV detection at 254 and 366 nm or by spraying the plates with anisaldehyde reagent followed by heating. Distilled and spectral grade solvents were used for column chromatography and spectroscopic measurements, respectively.

3.2. Fungal material and identification

The endophytic fungus was isolated from fresh, healthy stems of *O. violaceus* (L.) O. E. Schul (*Brassicaceae*), which were collected in April 2018 around Beijing, China. After 70% ethanol surface sterilization, the disinfected stems were dissected into small pieces of 0.5 cm length and placed on the fungal isolation medium (malt agar medium). The isolation of the fungal strain was achieved according to a standard procedure as described before.[18] It was identified as *Aplosporella javeedii* according to the DNA amplification and sequencing of the ITS region as described previously.[19] The sequence data were submitted to GenBank with the accession number MN720704. The fungal strain is kept in the Institute of Pharmaceutical Biology and Biotechnology, Heinrich-Heine University, Duesseldorf, Germany, with the ID code ZGB-B.

3.3. Cultivation, extraction and isolation

The fungus was cultivated on solid rice medium (100 g rice and 110 mL demineralized water) in ten Erlenmeyer flasks (1 L each). After autoclaving at 121 °C for 20 min and cooling down to room temperature, the fungal strain was added and cultivated for 20 days. After the fungus had completely overgrown the medium, the culture was extracted with 800 mL EtOAc followed by evaporation of the extract to dryness. The obtained brown extract (10.5 g) was subjected to a silica gel vacuum liquid chromatography column (VLC), using solvents in a gradient of increasing polarity (*n*-hexane, EtOAc, CH_2Cl_2, MeOH) to yield 12 fractions (V1 to V12). Fraction V3 (1.5 g) was subjected to a silica gel column with a gradient of *n*-hexane and EtOAc (20:1 to 0:100), affording eight subfractions (V3-S1 to V3-S8). Subfraction V3-S2 (80.2 mg) was purified by semi-preparative HPLC using MeOH-H_2O (70:30 to 100:0) to give **1** (8.3 mg). Fraction V4 (1.1 g) was also separated on a silica gel column with a *n*-hexane-EtOAc gradient (20:1 to 0:100), affording ten subfractions (V4-S1 to V4-S10). Subfraction V4-S2 (51.1 mg) was purified by semi-preparative HPLC using MeOH-H_2O (30:70 to 70:30) to give **5** (4.3 mg). Fraction V5 (235.9 mg) was subjected to a Sephadex LH-20 column using CH_2Cl_2-MeOH (1:1) as eluent to obtain seven subfractions (V5-S1 to V5-S7). Subfraction V5-S4 (27.8 mg) was purified by semi-preparative HPLC using MeOH-H_2O (30:70 to 70:30) to give **2** (3.6 mg) and **4** (10.5 mg). Fractions V7 (206.4 mg) and V8 (100.2 mg) were combined and further fractionated using a Sephadex LH-20 column with CH_2Cl_2-MeOH (1:1) as eluent to give four subfractions (V7-S1 to V7-S4). Subfraction V8-S3 (119.6 mg) were subjected to a silica gel column with a CH_2Cl_2-MeOH gradient (20:1 to 0:100), followed by purification with semi-preparative HPLC using MeOH-H_2O (10:90 to70:30) as mobile phase to give **3** (2.0 mg). Fraction V9 (1.0 g) was separated on a Sephadex LH-20 column using CH_2Cl_2-MeOH (1:1) to yielded six subfractions (V9-S1 to V9-S6). Subfraction V9-S4 (18.2 mg) was further purified by semi-preparative HPLC using MeCN-H_2O (10:90 to 20:80) to give **6** (1.5 mg).

Aplojaveediin A (**1**): Colorless crystal; UV (MeOH) λ_{max} 208, 220 and 298 nm; ^1H and ^{13}C NMR data, see Table 1; HRESIMS $[M+H]^+$ *m/z* 223.1332 (calcd for $C_{12}H_{19}O_3$ 223.1334), $[M-H]^-$ *m/z* 221.1178 (calcd for $C_{13}H_{17}O_3$ 221.1178).

Aplojaveediin B (**2**): Brown homogeneous oil; UV (MeOH) λ_{max} 218 and 301 nm; ^1H NMR and ^{13}C NMR data, see Table 1; HRESIMS $[M+H]^+$ *m/z* 239.1280 (calcd for $C_{13}H_{19}O_4$ 239.1283), $[M-H]^-$ *m/z* 237.1130 (calcd for $C_{13}H_{17}O_4$ 237.1127).

Aplojaveediin C (**3**): Brown homogeneous oil; $[\alpha]_D^{20}$ + 6 (*c* 0.2, MeOH); UV (MeOH) λ_{max} 206, 220 and 297 nm; ^1H and ^{13}C NMR data, see Table 1; HRESIMS $[M-H]^-$ *m/z* 253.1084 (calcd for $C_{13}H_{17}O_5$ 253.1076).

Aplojaveediin D (**4**): Colorless crystal; UV (MeOH) λ_{max} 220 and 300 nm; ^1H and ^{13}C NMR data, see Table 2; HRESIMS $[M-H]^-$ *m/z* 251.0923 (calcd for $C_{13}H_{15}O_5$ 251.0919).

Aplojaveediin E (**5**): Colorless crystals; UV (MeOH) λ_{max} 208, 220 and 298 nm; ^1H and ^{13}C NMR data, see Table 2; HRESIMS $[M-H]^-$ *m/z* 265.1082 (calcd for $C_{14}H_{17}O_5$ 265.1076).

Aplojaveediin F (**6**): White amorphous solid; UV (MeOH) λ_{max} 220 and 297 nm; ^1H and ^{13}C NMR data, see Table 2; HRESIMS $[M-H]^-$ *m/z* 223.0607 (calcd for $C_{11}H_{11}O_5$ 223.0606).

3.4. Antibacterial assay

The antibacterial activities were tested by calculating the MICs against *Mycobacterium tuberculosis* H37Rv, *Staphylococcus aureus* ATCC 29213, *S. aureus* ATCC 700699, *Enterococcus faecalis* ATCC 29212, *E. faecalis* ATCC 51299, *E. faecium* ATCC 35667, *E. faecium* ATCC 700221, *Bacillus subtilis* ATCC 169 and *Escherichia coli* ATCC 25922. The MIC values were determined by the broth microdilution method following the recommendation of the Clinical and Laboratory Standards Institute (CLSI).[20]

3.5. Antifungal assay

Compounds were tested against the nosocomial pathogen *Candida albicans* both grown in the yeast form and the hyphae form. The microbroth dilution method was done as recommended by CLSI guidelines.[20] *Candida albicans* was inoculated in YPD medium (yeast extract 10 g/L, peptone 20 g/L, D-glucose 20 g/L) and incubated at 37 °C with shaking at 180 rpm overnight to obtain the yeast form. For the hyphae form, YP + Proline medium (yeast extract 10 g/L, peptone 20 g/L, proline 20 g/L) was used, and cells were incubated at 30 °C with shaking at 60 rpm overnight. Afterwards, cells were seeded at a density of 1 × 10^6 CFU/mL in 96 well microplate containing two fold serial dilutions of compounds at a concentration ranging from 100 to 0.78 μM in a total volume 100 μL. DMSO at a maximal concentration of 1% was

used as solvent control, while hygromycin B served as antifungal positive control.[16,17] The plates were incubated at 37 °C overnight aerobically as static cultures before being evaluated macroscopically. All tests were repeated twice.

The disc diffusion method was used as an additional sensitivity test. Briefly, a preculture of *Candida albicans* (hyphae form) was adjusted to 2×10^8 CFU/mL. Subsequently, 100 µL culture aliquots were plated out on the surface of YP + Proline agar plates. Then, 5 µL of compound **1** (1 mmol/L, 10MIC) was spotted onto a sterile filter disc. Hygromycin B (3.12 µg in 5 µL, 10MIC) was used as positive and DMSO (5 µL) as negative control. The plates were incubated at 30 °C overnight aerobically. Subsequently, the inhibition zones were measured by a caliper. All tests were repeated once.

3.6. Cytotoxicity assay

Cytotoxicity studies were conducted with three human cell lines THP-1 (human monocytic leukemia cell line), CLS-54 (human lung epithelial cell line), and HUH7 (liver cell line). The cells were cultured in RPMI 1640 medium containing 10% fetal bovine serum (FBS) at 37 °C in a humidified atmosphere of 5% CO_2 for 5 days. Afterwards, the cells were suspended and adjusted to a density of 1×10^6 cells/ml. For the adherent cell lines HUH7 and CLS-54, prior trypsinization was done for cell detachment. Cells were then seeded into a 96-well plate in a total volume of 100 µL containing 2-fold serial dilutions of the tested compounds in a concentration ranging from 100 to 0.78 µM. DMSO and hygromycin B were used as negative and positive controls, respectively. After 48 h incubation at 37 °C in a humidified atmosphere of 5% CO_2, 10 µL resazurin solution (100 µg/mL) was added to each well and incubated for a further 4 h. A microplate reader (excitation 545 nm, emission 590 nm) was used to measure the fluorescence. Residual growth was calculated relative to uninoculated (0% growth) and untreated (100% growth) controls, respectively.

3.7. Determination of time-kill kinetic

Time-kill kinetic was tested for compound **1** against the hyphae form of *Candida albicans*. A preculture grown in YP + Proline medium was adjusted to a density of 3×10^7 CFU/ml and split into three aliquots, which were treated either with 4-fold MIC (400 µM) of compound **1**, hygromycin B (474 µM) as an antifungal positive control or DMSO as the solvent control. After 0, 3, 6, 9 and 24 h incubation, 100 µL culture aliquots were taken and plated on YPD agar plates, and CFU were quantified after overnight incubation at 30°C aerobically. In order to avoid the potential degradation of compounds, the medium was removed after 6 h incubation by centrifuging at 4000 rpm for 10 min and replaced with an equal volume of fresh medium containing the respective compound at the initial concentration.

Declaration of Competing Interest

The authors declare that they have no known competing financial interests or personal relationships that could have appeared to influence the work reported in this paper.

Acknowledgments

This work was supported by the Deutsche Forschungsgemeinschaft (DFG, German Research Foundation) – project number 270650915/GRK 2158 (to P.P. and R.K.). P.P. also wants to thank the Jürgen Manchot Foundation for support. W.L. wishes to thank the China Scholarship Council, the Ministry of Education of China, for a doctoral scholarship.

Appendix A. Supplementary material

Supplementary data to this article can be found online at https://doi.org/10.1016/j.bmc.2020.115456.

References

1. Liu S, Zhao Y, Heering C, et al. Sesquiterpenoids from the Endophytic Fungus *Rhinocladiella similis*. *J Nat Prod*. 2019;82:1055–1062.
2. Harwoko H, Daletos G, Stuhldreier F, et al. Dithiodiketopiperazine derivatives from endophytic fungi *Trichoderma harzianum* and *Epicoccum nigrum*. *Nat Prod Res*. 2019;1–9.
3. Liu S, Dai H, Orfali RS, Lin W, Liu Z, Proksch P. New fusaric acid derivatives from the endophytic fungus *Fusarium oxysporum* and their phytotoxicity to barley leaves. *J Agric Food Chem*. 2016;64:3127–3132.
4. Patil RH, Patil MP, Maheshwari VL. Chapter 5 - Bioactive secondary metabolites from endophytic fungi: a review of biotechnological production and their potential applications. In: Atta ur R, ed. *Studies in Natural Products Chemistry*. Elsevier205; 2016:189.
5. Gouda S, Das G, Sen SK, Shin HS, Patra JK. Endophytes: a treasure house of bioactive compounds of medicinal importance. *Front Microbiol*. 2016;7:1538.
6. Liu S, Dai H, Makhloufi G, et al. Cytotoxic 14-membered macrolides from a mangrove-derived endophytic fungus *Pestalotiopsis microspora*. *J Nat Prod*. 2016;79:2332–2340.
7. Moussa M, Ebrahim W, El-Neketi M, et al. Tetrahydroanthraquinone derivatives from the mangrove-derived endophytic fungus *Stemphylium globuliferum*. *Tetrahedron Lett*. 2016;57:4074–4078.
8. Luo P, Lan ZQ, Li ZY. *Orychophragmus violaceus*, a potential edible-oil crop. *Plant Breed*. 1994;113:83–85.
9. Zhou LR, Wu J, Wang S. Orychophragmus. In: Kole C, ed. *Wild Crop Relatives: Genomic and Breeding Resources*. Berlin, Heidelberg: Springer Berlin Heidelberg; 2011:199–225.
10. Medicinal Plant Images Database. School of Chinese Medicine, Hong Kong Baptist University; 2007. http://libproject.hkbu.edu.hk/was40/detail?lang=en&channelid=1288&searchword=herb_id=D00879.
11. Huo X, Liu C, Gao L, Xu X, Zhu N, Cao L. Hepatoprotective effect of aqueous Extract from the seeds of *Orychophragmus violaceus* against liver injury in mice and HepG2 cells. *Int J Mol Sci*. 2017;18:1197.
12. Jami F, Slippers B, Wingfield MJ, Gryzenhout M. *Botryosphaeriaceae* species overlap on four unrelated, native South African hosts. *Fungal Biol*. 2014;118:168–179.
13. Fan XL, Yang Q, Cao B, Liang YM, Tian CM. New record of *Aplosporella javeedii* on five hosts in China based on multi-gene analysis and morphology. *Mycotaxon*. 2015;130:749–756.
14. Zhu HY, Tian CM, Fan XL. Studies of botryosphaerialean fungi associated with canker and dieback of tree hosts in Dongling Mountain of China. *Phytotaxa*. 2018;348:63–76.
15. Jia H, Liu Z, Sungborn O, et al. First report of *Aplosporella javeedii* causing branch blight disease of Mulberry (*Morus alba*) in China. *J Plant Dis Prot*. 2019;126(5):475–477. https://doi.org/10.1007/s41348-019-00245-5.
16. Basso Jr LR, Bartiss A, Mao Y, et al. Transformation of *Candida albicans* with a synthetic hygromycin B resistance gene. *Yeast*. 2010;27:1039–1048.
17. Ta CA, Guerrero-Analco JA, Roberts E, et al. Antifungal saponins from the Maya medicinal plant *Cestrum schlechtendahlii* G. Don (Solanaceae). *Phytother Res*. 2016;30:439–446.
18. Debbab A, Aly AH, Edrada-Ebel R, et al. Bioactive metabolites from the endophytic fungus *Stemphylium globuliferum* isolated from *Mentha pulegium*. *J Nat Prod*. 2009;72:626–631.
19. Kjer J, Debbab A, Aly AH, Proksch P. Methods for isolation of marine-derived endophytic fungi and their bioactive secondary products. *Nat Protoc*. 2010;5:479–490.
20. CLSI. *Methods for dilution antimicrobial susceptibility tests for bacteria that grow aerobically*. CLSI standard M07 11th ed. Wayne, PA: Clinical and Laboratory Standards Institute; 2018.

Supporting Information

Antifungal polyketide derivatives from the endophytic fungus Aplosporella javeedii

Ying Gao[a], Lin Wang[a], Rainer Kalscheuer[a], Zhen Liu[a,b], Peter Proksch[a,b]

a Institute of Pharmaceutical Biology and Biotechnology, Heinrich Heine University Düsseldorf, Universitätsstrasse 1, 40225 Düsseldorf, Germany.

b Hubei Key Laboratory of Natural Products Research and Development, College of Biological and Pharmaceutical Sciences, China Three Gorges University, Yichang, 443002, People's Republic of China.

Data to this article can be found online at https://doi.org/10.1016/j.bmc.2020.115456.

Chapter 6-Discussion

6.1 Secondary metabolites from fungus *Clonostachys rosea* and their antimicrobial activities

Natural products are a key source in new drug discovery, especially for infectious diseases but also in other therapeutic areas like cancer and cardiovascular diseases. Along with the study for new natural products with antimicrobial activities, we developed the fermentation of the fungus *C. rosea*, which has a wide distribution all over the world. Previous study reported that *C. rosea* is a potent biocontrol agent with destructive effects against several plant pathogenic fungi.[1] Inhibitory activity to nematodes and insects were shown when *C. rosea* was combined with *Bacillus thuringiensis* isolates.[2-3]

From solid rice culture of *C. rosea*, twenty-four compounds were isolated including one unprecedented roseazine A containing a dioxolane carbon bridge piperazine skeleton and ten asperphenalenones, among four of them diversely linked as diterpenoid glycosides. Remarkably, glycosides were for the first time isolated from the rice culture of *C. rosea*, which further expanded the diversity of natural compounds this organism is able to produce. Additionally, five cytochalasins and eight biphenyl ethers were also identified from solid rice culture of *C. rosea*. The unprecedented roseazine A obtained from *C. rosea* represents a new carbon skeleton and although no antimicrobial bioactivity could be observed for this compound in the used test systems, it provides a structurally new candidate for the discovery of potential drugs in other therapeutic areas. Asperphenalenones were also for the first time obtained from *C. rosea,* while these compounds previously were commonly reported from *Aspergillus*, such as plant endophytic fungus *Aspergillus sp*. CPCC 400735 and soil fungus *Aspergillus sp*. PSURSPG185.[4-5] Cytochalasins were also for the first time reported from *C. rosea* as well in our study, while this group of mycotoxins has already often been described for fungi of several other genera. Cytochalasins were considered as potential candidates for drug discovery in early years. However, due to their general cytotoxic properties and very narrow therapeutic

specificity they have not yet found their way as therapeutics into the clinic. The total synthesis of cytochalasins has been established. For example, Gilbert Stork and co-workers were able to total synthesize cytochalasin B, after Eric Merifield and Eric J. Thomas announced total synthesis of cytochalasin D and O in the past century.[6-7] Based on the identification of the *che* gene cluster in *Penicillium expansum*, a biosynthetic pathway was proposed in which CheA and CheB act together to synthesize a nonaketide chain, which is then condensed with an activated tryptophan.[8] Subsequently, proposed early, middle, and late stages of cytochalasan biosynthesis were published successively in recent years.[9-10] Despite its potential importance as a biocontrol agent in agriculture, secondary metabolites of *C. rosea* have only scarcely been reported in the literature. Examples of secondary metabolites published previously for *C. rosea* include: (1) bisorbicillinoids possessing open-ended cage structures and displayed antibacterial activity.[11] (2) Dihydrovertinolide and clonostach acids A obtained from apple juice supplemented in solid rice medium and dihydrovertinolide exhibited phytotoxicity against lettuce.[12] (3) Unique cyclic heptapeptides exhibited significant cytotoxicity against the L5178Y mouse lymphoma cell with IC_{50} values of 0.1 μM.[13] (4) TMC 151 series of compounds were exclusively found in *C. rosea,*[14] and (5) eburicol was obtained by OSMAC in YES medium and displayed significant activity against MCF-7 cells.[15] (6) Finally, two novel indole alkaloids featuring clonorosins A and B were isolated, and clonorosins A was active against *Fusarium oxysporum*.[16]

To determine the antibacterial activity, all compounds isolated in the course of this thesis were tested against nosocomial pathogens, such as *S. aureus*, *E. faecium*, *E. faecalis* and *C. albicans*, as well as against *M. tuberculosis*. Interestingly, asperphenalenone F and G showed significant activities against Gram-positive bacteria *S. aureus*, *E. faecalis* and *E. faecium.* Especially asperphenalenone G exhibited stronger inhibitory activity against MRSA with MIC of 12.5 μM. In contrast, asperphenalenone E was inactive but only differes in position 1 and 7 compared to F and G. So from the structure-activity relationship aspect, if position 1 and 7 were substituted by methoxy group, their bioactivities will obviously increase. But their side chain

plays an indispensable role as well. If position 33 was substituted by sugar (mannose), the activity against MRSA was decreased from 12.5 to 100 μM compared to G and L. This deduction also can be demonstrated from F and M. Thus, on the one hand, diterpenoid glycoside in the side chain expand the diversity of compounds, on the other hand, they did not increase the activity against Gram-positive bacteria. Unfortunately, all asperphenalenones did not display activities against *M. tuberculosis* H37Rv and *C. albicans* neither in the yeast nor hyphae form. However, in previous studies asperphenalenone derivatives were not only active against Gram-positive bacteria but also Gram-negative bacteria like *Pseudomonas aeruginosa* and *E. coli*.[17] Another related aspergillussanones A displayed cytotoxic activity against human oral carcinoma (KB) cell lines.[5]

Based on the reported anti-virus (HIV and influenza) activity for several aspergillussanones, [4, 18] we tried to evaluate the anti-HIV activity of asperphenalenones. First, we tested their cytotoxic activity against human T lymphocyte cells to make sure compounds killed or inhibited the virus not by an underlying general cytotoxicity to the host cells. Asperphenalenone **G** and **H** were cytotoxic at concentration of 30.8 μM and 40 μM, respectively, which directed us to choose 80% of the growth-inhibiting concentration to work on the anti-HIV activity assay. Notably, asperphenalenone **E** showed potent activity resulting in around 70% decrease in viral RNA. Compared to the known compound asperphenalenone **A**, which displayed significant activity against HIV with IC_{50} values of 4.5 μM,[4] the difference between them was the side chain at position 30 substituted with hydroxyl group and position 33 substituted by a carboxyl group. Hence, we inferred that the presence of the hydroxyl and carboxyl group might change the density of electron cloud and increase anti-HIV activity.

Cytochalasins have been widely reported in isolation, organic synthesis, and bioactivity testing. Several potent biological activities have been described for this class of compounds. Most prominently, cytochalasins B and D are known to interact with actin filaments, leading to disturbance of the cytoskeleton and related cellular functions.[19] Yet, this is not the only

biological feature of cytochalasins, since some of them have been shown to inhibit glucose transporters,[20] offering the possibility of further development in physiology and cancer treatments,[21] or interfere with the release of hormones.[22] However, there have been few medicinal chemistry studies on this compound family probably because of their reputation of being generally toxic. Notably, our study put efforts on antibacterial activity screening with cytochalasins and showed potential activity not only against the Gram-positive bacterium *S. aureus* but also against *M. tuberculosis*. Indeed, the diversity of structures, their complexity and the distribution of these compounds in the microbial world suggest that they play a key role not only in microorganism communication and defense but also in the fitness of the microorganism hosts in symbiotic associations.

6.2 Natural products of pestalotic acid A as a new lead structure against methicillin-resistant *Staphylococcus aureus*

Natural product pestalotic acid derivatives were identified from the endophytic fungus *Pestalotiopsis chamaeropis*, which exhibited significant activity against Gram-positive pathogens including multidrug-resistant strains.

Pestalotiopsis is a highly creative genus with respect to the chemistry and bioactivity of secondary metabolites. To date, a number of studies described their diverse secondary metabolites and bioactivity. Alkaloids, terpenoids, isocoumarin derivatives, coumarins, chromones, quinones, semiquinones, peptides, xanthones, xanthone derivatives, phenols, phenolic acids, and lactones have been reported from species[23], making them a particularly rich source for bioprospecting.

In our study, nine natural compounds were obtained from solid rice culture under the guidance of *Pestalotiopsis* bioactivity screening isolation including a new glucoside, pestalotic acid A, and seven ambuic acid derivatives. In antibacterial activity screening, pestalotic acid A

showed significant activity against Gram-positive bacteria, especially against MRSA. On the foundation of pestalotic acid A, an "OSMAC" approach was carried out to increase fungal chemical diversity. As part of our efforts in the search for antibacterial compounds from the endophytic fungus *P. chamaeropis*, the "OSMAC" approach was utilized to expand natural products produced by the studied strains. The chemical profiles of *P. chamaeropis* were studied through addition of different salts into solid rice medium, including 3.5% NaBr, 3.5% NaF, 3.5% NaCl, 3.5% NaI, 3.5% $(NH_4)_2SO_4$, 3.5% $NaNO_3$, 5% L-Rhamnose, , a mixture of $MgSO_4$, $NaNO_3$ and NaCl, a mixture of $FeSO_4$, $NaNO_3$ and NaCl, and a mixture of $ZnSO_4$, $NaNO_3$ and NaCl. Interestingly, the addition of salts to the solid rice medium resulted in a significant change in fungal metabolite pattern as indicated by the HPLC chromatograms. For example, when L-Rhamnose was added to the rice medium, the activity of the corresponding organic extract against MRSA and *C. albicans* were obviously increased, but the diversity of products were not changed as assesses from HPLC chromatograms (Figure 6. 1-A). When metal ions were added to rice medium, the yield and bioactivity had dramatically changed. The possible reason might be that Mg^{2+} was a limiting growth factor for fungi, while Fe^{2+} was already available in saturated quantities so that exogenous addition did not influence yield and bioactivity much. In contrast, the presence of Zn^{2+} was toxic to the fungi, leading to slow grow and decreased production of secondary metabolites (Figure 6. 1- B,C,D). The addition of NaI led to disappearance of one main peak but enriched the production of pestalotic acid derivatives (Figure 6. 2) and showed activity against MRSA and *C. albicans* at 100 μg/mL, respectively (Table 6.1). Notably, pestalotic acids B-G and the new pestalotic acid H were undetected in cultures lacking the salts, indicating that those were induced by NaI.

Hence, salts are an important factor to induce biochemical processes within cultivation systems, and suitable salinity is needed for normal microbial growth.[24] Fungi exposed to different types of media with various salts or halogens can be triggered to activate silent biosynthetic gene clusters that consequently can lead to production of different structural

variants of compounds that are produced under "normal" culture conditions or even to formation of completely new types of molecules unrelated to the "regular" metabolite profile.[25] In our study, we successfully enhanced the expression of pestalotic acid derivatives and obtained eight derivatives. Interestingly, however, no halogenated natural products were discovered, indicating that the salts were not directly used as substrates in the activated pathways and incorporated into the compounds.

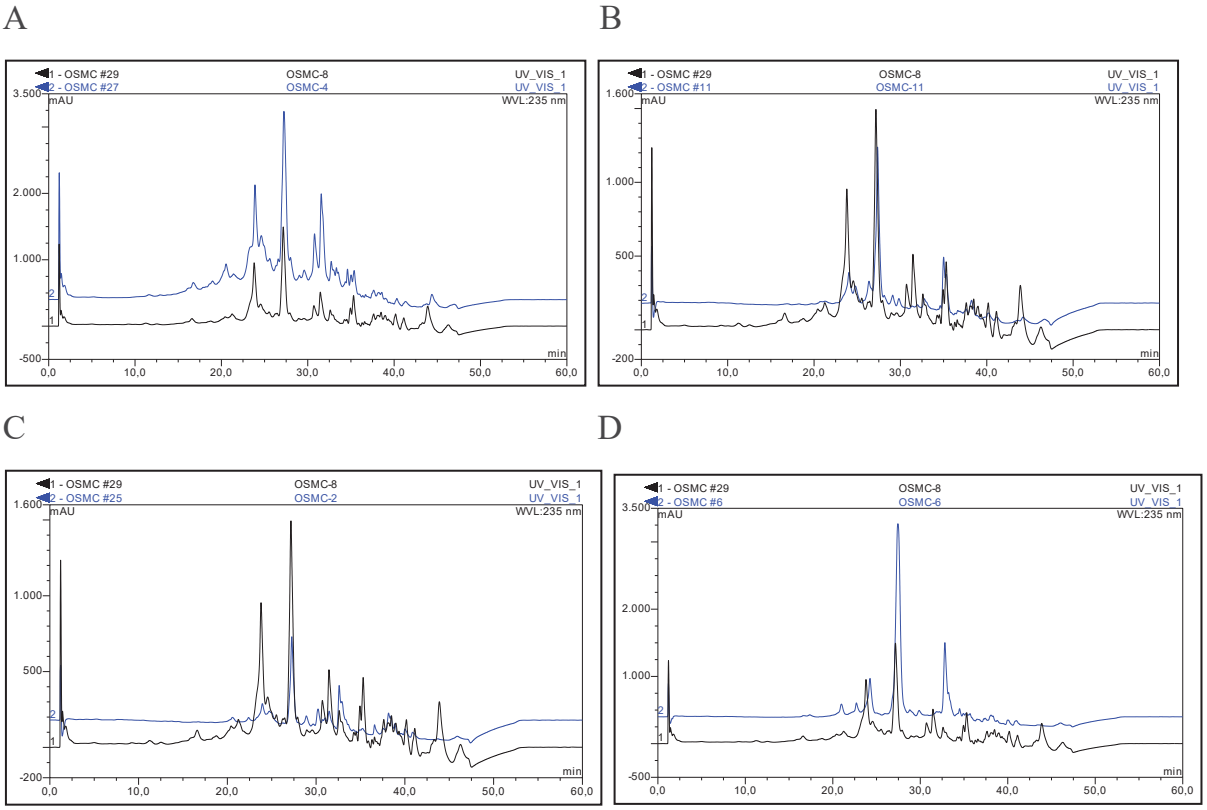

Figure 6. 1: HPLC chromatograms of EtOAc extract by "OSMAC". Black line represent HPLC chromatograms of rice; Blue line represent HPLC chromatograms of different medium. A: HPLC chromatograms of rice+L-Rhammnose. B: HPLC chromatograms of rice + $MgSO_4$+ $NaNO_3$+NaCl. C: HPLC chromatograms of rice+$FeSO_4$+$NaNO_3$+NaCl. D: HPLC chromatograms of rice+$ZnSO_4$ +$NaNO_3$+NaCl.

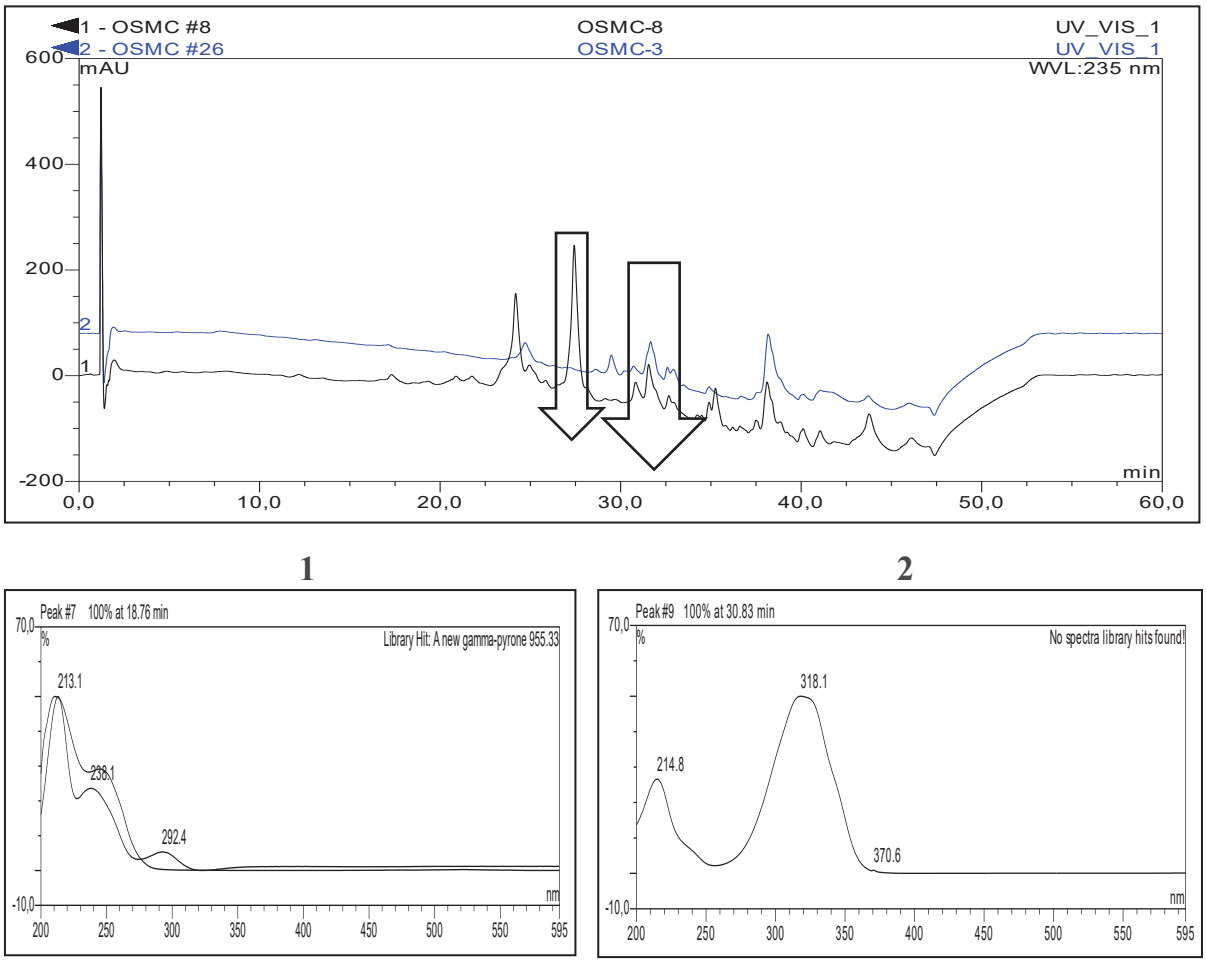

Figure 6. 2: HPLC chromatograms of EtOAc extract of *P. chamaeropis* cultured on solid rice medium (black) compared to culture on solid rice medium supplied with 3.5% NaI (blue).1: UV absorption of main peak; 2: UV absorption of pestalotic acid.

The biosynthetic pathway of pestalotic acid in fungi has not been elucidated until now. The proposed biosynthetic pathway of the structurally similar compound terrestric acid from *Pestalotiopsis crusotusm* shown in Figure 6.3 might be a useful reference. Acetyl-CoA, 3 x malonyl-CoA and L-malic acid are used as substrates by TraA to form carboxylcrustic acid. Afterwards dehydrogenation is mediated by TraG to get **4**. The responsible enzyme for the hydroxylation of **5** has not been identified yet. Next, spontaneously loss of a keto and hydroxyl group occurs to obtain **1**, followed by TraH to catalyze an oxidative decarboxylation of **1** to yield **3**. Subsequently, TraD is responsible for the stereospecific reduction of **3** to yield **2**. This study did not only reveal the proposed biosynthetic pathway of terrestric acid, but also explains

the biotransformation that is required for the sequential two-step reactions i.e., decarboxylation by TraH and oxidoreduction by TraD.[26]

Table 6.1: Activity against MRSA and *C. albicans* of EtOAc extracts obtained from *P. chamaeropis* by "OSMAC" approach.

NO.	Medium / condition	Weight (mg)	Yields (%)	Initial Concentration (mg/ml)	MRSA	*Candida albicans* (Hyphae form)	*Candida albicans* (Yeast form)
1	*Pestalatiopsis* + Rice	448	100%	10	>100 **µg/ml**	>100 **µg/ml**	>100 **µg/ml**
2	*Pestalatiopsis* + Rice + NaCl	616	137.50%	10	>100	>100	>100
3	*Pestalatiopsis* + Rice + NaBr	744	166.07%	10	**100**	>100	>100
4	*Pestalatiopsis* + Rice + NaI	522	116.52%	10	**100**	**100**	**100**
5	*Pestalatiopsis* + Rice + $NaNO_3$	541	120.76%	10	>100	>100	>100
6	*Pestalatiopsis* + Rice +$(NH_4)_2SO_4$	374	83.48%	10	>100	**100**	>100
7	*Pestalatiopsis* + Rice + $MgSO_4$ + $NaNO_3$ + NaCl	700	156.25%	10	>100	>100	>100
8	*Pestalatiopsis* + Rice + $FeSO_4$ + $NaNO_3$ + NaCl	535	119.42%	10	**100**	>100	>100
9	*Pestalatiopsis* + Rice + $ZnSO_4$ + $NaNO_3$ + NaCl	252	56.25%	10	>100	>100	>100
10	*Pestalatiopsis* + *Bacillus subtilis* + Rice	649	144.87%	10	**100**	>100	>100
11	*Pestalatiopsis* + Rice + L-Rhamnose	606	135.27%	10	**50**	**50**	**100**

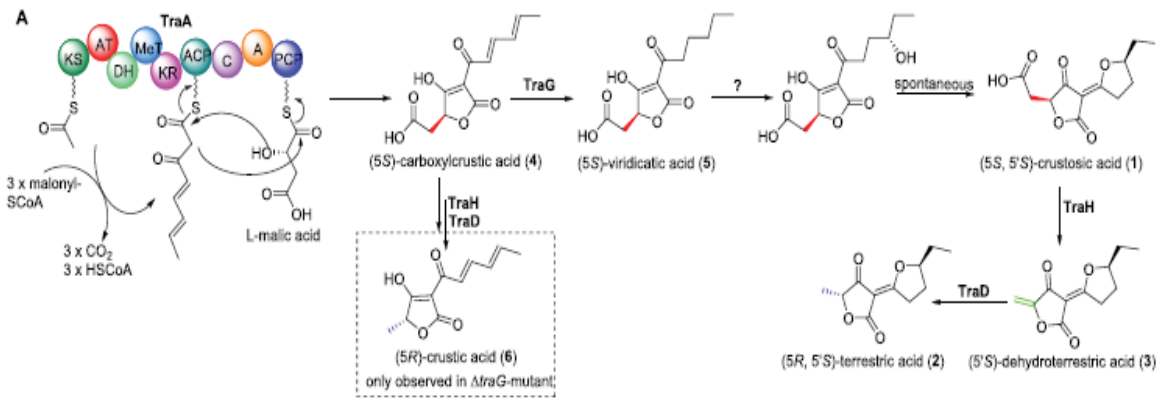

Figure 6.3: Proposed terrestric acid biosynthetic pathway in *P. crusotusm* PRB-2

To evaluate the bioactivity against bacteria, various Gram-positive pathogens including MRSA (ATCC 700699), Vancomycin-resistant *E. faecium* ATCC 700221, Vancomycin-resistant *E. faecalis* ATCC 51299, susceptible strain of *S. pneumonia* ATCC 49619, and *M. tuberculosis* H37Rv and the fungus *C. albicans* were tested with isolated compounds in minimal inhibitory concentration assay. Interestingly, pestalotic acid A and G demonstrated a significant effect against MRSA with an MIC_{90} of 6.25 μM while the other compounds were nearly devoid of antibacterial activity even at the highest tested concentration of 100 μM. Thus, from the structure-activity relationship aspect, substitution by a hydroxyl group, ketone group and ester group at the side chain obviously is not conducive for antibacterial activity. However, in previous studies pestalotic acid A did not exhibit activity against *S. aureus* Col (CGMCC 1.2465) strain and *S. pneumoniae* (CGMCC 1.1692). In contrast, pestalotic acid G displayed activity not only against MRSA but also *S. pneumoniae.* [27]

Furthermore, due to the specific structure of pestalotic acid A containing a decane linker, the molecule possesses high lipophilicity and thus might be able to interact with the phospholipid bilayers of the cell membrane. Pestalotic acid A might impair the integrity of the cell membrane might as indicated by detection of fluorescence in treated cells during the PI assay. Capacity of lysis on MRSA cells was confirmed by measurement of the fluorescence caused by PI after 40 mins incubation with pestalotic acid A. In addition, in vitro experiments were done to preliminary explore pharmacodynamic properties of the compound. Cytotoxic and hemolytic effects were only observed at higher concentrations. Therefore, the therapy selective index (SI) of pestalotic acid A in different human cell lines, such as HEK-293, THP-1, HUH-7, and H-4, had an appropriate therapeutic window against MRSA.

Future investigations might give further inspiring hints about the mechanisms of action,. For example, the morphology of bacterial cells treated with sublethal concentration of testing compounds can be analyzed under the microscope. This might reveal the effects on the bacterial envelope through the shape of the cells via electron microscopy, and potential damage of

membrane integrity might be observable by bleb formation or cell shape alteration.[28] If pestalotic acids can be linked to a fluorescence probe, it might be helpful for the localization of the compounds by fluorescence microscopy.[29-30] Transcriptome and proteome profiling are also useful in giving information about metabolic pathways by treatment with testing compounds. Proteome profile of the testing compound can be compared with profiles of antibiotics with known mode of action. This might indicate the affected pathway due to similar protein abundance patterns.[31] *B. subtilis* bio-reporter strains with fluorescent or bioluminescent reporter genes under control of selected promotor were used by others to identify interference with different biosynthetic pathways and could also represent a powerful tool in our mode-of-action study.[32]

References to chapter 6

[1] Roberti R, Veronesi A, Cesari A, et.al. Induction of PR proteins and resistance bynthe biocontrol agent *Clonostachys rosea* in wheat plants infected with *Fusarium culmorum*. *Plant Sci*. 2008; 175, 339−347.

[2] Baloyi MA, Laing MD, Yobo KS. Use of mixed cultures of biocontrol agents to control sheep nematodes. Vet. *Parasitol*. 2012; 184, 367−370.

[3] Mamarabadi M, Jensen DF, Lübeck M. An N-acetyl-β-Dglucosaminidase gene, cr-nag1, from the biocontrol agent *Clonostachys rosea* is up-regulated in antagonistic interactions with *Fusarium culmorum*. *Mycol. Res*. 2009; 113, 33−43.

[4] Pang X, Zhao JY, Fang XM, et.al. Metabolites from the plant endophytic fungus *aspergillus sp*. cpcc 400735 and their anti-HIV activities. *J. Nat. Prod*. 2017; 80, 2595-2601.

[5] Rukachaisirikul V, Rungsaiwattana N, Klaiklay S, et.al. γ-butyrolactone, cytochalasin, cyclic carbonate, eutypinic acid, and phenalenone derivatives from the soil Fungus *aspergillus sp*. PSURSPG185. *J. Nat. Prod*. 2014; 77, 2375−2382.

[6] Eric Merifield, Eric J. Thomas. Total synthesis of cytochalasin D: total synthesis and full structural assignment of cytochalasin O. *J. Chem. Soc., Perkin Trans*. 1, 1999; 22, 3269-3283.

[7] Stork G, Nakahara Y, Nakahara Y, et.al. Total synthesis of cytochalasin B. *J. Am. Chem. Soc.* 1978; 100, 24, 7775–7777.

[8] Schümann J, Christian H. Molecular basis of cytochalasan biosynthesis in fungi: gene cluster analysis and evidence for the involvement of a PKS-NRPS hybrid synthase by RNA silencing. *J. Am. Chem. Soc*. 2007, 129; 31, 9564-9565.

[9] Oikawa H, Yasunobu M, Akitami I. Biosynthetic study of chaetoglobosin A: origins of the oxygen and hydrogen atoms, and indirect evidence for biological Diels–Alder reaction. *J. Chem. Soc*. *Perkin Trans*. 1992; 1, 2955-2959.

[10] Hu Y, Dietrich D, Xu W, et al. A carbonate-forming Baeyer-Villiger monooxygenase. *Nat Chem Biol*.2014; 10, 552–554.

[11] Zhai MM, Qi FM, Li J, et.al. Isolation of secondary metabolites from the soil-derived fungus *clonostachys rosea* yrs-06, a biological control agent, and evaluation of antibacterial activity. *J. Agric. Food Chem*. 2016; 64, 2298−2306.

[12] Supratman U, Suzuki T, Nakamura T, et.al. New metabolites produced by endophyte *clonostachys rosea* B5-2. *Nat. Prod. Res*. 2021; 3, 1525-1531.

[13] Abdel-Wahab NM, Harwoko H, Müller WEG, et.al. Cyclic heptapeptides from the soil-derived fungus *clonostachys rosea*. *Bioorg Med Chem*. 2019; 27, 3954–3959.

[14] Okuda T, Kohno J, Kishi N, et.al. Production of TMC-151, TMC-154 and TMC-171, A new class of antibiotics, is specific to 'gliocladium roseum' group. *Mycoscience*. 2000; 41, 239-253.

[15] Dias ACDS, Couzinet-Mossion A, Ruiz N, et.al. Steroids from marine-derived fungi: evaluation of antiproliferative and antimicrobial activities of eburicol. *Mar. Drugs*. 2019; 17, 372.

[16] Jiang CX, Yu B, Miao YM, et.al. Indole alkaloids from a soil-derived *Clonostachys rosea*. *J. Nat. Prod*. 2021; 84, 2468−2474.

[17] Gombodorj S, Yang M.H, Shang ZC, et.al. New phenalenone derivatives from *Pinellia ternata* tubers derived Aspergillus sp. *fitote*. 2017; 120, 72-78.

[18] Zhao J, Wang J, Pang X, et al. An anti-influenza A virus microbial metabolite acts by degrading viral endonuclease PA. *Nat Commun*. 2022; 13, 1-11.

[19] Scherlach K, Boettger D, Remme Net.al. The chemistry and biology of cytochalasans. *Nat. Prod. Rep*. 2010; 27, 869-886.

[20] Rampal AL, Pinkofsky HB, Jung C Y. Structure of cytochalasins and cytochalasin B binding sites in human erythrocyte membranes. *Biochemistry*. 1980; 19, 679-683.

[21] Sellstedt M, Schwalfenberg M, Ziegler S, et.al. Trienamine catalyzed asymmetric synthesis and biological investigation of a cytochalasin B-inspired compound collection. *Org. Biomol. Chem*. 2016; 14, 50-54.

[22] Schofield JG. Cytochalasin B and release of growth hormone. *Nat New Biol*. 1971; 50, 215-216.

[23] Xu J, Ebada SS, Proksch P. Pestalotiopsis a highly creative genus: chemistry and bioactivity of secondary metabolites. *Fungal Divers*. 2010; 44, 15–31.

[24] Poolman B, Glaasker E. Regulation of compatible solute accumulation in bacteria. *Mol. Microbiol*. 1998; 29, 397–407.

[25] Pan R, Bai X, Chen J, et.al. Exploring structural diversity of microbe secondary metabolites using OSMAC strategy: a literature review. *Front. Microbiol*. 2019; 10, 294.

[26] Fan J, Liao G, Ludwig-Radtke L, et.al. Formation of Terrestric Acid in Penicillium crustosum Requires Redox-Assisted Decarboxylation and Stereoisomerization. *Org. Lett*. 2020, 22, 1, 88–92.

[27] Zhang F, Ding G, Li L, et.al. Isolation, antimicrobial activity, and absolute configuration of the furylidene tetronic acid core of pestalotic acids A–G. *Org. Biomol. Chem*. 2012; 10, 5307–5314.

[28] Hartmann M, Berditsch M, Hawecker J, et.al. Damage of the bacterial cell envelope by antimicrobial peptides gramicidin S and PGLa as revealed by transmission and scanning electron microscopy, *Antimicrob. Agents Chemother*. 2010; 54, 3132-3142.

[29] Tiyanont K, Doan T, Lazarus MB, et.al. Imaging peptidoglycan biosynthesis in *Bacillus subtilis* with fluorescent antibiotics. *PNAS*. 2006; 103, 11033-11038.

[30] Zhang B, Stone MRL, Sanjaya KC, et al. Application of antibiotic-derived fluorescent probes to bacterial studies. *Meth. Enzymol*. 2022; 665, 1-28.

[31] da Cunha BR, Zoio P, Fonseca LP, et.al. Technologies for High-throughput identification of antibiotic mechanism of action. *Antibiotics*. 2021; 10, 565.

[32] Reithuber E, Wixe T, Ludwig KC, et.al. THCz: Small molecules with antimicrobial activity that block cell wall lipid intermediates. *Proc Natl Acad Sci U S A*. 2021; 118, 47 e2108244118.

List of Abbreviations

A. baumannii	*Acinetobacter baumannii*
ATCC	American Type Culture Collection
ATP	Adenosine Tri-Phosphate
Bgc_s	Biosynthetic gene clusters
calcd.	Calculated
CCCP	Carbonyl Cyanide m-Chlorophenyl Hydrazone
CDC	Centre for Disease Control and Prevention
$CDCl_3$	Deuterated chloroform
CD_3OD	Deuterated methanol
CFU	Colony forming units
CH2Cl2, DCM	Dichloromethane
CLSI	Clinical and Laboratory Standards Institute
COSY	Correlated spectroscopy
CYP_3A_4	Cytochrome P450 3A4
DMEM	Dulbecco's Modified Eagles Medium
DMSO	Dimethyl sulfoxide
DNA	Deoxyribo-Nucleic Acid
DOI	Digital Object Identifier
ECD	Electronic circular dichroism
E. coli	Escherichia coli
E. faecalis	Enterococcus faecalis
E. faecium	Enterococcus faecium
e. g.	*Exempli gratia,* for example
et al.	Et altera (and others)
EtOAc	Ethyl acetate
FBS	fetal bovine serum
FDA	Food and Drug Administration
g	Gram
GFP	Green Fluorescent Protein
h	Hour (s)
HIV-1	Human immunodeficiency virus type 1
HMBC	Heteronuclear multiple bond connectivity
HPLC	High-performance liquid chromatography
HRESIMS	High-resolution electrospray ionization mass spectrometry
HSQC	Heteronuclear single quantum coherence
Hz	Hertz
IC_{50}	Half maximal inhibitory concentration

ITS	Internal transcribed spacer
L	Liter
LC-MS	liquid chromatography-mass spectrometry
LPS	Lipopolysaccharide
m	Multiplet signal
M	Molar
m/z	Mass per charge
MDR Multi-Drug Resistant	MDR Multi-Drug Resistant
MeCN	Acetonitrile
MeOH	Methanol
mg	Milligram
MgSO4	Magnesium sulfate
MH	Müller Hinton
MHz	Megahertz
MIC	Minimal inhibitory concentration
min	Minute
MRSA	Methicillin-resistant *Staphylococcus aureus*
MS	Mass spectrometry
M. tb.	*Mycobacterium tuberculosis*
NaBr	Sodium bromide
NaCl	Sodium chloride
NaF	Sodium fluoride
NaI	Sodium iodide
NaNO3	Sodium nitrate
$(NH_4)_2SO4$	Ammonium sulfate
nm	Nanometer
NMR	Nuclear magnetic resonance
NOE	Nuclear overhauser effect
NOESY	Nuclear overhauser effect spectroscopy
OD	Optical density
OSMAC	One strain many compounds
PBS	Phosphate buffered saline
PCR	Polymerase chain reaction
RNA Ribo-Nucleic Acid	RNA Ribo-Nucleic Acid
ROESY	Rotating-frame nuclear Overhauser effect correlation spectroscopy
RP	Reverse phase
rpm	Rounds per minute
S. aureus	*Staphylococcus aureus*
SAR	Structure-activity relationship
SI	Selectivity index

sp.	Species
TB	Tuberculosis
TLC	Thin layer chromatography
topo	Topoisomerase
UV	Ultra-violet
VLC	Vacuum liquid chromatography
WHO	World Health Organization
WT	Wild type
ZnSO4	Zinc sulfate
µg	*µM Gram*
µM	*µM Micromolar*

Research contributions

Publications

- Gao Y, **Wang L**, Kalscheuer R, Liu Z, Proksch P. Antifungal polyketide derivatives from the endophytic fungus *Aplosporella javeedii*. *Bioorg Med Chem*. 28, 115456 (2020).

  Overall contribution to this publication: 35%, second author, antifungal activity evaluation.

- Gao Y, Stuhldreier F, Schmitt L, Wesselborg S, **Wang L**, Müller WEG, Kalscheuer R, Guo Z, Zou K, Liu Z, Proksch P. Sesterterpenes and macrolide derivatives from the endophytic fungus *Aplosporella javeedii*. *Fitoterapia.* 146, 104652 (2020).

  Overall contribution to this publication: 15%, fourth author, antibacterial activity screening.

- Rehberg N, Sommer G, Drießen D, Kruppa M, Adeniyi ET, Chen S, **Wang L**, Wolf K, Tasch B, Ioerger TR, Zhu K, Müller TJJ, Kalscheuer R. Nature-inspired (di)azine-bridged bisindole alkaloids with potent antibacterial in vitro and in vivo efficacy against Methicillin-resistant *Staphylococcus aureus*. J Med Chem 63, 12623-12641 (2020).

  Overall contribution to this publication: 10%, third author, cytotoxicity assay.

- **Wang L**, Ma QY, Kong FD, Xie QY, Zhou LM, Dai HF, Kalscheuer R, Wu YG, Zhao YX. Chemical constituents and nematocidal activity of the fruiting body of *Ramaria stricta*. *Chem Nat Comp.* 57, 720-723 (2021).

Overall contribution to this publication: 90%, first author, Chemical constituent isolation from the fruiting body of *Ramaria stricta*, structure elucidation, anti-nematocidal activit testing and preparation of the manuscript.

- Eze PM, Simons V, Seidemann T, **Wang L**, Kiffe-Delf AL, Frank M, van Geelen L, Abba CC, Esimone CO, Okoye FBC, Kalscheuer R. Serratiochelins A and B from *Serratia marcescens* show xenosiderophoric characteristics towards *Acinetobacter baumannii* and *Mycobacterium tuberculosis*. *Trop J Pharm Res.* 20, 2551-2658 (2021).

Overall contribution to this publication: 10%, fourth author, helping in compounds isolation and structure elucidation.

- Xue Cao, Li Yang, Hao-Fu Dai, Yan-Mei Wei, Sheng-Zhuo Huang, Hao Wang, Cai-Hong Cai, **Lin Wang**, Wen-Li Mei, Hui-Qin Chen. One new lignin and one new fluorenone from Dendrobium nobile Lindl. *Phytochem. Lett.* 44, 164-168, (2021)

Overall contribution to this publication: 10%, eighth author, helping in structure elucidation and activity discussion.

Statutory Declaration

I declare under oath that I have compiled my dissertation independently and without any undue assistance by third parties under consideration of the “Principles for the Safeguarding of Good Scientific Practice at Heinrich-Heine-University Düsseldorf”.

I declare that I have not used sources or means without declaration in the text. All the passages taken from other works in the wording or in the meaning have been clearly indicated with sources. This thesis has not been used in the same or similar version to achieve an academic grading or is being published elsewhere.

Düsseldorf, 12.07.2022

_____

Lin Wang

Acknowledgement

First of all, I would like to express my sincere appreciation to Prof. Dr. Rainer Kalscheuer for giving me the precious opportunity to pursue my doctoral study with great topics in his research group at the Institute of Pharmaceutical Biology and Biotechnology, Heinrich Heine University. Further, I would like to express my deep thanks for his patient guidance, constructive suggestions, full trusts and freedom as well as continuous supports. Worthy, his rigorous scientific spirit, kind and generous attitude with students will inspire me in my all life.

My great thanks to my co-supervisor Prof. Dr. Peter Proksch for encouragements before came to Germany and professional suggestions during my doctoral research.

My special thanks to Prof. Dr. Haofu Dai (Institute of Tropical Bioscience and Biotechnology, Chinese Academy of Tropical Agriculture Science) for introducing me to Prof. Rainer Kalscheuer.

My sincere thanks to Prof. Dr. Youxin Zhao (Institute of Tropical Bioscience and Biotechnology, Chinese Academy of Tropical Agriculture Science) for caring and encouragements in the beginning of my doctoral research.

I would like to thank Dr. Zhen Liu for helping to improve my manuscripts, NMR data rechecking and valuable suggestions on my experiments.

I would like to thank to Prof. Dr. Tibor Kurtán (Department of Organic Chemistry, University of Debrecen) for helping CD measurements, ECD calculations and patiently answering with my stereochemical questions.

I would like to thank to Prof. Dr. Heiner Schaal (Institute of Virology, University Hospital Düsseldorf, Heinrich Heine University Düsseldorf) for his kindly help in HIV activity screening.

I would like to thank to Prof. Dr. Christoph Janiak (institute of ACI Section for nanoporous and nanoscale materials) for helping in single-crystal X-ray diffraction.

A honest thanks to all members my working group, especially Dr. Lasse van Geelen, Emmanuel Tola Adeniyi, Anna-Lene Kiffe-Delf, Kristin Schwechel, Viktor Simons, Tino seidemann, Dieter Meier, Steffen Schindler, Yvonne Gröner, Mohammed Rizwan Babu Sait for selfless helping in my whole doctoral study time. And also thanks Heike Goldbach-Gecke so much for professional teaching in cytotoxicity.

My deep thanks to the whole colleagues and friends at Institute of Pharmaceutical Biology and Biotechnology for the friendly help and fruitful cooperation, especially, Dr. Marian Frank, Dr. Nam Tran-Cong, Dr. Dina Faek Abdel-Kader Hassouna El-Kashef, Dr. Ying Gao, Dr. Xiaoqin Yu, Dr. Haiqian, Yu, Dr. Ni Putu Ariantari and Kim Le. Also thanks to Katja Friedrich, Simone Miljanovic and Claudia Eckelskemper for all the supports.

In the end, I would like to express my thanks to China Scholarship Council, Ministry of Education of China for the financial support in Germany.